UNIVERSITY OF CALIFORNIA, SAN DIEGO

Supramolecular Structures and Metal-Organic Frameworks Based on Metal Dipyrrin Building Blocks

A dissertation submitted in partial satisfaction of the

requirements for the degree Doctor of Philosophy

in

Chemistry

by

Sara R. Halper

Committee in charge:

Professor Seth M. Cohen, Chair
Professor Clifford P. Kubiak
Professor Charles L. Perrin
Professor Michael J. Sailor
Professor Jan B. Talbot

2006

The dissertation of Sara R. Halper is approved, and it is acceptable in quality and form for publication on microfilm:

_____

_____

_____

_____

_____

Chair

University of California, San Diego

2006

In dedication to my parents,

Jane and Steve Halper

TABLE OF CONTENTS

LIST OF SYMBOLS AND ABBREVIATIONS

α	alpha
Å	Ångstrøm; 10^{-10} m
$Å^3$	cubic Ångstrøm
acac	acetylacetonate
$AgBF_4$	silver hexafluorophosphate
APCI	Atmospheric Pressure Chemical Ionization
β	beta
bs	broad singlet (NMR)
C	carbon
°C	degree Celsius
Calcd	calculated
CCDC	Cambridge Crystallographic Data Centre
$CDCl_3$	deuterated chloroform
CF_3	tetrafluorocarbon
$CHCl_3$	chloroform
CH_2Cl_2	methylene chloride
CH_3CN	acetonitrile
Cl	chlorine, chloride
cm^{-1}	inverse centimeter
^{13}CNMR	carbon NMR

C=O	carbonyl
Cu	copper(II)
CuI	copper(I) iodide
°	degree
δ	chemical shift; ppm
Δ	heat
d	doublet (NMR)
d-DMSO	deuterated dimethyl sulfoxide
DDQ	2,3-Dichloro-5,6-dicyano-1,4-benzoquinone
DI	deionized
dpm	dipyrromethene
DSC	Differential Scanning Calorimetry
EDTA	ethylenediaminetetraacetic acid
EI	Electron Ionization
EPR	Electron Paramagnetic Resonance
ESI	electrospray ionization
ε	molar extinction coefficient; M^{-1} cm^{-1}
FAB	fast atom bombardment
F-F	fluorine-fluorine
γ	gamma
GC	gas chromatography
h	hour

hfacac	hexafluoroacetylacetonate
H_2O	water, hydrate
HRMS	high-resolution mass spectrometry
Hz	hertz
IR	infrared
J	spin-spin
K	Kelvin
KBr	potassium bromide
λ	wavelength, lambda
m	multiplet (NMR)
M	molar; mol L^{-1}
MALDI	Matrix-Assisted Laser Desorption/Ionization
MeOH	methanol
$MgSO_4$	magnesium sulfate
MHz	mega-hertz; 10^6 s^-
mg	milligram
min	minute
mL	mililiter
mM	milimolar
mmol	milimol
MOF	Metal-Organic Framework
MS	mass spectrometry

MW	molecular weight
m/z	mass to charge
N	nitrogen
nm	nanometer; 10^{-9} m
NMR	Nuclear Magnetic Resonance
O	oxygen
ORTEP	Oak Ridge Thermal Ellipsoid Presentation
%	Percent
PF_6^-	hexafluorophosphate anion
Ph	Phenyl
π	Pi; ratio of the circumference of a circle to its diameter
ppm	parts per million
pyr	pyridyl
q	quintuplet (NMR)
quin	quinolyl
ref.	reference
s	singlet (NMR)
SiO_2	silicon dioxide, silica gel
tfacac	trifluoroacetylacetonate
TFA	Trifluoroacetic acid
TGA	Thermogravimetric Analysis
THF	tetrahydrofuran

TLC	Thin Layer Chromatography
TMS	trimethylsilyl
UV/VIS	Ultra-Violet/Visible
ν	wave number, cm^{-1}
V	volts

LIST OF FIGURES

LIST OF SCHEMES

LIST OF TABLES

ACKNOWLEDGEMENTS

First and foremost I would like to acknowledge my parents for their unconditional support. I would not be where I am today without them.

I would like to thank Seth M. Cohen for allowing me to work in his lab. I would also like to thank other UCSD confidants: Lynne Keith McMullin, Dr. Barbara Sawrey, and Jill Weller for non-research related support. In addition, my time in lab would not have been as enjoyable without the companionship and support of my labmates: David Puerta, Misha Golynskiy, Talib Davis, Jana Lewis, Faith Jacobsen, Loi Do, Mitchell Malachowski, and Heather Delaney. Furthermore, the extensive X-ray crystallography performed would not have been possible without the assistance of Dr. Arnold L. Rheingold and Dr. Lev Zakharov.

I would like to thank the U.S. Department of Education and Lynne Keith McMullin for providing me with a Graduate Assistance in Areas of National Need (GAANN) Fellowship my first two years at UCSD. I would also like to thank the National Science Foundation (NSF) for granting me a Graduate Research Fellowship, which has supported me my last two and a half years at UCSD. I am eternally grateful to both because I would not have received this degree as promptly or with as many publications without them.

The text, schemes, and figures of chapters two, four, and five are in part reprints of the materials published in the following papers: Sara R. Halper and Seth M. Cohen, "Self-Assembly of Heteroleptic [Cu(dipyrrinato)(hfacac)] Complexes Driven

by Fluorine-Fluorine Interactions" *Inorg. Chem*. **2005**, 44, 4139-4141; Sara R. Halper and Seth M. Cohen, "Heterometallic Metal-Organic Frameworks Based on Tris(dipyrrinato) Coordination Complexes" *Inorg. Chem.* **2005**, 44, 486-488; Sara R. Halper and Seth M. Cohen, "Self-Assembly of Two Distinct Supramolecular Motifs in a Single Crystalline Framework" *Angew. Chem. Intl. Ed.* **2004**, 43, 2385-2388; Sara R. Halper, Mitchell R. Malachowski, Heather M. Delaney, and Seth M. Cohen, "Heteroleptic Copper Dipyrromethene Complexes: Synthesis, Structure, and Coordination Polymers" *Inorg. Chem.* **2004**, 43, 1242-1249; and Sara R. Halper and Seth M. Cohen, "Synthesis, Structure, and Spectroscopy of Phenylacetylene Rods Incorporating Meso-Substituted Dipyrrin Ligands" *Chem. Eur. J.* **2003**, 9, 4661-4669. The dissertation author was the primary researcher. The co-authors listed in the publications also participated in the research. The permissions to reproduce the papers are granted by the American Chemical Society, and John Wiley & Sons Inc.

VITA

Education

March 2006 - Ph.D. in Chemistry, University of California, San Diego
Advisor: Prof. Seth M. Cohen

June 2003 - Master of Science in Chemistry, University of California, San Diego

May 2001 - Bachelor in Chemistry, University of Arizona

Research Fellowships and Experiences

Sept. 2003 – March 2006	National Science Foundation (NSF) Graduate Research Fellowship
Sept. 2001 – Aug. 2003	U.S. Department of Education Graduate Assistance in Areas of National Need (GAANN) Fellowship
July 2001 – Aug. 2001	Research in Industry Summer Experience (RISE) Program, University of California, San Diego
May 2000 – Aug. 2000	National Science Foundation (NSF) Research Experience for Undergraduates (REU) Program, University of Florida
May 1999 – Aug. 1999	National Science Foundation (NSF) Research Experience for Undergraduates (REU) Program, University of Central Florida
Sept. 1999 – May 2000	Undergraduate Research Assistant, University of Arizona, with Prof. F. Ann Walker, Dr. Nadine Gruhn, and Prof. Dennis Lichtenburger
Oct. 1998 – May 2000	University of Arizona/NASA Space Grant Undergraduate Research Program, with Prof. John O. Kessler

Professional Affiliations

1998 – present	American Chemistry Society, Member

Presentations

Dec. 2005	ACS Pacifichem Meeting, Honolulu, HI. “Metal-organic frameworks based on tris-chelate metal dipyrrin building blocks” poster.
Aug. 2005	ACS National Meeting, Washington, DC. “Metal-organic Frameworks Based on Tris-Chelate Metal Dipyrrin Building Blocks” oral presentation.
March 2005	ACS National Meeting, San Diego, CA “Metal-organic Frameworks Based on Pyridine Substituted Dipyrromethene Metal Complexes” poster.
March 2004	ACS National Meeting, Anaheim, CA “Supramolecular Complexes Based on Dipyrromethene Compounds” poster.
Aug. 2002	16th International Conference on Physical Organic Chemistry (ICPOC-16), San Diego, CA “Supramolecular Complexes Based on Dipyrromethene Ligands” poster.
March 2000	ACS National Meeting, San Francisco, CA “Photoelectron Spectroscopy of Tetrakis-(2,6-Dihalophenyl)porphyrins” poster.
April 1999	Arizona NASA Space Grant Convention, Tempe, AZ “Velocity of Swimming Bacteria” oral presentation.

Publications

1. Sara R. Halper and Seth M. Cohen, "Self-Assembly of Heteroleptic [Cu(dipyrrinato)(hfacac)] Complexes Driven by Fluorine-Fluorine Interactions" *Inorg. Chem.* **2005**, 44, 4139-4141.

2. Sara R. Halper and Seth M. Cohen, "Heterometallic Metal-Organic Frameworks Based on Tris(dipyrrinato) Coordination Complexes" *Inorg. Chem.* **2005**, 44, 486-488.

3. Loi Do, Sara R. Halper, and Seth M. Cohen, "Helical Coordination Polymers and Cyclic Dimers Formed From Heteroleptic Thioether-Dipyrrinato Copper(II) Complexes" *Chem. Commun.* **2004**, 2662-2663.

4. Sara R. Halper and Seth M. Cohen, "Self-Assembly of Two Distinct Supramolecular Motifs in a Single Crystalline Framework" *Angew. Chem. Intl. Ed.* **2004**, 43, 2385-2388.

5. Sara R. Halper, Mitchell R. Malachowski, Heather M. Delaney, and Seth M. Cohen, "Heteroleptic Copper Dipyrromethene Complexes: Synthesis, Structure, and Coordination Polymers" *Inorg. Chem.* **2004**, 43, 1242-1249.

6. Sara R. Halper and Seth M. Cohen, "Synthesis, Structure, and Spectroscopy of Phenylacetylene Rods Incorporating Meso-Substituted Dipyrrin Ligands" *Chem. Eur. J.* **2003**, 9, 4661-4669.

7. Seth M. Cohen and Sara R. Halper, "Dipyrromethene Complexes of Iron" *Inorg. Chim. Acta* **2002**, 341, 12-16.

ABSTRACT OF THE DISSERTATION

Supramolecular Structures and Metal-Organic Frameworks Based on Metal Dipyrrin Building Blocks

by

Sara R. Halper

Doctor of Philosophy in Chemistry

University of California, San Diego, 2006

Professor Seth M. Cohen, Chair

Metal dipyrrin complexes have the potential to be incorporated into a variety of supramolecular systems and metal-organic frameworks (MOFs). Despite their potential, limited work has been done to study simple *meso*-substituted dipyrrin metal complexes for their use in supramolecular systems; therefore, dipyrrin ligands and metal complexes have been synthesized and studied. Metal dipyrrin complexes were prepared containing copper(II), iron(III), or cobalt(III) metal centers. Phenylacetylene spacers and perfluorophenyl groups were introduced and their effects were studied.

During the preparation of certain dipyrrins, new α-substituted dipyrrin ligands were identified and their metal-coordination was explored. Also in the preparation of certain dipyrrins, a wide variety of supramolecular structures containing heteroleptic copper(II) dipyrrin complexes emerged, ranging from one-dimensional coordination polymers to discrete supramolecular hexagons. One very unique structure emerged consisting of both discrete supramolecular hexagons and double-helical polymer chains in the same crystalline framework. The materials were characterized by various methods including single crystal X-ray diffraction. Studies on their topology and their structural driving forces such as F–F interactions were carried out.

Finally, a series of MOFs containing cobalt(III) and iron(III) metal dipyrrin complexes and silver(I) salts were prepared. The materials were primarily characterized by X-ray diffraction. Once again a wide variety of topologies emerged, ranging from two-dimensional hexagonal sheets to elaborate three-dimensional topologies. One particular combination of a dipyrrin complex and silver(I) salt formed a chiral MOF. Mixed-metal MOFs were also prepared, as well as MOFs containing large dipyrrin building blocks. The counterion was shown to template the formation of the frameworks; therefore anion templating and anion exchange studies were performed.

I. Introduction

1.1. Solid-State Materials

Recent advances have been made in the field of supramolecular chemistry towards the design of solid-state materials which can parallel and even improve upon the physical properties of zeolites for such purposes as catalysis, gas and solvent storage, and analyte sensing.[1] Supramolecular solid-state materials can be formed through simple organic or inorganic building blocks connected through different types of bonds to form elaborate two- and three-dimensional structures. Such materials can be built upon intermolecular forces such as hydrogen bonding,[2-4] π-π interactions,[5, 6] and metal-ligand coordination bonding.[7-9] Structures based on coordinative bonding can be very robust, especially when multidentate ligands bind to the metal. Supramolecular materials have an advantage over zeolites because they can be systematically designed with specific chemical properties and a desired topology. The topology of these materials is dictated by the symmetry of the building blocks and the coordination number and geometry of the linking metals. The physical properties of supramolecular materials can be tuned by slight modification of the building blocks.

1.2. Metal-Organic Frameworks

The term metal-organic framework (MOF) has been coined to classify materials consisting of an organic (or in some instances inorganic) ligand linked via metal ions or metal clusters to form a framework structure. A large number of one, two, and three-dimensional frameworks have been prepared.[10, 11] Three-dimensional topologies are commonly sought because they generally create robust solids. Altering

the organic ligand by appending functional groups or changing the ligand length can alter the physical properties of the framework. For example, using larger ligands can increase pore or channel size, and adding functional groups can alter the chemical environment of the pores or channels.

Zinc carboxylate-containing MOFs developed by Yaghi and others are prepared from carboxylic acid ligands and zinc(II) salts.[12, 13] The combination of a carboxylate ligand with zinc(II) nitrate yields extremely robust three-dimensional frameworks containing rigid organic ligands linked by $Zn_4O(CO_2)_6$ clusters (Figure 1-1). Similar MOFs have been prepared based on the interaction of carboxylates with metals such as zinc(II), lead(II), manganese(II), and others.[14] This class of MOFs has yielded materials with novel properties which have mimicked or even surpassed those of known zeolites. For example, the framework IRMOF-6 ($Zn_4O(R_6\text{-}BDC)_3\cdot(CHCl_3)_7$) formed from the organic ligand bicyclo[4.2.0]octa-1,3,5-triene-2,5-dicarboxylate (R_6-BDC) and zinc(II) nitrate, has shown levels of methane storage that are 2.75 times higher then the highest reported zeolite.[15] IRMOF-6 and IRMOF-8 (the latter of which is prepared from 2,6-naphthalenedicarboxylic acid) have also shown a very high hydrogen storage capacity, surpassing other known solid-state materials.[16] Finally, MOF-177, prepared from 4,4',4''-benzene-1,3,5-triyl-tri-benzoic acid (H_3BTB) and $Zn(NO_3)_2\cdot 6H_2O$, has the highest surface area of any solid-state material reported to date, five times larger then any reported zeolite.[17]

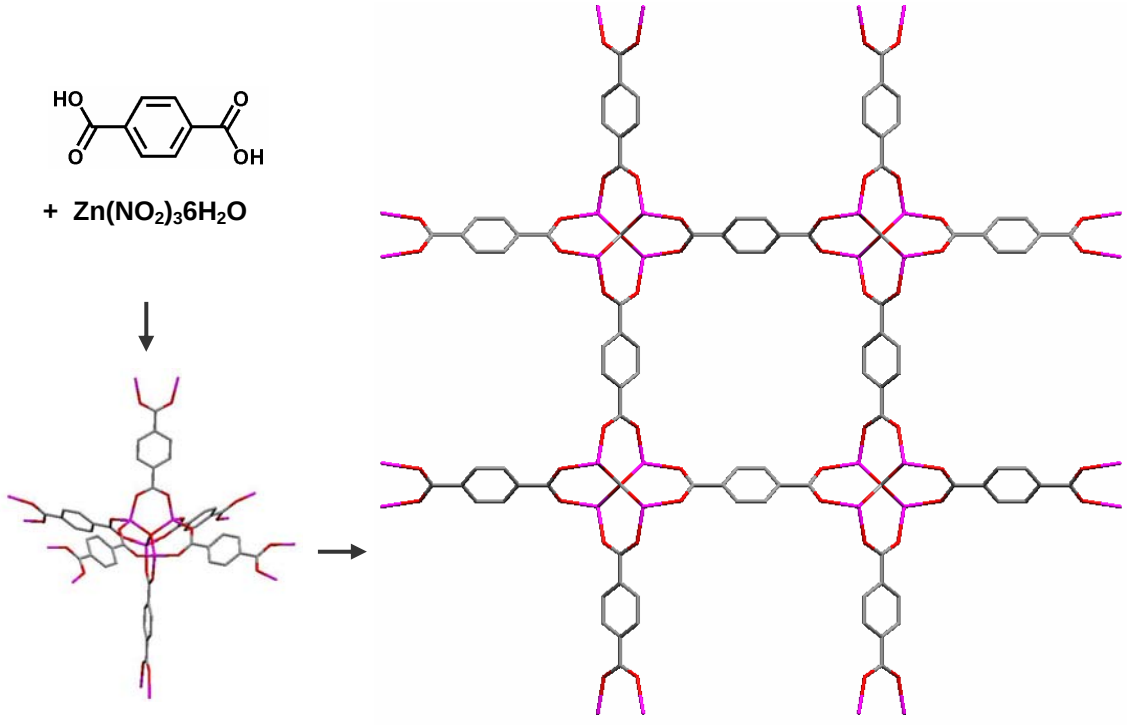

Figure 1-1. IRMOF-1 (right) consisting of 1,4-benzenedicarboxylate and $Zn(NO_2)_3 \cdot 6H_2O$ (top left), which generates octahedrally symmetric $Zn_4O(CO_2)_6$ clusters (bottom left). Hydrogen atoms have been omitted for clarity.

A number of research groups have explored MOFs constructed from silver(I) salts and multitopic coordinating ligands.[18, 19] In these systems, the coordinating ligands bind in a monodentate fashion to silver(I) ions. Of particular note, a number of systems in this family of MOFs containing pyrazine, thioether, and cyano ligands have been studied extensively by Lee, Moore, and coworkers.[20-25] Two- and three-fold symmetric organic ligands of various lengths have been used to create a number of one-, two-, and three-dimensional frameworks (Figure 1-2).

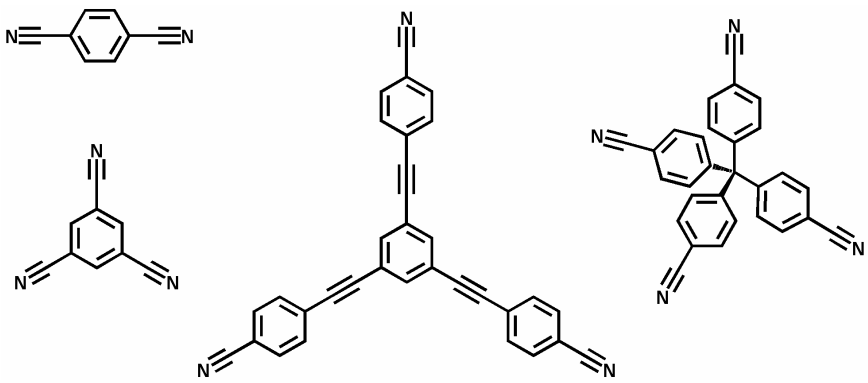

Figure 1-2. Several multitopic ligands that have been used in the synthesis of MOFs. Upon combination with silver(I) salts these ligands form one-, two-, and three-dimensional framework structures.

Of the aforementioned systems, the cyano-based MOFs have been the most widely studied. The MOF obtained from 1,3,5-tris(4-ethynylbenzonitrile)benzene (TEB) and silver(I) triflate (AgOTf, OTf = $^{-}O_3SCF_3$), exhibits three-dimensional interpenetrated frameworks with 15 Å × 22 Å channels (Figure 1-3). The chemical and physical attributes of the channels allow solvent exchange and vapor absorption of various small aromatic organic molecules.[24] The MOF is robust to the loss and reintroduction of small guest molecules. The same robust behavior is also observed in the MOF formed by 1,3,5-tris(3-ethynylbenzonitrile) and AgOTf; this framework also retains its integrity through moderate heating (110 °C).[23] These observations are very valuable because practical solid state materials need to remain robust to various solvent and heat conditions.

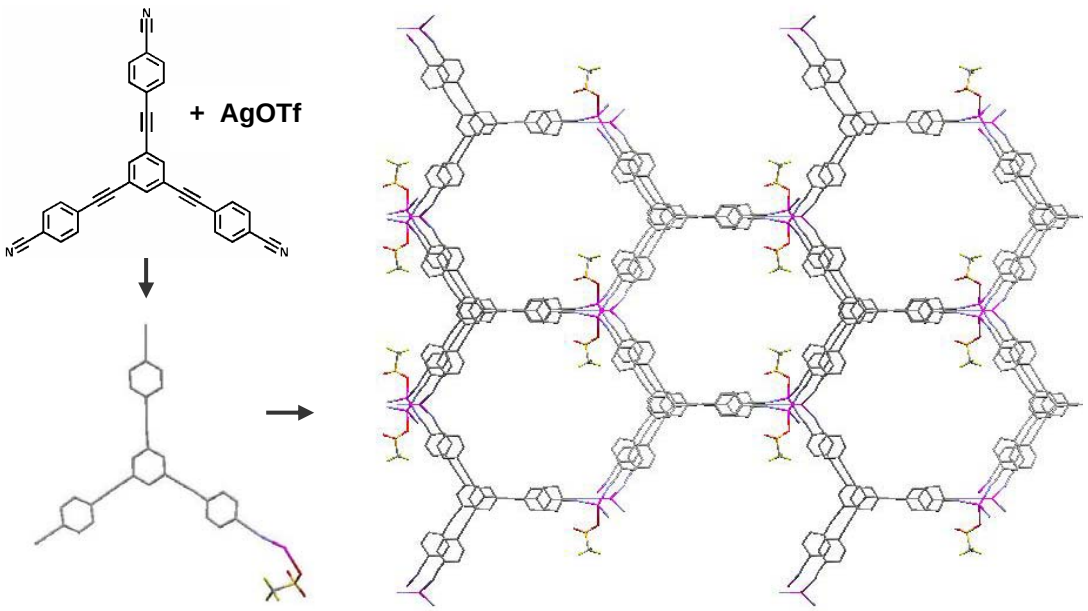

Figure 1-3. [TEB·AgOTf] MOF (right) consisting of 3,5-tris(4-ethynylbenzonitrile)benzene and silver(I) triflate (left). Hydrogen atoms have been omitted for clarity.

As previously mentioned, other functional groups have been utilized for the purpose of forming silver-containing MOFs such as thioether ligands,[26] nitrogenous ligands,[27-32] or a combination of various heterotopic ligands.[33-35] AgOTf is the most widely used silver(I) source; however, other silver(I) salts have been used to alter the chemical properties or topology of the frameworks. Pyridine ligands have been studied because they have been shown to coordinate to many silver(I) salts such as $AgBF_4$, $AgClO_4$, and $AgPF_6$ to form one-dimensional coordination polymers, as well as two- and three-dimensional frameworks, they have shown to be robust to thermal and solvent change, and they have exhibited zeolitic anion exchange properties.[27-32]

One desired physical property of zeolites that has yet to be achieved is chirality. Chiral MOFs have been prepared using chiral organic ligands such as

enantiometrically pure bipyridines and dicarboxylates combined with metal ions such as nickel(II), manganese(II) or cobalt(II).[36, 37] Chiral MOFs using homochiral phosphonate ligands bound to a variety of metal ions such as gadolinium(III), samarium(III), neodymium(III), and zirconium(III) have also been prepared and studied (Figure 1-4).[38-40] The ability to perform heterogeneous enantioselective separations was demonstrated by a chiral MOF comprised of a phosphonate ligand and a samarium(III) ion, which gave at best 14% enantiomeric separation of the racemic compound *trans*-1,2-diaminocyclohexane.[38]

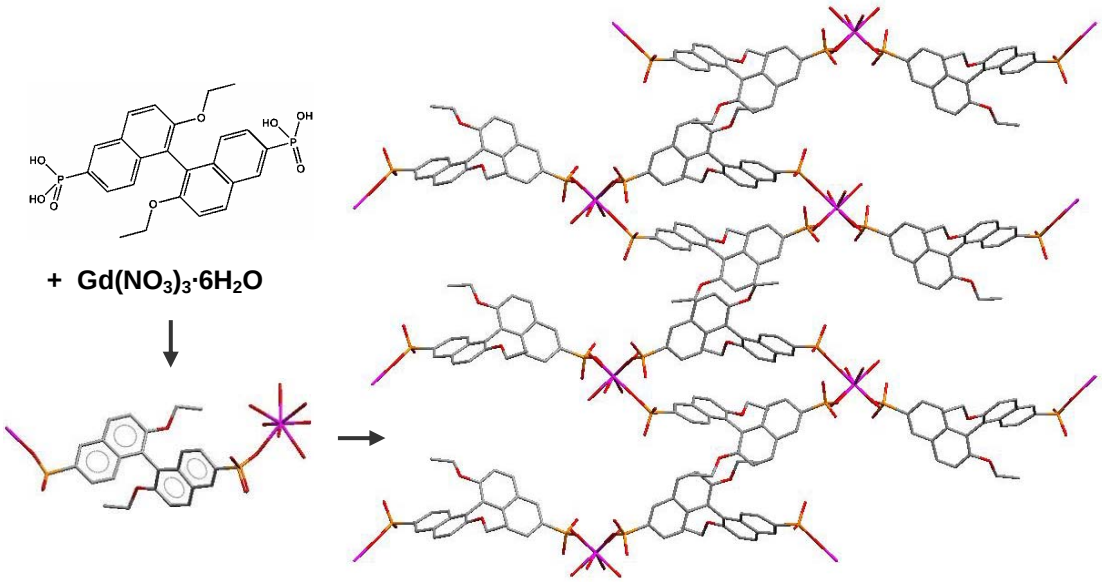

Figure 1-4. Phosphonate MOF (right) consisting of 2,2'-diethoxy-1,1'-binaphthalene-6,6'-bisphosphonic acid and $Gd(NO_3)_3 \cdot 6H_2O$ (left). Hydrogen atoms and solvent molecules have been omitted for clarity.

1.3. Metalloligands in MOFs

Despite the potential advantages of MOFs over traditional zeolites, complete exploitation of their metal ions has not been achieved because the metal ions or metal clusters in most MOFs generally serve a structural role. Therefore, efforts have been

made to integrate a second metal ion into the organic building block, thereby generating what is termed a ‘metalloligand’. Traditionally when a new metal ion is incorporated in a zeolite, it is not found to be evenly dispersed throughout the material.[41] One advantage of introducing a metal ion into the building block is upon formation of the MOF, the metal is covalently linked, evenly spaced, and accessible through pores or channels in the framework. For example, cadmium(II) has been coordinated with 4,4'-bipyridine and pyrazine which then were used in the preparation of the silver-containing MOFs $[Cd(bpy)_2(Ag(CN)_2)_2]$ and $[Cd(pyrz)(Ag(CN)_2)]$.[42, 43] However, this is an example of where adding a second metal center did not significantly enhance the physical properties of the framework. In contrast, the addition of a ‘functional’ metal center that provides useful physical, magnetic, or optical properties may greatly increase the potential utility of MOFs.

Among the most widely studied metalloligands are the metalloporphyrins. Metalloporphyrins have been linked through the *meso*-position to form frameworks via metal-ligand coordination bonding. Two- and three-dimensional arrays of metal and metal-free porphyrins have been synthesized using linking metal ions such as copper(I), zinc(II), cadmium(II), lead(II), palladium(II), and silver(I).[44-47] Metalloporphryins used for the preparation of MOFs have contained a variety of unsaturated open metal centers such as zinc(II), copper(II), and nickel(II). One disadvantage of using certain types of coordinating ligands such as pyridine is they can coordinate very well to a corresponding porphyrin metal center rather then the desired secondary metal ion or cluster.[48-50] Many porphyrin-based MOFs result in

fully saturated or partially saturated porphyrin metal centers due to the coordinating ligand. For example, Zn(5,10,15,20-Tetra(4-pyridyl)porphyrin) has been used as the building block of a silver-based MOF (Figure 1-5).[51] Upon formation of a framework, the zinc core became partially saturated by one pyridine ligand. Despite the coordination of the ligand to the porphyrin metal, it is still open to the binding of a second axial ligand, which could be useful for catalytic applications.

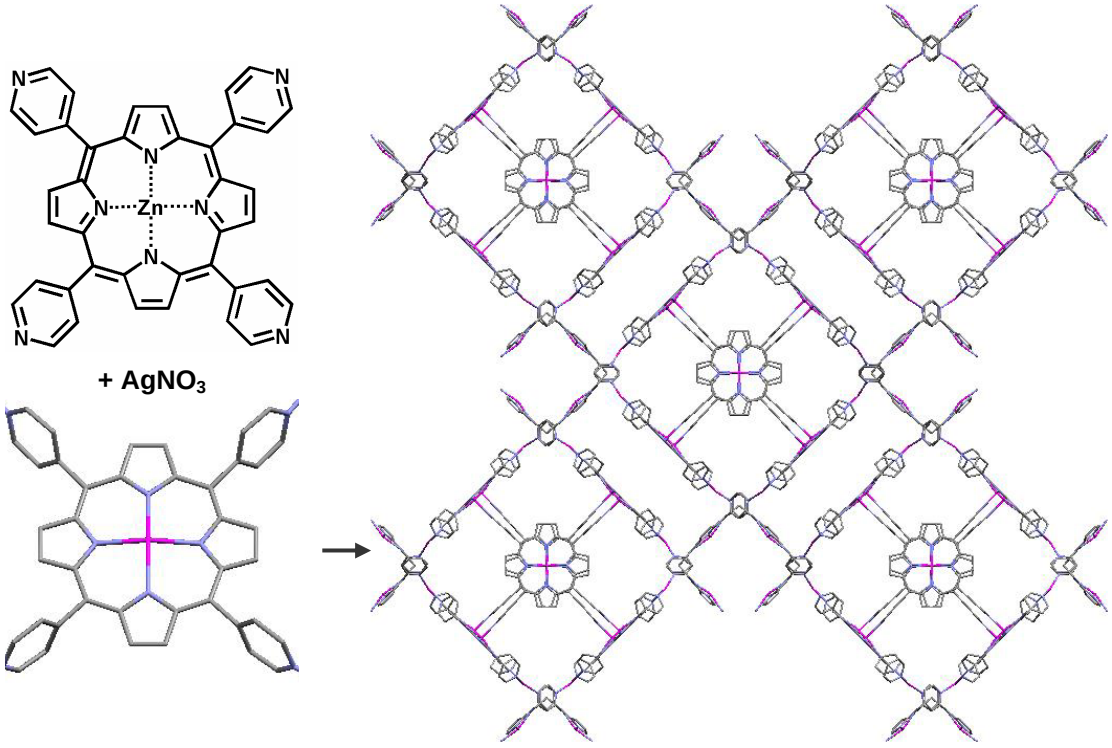

Figure 1-5. $[Ag_8(ZnTPyP)_7(H_2O)_2](NO_3)_8$ MOF (right) consisting of zinc 5,10,15,20-tetra(4-pyridyl)porphyrin and silver(I) nitrate (left). Hydrogen atoms and counter ions have been omitted for clarity.

Other metalloligands have been able to overcome the problem of self saturation. For example a metal *N*,*N*′-phenylenebis(salicylideneimine)dicarboxylate

(salphdc) metalloligand, decorated with carboxylate groups, has been reacted with zinc(II) nitrate to form an MOF containing zinc clusters similar to the carboxylate frameworks described earlier (Figure 1-6).[52] Unlike Zn(5,10,15,20-Tetra(4-pyridyl)porphyrin), the metal ion did not bind to the carboxylate ligands. Metal salicylidene-ethylenediamine (salen) complexes have been used extensively for catalysis and other biological applications.[53, 54] As anticipated, the framework contained large pores where the salen complex can be easily accessed; thus the material may be useful for chemisorption and catalytic applications.

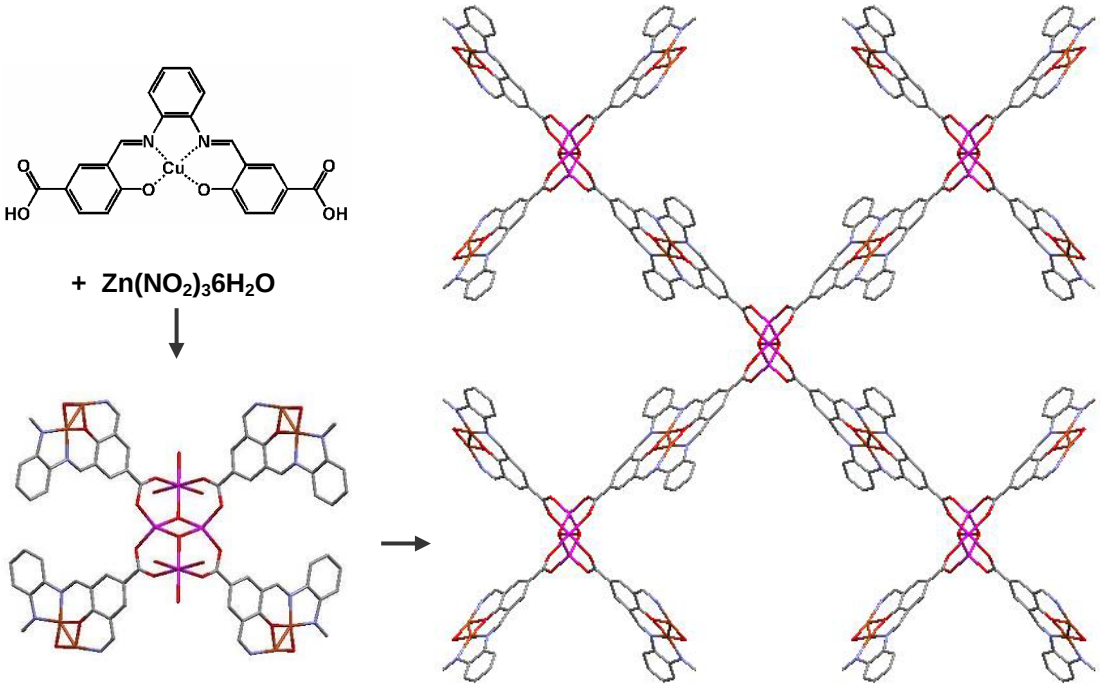

Figure 1-6. Salen MOF (right) comprised of M(salphdc) (M = Cu(II), Ni(II), and Co(II)) and $Zn(NO_2)_3 \cdot 6H_2O$ (top left), which generates octahedrally symmetric $Zn_4O(CO_2)_6$ clusters (bottom left). Hydrogen atoms and solvent molecules have been omitted for clarity.

Another class of metalloligands have been prepared from metal oxalate compounds.[55] Homo- and bimetallic MOFs have been obtained for a wide variety of metals such as nickel(II), iron(II), cobalt(II), zinc(II), manganese(II), and chromium(III). One preparation results in a two-dimensional honeycomb net containing iron(III) and manganese(II) (Figure 1-7).[56] Chiral three-dimensional frameworks have also been obtained from these metalloligands.[57] Metal oxalate MOFs have shown potential for a broad range of magnetic applications because the frameworks can exhibit either ferromagnetic or antiferromagnetic coupling.[56, 58] Finally, some oxalate-based MOFs have also shown to undergo cation exchange.[59] Oxalate building blocks can be disadvantageous because they have limited substitution capabilities, rendering it difficult to tune the physical and chemical attributes or add functionality. There are also certain types of topologies that cannot be achieved.

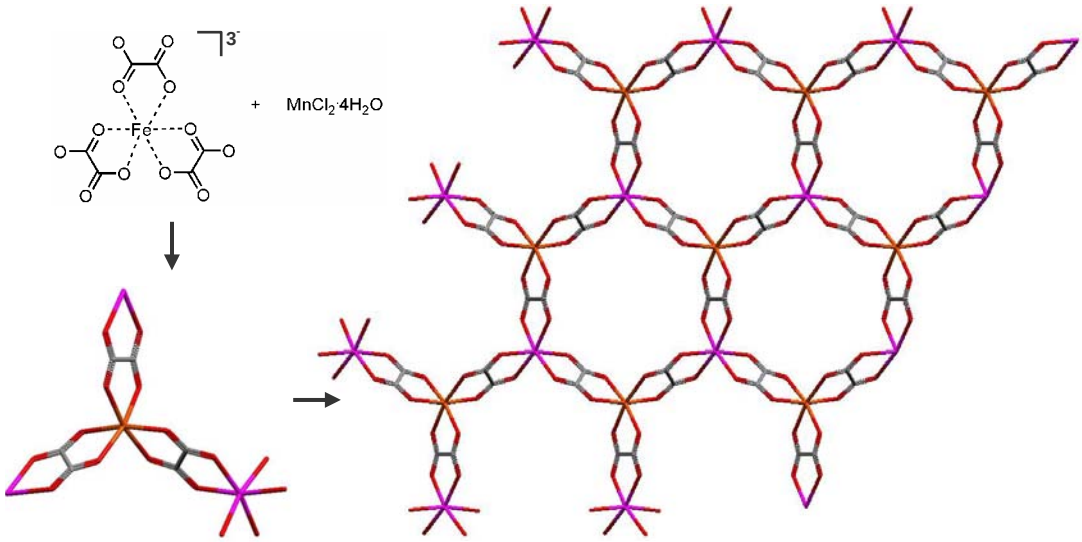

Figure 1-7. $[N(n\text{-}C_4H_9)_4][Mn^{II}Fe^{III}(C_2O_4)_3]$ MOF (right) comprised of $Fe(C_2O_4)_3$ and $MnCl_2{\cdot}4H_2O$ (left). Hydrogen atoms, solvent molecules, and templating cation have been removed for clarity.

1.4. Dipyrrin Complexes

The incorporation of dipyrrin metal complexes in MOFs has not been previously investigated. Dipyrrins are polypyrrolic aromatic bidentate ligands that can bind to a variety of metal ions. Some dipyrrin ligands have formed supramolecular dimers, trimers, and helical chains with metal ions such as zinc(II) and cobalt(II).[60-65] Almost all supramolecular dipyrrin structures reported to date contain α,β–substituted dipyrrins. While a variety of *meso*-substituted dipyrrin ligands have been reported,[66-68] few studies have utilized them for supramolecular structures.[69]

Meso-substituted dipyrrin ligands can be prepared on large scales and with a variety of functional groups appended.[66, 70] α,β–Unsaturated dipyrrin metal complexes have been prepared with iron(III), cobalt(III), nickel(II), copper(II), zinc(II), and palladium(II) (Scheme 1-1).[69, 71, 72] Four- and six-coordinate complexes can be prepared with a variety of coordination geometries including square planar, tetrahedral, and octahedral. Most dipyrrin metal complexes are charge neutral, highly crystalline, can be purified by standard chromatography methods, and are soluble in a variety of organic solvents such as chloroform, acetonitrile, and benzene.

Scheme 1-1. Synthesis of dipyrrin metal complexes from 5-phenyldipyrromethene.

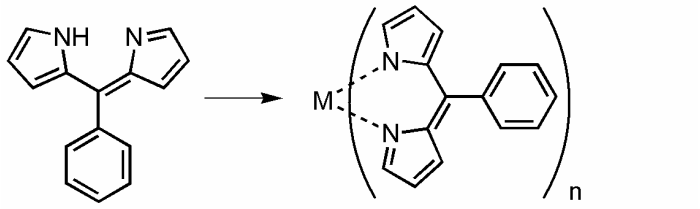

n = 3 M = Co(III), Fe(III)
n = 2 M = Cu(II), Ni(II), Zn(II), Pd(II)

The structure, symmetry, and absence of charge of dipyrrin metal complexes make them suitable as metalloligand analogs of organic building blocks already used in well established MOF systems (Figure 1-8). We can prepare a large variety of dipyrrin metal complexes and incorporate them into supramolecular structures such as MOFs. The advantage of incorporating dipyrrin metalloligands into MOFs is that they can be used to introduce new optical and physical properties not achievable with the corresponding organic building blocks.

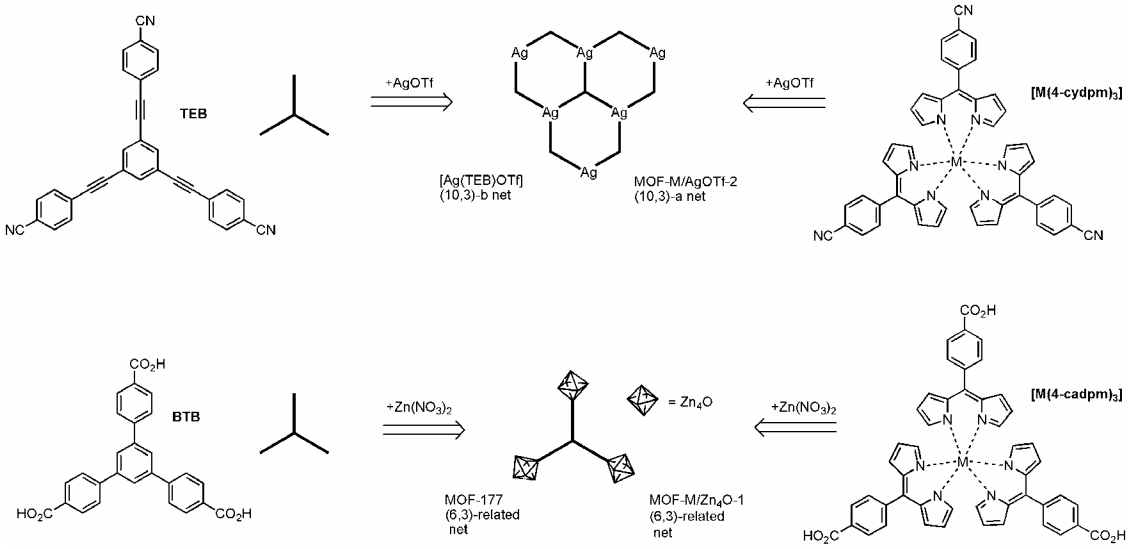

Figure 1-8. The organic building blocks TEB and BTB (left) used to create the MOFs [TEB·AgOTf] and MOF-177 (middle) and the dipyrrin complexes [M(4-cydpm)$_3$] and [M(4-cadpm)$_3$] (M = Co(III) and Fe(III)) (right) which can mimic the organic building blocks to create MOFs.

Dipyrrin complexes of zinc(II), copper(II), palladium(II) and nickel(II) form linear two-fold symmetric building blocks while cobalt(III) and iron(III) form three-fold symmetric building blocks. Square planar bis-chelate metal dipyrrin complexes

contain unsaturated metal centers, which if incorporated into MOFs, could be useful for applications such as catalysis and chemosensing. Tris–chelate metal complexes such as cobalt(III) or iron(III) dipyrrins are inherently chiral, therefore chiral MOFs may be obtained from these building blocks. Chiral MOFs could be very useful for performing chiral catalysis or enantiomeric separation.[73]

In addition to using dipyrrin building blocks to create unsaturated metal or chiral MOFs, fluorescent MOFs based on metal dipyrrin complexes may also be possible. Fluorescent MOFs may be useful as sensors. Boron-dipyrrin (BODIPY) complexes are highly fluorescent and have been studied extensively for a biological applications.[74-76] BODIPY derivatives would be difficult to incorporate in to supramolecular structures because a multitopic ligand cannot be prepared. Metal dipyrrin complexes are strong chromophores, and while most metal dipyrrin complexes are non-emissive, zinc(II) dipyrrins have been shown to be fluorescent.[69, 77] Other fluorescent dipyrrin complexes have not been explored but may be possible.

In addition to introducing new chemical properties, the dipyrrin building block can easily be altered to change the topology or functionality of the MOF. One of the goals in designing an MOF is to create pores or channels of a specific size. The dipyrrin building block can be lengthened with chemical groups such as phenylacetylene spacers to enlarge the building block, which could also enlarge the pore or channel size of the framework (depending on the interpenetration of the resulting framework). Another goal in designing MOFs is to incorporate certain functional attributes in the framework. Functional groups can easily be appended to

the dipyrrin ligand before introduction into the MOFs in order to alter or change the chemical environment within the framework. Despite the facile synthetic preparation of modified building blocks, it can be difficult to fully predict how certain physical characteristics of the frameworks will behave. Porosity may be undermined by interpenetration, or a functional group may interfere with the formation of a framework. Regardless, MOFs are usually prepared then the topology is identified, because in many cases, the actual topology is different from the expected topology.[78]

Dipyrrin metalloligands were chosen to reproduce several silver-containing MOFs.[20-25] Silver-containing MOFs have been shown to be easy to prepare from a one-step synthesis of the organic building block and silver(I) salt without the need for hydrothermal conditions, are robust to thermal changes, and have been extensively developed for applications such as solvent storage and exchange. Synthetically, a variety of different solvent conditions can be employed to produce crystals, and the topology can be structurally determined by X-ray diffraction.

Metal-organic frameworks containing metal dipyrrin complexes and silver(I) salts will be prepared and studied in great detail. Focus has been placed on tris-chelate metal complexes because they more closely mimic the three-fold organic ligands such as TEB[22] and BTB[17] and because the tris-chelate complexes contain a chiral metal center. The series of frameworks can be characterized and studied for their porosity, anion templating effect, and anion exchange properties.

Limited work has been done to study simple *meso*-substituted dipyrrin metal complexes for their use in supramolecular systems; therefore dipyrrin ligands and

metal complexes will also be prepared and studied in detail. In the preparation of MOFs, new α-substituted dipyrrin ligands were identified and their metal-coordination will be explored. Also in the preparation of MOFs, a wide variety of supramolecular structures have emerged, ranging from one-dimensional coordination polymers to discrete supramolecular hexagons. These materials may also hold promise for the development of advanced materials.

1.5. References

[1] *Comprehensive Supramolecular Chemistry, Vol. 6*, Elsevier, Oxford, **1996**.

[2] D. C. Sherrington, K. A. Taskinen, *Chem. Soc. Rev.* **2001**, *30*, 83.

[3] M. R. Ghadiri, J. R. Granja, R. A. Milligan, D. E. McRee, N. Khazanovich, *Nature* **1993**, *366*, 324.

[4] T. Amaya, J. J. Rebek, *J. Am. Chem. Soc.* **2004**, *126*, 14149.

[5] D. B. Amabilino, J. F. Stoddart, *Chem. Rev.* **1995**, *95*, 2727.

[6] D. Philip, J. F. Stoddart, *Angew. Chem. Int. Ed.* **1996**, *35*, 1154.

[7] O. R. Evans, W. Lin, *Acc. Chem. Res.* **2002**, *35*, 511.

[8] M. Oh, G. B. Carpenter, D. A. Sweigart, *Acc. Chem. Res.* **2004**, *37*, 1.

[9] O. Maury, H. L. Bozec, *Acc. Chem. Res.* **2005**, asap article.

[10] B. Moulton, M. J. Zaworotko, *Chem. Rev.* **2001**, *101*, 1629.

[11] S. Kitagawa, R. Kitaura, S.-i. Noro, *Angew. Chem. Int. Ed.* **2004**, *43*, 2334.

[12] O. M. Yaghi, H. Li, C. Davis, D. Richardson, T. L. Groy, *Acc. Chem. Res.* **1998**, *31*, 474.

[13] M. Eddaoudi, D. B. Moler, H. Li, B. Chen, T. M. Reineke, M. O'Keeffe, O. M. Yaghi, *Acc. Chem. Res.* **2001**, *34*, 319.

[14] N. L. Rosi, J. Kim, M. Eddaoudi, B. Chen, M. O'Keeffe, O. M. Yaghi, *J. Am. Chem. Soc.* **2005**, *127*, 1504.

[15] M. Eddaoudi, J. Kim, N. Rosi, D. Vodak, J. Wachter, M. O'Keeffe, O. M. Yaghi, *Science* **2002**, *295*, 469.

[16] N. L. Rosi, J. Eckert, M. Eddaoudi, D. Vodak, J. Kim, M. O'Keeffe, O. M. Yaghi, *Science* **2003**, *300*, 1127.

[17] H. K. Chae, D. Y. Siberio-Pérez, J. Kim, Y. Go, M. Eddaoudi, A. J. Matzger, M. O'Keeffe, O. M. Yaghi, *Nature* **2004**, *427*, 523.

[18] O. M. Yaghi, H. L. Li, *J. Am. Chem. Soc.* **1996**, *118*, 295.

[19] K. S. Min, M. P. Suh, *J. Am. Chem. Soc.* **2000**, *122*, 6834.

[20] D. Venkataraman, S. Lee, J. S. Moore, P. Zhang, K. A. Hirsch, G. B. Gardner, A. C. Covey, C. L. Prentice, *Chem. Mater.* **1996**, *8*, 2030.

[21] B. Chen, S. Lee, D. Venkataraman, F. J. DiSalvo, E. B. Lobkovsky, M. Nakayama, *Cryst. Growth Des.* **2001**, *2*, 101.

[22] G. B. Gardner, D. Venkataraman, J. S. Moore, S. Lee, *Nature* **1995**, *374*, 792.

[23] D. Venkataraman, G. B. Gardner, S. Lee, J. S. Moore, *J. Am. Chem. Soc.* **1995**, *117*, 11600.

[24] G. B. Gardner, Y.-H. Kiang, S. Lee, A. Asgaonkar, D. Venkataraman, *J. Am. Chem. Soc.* **1996**, *118*, 6946.

[25] Y.-H. Kiang, G. B. Gardner, S. Lee, Z. Xu, E. B. Lobkovsky, *J. Am. Chem. Soc.* **1999**, *121*, 8204.

[26] X.-H. Bu, W. Chen, M. Du, K. Biradha, W.-Z. Wang, R.-H. Zhang, *Inorg. Chem.* **2002**, *41*, 437.

[27] O.-S. Jung, Y. J. Kim, Y.-A. Lee, H. K. Chae, H. G. Jang, J. Hong, *Inorg. Chem.* **2001**, *40*, 2105.

[28] L. Carlucci, G. Ciani, D. W. v. Gudenberg, D. M. Prosperio, *Inorg. Chem.* **1997**, *36*, 3812.

[29] O.-S. Jung, Y. J. Kim, Y.-A. Lee, J. K. Park, H. K. Chae, *J. Am. Chem. Soc.* **2000**, *122*, 9921.

[30] D. Whang, K. Kim, *J. Am. Chem. Soc.* **1997**, *119*, 451.

[31] O.-S. Jung, Y. J. Kim, Y.-A. Lee, K.-M. Park, S. S. Lee, *Inorg. Chem.* **2003**, *42*, 844.

[32] C. L. Schauer, E. Matwey, F. W. Fowler, J. W. Lauher, *J. Am. Chem. Soc.* **1997**, *119*.

[33] P. Lin, R. A. Henderson, R. W. Harrington, W. Clegg, C.-D. Wu, X.-T. Wu, *Inorg. Chem.* **2004**, *43*, 181.

[34] Y.-B. Dong, J.-P. Ma, R.-Q. Huang, M. D. Smith, H.-C. zur Loye, *Inorg. Chem.* **2003**, *42*, 294.

[35] C.-L. Chen, C.-Y. Su, Y.-P. Cai, H.-X. Zhang, A.-W. Xu, B.-S. Kang, H.-C. zur Loye, *Inorg. Chem.* **2003**, *42*, 3738.

[36] Y. Cui, J. Lee, W. Lin, *J. Am. Chem. Soc.* **2003**, *125*, 6014.

[37] Y. Cui, O. R. Evans, H. L. Ngo, P. S. White, W. Lin, *Angew. Chem. Int. Ed.* **2002**, *41*, 1159.

[38] O. R. Evans, H. L. Ngo, W. Lin, *J. Am. Chem. Soc.* **2001**, *123*, 10395.

[39] H. L. Ngo, W. Lin, *J. Am. Chem. Soc.* **2002**, *124*, 14298.

[40] A. Hu, H. L. Ngo, W. Lin, *J. Am. Chem. Soc.* **2003**, *125*, 11490.

[41] P. A. Anderson, R. Armstrong, P. D. Barker, M. J. Edmondson, P. P. Edwards, A. Porch, *J. Chem. Soc., Dalton Trans.* **2004**, 3122.

[42] T. Soma, H. Yuge, T. Iwamoto, *Angew. Chem. Int. Ed.* **1994**, *33*, 1665.

[43] T. Soma, T. Iwamoto, *Acta. Crystallogr. Sect. C* **1996**, *52*, 1200.

[44] C. V. K. Sharma, G. A. Broker, J. G. Huddleston, J. W. Baldwin, R. M. Metzger, R. D. Rogers, *J. Am. Chem. Soc.* **1999**, *121*, 1137.

[45] T. N. Milic, N. Chi, D. G. Yablon, G. W. Flynn, J. D. Batteas, C. M. Drain, *Angew. Chem. Int. Ed.* **2002**, *41*, 2117.

[46] B. F. Abrahams, B. F. Hoskins, D. M. Michail, R. Robson, *Nature* **1994**, *369*, 727.

[47] D. Hagrman, P. J. Hagrman, J. Zubieta, *Angew. Chem. Int. Ed.* **1999**, *38*, 3165.

[48] K.-J. Lin, *Angew. Chem. Int. Ed.* **1999**, *38*, 2730.

[49] Y. Diskin-Posner, G. K. Patra, I. Goldberg, *J. Chem. Soc., Dalton Trans.* **2001**, *19*, 2775.

[50] L. Pan, S. Kelly, X. Huang, J. Li, *Chem. Commun.* **2002**, *20*, 2334.

[51] L. Carlucci, G. Ciani, D. M. Prosperio, F. Porta, *Angew. Chem. Int. Ed.* **2003**, *42*, 317.

[52] R. Kitaura, G. Onoyama, H. Sakamoto, R. Matsuda, S. Noro, S. Kitagawa, *Angew. Chem. Int. Ed.* **2004**, *43*, 2684.

[53] W. Zhang, J. L. Loebach, S. R. Wilson, E. N. Jacobsen, *J. Am. Chem. Soc.* **1990**, *112*, 2801.

[54] C. F. Works, P. C. Ford, *J. Am. Chem. Soc.* **2000**, *122*, 7592.

[55] S. Decurtins, H. W. Schmalle, P. Schneuwly, J. Ensling, P. A. Gtlich, *J. Am. Chem. Soc.* **1994**, *116*, 9521.

[56] R. Pellaux, H. W. Schmalle, R. Huber, P. Fischer, T. Hauss, B. Ouladdiaf, S. Decurtins, *Inorg. Chem.* **1997**, *36*, 2301.

[57] V. M. Russell, D. C. Craig, M. L. Scudder, I. G. Dance, *CrystEngComm* **2000**, *3*, 16.

[58] C. Mathoniere, C. J. Nuttall, S. G. Carling, P. Day, *Inorg. Chem.* **1996**, *35*, 1201.

[59] S. Neeraj, A. N. Noy, E. Jeanneau, T. Bataille, S. Raite, D. Louer, *Solid State Sci.* **2004**, *6*, 579.

[60] J. M. Sutton, E. Rogerson, C. J. Wilson, A. E. Sparke, S. J. Archibald, R. W. Boyle, *Chem. Commun.* **2004**, 1328.

[61] Q. Chen, Y. Zhang, D. Dolphin, *Tetrahedron Lett.* **2002**, *43*, 8413.

[62] A. Thompson, S. J. Rettig, D. Dolphin, *Chem. Commun.* **1999**, 631.

[63] Y. Zhang, A. Thompson, S. J. Rettig, D. Dolphin, *J. Am. Chem. Soc.* **1998**, *120*, 13537.

[64] A. Thompson, D. Dolphin, *Org. Lett.* **2000**, *2*, 1316.

[65] T. E. Wood, N. D. Dalgleish, E. D. Power, A. Thompson, X. Chen, Y. Okamoto, *J. Am. Chem. Soc.* **2005**, *127*, 5740.

[66] J. K. Laha, S. Dhanalekshmi, M. Taniguchi, A. Ambroise, J. S. Lindsey, *Org. Process Res. Dev.* **2003**, *7*, 799.

[67] D. Gryko, J. S. Lindsey, *J. Org. Chem.* **2000**, *65*, 2249.

[68] C.-H. Lee, J. S. Lindsey, *Tetrahedron* **1994**, *50*, 11427.

[69] L. Yu, K. Muthukumaran, I. V. Sazanovich, C. Kirmaier, E. Hindin, J. R. Diers, P. D. Boyle, D. F. Bocian, D. Holten, J. S. Lindsey, *Inorg. Chem.* **2003**, *42*, 6629.

[70] B. J. Littler, M. A. Miller, C.-H. Hung, R. W. Wagner, D. F. O'Shea, P. D. Boyle, J. S. Lindsey, *J. Org. Chem.* **1999**, *64*, 1391.

[71] C. Brückner, V. Karunaratne, S. J. Rettig, D. Dolphin, *Can. J. Chem.* **1996**, *74*, 2182.

[72] C. Brückner, Y. Zhang, S. J. Rettig, D. Dolphin, *Inorg. Chim. Acta* **1997**, *263*, 279.

[73] J. S. Seo, D. Whang, H. Lee, S. I. Jun, J. Oh, Y. J. Jeon, K. Kim, *Nature* **2000**, *404*, 982.

[74] J. Karolin, L. B.-A. Johansson, L. Strandberg, T. Ny, *J. Am. Chem. Soc.* **1994**, *116*, 7801.

[75] F. Li, S. I. Yang, Y. Ciringh, J. Seth, C. H. Martin III, D. L. Singh, D. Kim, R. R. Birge, D. F. Bocian, D. Holten, J. S. Lindsey, *J. Am. Chem. Soc.* **1998**, *120*, 10001.

[76] Y. Gabe, Y. Urano, K. Kikuchi, H. Kojima, T. Nagano, *J. Am. Chem. Soc.* **2004**, *126*, 3357.

[77] I. V. Sazanovich, C. Kirmaier, E. Hindin, L. Yu, D. F. Bocian, J. S. Lindsey, D. Holten, *J. Am. Chem. Soc.* **2004**, *126*, 2664.

[78] N. W. Ockwig, O. Delgado-Friedrichs, M. O'Keeffe, O. M. Yaghi, *Acc. Chem. Res.* **2005**, *38*, 176.

II. Development of Dipyrrins for Supramolecular Chemistry

2.1. Introduction

α,β-Unsubstituted dipyrrins have the potential for incorporation into a variety of supramolecular systems. They are stable, aromatic chromophores that have been shown to bind to some transition metals.[1, 2] Despite extensive studies on α,β-unsubstituted dipyrrin ligands, there have been few studies on their metal complexes and their development in supramolecular chemistry.

Phenylacetylenes are rigid organic spacers often found in molecular building blocks for creating different sized structures in supramolecular chemistry[3] and in liquid-crystalline materials.[4, 5] For incorporation in supramolecular structures, large phenylacetylene dipyrrin ligands can be prepared and coordinated to transition metals (Figure 2-1). The ability to extend the *meso*-substituent of dipyrrin ligands would allow for the creation of larger dipyrrin building blocks and incorporation into supramolecular structures. No previous work has been reported on phenylacetylene dipyrrin metal complexes and limited work has been reported on long phenylacetylene metal complexes.[6]

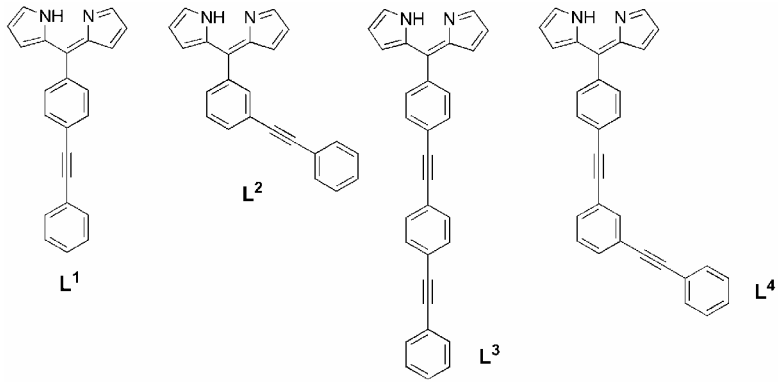

Figure 2-1. Diagram of the phenylacetylene dipyrrin ligands L^1, L^2, L^3, and L^4.

Fluorine–fluorine interactions of perfluoroarene complexes have been used to organize supramolecular structures.[7-9] In addition phenyl-perfluorophenyl interactions have also been used to drive the formation of interesting supramolecular structures.[7-9] Fluorinated arene compounds have exhibited liquid crystalline behavior.[10, 11] Perfluoroarene ligands have also been appended to porphyrin derivatives because of their electron withdrawing effect, which has shown to perturb the electronic nature of the porphyrin core.[12, 13] In light of these studies, perfluorophenyl dipyrrin ligands were prepared and coordinated with transition metals to form new fluorinated metal complexes.

2.2. Results and Discussion

2.2.1. Phenylacetylene Dipyrrins

The preparation of the first phenylacetylene dipyrrin ligand L^1 began with the Sonogashira coupling of 4-bromobenzaldehyde and phenylacetylene, followed by condensation with pyrrole, and oxidation with 2,3-dicloro-5,6-dicyanobenzoquinone (DDQ) (Scheme 2-1). The dipyrromethene is combined with iron(III) and copper(II) salts to form the dipyrrin metal complexes $[Fe(L^1)_3]$ and $[Cu(L^1)_2]$, respectively. The metal complexes are purified by column chromatography and characterized by mass spectrometry, electronic absorption, and infrared spectroscopy.

Scheme 2-1. Synthesis of L^1.

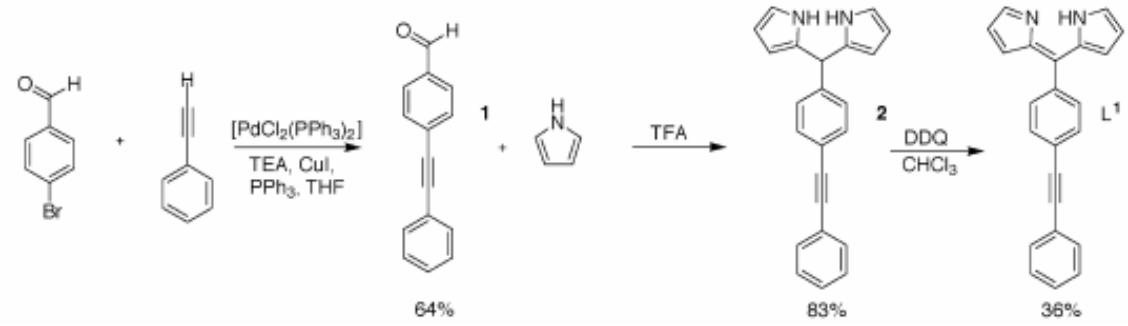

The iron(III) and copper(II) dipyrrin complexes $[Fe(L^1)_3]$ and $[Cu(L^1)_2]$ were characterized by X-ray diffraction (Figure 2-2). $[Fe(L^1)_3]$ exhibits a six-coordinate octahedral metal center with three dipyrrin ligands and Fe–N bond distances of 1.96 Å. The *meso*-phenyl group is rotated ~73º from the dipyrrin moiety and the second phenyl group is rotated ~50º from the *meso*-phenyl group. The crystal structure reveals a highly symmetric metal complex, which may prove useful in the formation of supramolecular structures and molecular solids.

$[Cu(L^1)_2]$ exhibits a four-coordinate distorted square planar geometry with two dipyrrin ligands and Cu–N bond distances of 1.94-1.95 Å. The *meso*-phenyl group is rotated ~55º from the dipyrrin moiety; however, the two phenyl groups are relatively planar with respect to each other.

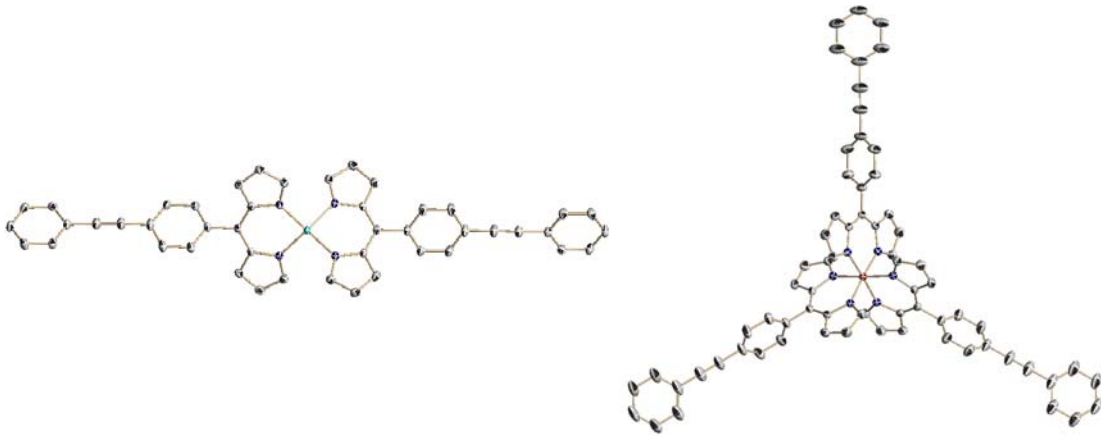

Figure 2-2. Structural diagram of $[Cu(L^1)_2]$ (left) and $[Fe(L^1)_3]$ (right) (ORTEP, 50% probability ellipsoids). Hydrogen atoms and solvent molecules have been omitted for clarity.

Because dipyrromethenes have been shown to be difficult to isolate prior to the synthesis of the metal complexes, a new procedure was desired to isolate the dipyrromethenes for characterization purposes. As stated, the metal complexes could easily be purified by column chromatography. De-metallization of the metal complexes was one possible route for the isolation of the dipyrrin ligands. The first attempt involved the addition of hydrochloric acid to the copper(II) complex. The metal was removed but the metal complex partially formed again when the ligand was isolated. De-metallization of various supramolecular metal complexes has been performed using potassium cyanide.[14] The addition of potassium cyanide proved much more successful, as the copper(II) ion was readily removed from $[Cu(L^1)_2]$ as could be seen by a solution color change from red to orange. The dipyrromethene was then extracted with methylene chloride and washed with water to remove the copper(II) and potassium cyanide by-products. The ligand L^1 was isolated in a moderate yield (57%) and no further purification was required. Later reactions

involving other types of dipyrrin ligands and identical reaction conditions would prove to be higher yielding (80-100%). This procedure has proven to be useful when the purified dipyrromethene is required for the synthesis of some dipyrrin metal complexes.

In order to explore various ligand geometries, a second phenylacetylene dipyrrin ligand L^2 (Figure 2-1) was also synthesized following a similar synthetic procedure to L^1. Iron(III) and copper(II) dipyrrin complexes $[Fe(L^2)_3]$ and $[Cu(L^2)_2]$ were prepared and isolated. The metal complexes show very interesting solubility properties, not only dissolving in common organic solvents such as benzene, methylene chloride, and chloroform, but also dissolving in more polar solvents such as acetone, methanol, and ethanol. The metal complexes formed with L^1 did not dissolve in the latter solvents. Suitable single crystals of $[Fe(L^2)_3]$ and $[Cu(L^2)_2]$ could not be obtained for X-ray diffraction analysis.

2.2.2. Extended Phenylacetylene Dipyrrins

To further explore the extension of dipyrrin ligands, an additional phenylacetylene group was appended to the L^1 ligand in two independent positions to obtain the ligands L^3 and L^4 (Figure 2-1). L^3 was obtained from the Sonogashira coupling of 4-(ethynyl)benzaldehyde with 1,4-diiodobenzene followed by a second Sonogashira coupling with phenylacetylene (Scheme 2-2). The iron(III) and copper(II) dipyrrin complexes $[Fe(L^3)_3]$ and $[Cu(L^3)_2]$ were prepared. The ligand and metal complexes did prove to be more challenging to prepare and handle due to

limited solubility; however, the materials could still be purified by column chromatography using common organic solvents.

Scheme 2-2. Synthesis of L^3.

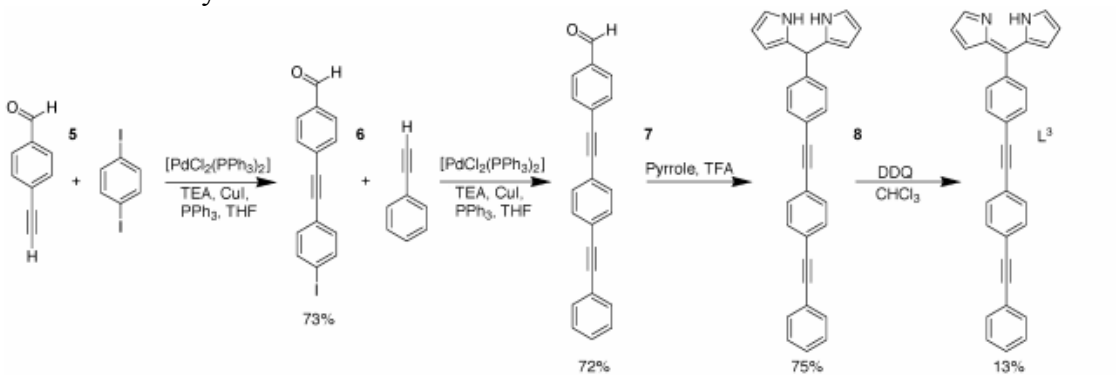

Thin plates of $[Fe(L^3)_3]$ were obtained and characterized by single crystal X-ray diffraction (Figure 2-10). The X-ray structure reveals a six-coordinate iron(III) center with three dipyrrin ligands. The Fe–N bond distances range from 1.93-1.99 Å. From the iron(III) center to the farthest hydrogen of the terminal phenyl group is ~22 Å. The structure appears to be bent along the phenylacetylene backbone (Figure 2-3). Single crystals could not be obtained for $[Cu(L^3)_2]$. In addition, the copper(II) complex became very difficult to redissolve in all solvents once it was isolated as a solid. This is probably due to interligand π–π stacking and subsequent aggregation.

Figure 2-3. Structural diagram of one $[Fe(L^3)_3]$ ligand showing the notable bending of the phenylacetylene portion of the ligand (ORTEP, 50% probability ellipsoids). Hydrogen atoms and solvent molecules have been omitted for clarity.

Extended phenylacetylene systems[15-17] and boron-dipyrrin compounds[18, 19] have been used in light-harvesting systems. Therefore, the ligands and metal complexes of the extended phenylacetylene system L^3 were measured for their fluorescent properties (Figure 2-4). The strongest fluorescent dipyrrin compound prepared is the dipyrromethane **8**, which emits at 352 and 368 nm with a smaller broad emission at 460 nm. The oxidized dipyrromethene L^3 is relatively non-fluorescent, probably due to quenching by the dipyrrin moiety. The metal complexes $[Fe(L^3)_3]$ and $[Cu(L^3)_2]$ are also non-florescent. While dipyrrins without any *meso*-substitution have been shown to be highly fluorescent, all *meso*-substituted dipyrrins studied here are non-fluorescent. All other dipyrrin ligands L^1, L^2, and L^4, and metal complexes formed are relatively non-fluorescent. While the iron(III) and copper(II) metal complexes are non-fluorescent, as has been seen with most dipyrrin metal complexes, zinc(II) dipyrrin complexes have shown to be fluorescent.[20]

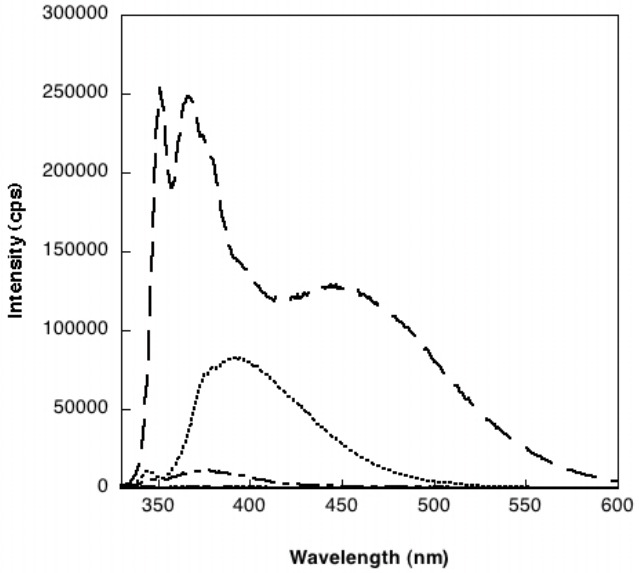

Figure 2-4. Fluorescence spectra for compounds **7** (····), **8** (---), L^3 (·–·–), $[Fe(L^3)_3]$ (——, no significant emission), and $[Cu(L^3)_2]$ (——, no significant emission).

Finally, iron(III) and copper(II) dipyrrin complexes were prepared from the extended ligand L^4. The solubility of $[Fe(L^4)_3]$ and $[Cu(L^4)_2]$ is much higher than the metal complexes of L^3. The solubility is very similar to the other metal complexes formed with the bent ligand L^2, dissolving in common organic solvents and polar solvents such as methanol. Also like the metal complexes formed with L^2, $[Fe(L^4)_3]$ and $[Cu(L^4)_2]$ could not be crystallized for X-ray diffraction analysis.

2.2.3. Electronic Absorption Spectra

All iron(III) and copper(II) dipyrrin complexes form red solutions when dissolved in organic solvents, but are dichroic red/green solids upon crystallization. All the iron(III) complexes $[Fe(L^1)_3]$, $[Fe(L^2)_3]$, $[Fe(L^3)_3]$, and $[Fe(L^4)_3]$ were analyzed by electronic absorption spectroscopy (Figure 2-5). As expected, all complexes

display metal–ligand charge transfer bands at 444 and 490 nm.[1] The features are independent of the *meso*-ligand substitution. The ligands all exhibit π–π* transitions in the range of 280-350 nm. The extended phenylacetylene metal complexes prepared from L^3 and L^4 include the addition of more intense π–π* transitions from the extended phenylacetylene ligand between 260-400 nm.[17]

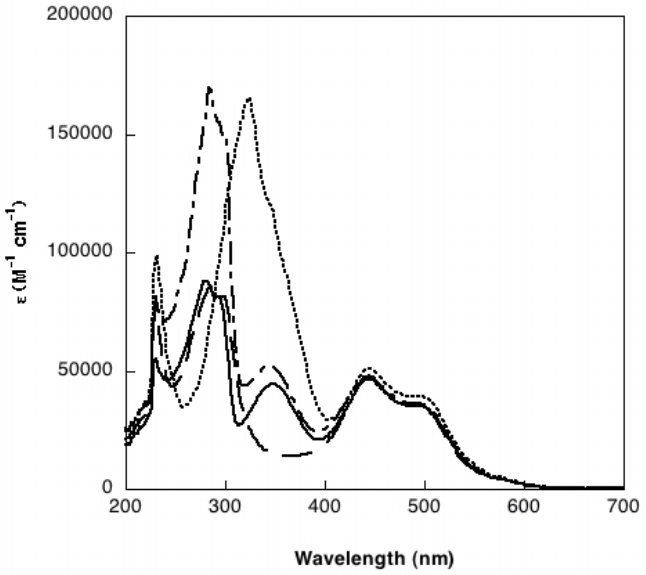

Figure 2-5. Electronic absorption spectra for iron(III) dipyrrin complexes $[Fe(L^1)_3]$ (——), $[Fe(L^2)_3]$ (---), $[Fe(L^3)_3]$ (····), and $[Fe(L^4)_3]$ (·–·–).

All the copper(II) complexes $[Cu(L^1)_2]$, $[Cu(L^2)_2]$, $[Cu(L^3)_2]$, and $[Cu(L^4)_2]$ were also analyzed by electronic absorption spectroscopy (Figure 2-6). All complexes display metal–ligand charge transfer bands at 468 and 500 nm.[2] Once again the ligands exhibit π–π* transitions in the range of 280-350 nm, and the extended phenylacetylene metal complexes prepared from L^3 and L^4 exhibit more intense π–π* transitions at 260-400 nm.

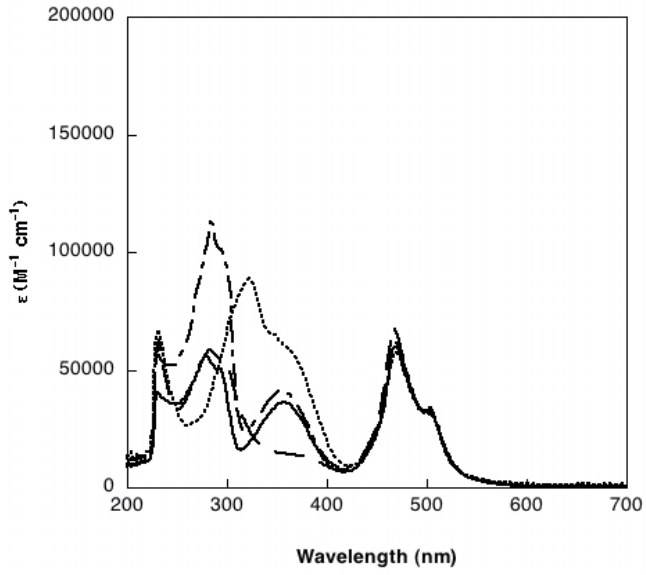

Figure 2-6. Electronic absorption spectra for copper(II) dipyrrin complexes $[Cu(L^1)_2]$ (——), $[Cu(L^2)_2]$ (---), $[Cu(L^3)_2]$ (····), and $[Cu(L^4)_2]$ (·–·–).

2.2.4. Fluorinated Dipyrrins

As stated earlier, fluorine–fluorine interactions of perfluoroarene complexes have been used to form supramolecular structures. Fluorinated dipyrrins could be useful for incorporation in to supramolecular structures. In addition, fluorinated dipyrrins make the dipyrrin moiety more stable because of the substituted electron withdrawing groups in the *meso*-position.[21]

The synthesis of the perfluorophenyl iron(III) dipyrrin complex was previously reported; however, no crystal structure was given.[21] The iron(III) dipyrrin complex, renamed $[Fe(phFdpm)_3]$, was prepared (Scheme 2-3) and crystallized (Figure 2-11). The octahedral iron(III) center has Fe–N bond distances of 1.95-1.98 Å. There are many F–F interactions at 3.0-3.4 Å. In addition, the cobalt(III) complex $[Co(phFdpm)_3]$ was also prepared and crystallized (Figure 2-12). The Co–N bond

distance is slightly shorter compared to other cobalt(III) dipyrrin complexes at 1.93-1.94 Å. There are also many F–F interactions at 3.0-3.4 Å.

Scheme 2-3. Synthesis of $[M(phFdpm)_3]$ (M = Co(III), Fe(III)).

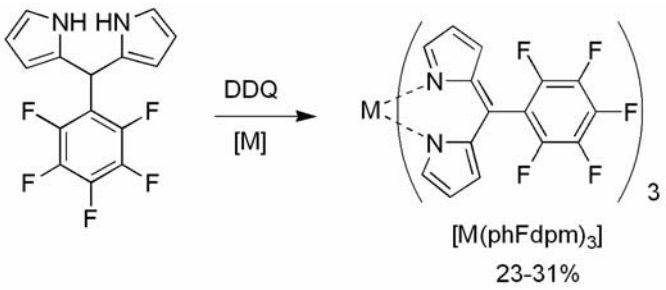

Both complexes were once again analyzed by electronic absorption spectroscopy. The iron(III) complex exhibits bands at 228 298, 451, and 500 (shoulder) nm, while the cobalt(III) complex exhibits bands at 301, 408, 477, and 517 nm. The more intense iron(III) and cobalt(III) metal-ligand charge transfer bands at 451 nm and 477 nm, respectively, are red-shifted 7 nm and 10 nm compared to the unfluorinated counterparts. The less intense metal-ligand charge transfer bands at 500 nm and 517 nm, respectively, exhibit an even bigger red-shift.

2.2.5. Extended Fluorinated Dipyrrins

To utilize both the phenylacetylene spacers and the perfluorophenyl groups of the previous dipyrrins, a new ligand L^5 and metal complex $[Fe(L^5)_3]$ were prepared (Scheme 2-4). Once again the synthesis involved the Sonogashira coupling of 4-

ethynylbenzaldehyde and iodopentafluorobenzene, condensation with pyrrole, oxidation with DDQ, and metal complexation with $FeCl_3 \cdot 6H_2O$.

Scheme 2-4. Synthesis of $[Fe(L^5)_3]$.

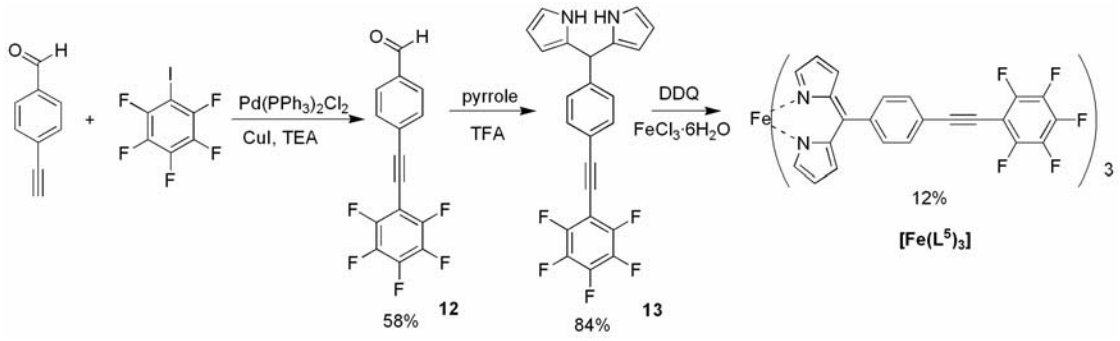

$[Fe(L^5)_3]$ exhibits electronic absorbance features similar to the previous unfluorinated iron(III) dipyrrin complexes, with transitions at 444 and 492 nm. Crystals of $[Fe(L^5)_3]$ were also analyzed by X-ray diffraction (Figure 2-13). The iron(III) center is six-coordinate with three dipyrrin ligands and Fe–N bond distances of 1.95-1.99 Å. Compared to the extended phenylacetylene complex $[Fe(L^3)_3]$, some of the ligands of $[Fe(L^5)_3]$ are bent rather then linear (Figure 2-7). There are many F–F interactions of corresponding perfluorophenyl groups at 3.0-3.4 Å. It appears as though the F–F interactions aggregate such that the perfluorophenyl ligands create fluorinated channels throughout the packing structure (Figure 2-14).

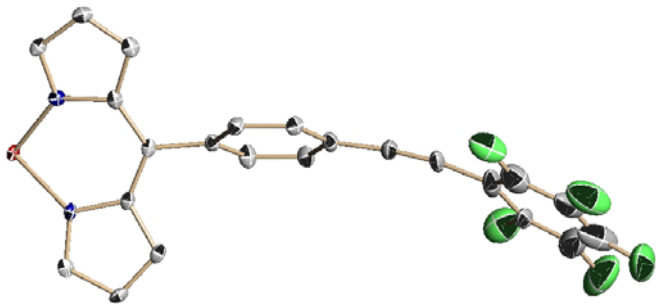

Figure 2-7. Structural diagram of one $[Fe(L^5)_3]$ ligand showing the notable bending of the ligand (ORTEP, 50% probability ellipsoids). Solvent molecules have been omitted for clarity.

2.2.6. Electrochemistry of Iron(III) Dipyrrins

Knowing the electrochemical behavior of the iron(III) dipyrrin complexes will be helpful for the incorporation of these complexes as building blocks for supramolecular structures. The electrochemical behavior of the iron(III) dipyrrin complexes $[Fe(L^1)_3]$, $[Fe(L^2)_3]$, $[Fe(L^3)_3]$, and $[Fe(L^4)_3]$ was examined by cyclic voltammetry. The complexes display quasireversible redox couples centered around -1.152 V (-0.692 V vs. SCE) with an average ΔE_p of 0.119 V (Table 2-1). The phenylacetylene moiety does not appear to significantly contribute to the electrochemical behavior of the metal center.

Table 2-1. Electrochemical data for $[Fe(L^1)_3]$, $[Fe(L^2)_3]$, $[Fe(L^3)_3]$, and $[Fe(L^4)_3]$.

Compound	Potential vs. $Fc^{0/+}$ (V)	Potential vs. SCE (V)	ΔE_p (V)
$[Fe(L^1)_3]$	-1.156	-0.697	0.105
$[Fe(L^2)_3]$	-1.147	-0.687	0.086
$[Fe(L^3)_3]$	-1.155	-0.695	0.145
$[Fe(L^4)_3]$	-1.150	-0.690	0.140

2.3. Conclusions

α,β-Unsubstituted dipyrrin ligands and their metal complexes have shown to be easy to prepare from a variety of aldehydes. In addition, variable length phenylacetylene groups and perfluorophenyl groups can also be appended for incorporation into supramolecular structures. The packing of $[Co(phFdpm)_3]$, $[Fe(phFdpm)_3]$ and $[Fe(L^5)_3]$ also appear to be driven by the F–F interactions of the perfluorophenyl groups.

2.4. Experimental Section

General Procedures/Methods: Unless otherwise noted, starting materials were obtained from commercial suppliers and used without further purification. Pyrrole was freshly distilled. Mass spectrometry was performed either at the University of California, San Diego Mass Spectrometry Facility in the Department of Chemistry and Biochemistry, or at University of Arizona Mass Spectrometry Facility in the Department of Chemistry. A ThermoFinnigan LCQ-DECA mass spectrometer was used for the ESI or APCI analysis, and the data were analyzed using the Xcalibur software suite. A ThermoFinnigan MAT 900XL mass spectrometer was used to acquire the data for the high resolution mass spectra (HRMS). Elemental analysis was performed at the University of California, Berkeley Analytical Facility or NuMega Resonance Labs, Inc. San Diego, CA. Infrared spectra were collected on a Mattson Research Series FT-IR instrument (using KBr pellets or NaCl plates, laboratory of Prof. Clifford P. Kubiak) at the Department of Chemistry and Biochemistry,

University of California, San Diego. $^{1}H/^{13}C$NMR spectra were recorded on a Varian FT-NMR spectrometer running at 300 MHz, 400 MHz and 500 MHz at the Department of Chemistry and Biochemistry, University of California, San Diego. UV-visible spectra were recorded in CH_2Cl_2 using a Hewlett-Packard 4582A spectrophotometer under PC control using the ChemStation software suite or a Perkin-Elmer Lambda 25 spectrophotometer with the UVWinLab 4.2.0.0230 software package.

Complex Synthesis and Characterization:

4-(Phenylacetyl)benzaldehyde (1). A mixture of 4-bromobenzaldehyde (0.150 g, 0.81 mmol), phenylacetylene (0.331 g, 3.24 mmol), triethylamine (0.123 g, 1.22 mmol), $Pd(PPh_3)_2Cl_2$ (0.028 g, 0.04 mmol), triphenylphosphine (0.005 g, 0.02 mmol), CuI (0.002 g, 0.008 mmol), and 15 mL of dry THF was stirred under nitrogen for 24 h. The reaction mixture was diluted with 50 mL of CH_2Cl_2, was washed with 50 mL 0.1 M EDTA and 50 mL brine, and then was dried over $MgSO_4$. The $MgSO_4$ was removed by vacuum filtration, and the filtrate was evaporated to dryness. The resulting brown oil was purified by column chromatography (SiO_2; hexanes/CH_2Cl_2, 4:1) to afford a yellow solid. Yield: 64% (0.107 g). ^{1}HNMR ($CDCl_3$ 400MHz, 25°C): δ 7.34-7.36 (m, 3H), 7.51-7.54 (m, 2H), 7.67 (d, 2H, J = 8.0 Hz), 7.85 (d, 2H, J = 8.4 Hz), 9.99 ppm (s, 1H, CHO). ^{13}CNMR ($CDCl_3$ 100MHz, 25 °C): δ 88.4, 93.7, 122.6, 128.7, 129.2, 129.7, 132.0, 132.2, 132.6, 135.5, 191.4 ppm. APCI-MS: *m/z* 207.2 $[M+H]^+$. λ_{max} = 312, 326 nm.

5-(4-Phenylacetylphenyl)dipyrromethane (2). Aldehyde **1** (0.107 g, 0.52 mmol) was dissolved in neat pyrrole (10 mL) and degassed by bubbling with nitrogen for 20 min. Trifluoroacetic acid (0.01 mL, 0.09 mmol) was added. The solution was stirred for 10 min. It was diluted with 50 mL of CH_2Cl_2, washed with 50 mL 0.1 M NaOH and 50 mL water then dried over $MgSO_4$. The $MgSO_4$ was removed by vacuum filtration and the filtrate was evaporated to remove CH_2Cl_2. The remaining pyrrole was removed by vacuum distillation with gentle heating. The product was purified by column chromatography (SiO_2; hexanes/CH_2Cl_2, 1:1) to afford a yellow foam. Yield: 83% (0.139 g). ^{1}HNMR ($CDCl_3$ 400MHz, 25 °C): δ 5.46 (s, 1H) 5.95 (s, 2H), 6.23 (q, 2H, J = 2.8 Hz, J = 2.8 Hz), 6.71 (m, 2H), 7.23 (d, 2H, J = 8.4 Hz), 7.39-7.41 (m, 3H), 7.55 (d, 2H, J = 8.4 Hz), 7.58-7.61 (m, 2H), 7.88 ppm (bs, 2H, NH). ^{13}CNMR ($CDCl_3$ 100MHz, 25°C): δ 44.2, 89.5, 89.8, 107.7, 108.7, 117.7, 122.1, 123.4, 128.5, 128.6, 128.7, 131.8, 132.0, 132.2, 142.6 ppm. APCI-MS: *m/z* 323.1 $[M+H]^+$, 256.3 [M-pyrrole]$^+$. λ_{max} = 288, 306 nm.

5-(4-Phenylacetylphenyl)-4,6-dipyrromethene (L^1). *Method 1.* Dipyrromethane **2** (0.080 g, 0.25 mmol) was dissolved in 150 mL $CHCl_3$ and stirred in an ice bath. DDQ (0.057 g, 0.25 mmol) was dissolved in 100 mL benzene and added slowly dropwise over the course of 1 h. The solvent was then evaporated and the product was purified by column chromatography (SiO_2; $CHCl_3$) to afford a yellow film. Yield: 30% (0.024 g). ^{1}HNMR ($CDCl_3$ 400MHz, 25 °C): δ 6.43 (d, 2H, J = 4.4 Hz), 6.63 (d, 2H, J = 4.4 Hz), 7.38-7.41 (m, 3H), 7.52 (d, 2H, J = 8.1 Hz), 7.58-7.60 (m, 2H), 7.64 (d, 2H, J = 8.1 Hz), 7.66 ppm (bs, 2H). ^{13}CNMR ($CDCl_3$ 100MHz,

25°C): δ 88.8, 90.7, 117.6, 122.8, 123.8, 128.2, 128.3, 128.4, 130.6, 130.7, 131.5, 137.0, 140.5, 140.8, 143.6 ppm. ESI-MS: *m/z* 321.3 $[M+H]^+$. λ_{max} = 286, 342, 436 nm.

Method 2. Dipyrromethane **2** (0.139 g, 0.43 mmol) was dissolved in 150 mL $CHCl_3$ and stirred in an ice bath. DDQ (0.109 g, 0.48 mmol) was dissolved in 100 mL benzene and added slowly dropwise. The solvent was then evaporated to one-half the volume and $Cu(acac)_2$ (0.068 g, 0.26 mmol) was added to form the copper complex, which was purified by column chromatography (vide infra). The copper complex was dissolved in 75 mL of THF. Potassium cyanide (0.200 g, 3.07 mmol) dissolved in 20 mL of H_2O was added to the copper complex, and the mixture was stirred overnight. The solution turned from red to orange. The reaction mixture was evaporated to dryness and the resulting residue was dissolved in 50 mL of CH_2Cl_2, washed with 50 mL brine and 50 mL H_2O, dried with $MgSO_4$, vacuum filtered, and the filtrate evaporated to dryness to afford a yellow film. Yield: 36% (0.050 g, from **2**; 57% from $[Cu(\mathbf{L^1})_2]$).

$[Cu(\mathbf{L^1})_2]$. Dipyrromethane **2** (0.139 g, 0.43 mmol) was dissolved in 150 mL $CHCl_3$ and stirred in an ice bath. DDQ (0.109 g, 0.48 mmol) was dissolved in 100 mL benzene and added slowly dropwise. The solvent was then evaporated to one-half the volume and $Cu(acac)_2$ (0.068 g, 0.26 mmol) was added and the solution was stirred at room temperature for 5-10 min. The reaction mixture was then evaporated to dryness and the resulting residue was purified by column chromatography (SiO_2; $CHCl_3$) to afford a dichroic red/green film. Yield: 63% (0.095 g). APCI-MS: *m/z* 702.1 $[M+H]^+$.

Anal. Calcd for $C_{46}H_{30}N_4Cu{\cdot}H_2O{\cdot}$benzene: C, 78.22; H, 4.80; N, 7.02. Found C, 78.40; H, 4.66; N, 6.99. λ_{max} = 282, 292, 356, 468, 502 nm.

[Fe(L^1)$_3$]. Dipyrromethane **2** (0.150 g, 0.47 mmol) was dissolved in 150 mL $CHCl_3$ and stirred in an ice bath. DDQ (0.117 g, 0.51 mmol) was dissolved in 100 mL benzene and added slowly dropwise. After addition, the reaction mixture was then evaporated to dryness and the resulting dark residue was redissolved in 100 mL of a 1:1 mixture of $CHCl_3$/MeOH. Triethylamine (2 mL) and $FeCl_3{\cdot}6H_2O$ dissolved in 5 mL of MeOH was added to the $CHCl_3$/MeOH solution. The resulting mixture was heated to reflux overnight (~14 h). The solution was evaporated to dryness and the product was purified by column chromatography (SiO_2; $CHCl_3$) to afford a dichroic red/green film. Yield: 59% (0.092 g). APCI-MS: *m/z* 1013.7 $[M+H]^+$. Anal. Calcd for $C_{69}H_{45}N_6Fe{\cdot}H_2O{\cdot}$hexane: C, 80.56; H, 5.50; N, 7.52. Found C, 80.37; H, 5.18; N, 7.66. λ_{max} = 280, 292, 348, 444, 490 nm.

3-(Phenylacetyl)benzaldehyde (3). The same procedure was used as in the synthesis of **1**, starting from 3-iodobenzaldehyde (0.250 g, 1.08 mmol). Yield: 77% (0.171 g). ^{1}HNMR ($CDCl_3$ 400MHz, 25 °C): δ 7.35-7.37 (m, 3H), 7.49 (t, 1H, J = 15.6 Hz), 7.54-7.56 (m, 2H), 7.74-7.76 (dt, 1H, J = 8.4 Hz), 7.80-7.83 (dt, 1H, J = 8.0 Hz), 8.01 (t, 1H, J = 1.2 Hz), 9.99 ppm (s, 1H, CHO). ^{13}CNMR ($CDCl_3$ 100MHz, 25 °C): δ 88.0, 91.1, 122.7, 124.6, 128.5, 128.8, 128.9, 129.2, 131.7, 133.0, 136.5, 137.1, 191.5 ppm. GC-EIMS: *m/z* 206.1 $[M^{\cdot}]^+$. λ_{max} = 282, 298 nm.

5-(3-Phenylacetylphenyl)dipyrromethane (4). The same procedure was used as in the synthesis of **2**, starting from **3** (0.171 g, 0.83 mmol). Yield: 76% (0.204 g).

^{1}HNMR (CD_2Cl_2 400MHz, 25 °C): δ 5.48 (s, 1H), 5.96 (m, 2H), 6.23 (q, 2H, J = 2.8, Hz J = 2.4 Hz), 6.73 (q, 2H, J = 2.0, Hz J = 2.4 Hz), 7.26 (d, 1H, J = 8.4 Hz), 7.38 (t, 1H, J = 7.6 Hz), 7.42-7.45 (m, 3H), 7.47 (s, 1H), 7.52 (d, 1H, J = 8.0 Hz), 7.60-7.62 (m, 2H), 7.99 ppm (bs, 2H, NH). ^{13}CNMR ($CDCl_3$ 100MHz, 25 °C): δ 44.1, 89.5, 89.6, 107.5, 108.6, 117.7, 123.3, 123.6, 128.6, 128.7, 128.9, 130.3, 131.5, 131.8, 132.3, 143.1 ppm. APCI-MS: *m/z* 323.1 $[M+H]^+$, 256.3 [M-pyrrole]$^+$. λ_{max} = 284, 302 nm.

5-(3-Phenylacetylphenyl)-4,6-dipyrromethene (L^2). The same procedure was used as in the synthesis of L^1 (Method 1), starting from **4** (0.204 g, 0.63 mmol). Yield: 42% (0.086 g). ^{1}HNMR ($CDCl_3$ 400MHz, 25 °C): δ 6.42 (dd, 2H, J = 2.8 Hz), 6.62 (dd, 2H, J = 2.8 Hz), 7.33-7.34 (m, 3H), 7.42-7.43 (m, 2H), 7.51-7.53 (m, 2H), 7.64-7.66 (m, 2H), 7.70 ppm (t, 2H, J = 1.2 Hz). ^{13}CNMR ($CDCl_3$ 100MHz, 25 °C): δ 88.6, 90.1, 117.6, 122.7, 122.8, 127.6, 128.2, 128.3, 129.6, 130.4, 131.5, 132.0, 133.4, 137.2, 139.3, 143.7 ppm. APCI-MS: *m/z* 321.3 $[M+H]^+$. λ_{max} = 288, 434 nm.

[Cu(L^2)$_2$]. The same procedure was used as in the synthesis of [Cu(L^1)$_2$], starting from purified L^2 (0.034 g, 0.11 mmol). Yield: 81% (0.030 g). MALDI-TOF-MS: *m/z* 702.58 $[M+H]^+$. Anal. Calcd for $C_{46}H_{30}N_4Cu$: C, 78.67; H, 4.31; N, 7.98. Found C, 78.85; H, 4.42; N, 7.68. λ_{max} = 284, 298, 468, 500 nm.

[Fe(L^2)$_3$]. The same procedure was used as in the synthesis of [Fe(L^1)$_3$], starting from purified L^2 (0.026 g, 0.081 mmol). Yield: 91% (0.025 g). APCI-MS: *m/z* 1013.8 $[M+H]^+$. Anal. Calcd for $C_{69}H_{45}N_6Fe$: C, 81.73; H, 4.47; N, 8.29. Found C, 81.70; H, 4.55; N, 8.22. λ_{max} = 284, 300, 444, 496 nm.

4-(Ethynyl)benzaldehyde (5). 4-[(Trimethylsilyl)ethynyl]benzaldehyde (1.00 g, 4.94 mmol) was dissolved in 50 mL methanol to which potassium carbonate (0.500 g, 3.62 mmol) was added. The reaction was stirred for 15 min at which point the starting material was completely consumed as judged by TLC and GC-MS. The reaction mixture was evaporated to dryness and dissolved in 50 mL CH_2Cl_2, washed with 50 mL aqueous sodium bicarbonate, and dried over $MgSO_4$. The $MgSO_4$ was removed by vacuum filtration, and the filtrate was evaporated to dryness to afford a yellow solid. Yield: 96% (0.617 g). ^{1}HNMR ($CDCl_3$ 400MHz, 25 °C): δ 3.30 (s, 1H), 7.57 (d, 2H, J = 8.0 Hz), 7.78 (d, 2H, J = 8.4 Hz), 9.94 ppm (s, 1H, CHO). ^{13}CNMR ($CDCl_3$ 100MHz, 25 °C): δ 81.5, 82.9, 128.3, 129.6, 132.8, 136.0, 191.3 ppm. GC-EIMS: *m/z* 130.7 $[M^{\cdot}]^+$.

4-(4-Iodophenylacetyl)benzaldehyde (6). A mixture of **5** (0.300 g, 2.31 mmol), 1,4-diiodobenzene (3.042 g, 9.22 mmol), triethylamine (0.349 g, 3.46 mmol), $Pd(PPh_3)_2Cl_2$ (0.081 g, 0.12 mmol), triphenylphosphine (0.015 g, 0.06 mmol), CuI (0.009 g, 0.05 mmol), and 15 mL of dry THF was stirred under nitrogen for 4 days. The reaction mixture was diluted with 50 mL of CH_2Cl_2, washed with 50 mL 0.1 M EDTA and 50 mL brine, and was then dried over $MgSO_4$. The $MgSO_4$ was removed by vacuum filtration and the filtrate was evaporated to dryness. The remaining residue was purified by column chromatography (SiO_2; hexanes/CH_2Cl_2, 1:1) to afford a yellow solid. Yield: 73% (0.560 g). ^{1}HNMR ($CDCl_3$ 400MHz, 25 °C): δ 7.28 (d, 2H, J = 8.4 Hz), 7.67 (d, 2H, J = 8.4 Hz), 7.72 (d, 2H, J = 8.4 Hz), 7.87 (d, 2H, J = 8.4 Hz), 10.02 ppm (s, 1H, CHO). ^{13}CNMR ($CDCl_3$ 100MHz, 25 °C): δ 89.8, 92.3, 95.0, 121.8,

127.7, 129.0, 129.4, 131.8, 133.0, 137.5, 191.0 ppm. GC-EIMS: *m/z* 332.1 $[M^{\cdot}]^{+}$. λ_{max} = 320, 334 nm.

4-[4-(Phenylacetyl)phenylacetyl]benzaldehyde (7). The same procedure was used as in the synthesis of **1**, starting from **6** (0.200 g, 0.60 mmol) and phenylacetylene (0.184 g, 1.8 mmol). After 3 days, the reaction mixture was diluted with 50 mL of CH_2Cl_2, washed with 50 mL 0.1 M EDTA and 50 mL brine, and was then dried over $MgSO_4$. The $MgSO_4$ was removed by vacuum filtration and the filtrate was evaporated to dryness. The remaining residue was purified by column chromatography (SiO_2; CH_2Cl_2) to afford a yellow solid. Yield: 72% (0.133 g). ^{1}HNMR ($CDCl_3$ 400MHz, 25 °C): δ 7.36 (m, 3H), 7.54 (m, 6H), 7.69 (d, 2H, *J* = 8.0 Hz), 7.89 (d, 2H, *J* = 8.0 Hz), 10.03 ppm (s, 1H, CHO). ^{13}CNMR ($CDCl_3$ 100MHz, 25 °C): δ 88.9, 90.2, 91.6, 93.0, 122.1, 122.7, 123.8, 128.3, 128.4, 129.2, 129.5, 131.5, 131.6, 132.0, 135.3, 191.1 ppm. GC-EIMS: *m/z* 306.3 $[M^{\cdot}]^{+}$. λ_{max} = 338 nm.

5-[4-((Phenylacetyl)phenylacetyl)phenyl]dipyrromethane (8). The same procedure was used as in the synthesis of **2**, starting from **7** (0.133 g, 0.43 mmol). Yield: 75% (0.138 g). ^{1}HNMR ($CDCl_3$ 400MHz, 25 °C): δ 5.48 (s, 1H), 5.93 (m, 2H), 6.19 (q, 2H, *J* = 2.8 Hz, *J* = 3.2 Hz), 6.71 (m, 2H), 7.22 (d, 2H, *J* = 8.0 Hz), 7.37 (m, 3H), 7.49-7.57 (m, 8H), 7.90 ppm (bs, 2H, NH). ^{13}CNMR ($CDCl_3$ 100MHz, 25 °C): δ 43.8, 89.0, 89.1, 90.9, 91.2, 107.3, 108.4, 117.3, 121.5, 122.8, 122.9, 123.0, 128.2, 128.3, 131.3, 131.4, 131.7, 131.8, 142.3 ppm. MALDI-TOF-MS: *m/z* 422.23 $[M+H]^{+}$. λ_{max} = 324, 346 nm.

5-[4-((Phenylacetyl)phenylacetyl)phenyl]-4,6-dipyrromethene (L^3). The same procedure was used as in the synthesis of L^1 (Metod 2) starting from **8** (0.202 g, 0.48 mmol). Yield: 13% (0.026 g). ^{1}HNMR ($CDCl_3$ 400MHz, 25 °C): δ 6.42 (d, 2H, J = 2.8 Hz), 6.62 (d, 2H, J = 3.2 Hz), 7.36-7.39 (m, 3H), 7.52 (d, 2H, J = 8.0 Hz), 7.55-7.57 (m, 6H), 7.63 (d, 2H, J = 8.0 Hz), 7.66 ppm (s, 2H). ^{13}CNMR ($CDCl_3$ 100MHz, 25 °C): δ 89.0, 90.4, 90.6, 91.4, 117.7, 122.6, 122.8, 123.2, 123.6, 128.3, 128.4, 128.5, 130.7, 130.8, 131.3, 131.4, 131.5, 137.2, 140.5, 140.8, 143.7 ppm. ESI-MS: *m/z* 421.3 $[M+H]^+$. λ_{max} = 324, 436 nm.

[Cu(L^3)$_2$]. The same procedure was used as in the synthesis of [Cu(L^1)$_2$], starting from **8** (0.130 g, 0.31 mmol). Yield: 69% (0.096 g). MALDI-TOF-MS: *m/z* 902.40 $[M+H]^+$. Anal. Calcd for $C_{62}H_{38}N_4Cu$: C, 82.51; H, 4.24; N, 6.21. Found C, 82.43; H, 4.58; N, 5.97. λ_{max} = 322, 468, 500 nm.

[Fe(L^3)$_3$]. The same procedure was used as in the synthesis of [Fe(L^1)$_3$], starting from **8** (0.340 g, 0.80 mmol). Yield: 48% (0.170 g). MALDI-TOF-MS: *m/z* 1313.44 $[M+H]^+$. Anal. Calcd for $C_{93}H_{57}N_6Fe$: C, 84.99; H, 4.37; N, 6.39. Found C, 85.00; H, 4.36; N, 6.50. λ_{max} = 320, 444, 490 nm.

4-(3-Iodophenylacetyl)benzaldehyde (9). A mixture of **5** (0.200 g, 1.54 mmol), 1,3-diiodobenzene (1.52 g, 4.61 mmol), triethylamine (0.155 g, 1.54 mmol), $Pd(PPh_3)_2Cl_2$ (0.054 g, 0.08 mmol), triphenylphosphine (0.010 g, 0.04 mmol), CuI (0.006 mg, 0.03 mmol), and 15 mL of dry THF was stirred under nitrogen for 3 days. The reaction mixture was diluted with 50 mL of CH_2Cl_2, washed with 50 mL 0.1 M EDTA and 50 mL brine, and was then dried over $MgSO_4$. The $MgSO_4$ was removed

by vacuum filtration and the filtrate was evaporated to dryness. The remaining residue was purified by column chromatography (SiO_2; hexanes/CH_2Cl_2, 1:1) to afford a yellow solid. Yield: 82% (0.420 g). ^{1}HNMR ($CDCl_3$ 400MHz, 25 °C): δ 7.11 (t, 1H, J = 8.0 Hz), 7.52 (dt, 1H, J = 8.0 Hz), 7.67 (d, 2H, J = 8.0 Hz), 7.72 (dt, 1H, J = 8.0 Hz), 7.88 (d, 2H, J = 8.4 Hz), 7.91 (t, 1H, J = 2.0 Hz), 10.02 ppm (s, 1H, CHO). ^{13}CNMR ($CDCl_3$ 100MHz, 25 °C): δ 89.6, 91.4, 93.7, 124.4, 128.8, 129.4, 129.80, 130.7, 132.0, 135.4, 137.7, 140.1, 191.1 ppm. GC-EIMS: *m/z* 332.1 $[M^{\cdot}]^+$. λ_{max} = 310, 328 nm.

4-[3-(Phenylacetyl)phenylacetyl]benzaldehyde (10). The same procedure was used as in the synthesis of **1**, starting from **9** (0.400 g, 1.20 mmol) and phenylacetylene (0.369 g, 3.60 mmol). After 3 days, the reaction mixture was diluted with 50 mL of CH_2Cl_2, washed with 50 mL 0.1 M EDTA and 50 mL brine, and was then dried over $MgSO_4$. The $MgSO_4$ was removed by vacuum filtration and the filtrate was evaporated to dryness. The remaining residue was purified by column chromatography (SiO_2; CH_2Cl_2) to afford a yellow solid. Yield: 90% (0.332 g). ^{1}HNMR ($CDCl_3$ 400MHz, 25 °C): δ 7.33-7.37 (m, 4H), 7.49-7.56 (m, 4H), 7.68 (d, 2H, J = 7.6 Hz), 7.74 (s, 1H), 7.87 (d, 2H, J = 8.0 Hz), 10.01 ppm (s, 1H, CHO). ^{13}CNMR ($CDCl_3$ 100MHz, 25 °C): δ 88.2, 89.0, 90.2, 92.4, 122.6, 122.7, 123.6, 128.2, 128.3, 128.4, 129.0, 129.4, 131.2, 131.4, 131.7, 131.9, 134.5, 135.3, 191.0 ppm. GC-EIMS: *m/z* 306.3 $[M^{\cdot}]^+$. λ_{max} = 286, 304 nm.

5-[3-((Phenylacetyl)phenylacetyl)phenyl]dipyrromethane (11). The same procedure was used as in the synthesis of **2**, starting from 0.330 g (1.08 mmol) of **10**.

Yield: 90% (0.410 g). ^{1}HNMR ($CDCl_3$ 400MHz, 25 °C): δ 5.49 (s, 1H), 5.93 (m, 2H), 6.18 (q, 2H, *J* = 3.2 Hz, *J* = 2.8 Hz), 6.72 (m, 2H), 7.22 (d, 2H, *J* = 8.0 Hz), 7.32-7.38 (m, 4H), 7.48-7.51 (m, 4H), 7.55-7.56 (m, 2H), 7.72 (t, 1H, *J* = 1.6 Hz), 7.94 ppm (bs, 2H, NH). ^{13}CNMR ($CDCl_3$ 100MHz, 25 °C): δ 43.9, 88.4, 88.5, 89.6, 89.9, 107.3, 108.4, 117.3, 121.5, 122.8, 123.4, 123.5, 128.2, 128.3, 131.1, 131.5, 131.7, 134.4, 142.3 ppm. MALDI-TOF-MS: *m/z* 421.23 $[M+H]^+$. λ_{max} = 286, 302 nm.

5-[3-((Phenylacetyl)phenylacetyl)phenyl]-4,6-dipyrromethene (L^4). The same procedure was used as in the synthesis of L^1 (Method 2), starting from **11** (0.250 g, 0.59 mmol). Yield: 36% (0.090 g). ^{1}HNMR ($CDCl_3$ 400MHz, 25 °C): δ 6.43 (d, 2H, *J* = 2.8 Hz), 6.64 (d, 2H, *J* = 3.2 Hz), 7.37-7.39 (m, 4H), 7.51-7.58 (m, 6H), 7.63 (d, 2H, *J* = 8.8 Hz), 7.67 (s, 2H), 7.79 ppm (s, 1H). ^{13}CNMR ($CDCl_3$ 100MHz, 25 °C): δ 88.4, 89.4, 89.9, 90.1, 117.7, 122.8, 123.2, 123.5, 123.6, 128.2, 128.3, 128.4, 128.5, 130.7, 131.1, 131.3, 131.5, 134.5, 137.2, 140.5, 140.8, 143.6 ppm. ESI-MS: *m/z* 421.3 $[M+H]^+$. λ_{max} = 286, 302, 432 nm.

[Cu(L^4)$_2$]. The same procedure was used as in the synthesis of [Cu(L^1)$_2$], starting from **11** (0.250 g, 0.59 mmol). Yield: 47% (0.125 g). MALDI-TOF-MS: *m/z* 901.20 $[M+H]^+$. Anal. Calcd for $C_{62}H_{38}N_4Cu$: C, 82.51; H, 4.24; N, 6.21. Found C, 82.25; H, 4.36; N, 6.23. λ_{max} = 284, 354, 470, 502 nm.

[Fe(L^4)$_3$]. The same procedure was used as in the synthesis of [Fe(L^1)$_3$], starting from **11** (0.150 g, 0.36 mmol). Yield: 57% (0.088 g). MALDI-TOF-MS: *m/z* 1313.38 $[M+H]^+$. Anal. Calcd for $C_{93}H_{57}N_6Fe$: C, 84.99; H, 4.37; N, 6.39. Found C, 84.77; H, 4.55; N, 6.45. λ_{max} = 284, 344, 444, 494 nm.

[Fe(phFdpm)$_3$]. 5-(Pentafluorophenyl)dipyrromethane[22] (0.45 g, 1.44 mmol) was dissolved in 200 mL $CHCl_3$ and stirred in an ice bath. DDQ (0.33 g, 1.44 mmol) was dissolved in 125 mL benzene and added slowly dropwise. After addition, the reaction mixture was then evaporated to 50 mL. Triethylamine (1 mL) was added. $FeCl_3 \cdot 6H_2O$ (0.13g, 0.47 mmol) was predissolved in 50 mL of MeOH and added to the reaction mixture. The resulting mixture was heated to reflux overnight (~14 h). The solution was evaporated to dryness and the product was purified by column chromatography (SiO_2; CH_2Cl_2:hexanes 1:1) to afford an red/green solid. Yield: 31% (0.143 g). ESI-MS: *m/z* 983.77 $[M+H]^+$. HR-FABMS: *m/z* 983.0675 $[M]^+$ (Calcd. *m/z* 983.0697). λ_{max} = 228 298, 451, 500(shoulder) nm. IR (film from CH_2Cl_2): *v* 2926, 1568, 1517, 1498, 1381, 1338, 1244, 1039, 989, 887, 841, 752 cm^{-1}.

[Co(phFdpm)$_3$]. A similar procedure to [Fe(phFdpm)$_3$] was used with 5-(pentafluorophenyl)dipyrromethane[22] (0.55 g, 1.76 mmol) and $[Co(pyr)_4Cl_2]Cl$ (0.25 g, 0.53 mmol) to afford an orange solid. Yield: 23% (0.131 g). ESI-MS: *m/z* 986.69 $[M+H]^+$. HR-FABMS: *m/z* 986.0669 $[M]^+$ (Calcd. *m/z* 986.0680). ^{1}HNMR ($CDCl_3$ 400MHz, 25 °C): δ 6.41 (d, 6H, *J* = 4.0 Hz), 6.54 (s, 2H), 6.71 ppm (d, 2H, *J* = 4.0 Hz). λ_{max} = 301, 408, 477, 517 nm. IR (film from CH_2Cl_2): *v* 2930, 1569, 1518, 1498, 1380, 1348, 1249, 1039, 1028, 995, 887, 839, 752 cm^{-1}.

4-((Perfluorophenyl)ethynyl)benzaldehyde (12). 4-Ethynylbenzaldehyde (0.15 g, 1.13 mmol), iodopentaflurobenzene (0.40 g, 1.36 mmol), $Pd(PPh_3)_3Cl_2$ (0.09 g, 0.13 mmol), and CuI (0.02 g, 0.11 mmol) were dissolved in dried, degassed triethylamine (15 mL). The reaction was heated to 35 ºC and stirred for 12 h. The

triethylamine was evaporated and the reaction mixture was diluted with 50 mL of CH_2Cl_2, washed with 50 mL 0.1 M EDTA and 50 mL brine, and was dried over $MgSO_4$. The $MgSO_4$ was removed by vacuum filtration and the filtrate was evaporated to dryness. The remaining residue was purified by column chromatography (SiO_2; hexanes/CH_2Cl_2, 1:4) to afford a yellow solid. Yield: 58% (0.20 g). ^{1}HNMR ($CDCl_3$ 400MHz, 25 °C): δ 7.71 (d, 2H, J = 8.0 Hz), 7.90 (d, 2H, J = 8.4 Hz), 10.02 ppm (s, 1H, CHO). ^{13}CNMR ($CDCl_3$ 100MHz, 25 °C): δ 76.7, 77.0, 77.3, 100.0, 127.3, 129.4, 132.2, 190.8 ppm. GC-EIMS: *m/z* 296.1 $[M^{\cdot}]^+$.

5-[4-((Perfluorophenyl)ethynyl)phenyl]dipyrromethane (13). The same procedure was used as in the synthesis of **2**, starting from **12** (0.20 g, 0.68 mmol). Yield: 84% (0.23 g). ^{1}HNMR ($CDCl_3$ 400MHz, 25 °C): δ 5.47 (s, 1H), 5.94 (s, 2H), 6.22 (q, 2H), 6.70 (q, 2H), 7.26 (d, 2H, J = 8.0 Hz), 7.56 (d, 2H, J = 8.0 Hz), 7.85 ppm (s, 2H, NH). ^{13}CNMR ($CDCl_3$ 100MHz, 25 °C): δ 43.8, 73.0, 101.2, 107.4, 108.4, 117.4, 119.9, 128.4, 131.6, 131.9, 143.8 ppm. APCI-MS: *m/z* 411.17 $[M+H]^+$.

$[Fe(L^5)_3]$. The same procedure was used as in the synthesis of $[Fe(L^1)_3]$, starting from **13** (0.23 g, 0.42 mmol). Yield: 12% (0.029 g). APCI-MS: *m/z* 1282.97 $[M+H]^+$. λ_{max} = 230, 284, 332, 444, 492 nm.

2.5. Acknowledgment

Text, schemes, and figures of this chapter, in part, are reprints of the materials published in the following paper: Sara R. Halper and Seth M. Cohen, "Synthesis, Structure, and Spectroscopy of Phenylacetylene Rods Incorporating Meso-Substituted

Dipyrrin Ligands" *Chem. Eur. J.* **2003**, 9, 4661-4669. The dissertation author was the primary researcher. The permission to reproduce this paper was granted by John Wiley & Sons Inc., Copyright 2003.

2.6. Appendix

X-ray Crystal Structure Determination

Details: Single crystals of each compound suitable for X-ray diffraction structural determination were mounted on quartz capillaries with Paratone oil and were cooled in a nitrogen stream on the diffractometer. Data were collected on either a Bruker AXS or a Bruker P4 diffractometer each equipped with area detectors. Peak integrations were performed with the Siemens SAINT software package. Absorption corrections were applied using the program SADABS. Space group determinations were performed by the program XPREP. The structures were solved by either Patterson or direct methods and refined with the SHELXTL software package (Sheldrick, G. M. *SHELXTL vers. 5.1 Software Reference Manual*; Bruker AXS: Madison, WI, 1997). All hydrogen atoms were fixed at calculated positions with isotropic thermal parameters, and all non-hydrogen atoms were refined anisotropically unless otherwise noted.

Structure of $[Cu(L^1)_2]$. Dark green blocks suitable for X-ray diffraction structural determination were grown from a solution of the complex dissolved in benzene diffused with hexanes. The complex co-crystallized with one molecule of benzene in the asymmetric unit.

Structure of [Fe(L^1)$_3$]. Dark green hexagons suitable for X-ray diffraction structural determination were grown from a solution of the complex dissolved in benzene diffused with hexanes. The complex co-crystallized with one disordered molecule of benzene, which was treated as a diffuse contribution using the program SQUEEZE (A. Spek, Platon Library). Electron count/unit cell: 92 (found), 84 (expected).

Structure of [Fe(L^3)$_3$]. Dark green thin plates suitable for X-ray diffraction structural determination were grown from a solution of the complex dissolved in benzene diffused with cyclohexane. The complex co-crystallized with one molecule of cyclohexane in the asymmetric unit.

Structure of [Fe(phFdpm)$_3$]. Green rods suitable for X-ray diffraction structural determination were grown from a solution of the complex dissolved in $CHCl_3$ diffused with hexanes. The complex co-crystallized with one disordered molecule of hexane, which was treated as a diffuse contribution using the program SQUEEZE (A. Spek, Platon Library). Electron count/unit cell: 195 (found), 200 (expected).

Structure of [Co(phFdpm)$_3$]. Red blocks suitable for X-ray diffraction structural determination were grown from a solution of the complex dissolved in $CHCl_3$ diffused with hexanes. The complex co-crystallized with one molecule of hexane which was partially occupied and disordered and one molecule of chloroform which was partially occupied. They were both treated as a diffuse contribution using

the program SQUEEZE (A. Spek, Platon Library). Electron count/unit cell: 154 (found), 216 (expected).

Structure of $[Fe(L^5)_3]$. Green thin plates suitable for X-ray diffraction structural determination were grown from a solution of the complex dissolved in CH_2Cl_2 diffused with hexanes. The complex co-crystallized with half a molecule of pentane per asymmetric unit which was disordered. It was treated as a diffuse contribution using the program SQUEEZE (A. Spek, Platon Library). Electron count/unit cell: 42 (found), 42 (expected).

X-ray Crystal Structure Details for $[Fe(L^1)_3]$

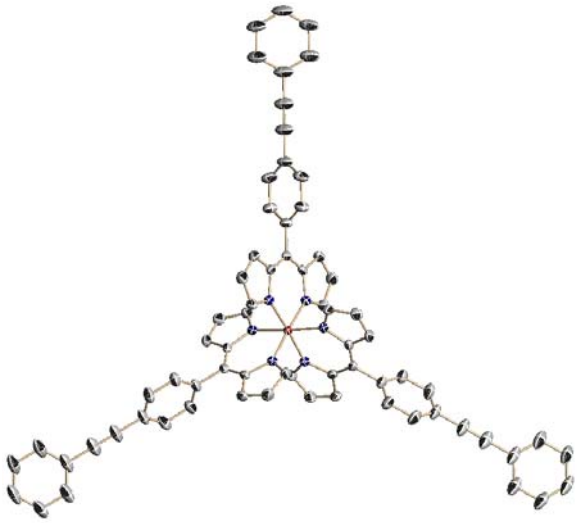

Figure 2-8. Structural Diagram of $[Fe(L^1)_3]$ with partial atom numbering schemes (ORTEP, 50% probability ellipsoids). Hydrogen atoms and disordered solvent have been omitted for clarity.

Table 2-2. Crystal Data for $[Fe(L^1)_3]$.

Empirical formula	$FeC_{75}H_{51}N_6$	
Temperature	100(2) K	
Crystal system	Rhombohedral	
Space group	*R*-3*c*	
Unit cell dimensions	a = 14.455(1) Å	α = 84.738(1)°
	b = 14.455(1) Å	β = 84.738(1)°
	c = 14.455(1) Å	γ = 84.738(1)°
Volume	2984.2 (2) $Å^3$	
Z	2	
Crystal size	0.34 × 0.32 × 0.12 mm^3	
Reflections collected	24747	
Independent reflections	2298 [*R*(int) = 0.0326]	
Data / restraints / parameters	2298 / 0 / 119	
Goodness-of-fit on F^2	1.075	
Final *R* indices [I>2sigma(I)]	*R*1 = 0.0393, w*R*2 = 0.0999	
R indices (all data)	*R*1 = 0.0497, w*R*2 = 0.1043	

X-ray Crystal Structure Details for $[Cu(L^1)_2]$

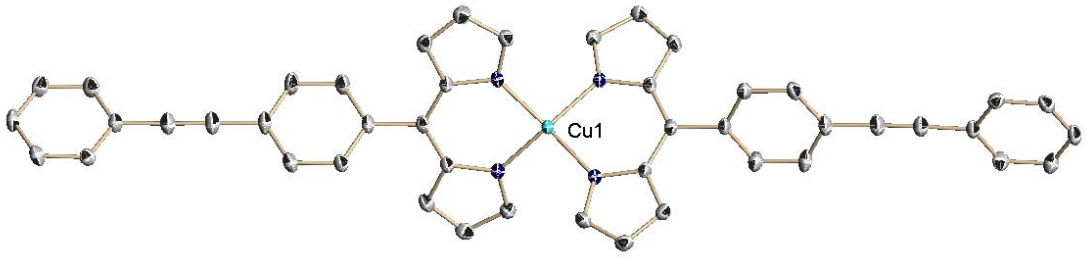

Figure 2-9. Structural Diagram of $[Cu(L^1)_2]$ with partial atom numbering schemes (ORTEP, 50% probability ellipsoids). Hydrogen atoms and disordered solvent have been omitted for clarity.

Table 2-3. Crystal Data for $[Cu(L^1)_2]$.

Empirical formula	$CuC_{52}H_{36}N_4$	
Temperature	100(2) K	
Crystal system	Triclinic	
Space group	*P*-1	
Unit cell dimensions	a = 9.378(1) Å	α = 104.721(2)°
	b = 13.821(1) Å	β = 99.250(2)°
	c = 16.635(2) Å	γ = 104.753(2)°
Volume	1957.2 (3) $Å^3$	
Z	2	
Crystal size	0.21 × 0.20 × 0.20 mm^3	
Reflections collected	16330	
Independent reflections	8499 [R(int) = 0.0253]	
Data / restraints / parameters	8499 / 0 / 514	
Goodness-of-fit on F^2	1.034	
Final R indices [I>2sigma(I)]	$R1$ = 0.0518, w$R2$ = 0.1445	
R indices (all data)	$R1$ = 0.0551, w$R2$ = 0.1477	

X-ray Crystal Structure Details for $[Fe(L^3)_3]$

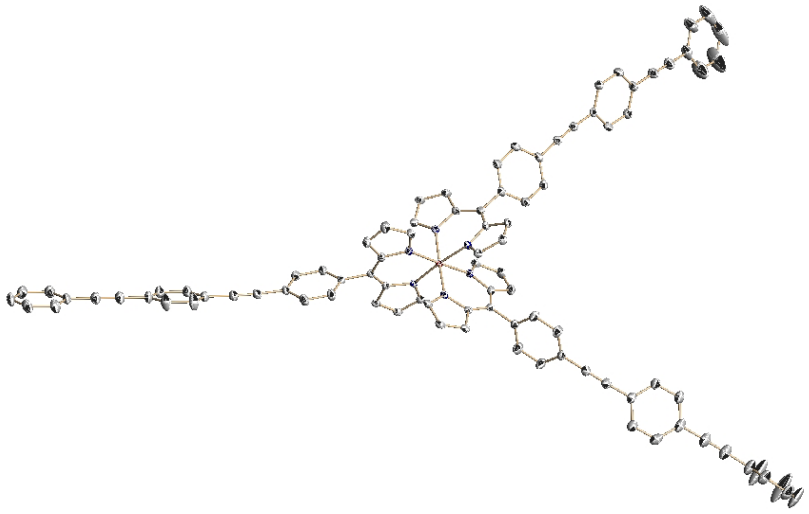

Figure 2-10. Structural Diagram of $[Fe(L^3)_3]$ with partial atom numbering schemes (ORTEP, 50% probability ellipsoids). Hydrogen atoms and solvent have been omitted for clarity.

Table 2-4. Crystal Data and Structure Refinement for $[Fe(L^3)_3]$.

Empirical formula	$FeC_{99}H_{69}N_6$	
Temperature	100(2) K	
Crystal system	Monoclinic	
Space group	*P*2(1)/*c*	
Unit cell dimensions	$a = 28.896(2)$ Å	$\alpha = 90°$
	$b = 15.122(1)$ Å	$\beta = 91.484(1)°$
	$c = 17.094(1)$ Å	$\gamma = 90°$
Volume	7466.7(8) $Å^3$	
Z	4	
Crystal size	$0.48 \times 0.35 \times 0.03$ mm^3	
Reflections collected	45623	
Independent reflections	16911 [*R*(int) = 0.0426]	
Data / restraints / parameters	11691 / 0 / 955	
Goodness-of-fit on F^2	1.023	
Final *R* indices [I>2sigma(I)]	*R*1 = 0.0510, w*R*2 = 0.1164	
R indices (all data)	*R*1 = 0.0821, w*R*2 = 0.1292	

X-ray Crystal Structure Details for [Fe(phFdpm)$_3$]

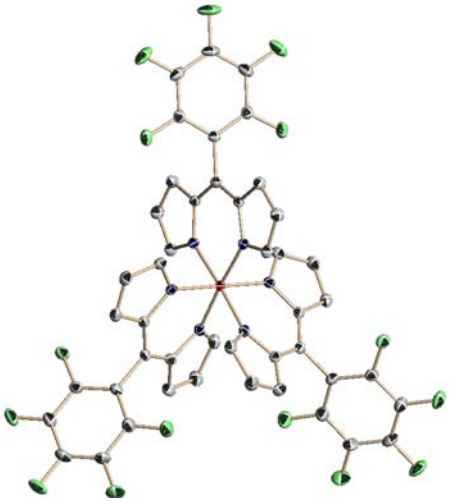

Figure 2-11. Structural Diagram of [Fe(phFdpm)$_3$] with partial atom numbering schemes (ORTEP, 50% probability ellipsoids). Hydrogen atoms and disordered solvent have been omitted for clarity.

Table 2-5. Crystal Data for [Fe(phFdpm)$_3$].

Empirical formula	$FeC_{51}H_{32}N_6F_{15}$	
Temperature	100(2) K	
Crystal system	Monoclinic	
Space group	*C*2/*c*	
Unit cell dimensions	a = 18.331(2) Å	α = 90°
	b = 20.476(2) Å	β = 121.8830(10)°
	c = 14.1040(16) Å	γ = 90°
Volume	4495.3(9) Å^3	
Z	4	
Crystal size	0.55 × 0.30 × 0.20 mm^3	
Reflections collected	19218	
Independent reflections	5057 [*R*(int) = 0.0247]	
Data / restraints / parameters	5057 / 0 / 305	
Goodness-of-fit on F^2	1.062	
Final *R* indices [I>2sigma(I)]	*R*1 = 0.0319, w*R*2 = 0.0852	
R indices (all data)	*R*1 = 0.0345, w*R*2 = 0.0867	

X-ray Crystal Structure Details for [Co(phFdpm)$_3$]

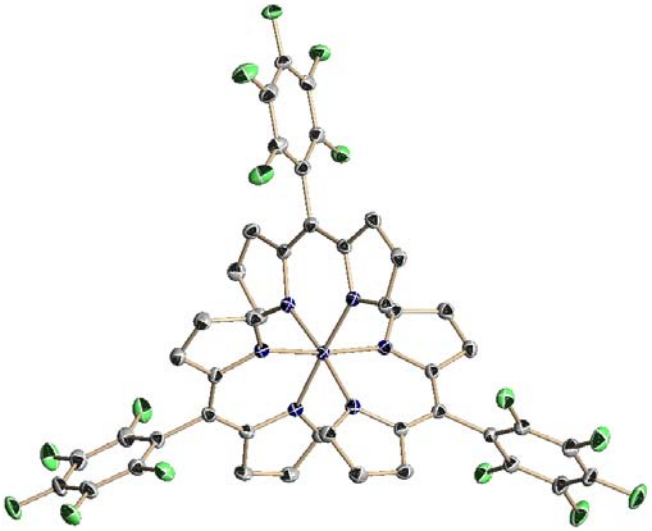

Figure 2-12. Structural Diagram of [Co(phFdpm)$_3$] with partial atom numbering schemes (ORTEP, 50% probability ellipsoids). Hydrogen atoms and disordered solvent have been omitted for clarity.

Table 2-6. Crystal Data for [Co(phFdpm)$_3$].

Empirical formula	$CoC_{52}H_{33}N_6F_{15}Cl_3$	
Temperature	100(2) K	
Crystal system	Triclinic	
Space group	*P*-1	
Unit cell dimensions	a = 12.7899(17) Å	α = 83.368(2)°
	b = 13.1878(17) Å	β = 74.290(2)°
	c = 15336(2) Å	γ = 70.280(2)°
Volume	2343.2(5) Å^3	
Z	2	
Crystal size	0.27 × 0.25 × 0.17 mm^3	
Reflections collected	20096	
Independent reflections	10240 [R(int) = 0.0173]	
Data / restraints / parameters	10240 / 0 / 604	
Goodness-of-fit on F^2	1.086	
Final R indices [I>2sigma(I)]	R1 = 0.0325, wR2 = 0.0886	
R indices (all data)	R1 = 0.0355, wR2 = 0.0904	

X-ray Crystal Structure Details for $[Fe(L^5)_3]$

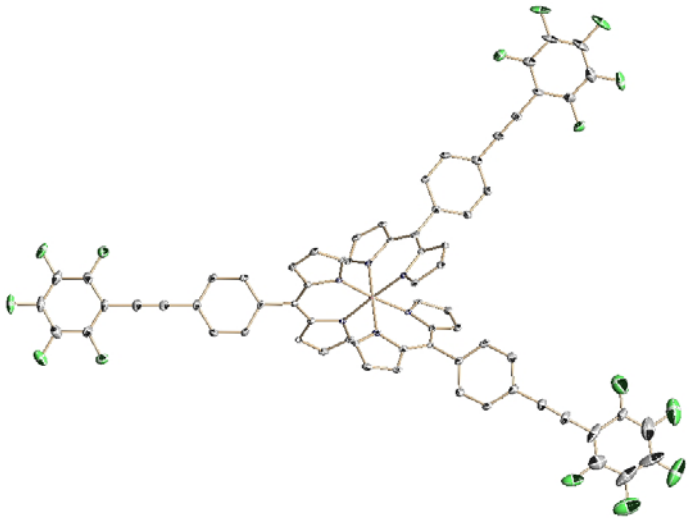

Figure 2-13. Structural Diagram of $[Fe(L^5)_3]$ with atom numbering schemes (ORTEP, 50% probability ellipsoids). Hydrogen atoms and solvent have been omitted for clarity.

Table 2-7. Crystal Data for $[Fe(L^5)_3]$.

Empirical formula	$FeC_{71.5}H_{36}N_6F_{15}$	
Temperature	100(2) K	
Crystal system	Triclinic	
Space group	*P*-1	
Unit cell dimensions	a = 11.420(5) Å	α = 95.743(7)°
	b = 13.231(6) Å	β = 101.872(7)°
	c = 21.568(9) Å	γ = 113.042(6)°
Volume	2875 (2) $Å^3$	
Z	2	
Crystal size	0.30 × 0.19 × 0.10 mm^3	
Reflections collected	24176	
Independent reflections	12682 [R(int) = 0.0494]	
Data / restraints / parameters	12682 / 0 / 821	
Goodness-of-fit on F^2	1.048	
Final R indices [I>2sigma(I)]	$R1$ = 0.0904, w$R2$ = 0.2088	
R indices (all data)	$R1$ = 0.1284, w$R2$ = 0.2270	

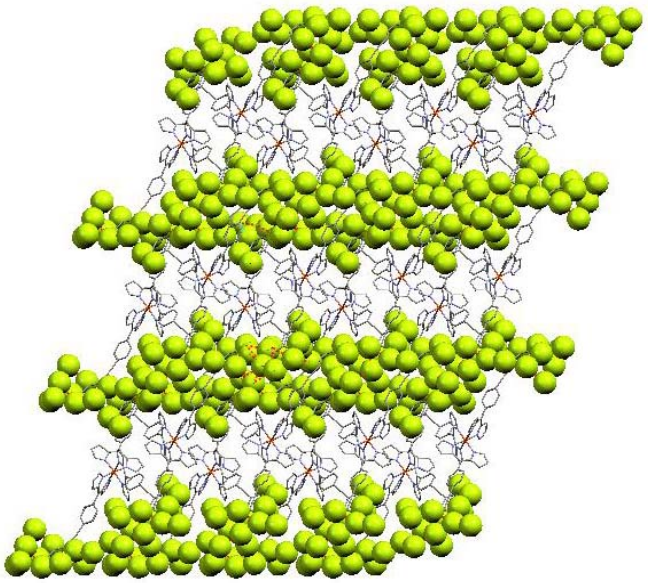

Figure 2-14. Packing diagram of $[Fe(L^5)_3]$ viewed down the crystallographic *a*-axis (F atoms: space filling model; all other atoms: stick form). Solvent molecules have been omitted for clarity.

2.7. References

[1] C. Brückner, Y. Zhang, S. J. Rettig, D. Dolphin, *Inorg. Chim. Acta* **1997**, *263*, 279.

[2] C. Brückner, V. Karunaratne, S. J. Rettig, D. Dolphin, *Can. J. Chem.* **1996**, *74*, 2182.

[3] O. Henze, D. Lentz, A. D. Schlüter, *Chem. Eur. J.* **2000**, *6*, 2362.

[4] J. Zhang, J. S. Moore, *J. Am. Chem. Soc.* **1994**, *116*, 2655.

[5] S. Höger, V. Enkelmann, K. Bonrad, C. Tschierske, *Angew. Chem. Int. Ed.* **2000**, *39*, 2267.

[6] R. D. Adams, T. Barnard, A. Rawlett, J. M. Tour, *Eur. J. Inorg. Chem.* **1998**, 429.

[7] G. W. Coates, A. R. Dunn, L. M. Henling, D. A. Dougherty, R. H. Grubbs, *Angew. Chem. Int. Ed.* **1997**, *36*, 248.

[8] M. Gdaniec, W. Jankowski, M. J. Milewska, T. Polonski, *Angew. Chem. Int. Ed.* **2003**, *42*, 3903.

[9] F. Ponzini, R. Zagha, K. Hardcastle, J. S. Siegel, *Angew. Chem. Int. Ed.* **2000**, *39*, 2323.

[10] C. Dai, P. Nguyen, T. B. Marder, A. J. Scott, W. Clegg, C. Viney, *Chem. Commun.* **1999**, 2493.

[11] M. Weck, A. R. Dunn, K. Matsumoto, G. W. Coates, E. B. Lobkovsky, R. H. Grubbs, *Angew. Chem. Int. Ed.* **1999**, *38*, 2741.

[12] Z. Gross, N. Galili, I. Saltsman, *Angew. Chem. Int. Ed.* **1999**, *38*, 1427.

[13] H. Maeda, A. Osuka, Y. Ishikawa, I. Aritome, Y. Hisaeda, H. Furuta, *Org. Lett.* **2003**, *5*, 1293.

[14] J.-P. Sauvage, *Acc. Chem. Res.* **1990**, *23*, 319.

[15] Z. Xu, M. Kahr, K. L. Walker, C. L. Wilkins, J. S. Moore, *J. Am. Chem. Soc.* **1994**, *116*, 4537.

[16] C. Devadoss, P. Bharathi, J. S. Moore, *J. Am. Chem. Soc.* **1996**, *118*, 9635.

[17] J. S. Melinger, Y. Pan, V. D. Kleiman, Z. Peng, B. L. Davis, D. McMorrow, M. Lu, *J. Am. Chem. Soc.* **2002**, *124*, 12002.

[18] R. W. Wagner, J. S. Lindsey, *Pure & Appl. Chem.* **1996**, *68*, 1373.

[19] F. Li, S. I. Yang, Y. Ciringh, J. Seth, C. H. Martin III, D. L. Singh, D. Kim, R. R. Birge, D. F. Bocian, D. Holten, J. S. Lindsey, *J. Am. Chem. Soc.* **1998**, *120*, 10001.

[20] I. V. Sazanovich, C. Kirmaier, E. Hindin, L. Yu, D. F. Bocian, J. S. Lindsey, D. Holten, *J. Am. Chem. Soc.* **2004**, *126*, 2664.

[21] J.-Y. Shin, D. Dolphin, B. O. Patrick, *Crystal Growth & Design* **2004**, *4*, 659.

[22] B. J. Littler, M. A. Miller, C.-H. Hung, R. W. Wagner, D. F. O'Shea, P. D. Boyle, J. S. Lindsey, *J. Org. Chem.* **1999**, *64*, 1391.

III. Asymmetric α-Substituted Alkoxy Dipyrrins and Their Metal Complexes

3.1. Introduction

Asymmetrically-substituted dipyrromethanes and dipyrromethenes (dipyrrins) have been used extensively in the synthesis of porphyrins,[1-3] boron-dipyrrin (BODIPY) dyes,[4, 5] and supramolecular dimers and trimers.[6-9] *Meso*-substituted dipyrrins have been found to form discrete supramolecular structures.[10] Asymmetrically α-substituted *meso*-dipyrrin compounds and their corresponding metal complexes (Figure 3-1) have been prepared as precursors to some porphyrins, porphyrin derivatives, and have been isolated as side products during porphyrin syntheses.[11-15] The addition of alkoxy groups in the α-position of N-confused porphyrins has also been observed.[16-23] The α-position of dipyrrins and N-confused porphyrins is known to be reactive, undergoing transformations such as the addition of bromine,[24] Diels-Alder reactions,[25] and ring fusion.[24, 26] Polypyrrolic compounds with oxygen atoms in the α-position have been identified in several natural products and natural product derivatives[27] including, phycobilins,[28] phytochromes,[29] and bile pigments.[30, 31] More specifically, a highly α,β-substituted bile derivative was observed containing a methoxy ligand in the α-position.[32]

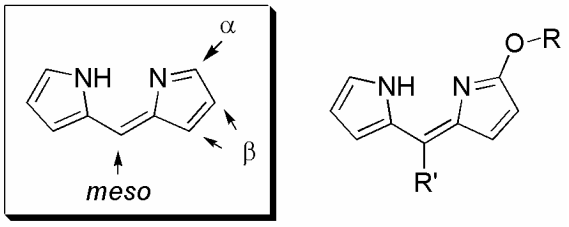

Figure 3-1. The α-, β-, and *meso*- positions of dipyrrins (left), and the generic structure of asymmetric α-alkoxy *meso*-substituted dipyrrins (right).

Herein, a new route to asymmetric α-substituted *meso*-dipyrrins is discovered and investigated. The compounds are formed by the addition of an alkoxy group in the α-position of a dipyrromethane during metal complexation (Figure 3-1). These compounds were initially detected as side products from the synthesis of metal dipyrrinato complexes. Further experiments reveal more favorable conditions to obtain the alkoxy dipyrrin, without the formation of any metal complexes. A series of asymmetric α-alkoxy dipyrrins, as well as metal complexes with cobalt(III) and zinc(II), are prepared and characterized. The synthetic route to asymmetric α-alkoxy dipyrrins described here may prove useful, upon further optimization, for the synthesis of natural products containing this functional motif.

3.2. Results and Discussion

3.2.1. Discovery of Asymmetric α-Alkoxy Dipyrrins

In ongoing synthetic efforts towards dipyrrin complexes, *meso*-substituted dipyrromethanes were prepared using standard methods,[33-36] followed by oxidation with 2,3-dichloro-5,6-dicyano-1,4-benzoquinone (DDQ) or 2,3,5,6-tetrachloro-1,4-benzoquinone (*p*-chloranil) to form dipyrromethenes in situ for use in the synthesis of dipyrrinato metal complexes.[37-39] During certain preparations, the formation of a new compound via TLC is observed (as a mobile yellow band), an apparent side product during metal complexation.

The initial observation of the new compound was from the reaction of 5-(4-

cyanophenyl)-4,6-dipyrromethene (4-cydpm), $Na_3[Co(NO_2)_6]$, and triethylamine in a 1:5 mixture of methanol and chloroform (Scheme 3-1), which was designed to form the complex $[Co(4\text{-cydpm})_3]$ but produced three products in modest yields (~25-35% each). The components of the mixture were separated by silica column chromatography for identification. The first product to elute from the column was isolated as a red solid and identified as the desired $[Co(4\text{-cydpm})_3]$ complex.[40] The second product to elute was isolated as a yellow solid and after extensive characterization determined to be an α-methoxy dipyrrin (α-OMe-4-cydpm). The last product to elute from the column was found to be a dark red solid, suggestive of a cobalt(III) dipyrrinato complex. NMR spectroscopy and mass spectrometry indicates that this was indeed a cobalt(III) complex containing an unusual ligand set of two unaltered dipyrrinato ligands and one α-methoxy dipyrrinato ligand ($[Co(\alpha\text{-OMe-4-cydpm})(4\text{-cydpm})_2]$). This heteroleptic cobalt(III) complex was the first indication that these α-alkoxy dipyrrins could act as metal chelators.

Scheme 3-1. Synthesis of α-OMe-4-cydpm, $[Co(4\text{-cydpm})_3]$, and $[Co(\alpha\text{-OMe-4-cydpm})(4\text{-cydpm})_2]$.

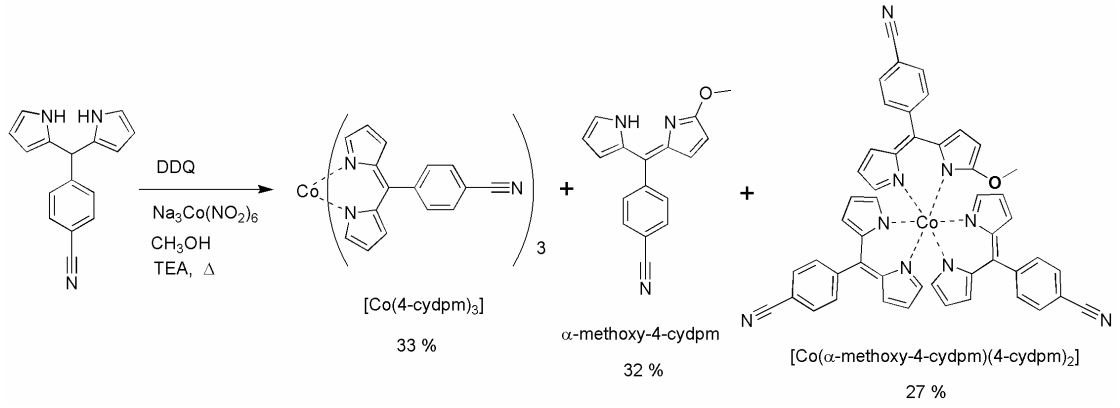

3.2.2. Exploration of the Reaction Conditions

Various reaction conditions were used to examine the formation of the asymmetric dipyrrin compounds. It was found that the formation of the alkoxy compounds do not require the presence of a base but do require a metal salt. The use of bases such as triethylamine promote the formation of the dipyrrinato metal complexes over the formation of the new alkoxy dipyrrins. In the absence of base, formation of the metal complex is minimized, with no effect on the formation of the alkoxy species. Reducing the quantity of metal salts to catalytic amounts (5% mol, $Na_3[Co(NO_2)_6]$) results in very slow reaction rates and lower yields (over the course of days at room temperature), therefore 0.3–0.4 equiv of the metal source is used (as employed in our initial discovery) and the reaction is heated to reflux. The modified reaction conditions provide a general approach to the preparation of asymmetric α-alkoxy dipyrrins, consisting of the oxidation of a dipyrromethane followed by in situ reaction of the resulting dipyrrin with a metal salt in the presence of an alcohol. While these conditions did not improve the yield of the asymmetric α-alkoxy dipyrrin (based on our original discovery, see Scheme 3-1), it did reduce the number of reaction products, such that the asymmetric α-alkoxy dipyrrin was the only major product formed, thereby facilitating purification by column chromatography. It is anticipated that a more comprehensive investigation of the reaction conditions may provide higher yielding synthetic preparations.

Further attempts to probe the reaction conditions by using alternative solvents,

alcohols, oxidants, metal salts, and dipyrrin precursors were also investigated. The results are summarized in Table 3-1. Non- or weakly-coordinating solvents such as methylene chloride, tetrahydrofuran, and benzene are tolerated, while more polar coordinating solvents such as ethyl acetate and acetonitrile inhibit product formation. The use of alcohol substrates other than methanol, such as ethanol, propanol, isopropanol, and benzyl alcohol could be successfully coupled to the dipyrrin moiety; however, the addition of the more sterically demanding isopropanol and benzyl alcohol products are very low yielding (as judged by TLC and electronic absorption analysis). No attempts to further optimize the reaction conditions for these bulky substrates were explored. Several metal salts were tested and found to be competent to perform the desired reaction (albeit in lower isolated yields), including $Mn(OAc)_2 \cdot 4H_2O$, $FeCl_3 \cdot 6H_2O$, and $[Co(pyr)_4Cl_2]Cl$. In contrast, $Cu(acac)_2$ fails to promote the reaction, which is likely due to the fact that dipyrrinato ligands rapidly form copper(II) complexes in the absence of added base (Chapter 2). We conclude the reaction scope is limited to metal ions that cannot readily form dipyrrinato complexes under the reaction conditions.

Table 3-1. Reaction conditions evaluated for the formation of α-alkoxy dipyrrins. Reactions deemed successful but not fully characterized were evaluated by TLC and electronic absorption spectroscopy (mec = methoxycarbonylphenyl, mt = methylthiophenyl, cy = cyanophenyl).

Dipyrromethane	Oxidant	Solvent	Alcohol	Metal Salt	Yield or Conversion
5-(4-mec)-4,6-dipyrromethane	DDQ	$CHCl_3$	MeOH	$Na_3[Co(NO_2)_6]$	19% yield
5-(4-mec)-4,6-dipyrromethane	*p*-chloranil	$CHCl_3$	MeOH	$Na_3[Co(NO_2)_6]$	35% yield
5-(4-cy)-4,6-dipyrromethane	DDQ	$CHCl_3$	MeOH	$Na_3[Co(NO_2)_6]$	15% yield
5-(4-phenyl)-4,6-dipyrromethane					detected by TLC
5-(4-mt)-4,6-dipyrromethane					detected by TLC
5-(4-nitrophenyl)-4,6-dipyrromethane					no product detected
5-(4-mec)-4,6-dipyrromethane	DDQ	CH_2Cl_2	MeOH	$Na_3[Co(NO_2)_6]$	detected by TLC
		THF			detected by TLC
		benzene			detected by TLC
		EtOAc			no product detected
		CH_3CN			no product detected
5-(4-mec)-4,6-dipyrromethane	DDQ	$CHCl_3$	EtOH	$Na_3[Co(NO_2)_6]$	35% yield
			PrOH		38% yield
			iPrOH		small amount detected by TLC
			BnOH		small amount detected by TLC
5-(4-mec)-4,6-dipyrromethane	DDQ	$CHCl_3$	MeOH	$Mn(OAc)_2{\cdot}4H_2O$	13% yield
				$FeCl_3{\cdot}6H_2O$	15% yield
				$[Co(pyr)_4Cl_2]Cl$	detected by TLC

3.2.3. Spectroscopic and Structural Features of α-Alkoxy Dipyrrins

Several of the α-alkoxy dipyrrin compounds have been fully characterized by mass spectrometry, electronic, infrared, and NMR spectroscopy. The electronic absorption spectrum of the α-alkoxy dipyrrin moiety has an absorbance maximum at

407 nm (attributed to a π-π* transition), which is shifted to higher energy when compared to that of the corresponding unsubstituted dipyrrins (~435 nm). The NMR spectrum of the α-alkoxy dipyrrins also clearly have distinguishing features from the parent unsubstituted dipyrrins. For example, the ^{1}HNMR spectra of α-OMe-4-cydpm (Figure 3-2) shows the expected five unique resonances for each of the pyrrolic protons between 6.0-7.2 ppm (compared with three resonances for the symmetric dipyrrin ligand). The hydrogen bound to the pyrrolic nitrogen atom, which is generally not observed in the NMR spectra of the dipyrrin precursors, is readily located at 12.1 ppm for α-OMe-4-cydpm.

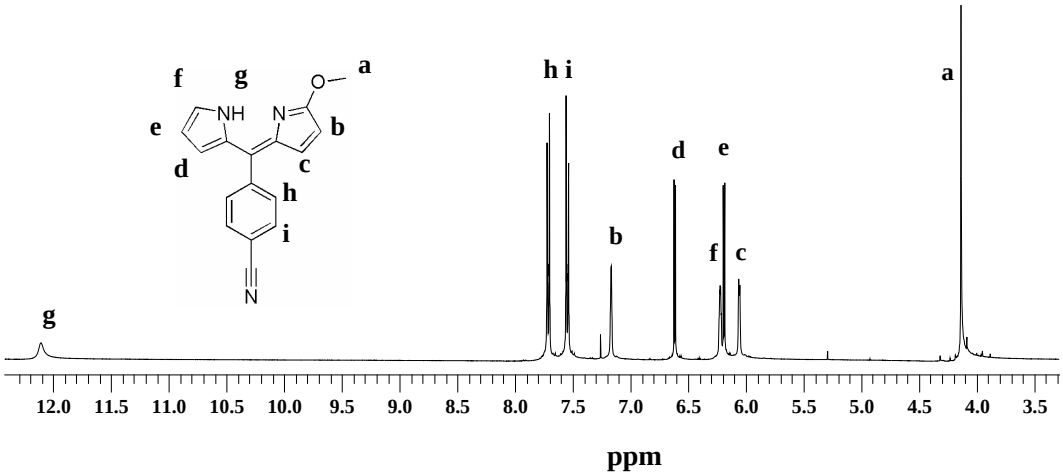

Figure 3-2. ^{1}HNMR of α-OMe-4-cydpm in $CDCl_3$ with full assignments.

In addition to complete spectroscopic characterization, the compound α-OMe-4-cydpm was crystallized and the structure was determined by X-ray diffraction (Figure 3-3). The crystal structure reveals several interesting features, which again distinguishes the compound from the parent unsubstituted dipyrromethenes. First, the structure unambiguously reveals the constitution of the molecule, showing the

methoxy substituent in the α-position of one of the pyrrolic subunits of the dipyrrin. Second, unlike the fully delocalized aromatic structure of unsubstituted dipyrrins, the crystal structure of α-OMe-4-cydpm reveals a distinct asymmetry in the dipyrrin chromophore bond lengths. The structure reveals alternating short and long C–C and C–N bond distances in the α-substituted pyrrolic ring: 1.30 Å (C9–N2), 1.45 Å (C8–C9), 1.35 Å (C7–C8), and 1.46 Å (C6–C7). Interestingly, this does not appear to disrupt the delocalized nature of the unsubstituted pyrrole ring, which has bond distances of 1.36 Å (N1–C1), 1.38 Å (C1–C2), 1.41 Å (C2–C3), and 1.39 Å (C3–C4). Also, the unsubstituted dipyrrins favor a planar arrangement of the pyrrole rings;[37, 38] however, in α-OMe-4-cydpm the two pyrrolic rings are twisted relative to one another. The dihedral torsion angle between C1, C3, C7, C9 (which should be 0° for a planar dipyrrin) is 15.35°. The out of plane twist does not agree with an earlier crystal structure of an asymmetric α-methoxy dipyrrin; however, the unequivalent bond lengths agrees with this earlier structure.[32] Finally, the nitrogen-bound pyrrolic hydrogen atom (H1N), typically bound equally by both pyrrole rings in an unsubstituted dipyrrin, is clearly identified in the electron density difference map, where it is localized on the nitrogen atom of the unmodified pyrrole ring (Figure 3-3). This may explain why this proton was readily observed by ^{1}HNMR, and indicates the alkoxy group sufficiently changes the basicity of the pyrrolic nitrogen atoms to favor a single tautomeric form.

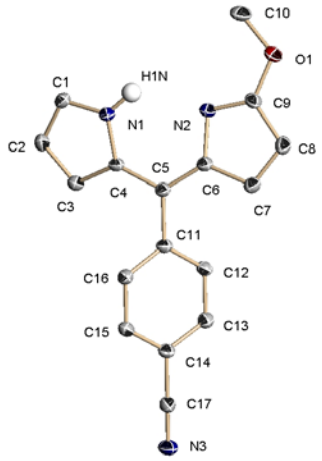

Figure 3-3. Structural diagram of α-OMe-4-cydpm with full atom numbering scheme (ORTEP, 50% probability ellipsoids). Hydrogen atoms (except for pyrrolic hydrogen) have been omitted for clarity.

3.2.4. α-Alkoxy Dipyrrinato Metal Complexes

As described earlier, an α-alkoxy dipyrrin demonstrated the capacity to bind cobalt(III) in the reaction mixture from which the compound was first identified. A complex containing a single α-OMe-4-cydpm and two 4-cydpm ligands ([Co(α-OMe-4-cydpm)(4-cydpm)$_2$]) was isolated from the mixture of products. The cobalt(III) complex was characterized by high-resolution mass spectrometry, ^{1}HNMR, electronic, and infrared spectroscopy. The α-methoxy substituent was found to significantly perturb the ligand-to-metal charge transfer (LMCT) band relative to the unsubstituted dipyrrinato complexes. As shown in Figure 3-4, the electronic absorbance spectra of the unsubstituted and α-methoxy-substituted dipyrrinato cobalt(III) complexes are easily distinguishable. The unsubstituted homoleptic complex [Co(4-cydpm)$_3$] has absorbance maxima at 469 and 506 nm, while the heteroleptic methoxy-substituted

[Co(α-OMe-4-cydpm)(4-cydpm)$_2$] has an absorbance maximum at 490 nm (Figure 3-4). Therefore, even though the complex [Co(α-OMe-4-cydpm)(4-cydpm)$_2$] contains only a single modified ligand, it is still readily distinguished from the unsubstituted cobalt(III) complex by absorption spectroscopy.

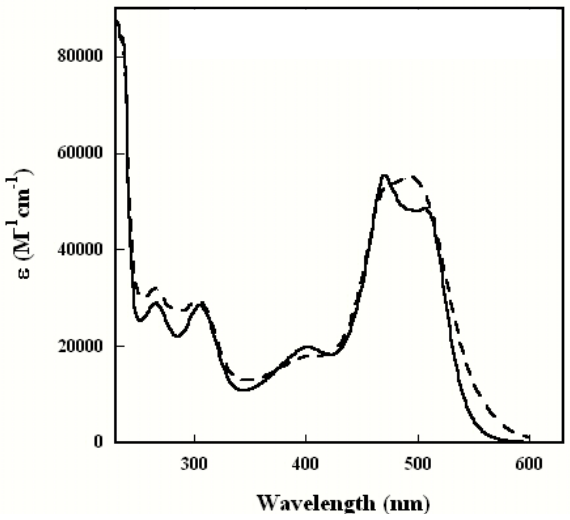

Figure 3-4. Electronic absorption spectra for [Co(4-cydpm)$_3$] (—) and [Co(α-OMe-4-cydpm)(4-cydpm)$_2$] (---) in CH_2Cl_2.

The presence of the α-OMe-4-cydpm ligand in [Co(α-OMe-4-cydpm)(4-cydpm)$_2$] also has a pronounced effect on the NMR spectra of the complex (Figure 3-5). The homoleptic metal dipyrrin complex [Co(4-cydpm)$_3$], is of the point group D_3 and the dipyrrin ligands are symmetry-related, therefore exhibiting chemical shifts readily assigned to a single ligand type with three resonances for the dipyrrin units from 6.0-7.0 ppm, and two resonances for the *meso*-phenyl rings from 7.0-8.0 ppm. For the heteroleptic [Co(α-OMe-4-cydpm)(4-cydpm)$_2$] complex, the symmetry is reduced to the C_s point group and the dipyrrin ligands are no longer symmetry-related.

Almost every dipyrrin proton on each dipyrrin ligand exhibits a unique chemical shift in the ^{1}HNMR spectra as can be seen by the numerous resonances from 6.0-7.0 ppm. The resonances appear as a combination of singlets, associated with the α-proton, and doublets associated with the β-protons. The phenyl protons of all three ligands also exhibit a variety of unique chemical shifts as can be seen by the multiplets at 7.4-7.8 ppm. All dipyrrin protons, phenyl protons, and methoxy protons correspond to a relative integration of 18, 12, and 3 protons respectively, showing that the compound contains only one methoxy substituted dipyrrin ligand per metal complex.

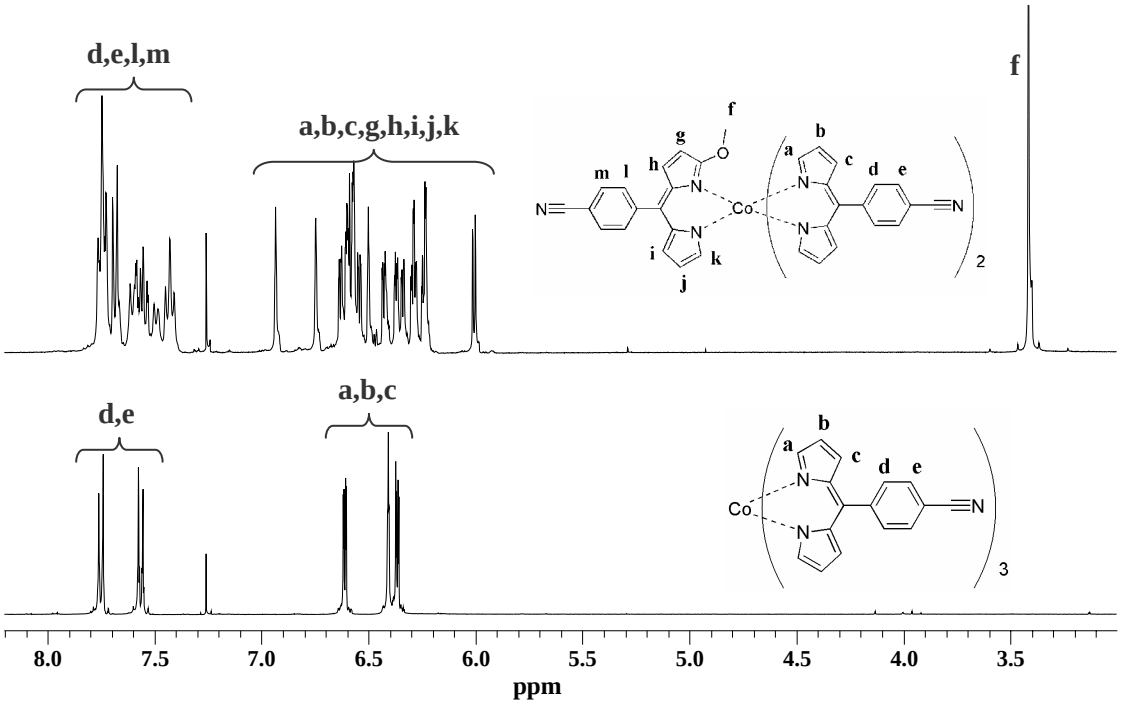

Figure 3-5. ^{1}HNMR of [Co(α-OMe-4-cydpm)(4-cydpm)$_2$] (top) and [Co(4-cydpm)$_3$] (bottom) in $CDCl_3$.

A similar heteroleptic cobalt(III) complex, [Co(α-OMe-4-mecdpm)(4-mecdpm)$_2$] (4-mecdpm = 5-(4-methoxycarbonylphenyl)-4,6-dipyrromethene), was

also obtained under the same reaction conditions as described for [Co(α-OMe-4-cydpm)(4-cydpm)$_2$]. The second cobalt(III) complex was characterized by mass spectrometry and electronic absorption spectroscopy. Attempts to prepare homoleptic tris-chelate cobalt(III) complexes with three α-methoxy substituted ligands were unsuccessful, likely due to steric limitations imposed by the α-methoxy substitutents.

In an attempt to prepare a homoleptic metal complex with an α-alkoxy dipyrrinato ligand, it was anticipated that a four-coordinate metal ion such as zinc(II) would better accommodate the sterics of this ligand system. Indeed, metal complexes of zinc(II) with asymmetric dipyrrins have been reported in the literature.[13, 15] The combination of α-OMe-4-mecdpm, $Zn(OAc)_2{\cdot}2H_2O$, and triethylamine in a chloroform/methanol mixture at room temperature generated the desired zinc(II) dipyrrin complex, which was isolated by crystallization after slow evaporation of the reaction mixture. Unlike other zinc(II) dipyrrinato complexes studied in our laboratory, [Zn(α-OMe-4-mecdpm)$_2$] was not stable to purification by column chromatography;[37, 39] exposure of [Zn(α-OMe-4-mecdpm)$_2$] to silica regenerated the free ligand. Electronic absorption spectroscopy confirms the formation of a zinc(II) complex with an absorption maximum at 486 nm (compared to the ligand α-OMe-4-cydpm at 407 nm, and other zinc(II) dipyrrins at 482-486 nm).[39]

[Zn(α-OMe-4-mecdpm)$_2$] was characterized by mass spectrometry, NMR, electronic, and infrared spectroscopy. Single crystals were also obtained and X-ray structural analysis confirmed the formation of the desired complex (Figure 3-6). The zinc(II) center is four-coordinate with two dipyrrin ligands and Zn–N bond distances

of 1.95-2.01 Å. The geometry of an ideal tetrahedral zinc(II) metal center would place the chelators mutually perpendicular to one another with torsion (dihedral) angles of 90°[41] and interligand L–M–L (L = ligand, M = metal) bond angles of 109.5°.[42] However, upon close examination of the [Zn(α-OMe-4-mecdpm)$_2$] structure, several unusual features not seen in other zinc(II) dipyrrinato complexes are found. For [Zn(α-OMe-4-mecdpm)$_2$], the torsion angles between the two ligands are 76° and 113°, and the interligand N1–Zn–N3 and N2–Zn–N4 angles are 119° and 99°, respectively (Figure 3-7). Because two of the bond angles in [Zn(α-OMe-4-mecdpm)$_2$] are fixed due to the bidentate ligands, the two other bond angles will be distorted from the ideal 109.5°, but should be identical to each other; however, they are different, making the complex quite distorted from the ideal geometry. The complex is distorted such that the two methoxy groups are brought close to each other in a *cis* fashion. In comparison, a previously reported α,β-unsubstituted zinc(II) dipyrrin complex was much closer to the ideal angles with torsion angles between the two ligands of 80°-90°, and L–Zn–L bond angles of 119-121°.[39] The dipyrrin moieties of each ligand in [Zn(α-OMe-4-mecdpm)$_2$] are nearly planar with dihedral torsion angles of 7.4° and 6.3°, which is closer to planarity then the free ligand (vide supra), but are more distorted then other reported dipyrrinato complexes.[37, 38, 43]

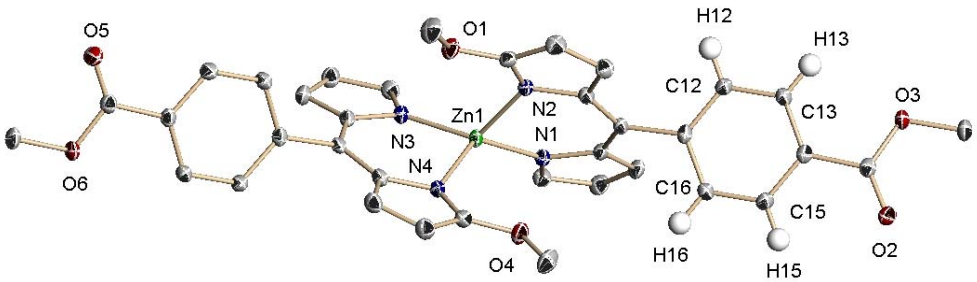

Figure 3-6. Structural diagram of [Zn(α-OMe-4-mecdpm)$_2$] with a partial atom numbering scheme (ORTEP, 50% probability ellipsoids). Most hydrogen atoms have been omitted for clarity.

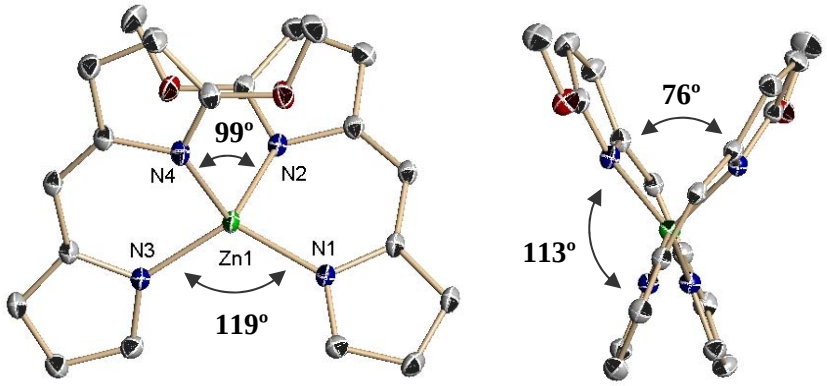

Figure 3-7. [Zn(α-OMe-4-mecdpm)$_2$] metal core viewed along two different off-axis directions with partial atom numbering schemes (ORTEP, 50% probability ellipsoids). The figure on the left displays the two bond angles (L–M–L) and the figure on the right displays the two torsion angles. The *meso*-phenyl ring and hydrogen atoms have been removed for clarity.

3.2.5. Solution Dynamics of [Zn(α-OMe-4-mecdpm)$_2$]

Upon close examination of the ^{1}HNMR spectrum of [Zn(α-OMe-4-mecdpm)$_2$], the resonances associated with phenyl protons H12 and H16 (Figure 3-6) appear as a doublet of doublets (Figure 3-8). This is in contrast to the same protons in the free ligand and of other metal dipyrrinato complexes where these protons appear as a

doublet.[37-39] This observation indicates that the highly distorted, *cis* geometry observed in the X-ray structure of [Zn(α-OMe-4-mecdpm)$_2$] is maintained in solution. The *cis* configuration of the ligands around the metal center results in two different chemical environments for the protons H12 and H16 (Figure 3-6) on either side of the *meso*-phenyl substituent. The chemical inequivalence of these protons was used as a probe for inversion of the ligand geometry about the zinc(II) center. Using variable temperature NMR (Figure 3-8), as the temperature was increased, the doublets of H12 and H16 coalesced at a $T_c \approx 86$ °C (359 K). This corresponds to a free energy of activation of $\Delta G^{\ddagger} = 72.4$ kJ mol^{-1} (calculated according to the formula $\Delta G^{\ddagger} = (19.13 \times 10^{-3})T_c(9.62 + \log T_c - \log \Delta\nu)$) for interconversion around the zinc(II) center between the *cis* and *trans* structural isomers.[44] The distal phenyl protons H13 and H15 (Figure 3-6) also undergo a less pronounced splitting, which also coalesce at elevated temperatures. Furthermore, two unique resonances are observed in the ^{13}CNMR spectrum of [Zn(α-OMe-4-mecdpm)$_2$] for the phenyl carbon atoms C12 and C16 (131.6 and 131.5 ppm, respectively, Figure 3-11), also coalescing at elevated temperatures, consistent with the solid-state structure and solution dynamics of the complex.

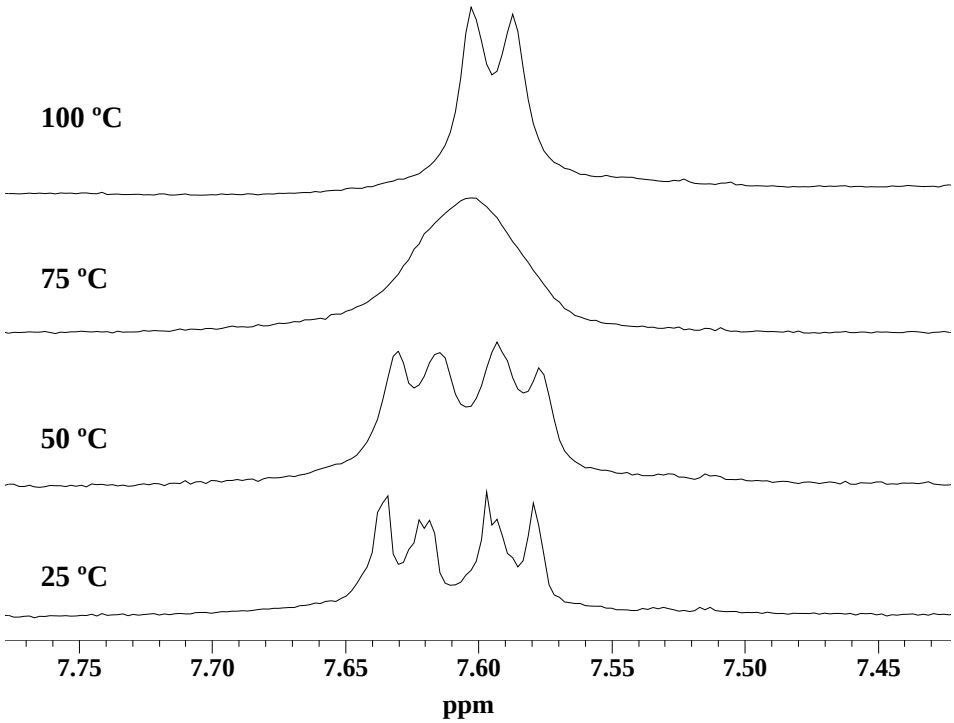

Figure 3-8. Variable temperature ^{1}HNMR spectra of the phenyl protons H12 and H16 (see Figure 3-6) of [Zn(α-OMe-4-mecdpm)$_2$] in d^6-DMSO. The resonances coalesce upon heating, indicative of a *cis*-to-*trans* interconversion of the ligands around the zinc(II) ion.

3.2.6. Details of the Reaction

Further exploration of the reaction conditions reveals the essential components involved in the formation of the α-alkoxy dipyrrins. When the *purified* dipyrrin is combined with a metal salt in the presence of an alcohol, the α-addition does not occur. Upon the addition of an equivalent of DDQ to the oxidized dipyrrin, metal salt, and alcohol, the alkoxy addition still does not occur. Because oxidation of all dipyrromethanes would reduce the DDQ to 2,3-dichloro-5,6-dicyanohydroquinone, the hydroquinone would be present in the reaction mixture after oxidation and during the metal complex formation. To determine the necessity of the hydroquinone,

2,3,5,6-tetrachlorohydroquinone (the reduced form of *p*-chloranil) was added to the reaction mixture containing pure 5-(4-methoxycarbonylphenyl)-4,6-dipyrromethene, $Na_3[Co(NO_2)_6]$, and methanol. Interestingly, the methoxy compound was formed, showing that the hydroquinone is required for the alkoxy addition to occur (Scheme 3-2).

Scheme 3-2. Detailed synthesis of the alkoxy α-substituted dipyrromethenes involving the hydroquinone.

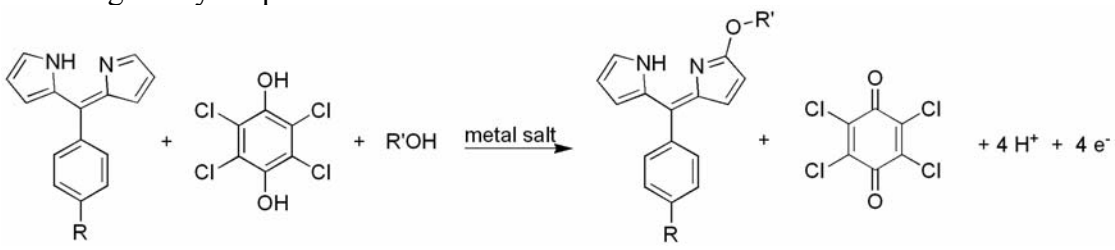

The contribution of the hydroquinone in the formation of the α-substituted dipyrrins is consistent with a mechanism proposed by Dolphin and coworkers involving an alkoxy addition to an N-confused porphyrin (Scheme 3-3).[16] The reaction involved the addition of $NaOCH_3$ and DDQ to an N-confused porphyrin in a mixture of methylene chloride/methanol, forming a methoxy α-substituted N-confused porphyrin in 9% yield. In comparison to their mechanism, the re-oxidized hydroquinone (*p*-chloranil) was isolated from the reaction mixture. However, in contrast to their reaction conditions and proposed mechanism, a strong nucleophile such as $NaOCH_3$ was not needed or a second equivalent of DDQ to form the final product. 2,3,5,6-Tetrachlorohydroquinone was also able to be used, rather than 2,3-

dichloro-5,6-dicyanohydroquinone. Therefore despite some similarities, the addition of an alkoxy group to dipyrromethenes described here does not appear undergo the same mechanism proposed by Dolphin.

Osuka and Furuta have also isolated a variety N-confused porphyrins that involved the addition or substitution of an methoxy or ethoxy group in the α-position both during and after the formation of certain porphyrins (Scheme 3-3).[17-23] The additions have been observed under a variety of reaction conditions, and no mechanism has been proposed.

Scheme 3-3. Synthesis of methoxy-substituted N-confused porphyrin (top) and ethoxy-substituted N-confused porphyrin (bottom).

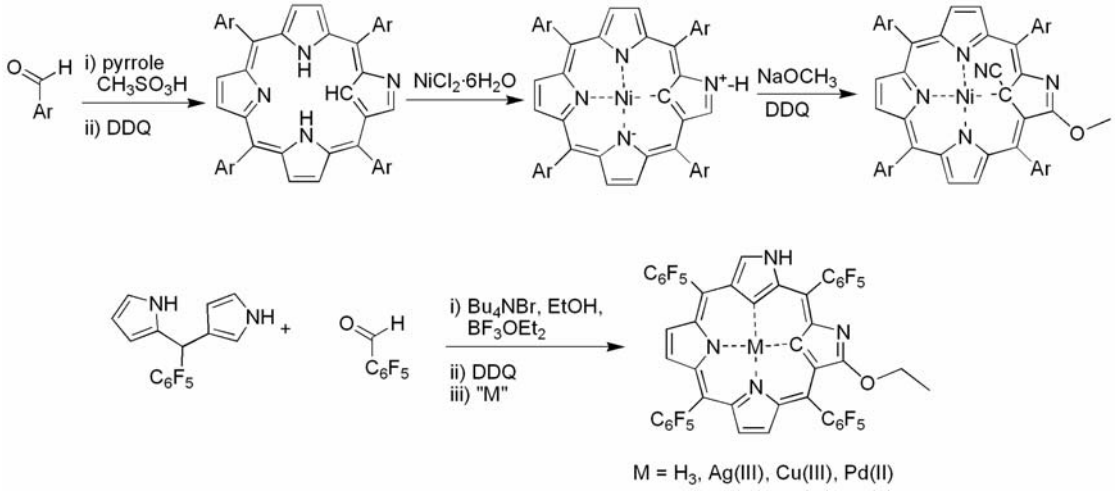

3.3. Conclusions

The α-alkoxy substitution of an imine mediated by a hydroquinone and metal salt has not been observed in the literature outside of porphyrin derivatives. The

formation of α-alkoxy dipyrrins has been shown to occur with a variety of alcohols and dipyrrins, using non-coordinating solvents with metal salts of manganese(II), iron(III), and cobalt(III). The presence of a hydroquinone has shown to be vital to the formation if the compounds. The synthesis of both hetero- and homoleptic metal complexes has been described and their structure has been probed both in solution and in the solid state.

The potential utility of this synthetic methodology could be explored further by optimization and exploration of the reaction conditions. The fluorescence of the alkoxy-inserted dipyrrin ligands also could be determined. Once the effect of the alkoxy ligand has been determined, its use in practical applications such as fluorescent tags can be explored.

3.4. Experimental Section

General Procedures/Methods: Unless otherwise noted, starting materials were obtained from commercial suppliers and used without further purification. Pyrrole was freshly distilled. Elemental analyses were performed at NuMega Resonance Labs, San Diego, California. $^{1}H/^{13}C$NMR spectra were recorded on a Varian FT-NMR spectrometer running at 400 MHz or 500 MHz at the Department of Chemistry and Biochemistry, University of California, San Diego. Infrared spectra were collected on a Mattson Research Series FT-IR instrument (using KBr pellets, laboratory of Prof. Clifford P. Kubiak) at the Department of Chemistry and Biochemistry, University of California, San Diego. UV-Visible spectra were recorded

using a Perkin-Elmer Lambda 25 spectrophotometer with the UVWinLab 4.2.0.0230 software package. Mass spectra were acquired at the Small Molecule Mass Spectrometry Facility located in the Department of Chemistry and Biochemistry, University of California, San Diego. A ThermoFinnigan LCQDECA mass spectrometer was used for the ESI or APCI analysis, and the data were analyzed using the Xcalibur software suite. A ThermoFinnigan MAT 900XL mass spectrometer was used to acquire the data for the high resolution mass spectra (HRMS).

Complex Synthesis and Characterization:

[5-(4-cyanophenyl)-1-methoxy-4,6-dipyrrinato]Bis[5-(4-cyanophenyl)-4,6-dipyrrinato]Co(III) [Co(α-OMe-4-cydpm)(4-cydpm)$_2$]. 5-(4-Cyanocarbonyl phenyl)-4,6-dipyrromethane (0.20 g, 0.81 mmol) was dissolved in 150 mL $CHCl_3$ and stirred in an ice bath. DDQ (0.20 g, mmol) was dissolved in benzene (150 mL) and added slowly dropwise. The solvent was then evaporated and the resulting dark residue was redissolved in a 1:1 mixture of $CHCl_3$/MeOH (100 mL). $Na_3[Co(NO_2)_6]$ (0.11 g, 0.27 mmol) dissolved in a 1:1 mixture of H_2O/MeOH (6 mL). Triethylamine (1 mL) was added to the solution. The resulting mixture was heated to 70 ºC overnight. The solution was evaporated to dryness and the product was purified by column chromatography (SiO_2; 3:2 to 9:1 CH_2Cl_2:hexanes) to afford three products: α-OMe-4-cydpm (yellow film, 0.064 g, 32% yield), [Co(4-cydpm)$_3$][40] (orange solid, 0.070 g, 33% yield), and **[Co(α-OMe-4-cydpm)(4-cydpm)$_2$]** (red solid, 0.060 g, 27% yield). [**Co(α-OMe-4-cydpm)(4-cydpm)$_2$]:** ^{1}HNMR ($CDCl_3$ 400 MHz, 25 ºC): δ

3.41 (s, 3H), 6.00 (d, 1H, *J* = 4.8 Hz), 6.24 (m, 2H), 6.29 (m, 2H), 6.34 (m, 1H), 6.37 (m, 1H), 6.42 (m, 1H), 6.50 (s, 1H), 6.55 (d, 1H, *J* = 4.8 Hz), 6.57 (m, 2H), 6.60 (m, 2H) 6.63 (d, 2H, *J* = 4.4 Hz), 6.75 (s, 1H), 6.94 (s, 1H), 7.43 (t, 2H, *J* = 8.8 Hz), 7.49-7.62 (m, 4H), 7.68 (d, 2H, *J* = 8.8 Hz), 7.73-7.77 ppm (m, 4H). APCI-MS: *m/z* 821.85 $[M+H]^+$. HR-FABMS: *m/z* 822.2146 $[M+H]^+$ (Calcd *m/z* 822.2135). λ_{max} (CH_2Cl_2 solution): 236, 266, 304, 408, 493 nm. IR (thin film CH_2Cl_2): *v* 2926, 2857, 2229, 1566, 1381, 1347, 1249, 1033, 998, 812 cm^{-1}.

5-(4-cyanophenyl)-1-methoxy-4,6-dipyrromethene (α-OMe-4-cydpm). 5-(4-Cyanophenyl)-4,6-dipyrromethane[33] (0.20 g, 0.81 mmol) was dissolved in 100 mL $CHCl_3$ and stirred in an ice bath. DDQ (0.18 g, 0.81 mmol) was dissolved in 100 mL benzene and added dropwise over ~1 h. After addition, the reaction mixture was then evaporated to dryness and the resulting dark residue was redissolved in 25 mL MeOH and 25 mL $CHCl_3$. $Na_3[Co(NO_2)_6]$ (0.11 g, 0.27 mmol), dissolved in 2 mL H_2O and 1 mL MeOH, was added to the solution. The resulting mixture was heated to reflux while stirring overnight. The solution was evaporated to dryness and the product was purified by column chromatography (SiO_2; 4:1 CH_2Cl_2:hexanes) to afford a yellow solid. Yield: 18% (0.041 g). ^{1}HNMR ($CDCl_3$ 400 MHz, 25 °C): δ 4.14 (s, 3H), 6.06 (m, 1H), 6.19 (d, 1H, *J* = 4.4 Hz), 6.22 (m, 1H), 6.62 (d, 1H, *J* = 4.4 Hz), 7.17 (bs, 1H), 7.56 (d, 2H, *J* = 8.0 Hz), 7.72 (d, 2H, *J* = 8.0 Hz), 12.11 ppm (bs, 1H, NH). ^{13}CNMR ($CDCl_3$ 100 MHz, 25 °C): δ 56.0, 110.3, 112.0, 117.4, 117.8, 118.4, 124.6, 131.0, 131.3, 131.6, 136.9, 141.9, 143.6, 175.3 ppm. APCI-MS: *m/z* 276.117 $[M+H]^+$. HR-FABMS: *m/z* 275.1054 $[M]^+$ (Calcd *m/z* 275.1053). λ_{max} (CH_2Cl_2 solution) = 235,

264, 285, 407 nm. IR (thin film CH_2Cl_2): *v* 2936, 2229, 1598, 1557, 1532, 1406, 1377, 1290, 1122, 1089, 1041, 937, 804, 775, 746, 691 cm^{-1}.

5-(4-methoxycarbonylphenyl)-1-methoxy-4,6-dipyrromethene (α-OMe-4-mecdpm). The same procedure was used as in the synthesis of α-OMe-4-cydpm, starting from 5-(4-methoxycarbonylphenyl)-4,6-dipyrromethane[43] (0.20 g, 0.71 mmol) to afford a yellow film. Yield: 19% (0.043 g). ^{1}HNMR ($CDCl_3$ 400 MHz, 25 °C): δ 3.96 (s, 3H), 4.13 (s, 3H), 6.11 (bd, 1H, *J* = 3.2 Hz), 6.17 (d, 1H, *J* = 4.8 Hz), 6.21 (bt, 1H, *J* = 3.2 Hz), 6.68 (d, 1H, *J* = 4.4 Hz), 7.15 (bs, 1H), 7.53 (d, 2H, *J* = 8.4 Hz), 8.10 (d, 2H, *J* = 8.4 Hz), 12.15 ppm (bs, 1H, NH). ^{13}CNMR ($CDCl_3$ 100 MHz, 25 °C): δ 52.2, 55.9, 110.3, 117.3, 117.7, 124.5, 128.8, 129.9, 130.8, 132.2, 132.4, 137.5, 142.0, 143.7, 166.8, 175.3 ppm. ESI-MS: *m/z* 309.15 $[M+H]^+$. HR-FABMS: *m/z* 309.1239 $[M+H]^+$ (Calcd *m/z* 309.1234). λ_{max} (CH_2Cl_2 solution) = 236, 289, 407 nm. IR (thin film CH_2Cl_2): *v* 3446, 2950, 1713, 1598, 1557, 1545, 1406, 1392, 1376, 1288, 1276, 1115, 1090, 1041, 764, 745, 718 cm^{-1}.

5-(4-methoxycarbonylphenyl)-1-ethoxy-4,6-dipyrromethene (α-OEt-4-mecdpm). The same procedure was used as in the synthesis of α-OMe-4-cydpm, starting from 5-(4-methoxycarbonylphenyl)-4,6-dipyrromethane[43] (0.20 g, 0.71 mmol) and ethanol (10 mL). Yield: 35% (0.081 g). ^{1}HNMR ($CDCl_3$ 400 MHz, 25 °C): δ 1.50 (t, 3H, *J* = 7.2 Hz), 3.96 (s, 3H), 4.53 (q, 2H, *J* = 7.6 Hz, *J* = 6.8 Hz), 6.11 (bd, 1H, *J* = 3.6 Hz), 6.16 (d, 1H, *J* = 4.4 Hz), 6.21 (bs, 1H), 6.67 (d, 1H, *J* = 4.8 Hz), 7.14 (bs, 1H), 7.53 (d, 2H, *J* = 8.8 Hz), 8.10 (d, 2H, *J* = 8.4 Hz), 12.14 ppm (bs, 1H, NH). ^{13}CNMR ($CDCl_3$ 100 MHz, 25 °C): δ 14.5, 52.2, 64.6, 110.2, 117.5, 117.6,

124.3, 128.8, 129.9, 130.8, 132.1, 132.2, 137.3, 142.0, 143.9, 166.8, 174.7 ppm. ESI-MS: *m/z* 323.05 $[M+H]^+$. HR-FABMS: *m/z* 323.1388 $[M+H]^+$ (Calcd *m/z* 323.1390). λ_{max} (CH_2Cl_2 solution) = 237, 290, 407 nm. IR (thin film CH_2Cl_2): *v* 3446, 3301, 2976, 2950, 1724, 1597, 1549, 1531, 1406, 1392, 1378, 1346, 1286, 1257, 1112, 1090, 1039, 764, 741, 724 cm^{-1}.

5-(4-methoxycarbonylphenyl)-1-propoxy-4,6-dipyrromethene (α-OPr-4-mecdpm). The same procedure was used as in the synthesis of α-OMe-4-cydpm, starting from 5-(4-methoxycarbonylphenyl)-4,6-dipyrromethane[43] (0.20 g, 0.71 mmol) and propanol (10 mL). Yield: 38% (0.091 g). ^{1}HNMR ($CDCl_3$ 400MHz, 25 °C): δ 1.09 (t, 3H, *J* = 7.6 Hz), 1.90 (m, 2H), 4.43 (t, 2H, *J* = 6.4 Hz), 6.11 (bd, 1H, *J* = 3.2 Hz), 6.18 (d, 1H, *J* = 4.8 Hz), 6.21 (bs, 1H), 6.68 (d, 1H, *J* = 4.8 Hz), 7.15 (bs, 1H), 7.53 (d, 2H, *J* = 8.4 Hz), 8.10 (d, 2H, *J* = 8.0 Hz), 12.16 ppm (bs, 1H, NH). ^{13}CNMR ($CDCl_3$ 100MHz, 25°C): δ 10.5, 22.2, 52.1, 70.3, 110.1, 117.5, 117.6, 124.3, 128.8, 129.8, 130.8, 132.0, 132.2, 137.2, 142.0, 143.9, 166.7, 174.9 ppm. FAB-MS: *m/z* 336.2 $[M]^+$. HR-FABMS: *m/z* 336.1459 $[M]^+$ (Calcd *m/z* 336.1468). λ_{max} (CH_2Cl_2 solution) = 237, 289, 407 nm. IR (thin film): *v* 3278, 2964, 2953, 2881, 1725, 1597, 1549, 1532, 1407, 1364, 1338, 1286, 1279, 1101, 1091, 1040, 960, 763, 742, 725 cm^{-1}.

Bis[5-(4-methoxycarbonylphenyl)-1-methoxy-4,6-dipyrrinato]Zn(II) [Zn(α-OMe-4-mecdpm)$_2$]. α-OMe-4-mecdpm (0.172 g, 0.558 mmol) was dissolved in 25 mL of $CHCl_3$ and 25 mL of MeOH. $Zn(OAc)_2{\cdot}2H_2O$ was dissolved in 5 mL of MeOH and added to the solution. Triethylamine (0.5 mL) was added and the reaction

was stirred overnight. The solution was then slowly evaporated to yield bright orange crystals, which were washed 3 times with 5 mL of MeOH. Yield: 77% (0.146 g). ^{1}HNMR ($CDCl_3$ 400 MHz, 25 °C): δ 3.76 (s, 6H), 3.98 (s, 6H), 6.00 (d, 2H, J = 4.4 Hz), 6.33 (d, 2H, J = 4.4 Hz), 6.41 (d, 2H, J = 3.6 Hz), 6.65 (d, 2H, J = 4.4 Hz), 7.37 (s, 2H), 7.60 (q, 4H, J = 5.2Hz, J = 7.6 Hz), 8.12 ppm (m, 4H). ^{13}CNMR ($CDCl_3$ 100 MHz, 25 °C): δ 52.3, 57.4, 103.9, 114.2, 127.4, 128.2, 128.3, 129.7, 130.7, 130.8, 134.1, 136.9, 138.1, 142.2, 143.5, 144.0, 166.7, 171.8 ppm. FAB-MS: *m/z* 678.4 $[M]^+$. HR-FABMS: *m/z* 678.1437 $[M]^+$ (Calcd. *m/z* 678.1451). λ_{max} (CH_2Cl_2 solution) = 240, 306, 486 nm. IR (thin film CH_2Cl_2): ν 3012, 3050, 2951, 2926, 2846, 1723, 1556, 1508, 1497, 1404, 1379, 1346, 1318, 1276, 1269, 1194, 1113, 1048, 1005, 962, 829, 763, 725 cm^{-1}.

3.5. Acknowledgment

Loi Do and Dr. Drew Murphy are acknowledged for some synthetic assistance and helpful discussions.

3.6. Appendix

X-ray Crystal Structure Determination

Details: Single crystals of each compound suitable for X-ray diffraction structural determination were mounted on quartz capillaries with Paratone oil and were cooled in a nitrogen stream on the diffractometer. Data were collected on either a Bruker AXS or a Bruker P4 diffractometer each equipped with area detectors. Peak

integrations were performed with the Siemens SAINT software package. Absorption corrections were applied using the program SADABS. Space group determinations were performed by the program XPREP. The structures were solved by either Patterson or direct methods and refined with the SHELXTL software package (Sheldrick, G. M. *SHELXTL vers. 5.1 Software Reference Manual*; Bruker AXS: Madison, WI, 1997). All hydrogen atoms were fixed at calculated positions with isotropic thermal parameters, and all non-hydrogen atoms were refined anisotropically unless otherwise noted.

Structure of α-OMe-4-cydpm. Orange blocks of α-OMe-4-cydpm suitable for X-ray diffraction structural determination were grown by evaporation from a solution of the compound dissolved in CH_2Cl_2 and hexanes. No solvent molecules were found co-crystallized with the compound. The hydrogen atom on the nitrogen (H1N) was found in the difference map, and the position was refined.

Structure of [Zn(α-OMe-4-mecdpm)$_2$]. Orange rods of [Zn(α-OMe-4-mecdpm)$_2$] suitable for X-ray diffraction structural determination were grown by evaporation from a solution of the complex dissolved in $CHCl_3$, MeOH, and triethylamine. No solvent molecules were found co-crystallized with the complex.

X-ray Crystal Structure Details for α-OMe-4-cydpm

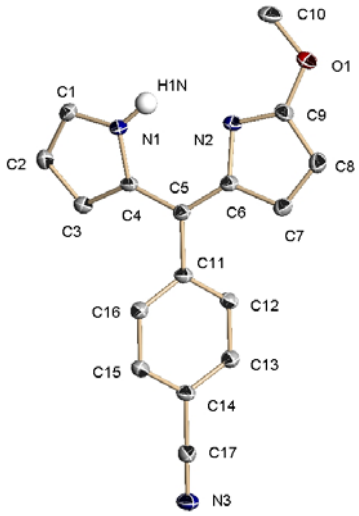

Figure 3-9. Structural diagram and labeling scheme of α-OMe-4-cydpm. Thermal ellipsoids at the 50% probability level. Hydrogen atoms have been omitted for clarity.

Table 3-2. Crystal Data for α-OMe-4-cydpm.

Empirical formula	$C_{17}H_{13}N_3O$	
Temperature	100(2) K	
Crystal system	Triclinic	
Space group	*P*-1	
Unit cell dimensions	a = 8.8386(9) Å	α = 63.7840(10)°
	b = 9.3207(9) Å	β = 68.1580(10)°
	c = 10.0246(10) Å	γ = 78.077(2)°
Volume	686.82(12) Å^3	
Z	2	
Crystal size	0.30 × 0.17 × 0.15 mm^3	
Reflections collected	5831	
Independent reflections	2979 [R(int) = 0.0182]	
Data / restraints / parameters	2979 / 0 / 195	
Goodness-of-fit on F^2	1.066	
Final R indices [I>2σ(I)]	$R1$ = 0.0455, $wR2$ = 0.1228	
R indices (all data)	$R1$ = 0.0507, $wR2$ = 0.1272	

X-ray Crystal Structure Details for [Zn(α-OMe-4-mecdpm)$_2$]

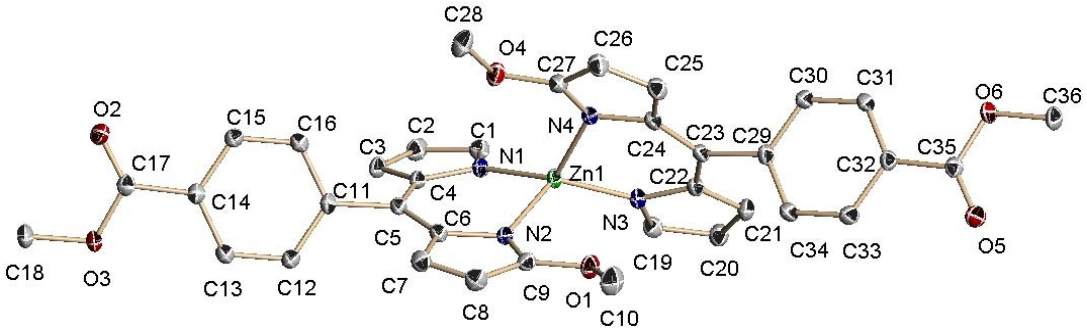

Figure 3-10. Structural diagram and labeling scheme of [Zn(α-OMe-4-mecdpm)$_2$]. Thermal ellipsoids at the 50% probability level. Hydrogen atoms have been omitted for clarity.

Table 3-3. Crystal Data for [Zn(α-OMe-4-mecdpm)$_2$].

Empirical formula	$ZnC_{36}H_{30}N_4O_6$	
Temperature	100(2) K	
Crystal system	Triclinic	
Space group	*P*-1	
Unit cell dimensions	a = 11.9083(7) Å	α = 69.4810(10)°
	b = 11.9234(7) Å	β = 88.6430(10)°
	c = 12.0192(7) Å	γ = 78.7560(10)°
Volume	1565.77(16) Å^3	
Z	2	
Crystal size	0.40 × 0.19 × 0.15 mm^3	
Reflections collected	13652	
Independent reflections	6804 [R(int) = 0.0155]	
Data / restraints / parameters	6804 / 0 / 428	
Goodness-of-fit on F^2	1.025	
Final R indices [I>2σ(I)]	R1 = 0.0293, wR2 = 0.0777	
R indices (all data)	R1 = 0.0310, wR2 = 0.0791	

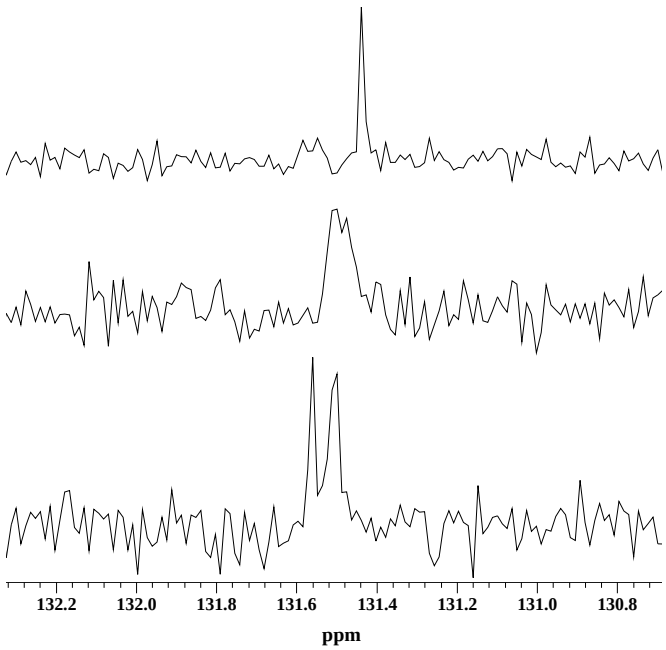

Figure 3-11. ^{13}CNMR of C12 and C16 (Figure 3-6) [Zn(α-OMe-4-mecdpm)$_2$] in *d*-DMSO at 25 °C (bottom), 50 °C (middle) and 100 °C (top). The two carbon atoms coalesce at elevated temperatures.

3.7. References

[1] D. M. Wallace, S. H. Leung, M. O. Senge, K. M. Smith, *J. Org. Chem.* **1993**, *58*, 7245.

[2] C.-H. Lee, F. Li, K. Iwamoto, J. Dadok, A. A. Bothner-By, J. S. Lindsey, *Tetrahedron* **1995**, *51*, 11645.

[3] P. D. Rao, B. J. Littler, G. R. Geier, J. S. Lindsey, *J. Org. Chem.* **2000**, *65*, 1084.

[4] M. Kollmannsberger, T. Gareis, S. Heinl, J. Breu, J. Daub, *Angew. Chem. Int. Ed.* **1997**, *36*, 1333.

[5] J. Karolin, L. B.-A. Johansson, L. Strandberg, T. Ny, *J. Am. Chem. Soc.* **1994**, *116*, 7801.

[6] Y. Zhang, A. Thompson, S. J. Rettig, D. Dolphin, *J. Am. Chem. Soc.* **1998**, *120*, 13537.

[7] A. Thompson, D. Dolphin, *Org. Lett.* **2000**, *2*, 1316.

[8] A. Thompson, S. J. Rettig, D. Dolphin, *Chem. Commun.* **1999**, 631.

[9] T. E. Wood, N. D. Dalgleish, E. D. Power, A. Thompson, X. Chen, Y. Okamoto, *J. Am. Chem. Soc.* **2005**, *127*, 5740.

[10] J. M. Sutton, E. Rogerson, C. J. Wilson, A. E. Sparke, S. J. Archibald, R. W. Boyle, *Chem. Commun.* **2004**, 1328.

[11] G. R. Geier, J. S. Lindsey, *J. Chem. Soc., Perkin Trans. 2* **2001**, 677.

[12] J.-P. Strachan, D. F. O'Shea, T. Balasubramanian, J. S. Lindsey, *J. Org. Chem.* **2000**, *65*, 3160.

[13] C. L. Hill, M. M. Williamson, *J. Chem. Soc., Chem. Commun.* **1985**, 1228.

[14] L. Simkhovich, I. Goldberg, Z. Gross, *Org. Lett.* **2003**, *5*, 1241.

[15] M. M. Williamson, C. M. Prosser-McCartha, J. S. Mukundan, C. L. Hill, *Inorg. Chem.* **1988**, *27*, 1061.

[16] Z. Xiao, B. O. Patrick, D. Dolphin, *Chem. Commun.* **2003**, 1062.

[17] H. Furuta, Y. Ishikawa, A. Osuka, T. Ogawa, *J. Am. Chem. Soc.* **1999**, *121*, 2945.

[18] H. Furuta, H. Maeda, A. Osuka, *J. Am. Chem. Soc.* **2000**, *122*, 803.

[19] K. Araki, H. Winnischofer, H. E. Toma, H. Maeda, A. Osuka, H. Furuta, *Inorg. Chem.* **2001**, *40*, 2020.

[20] Y. Ishikawa, A. Osuka, H. Furuta, *Angew. Chem. Int. Ed.* **2004**, *43*, 5077.

[21] H. Maeda, A. Osuka, H. Furuta, *Tetrahedron* **2004**, *60*, 2427.

[22] H. Furuta, H. Maeda, A. Osuka, M. Yasutake, T. Shinmyozu, Y. Ishikawa, *Chem. Commun.* **2000**, 1143.

[23] H. Maeda, A. Osuka, H. Furuta, *J. Am. Chem. Soc.* **2003**, *125*, 15690.

[24] H. Furuta, Y. Ishikawa, A. Osuka, T. Ogawa, *J. Am. Chem. Soc.* **2000**, *122*, 5748.

[25] Z. Xiao, B. O. Patrick, D. Dolphin, *Chem. Commun.* **2002**, 1816.

[26] H. S. Gill, I. Finger, I. Božidarevic, F. Szydlo, M. J. Scott, *New J. Chem.* **2005**, *29*, 68.

[27] G. Park, J. T. Tomlinson, M. S. Melvin, M. W. Wright, C. S. Day, R. A. Manderville, *Org. Lett.* **2003**, *5*, 113.

[28] S. I. Beale, J. Cornejo, *J. Biol. Chem.* **1991**, *266*, 22341.

[29] C. Fankhauser, *J. Biol. Chem.* **2001**, *276*, 11453.

[30] W. Rudiger, *Angew. Chem. Int. Ed.* **1970**, *9*, 473.

[31] H. Falk, *The Chemistry of Linear Oligopyrroles and Bile Pigments*, Springer-Verlag, Wien, **1989**.

[32] J. K. Dattagupta, E. F. Meyer Jr, D. L. Cullen, H. Falk, S. Gergely, *Acta Cryst.* **1983**, *C39*, 1384.

[33] P. D. Rao, S. Dhanalekshmi, B. J. Littler, J. S. Lindsey, *J. Org. Chem.* **2000**, *65*, 7323.

[34] C.-H. Lee, J. S. Lindsey, *Tetrahedron* **1994**, *50*, 11427.

[35] B. J. Littler, M. A. Miller, C.-H. Hung, R. W. Wagner, D. F. O'Shea, P. D. Boyle, J. S. Lindsey, *J. Org. Chem.* **1999**, *64*, 1391.

[36] J. K. Laha, S. Dhanalekshmi, M. Taniguchi, A. Ambroise, J. S. Lindsey, *Org. Process Res. Dev.* **2003**, *7*, 799.

[37] C. Brückner, V. Karunaratne, S. J. Rettig, D. Dolphin, *Can. J. Chem.* **1996**, *74*, 2182.

[38] C. Brückner, Y. Zhang, S. J. Rettig, D. Dolphin, *Inorg. Chim. Acta* **1997**, *263*, 279.

[39] L. Yu, K. Muthukumaran, I. V. Sazanovich, C. Kirmaier, E. Hindin, J. R. Diers, P. D. Boyle, D. F. Bocian, D. Holten, J. S. Lindsey, *Inorg. Chem.* **2003**, *42*, 6629.

[40] D. L. Murphy, M. R. Malachowski, C. Campana, S. M. Cohen, *Chem. Commun.* **2005**, 5506.

[41] S. Knapp, T. P. Keenan, X. Zhang, R. Fikar, J. A. Potenza, H. J. Schugar, *J. Am. Chem. Soc.* **1990**, *112*, 3452.

[42] P. Atkins, L. Jones, *Chemistry: Molecules, Matter, and Change*, 3rd ed., Freeman, New York, **1997**.

[43] S. M. Cohen, S. R. Halper, *Inorg. Chim. Acta* **2002**, *341*, 12.

[44] R. J. Abraham, P. Loftus, *Proton and Carbon-13 NMR Spectroscopy: An Integrated Approach*, Heyden, London, **1978**.

IV. Dipyrrin-Containing Coordination Polymers

4.1. Introduction

Coordination polymers have received a great deal of attention in recent years because they hold promise for developing novel magnetic, electronic, and functionalized materials.[1, 2] Unlike organic polymers, the monomeric units in coordination polymers are linked through metal coordination bonds rather than covalent bonds. Many recent studies have focused on creating coordination polymers with specific topologies and chemical properties.[3-9] One-dimensional coordination polymers can form topologies including zigzag, helical, and many others (Figure 4-1).

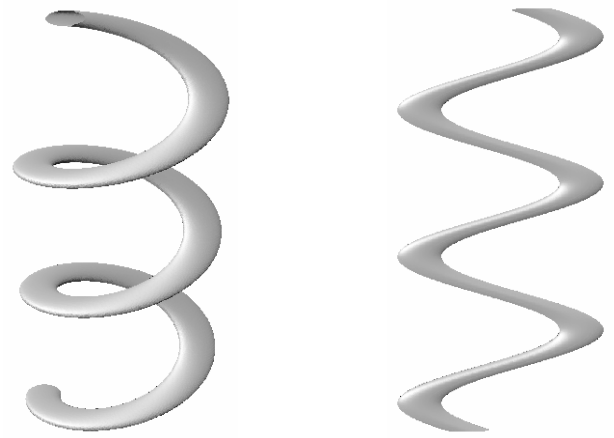

Figure 4-1. Cartoon representation of a helical (left) and zigzag (right) topology.

$Cu(acac)_2$ (acac = acetylacetonato) and $Cu(hfacac)_2$ (hfacac = hexafluoroacetylacetonato) have been bound to pyridine derivatives to form molecular complexes,[10-12] discrete supramolecular structures,[13, 14] and coordination polymers.[15-18] Herein, several coordination polymers and other supramolecular assemblies containing pyridine- and quinoline-substituted dipyrromethenes combined with fluorinated and unfluorinated copper(II) acac metal complexes are prepared and

studied. The coordination polymers are formed when a self-complementary, self-assembling building block contains a heteroatom donor group in the *meso*-position of the dipyrrin ligand, which binds to the axial position of a neighboring square planar metal center as the material is crystallized. This results in a square pyramidal copper(II) center and the formation of a coordination polymer (Figure 4-2). A variety of structures, from discrete complexes to zigzag and helical coordination polymers, are described. The metal complexes have been characterized by mass spectrometry, electronic absorption, and infrared spectroscopy. Most of the metal complexes have been characterized by single-crystal X-ray diffraction.

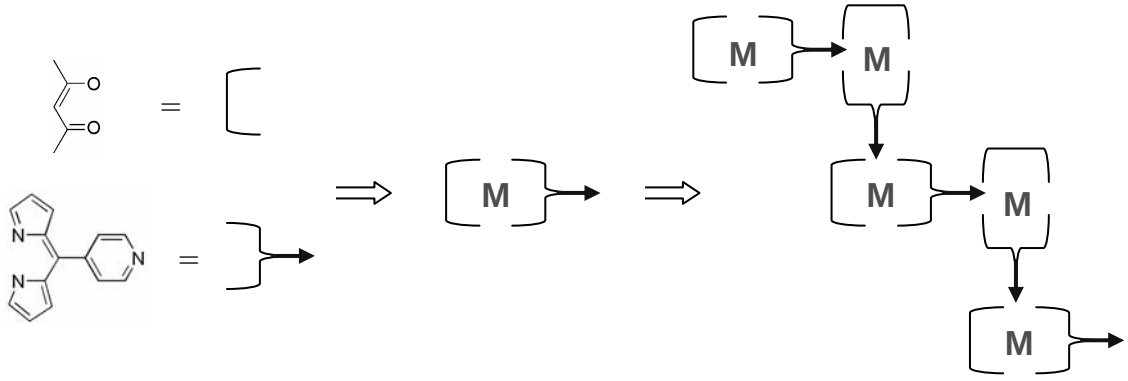

Figure 4-2. Cartoon representation of self-complimentary coordination polymer (right) formed by a dipyrrin ligand, acac ligand, and metal center (M = metal).

Previously, fluorine–fluorine interactions have been shown to drive the assembly of supramolecular materials.[19-21] Specifically, fluorination of an acac ligand has also previously been shown to have an effect on the assembly of compounds in the solid-state.[12] Overall, the formation of the dipyrrin coordination polymers described here is driven by fluorine–fluorine interactions, sterics around the

meso-donor atom, and the electronic nature of the copper(II) center.

4.2. Results and Discussion

4.2.1. *Meso*-Pyridyl Dipyrrins

The synthesis of the pyridyl dipyrromethane precursors has previously been reported.[22] The dipyrromethanes are oxidized with 2,3-dichloro-5,6-dicyano-1,4-benzoquinone (DDQ) to form pyrdpm (pyrdpm = pyridyldipyrromethene). When 0.5 equivalents of $Cu(acac)_2$ (relative to the initial dipyrromethane) is added to the oxidized dipyrrin, a homoleptic copper(II) dipyrrin complex $[Cu(pyrdpm)_2]$ is formed. When 1.0 equivalent of $Cu(acac)_2$ is added to the dipyrromethene, the heteroleptic complex [Cu(pyrdpm)(acac)] is produced. Both products form rapidly without the use of any base and are purified by column chromatography on silica gel to yield red solids that crystallize as orange/green crystals. The latter compounds rapidly decompose when exposed to alumina.

The homoleptic copper(II) pyridine dipyrrin complexes $[Cu(4\text{-}pyrdpm)_2]$ (4-pyrdpm = 5-(4-pyridyl)dipyrromethene) and $[Cu(3\text{-}pyrdpm)_2]$ (3-pyrdpm = 5-(3-pyridyl)dipyrromethene) were prepared, purified, and characterized by a variety of methods. Electronic absorption shows characteristic absorption maxima at 468-470 nm with a shoulder at 502 nm (Figure 4-3), similar to the previously reported dipyrrin complex bis[5-(4-nitrophenyl)-4,6-pyrrinato]Cu(II)[23] and other copper(II) dipyrrin complexes prepared with phenylacetylene dipyrrin ligands (Chapter 2).

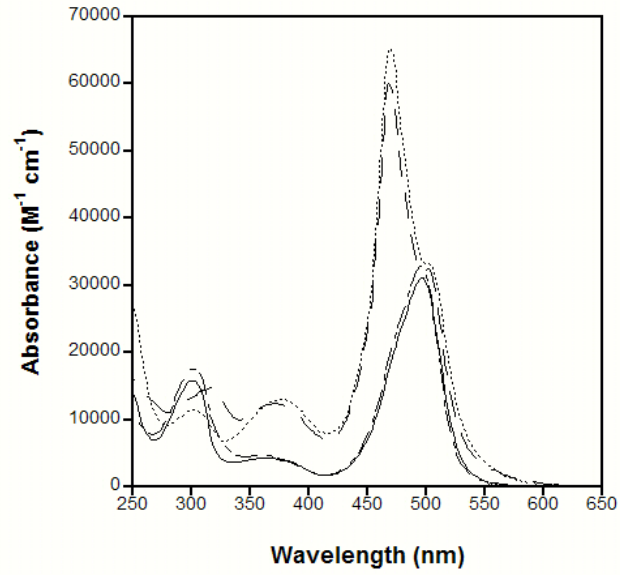

Figure 4-3. Electronic absorption spectra for [Cu(4-pyrdpm)$_2$] (····), [Cu(3-pyrdpm)$_2$] (---), [Cu(4-pyrdpm)(acac)] (—), and [Cu(3-pyrdpm)(acac)] (·-·-).

Single crystals of [Cu(4-pyrdpm)$_2$] were obtained and characterized by X-ray diffraction (Figure 4-24). The structure is a discrete mononuclear complex. The copper(II) center binds to two dipyrrin ligands and exhibits a distorted square planar geometry. The Cu–N_{dpm} bond distance is 1.95 Å, and the twist angle between the two dipyrrin ligands is 44°. The pyridyl ring is rotated 65-68° from the dipyrrin moiety. Though coordination numbers >4 are known for copper(II) centers,[24] the bulky dipyrrin ligands create a distorted square planar geometry around the metal center, which in turn obstructs the coordination of a fifth ligand.

Heteroleptic complexes [Cu(4-pyrdpm)(acac)], [Cu(3-pyrdpm)(acac)], and [Cu(2-pyrdpm)(acac)] (2-pyrdpm = 5-(2-pyridyl)dipyrromethene) were also prepared, purified, and characterized. The heteroleptic complexes are easily distinguished from the homoleptic complexes by electronic absorbance and infrared spectroscopy. The

complexes display an electronic absorption spectrum with maxima at 496-498 nm, blue-shifted relative to the corresponding homoleptic complexes (Figure 4-3). The infrared spectra also display multiple new stretches associated with the carbonyl groups of the acac ligands between 1518-1588 cm^{-1}.

Single crystals of [Cu(4-pyrdpm)(acac)] were obtained and analyzed by X-ray diffraction (Figure 4-25). The copper(II) center contains one dipyrrin ligand with a Cu–N_{dpm} bond distance slightly longer then the homoleptic complex at 1.98 Å, and one ancillary acac ligand with a Cu–O bond distance of 1.96 Å. Unlike the homoleptic complex at 65-68°, the pyridyl ring is nearly perpendicular to the dipyrrin moiety at 88°. Also unlike the homoleptic complex, the pyridine nitrogen coordinates to a neighboring copper(II) complex to create a square pyramidal copper(II) center and a one-dimensional coordination polymer with a Cu–N_{pyr} bond distance of 2.32 Å (Figure 4-4). The chains are aligned along the crystallographic *a*-axis, and a zigzag topology is formed.

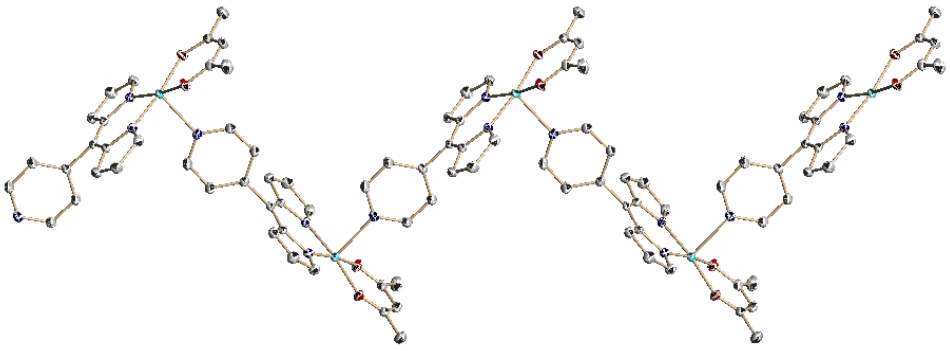

Figure 4-4. Structural diagram of the zigzag coordination polymer formed by [Cu(4-pyrdpm)(acac)] (ORTEP, 50% probability ellipsoids). Hydrogen atoms have been omitted for clarity.

[Cu(3-pyrdpm)(acac)] was also crystallized and analyzed by X-ray diffraction (Figure 4-26). Crystals were grown by slow evaporation of the complex dissolved in methylene chloride. The Cu–N_{dpm} and Cu–O bond distances are almost identical to [Cu(4-pyrdpm)(acac)] with bond distances of 1.96-1.98 Å and 1.95-1.97 Å, respectively. The connectivity also leads to a one-dimensional coordination polymer with a Cu–N_{pyr} bond distance of 2.29 Å, slightly shorter than [Cu(4-pyrdpm)(acac)]. The polymer appears to form a herringbone type chain (Figure 4-5). The chains are aligned along the crystallographic *a*-axis and in an antiparallel fashion with the ancillary acac ligands interdigitating with a neighboring chain. The complex also appears to be more bent compared to [Cu(4-pyrdpm)(acac)].

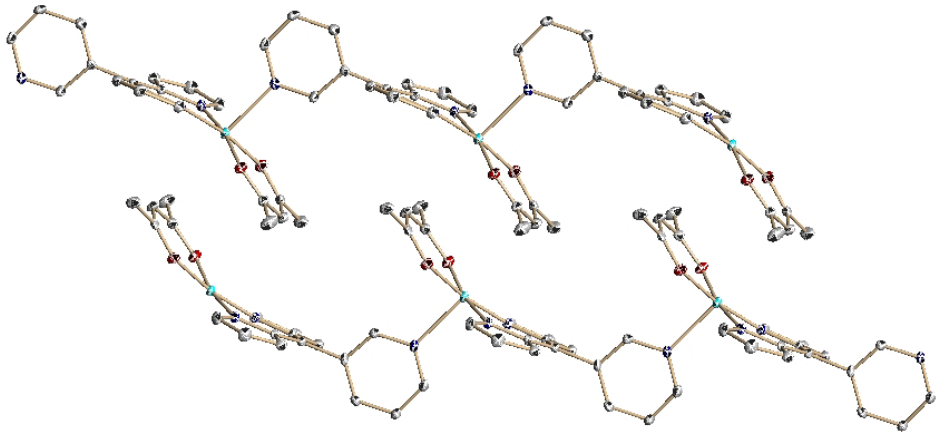

Figure 4-5. Structural diagram of two chains of the coordination polymer formed by [Cu(3-pyrdpm)(acac)] (ORTEP, 50% probability ellipsoids). Hydrogen atoms and solvent molecules have been omitted for clarity.

[Cu(3-pyrdpm)(acac)] co-crystallized with one molecule of methylene chloride per two monomer units. The inclusion of solvent is surprising as the crystal was

allowed to air-dry for several days before X-ray analysis. To confirm the amount of methylene chloride trapped in the structure, and to determine the framework stability with and without the ordered solvent molecules, thermogravimetric analysis (TGA) and differential scanning calorimetry (DSC) were employed. DSC shows a broad small endothermic transition, usually attributed to a loss of solvent, at ~94 ºC. TGA shows a weight loss of 8.3% around 80 ºC. This would account for slightly less than 0.5 equivalents of methylene chloride to the [Cu(3-pyrdpm)(acac)] complex (estimated weight loss of 10%). This is in good agreement with the ratio of the solvent molecule to dipyrrin complex found in the crystal structure. A second endothermic transition and weight loss of 18% is also detected at 225 ºC, which is accounted for by the loss of the acac ligand (estimated to be 23%). Finally, to determine the DSC transition and TGA weight loss below 100 ºC are not attributed to another component of the polymer, [Cu(4-pyrdpm)(acac)], which contains no solvent molecules, was also analyzed. No transitions or weight loss is detected until 225 ºC, also corresponding to the loss of the acac ligand. Notably, the [Cu(3-pyrdpm)(acac)] crystals could be heated to above 100 ºC to liberate the methylene chloride and then cooled again to produce a desolvated crystal. Attempts to reintroduce solvent molecules into the network by exposing the de-solvated crystals to methylene chloride vapors were unsuccessful. Submerging the crystal in a solution of methylene chloride would dissolve the crystal.

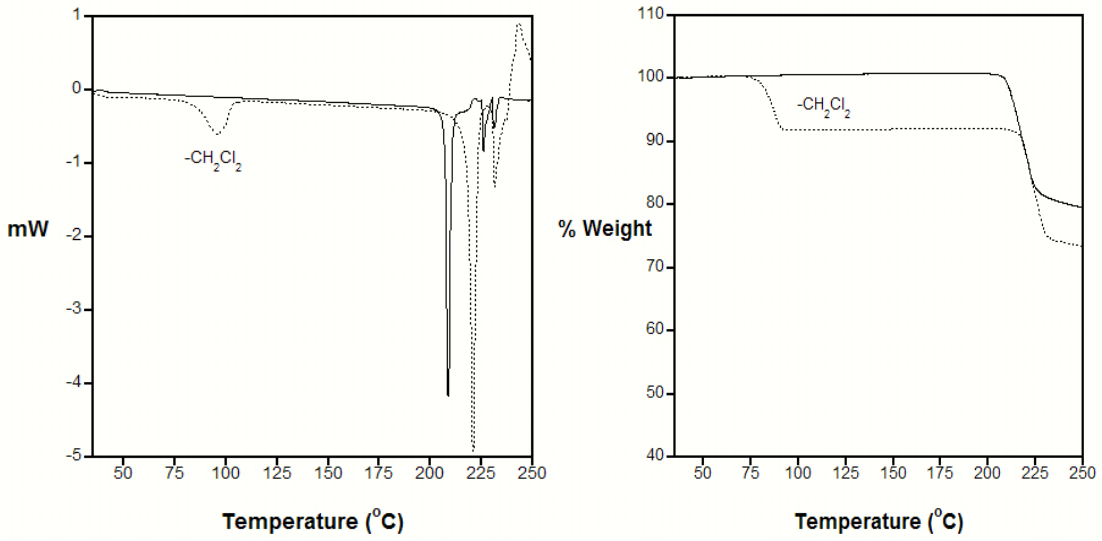

Figure 4-6. DSC (left) and TGA (right) of [Cu(4-pyrdpm)(acac)] (—) and [Cu(3-pyrdpm)(acac)] (····).

Finally, [Cu(2-pyrdpm)(acac)] was crystallized and analyzed by X-ray diffraction (Figure 4-27). Unlike the previous two heteroleptic complexes, the 2-pyrdpm analog forms a discrete mononuclear structure upon crystallization. The pyridine is not positioned in close proximity to the copper(II) center of any neighboring dipyrrin complex with the shortest Cu–N_{pyr} distance of >6.0 Å. The copper(II) center is square planar with Cu–N_{dpm} and Cu–O bond distances of 1.95-1.96 Å and 1.93-1.95 Å, respectively, slightly shorter then the 3-pyrdpm and 4-pyrdpm heteroleptic complexes. The pyridine ring most likely does not coordinate to any corresponding copper(II) center because of limited accessibility due to sterics around the nitrogen atom. DSC measurements show a substantially lower endothermic transition at ~120 ºC, confirming that [Cu(2-pyrdpm)(acac)] does not form a coordination polymer.

4.2.2. Fluorinated Ancillary Ligands

Besides altering the *meso*-group of the dipyrrin ligand, the ancillary acac ligand can also be altered in order to change certain properties of the coordination polymers. The addition of fluorine groups would not only alter the chemical composition of the framework, but could also change the polymer topology due to the F–F interactions that could occur. $Cu(tfacac)_2$ (tfacac = trifluoroacetylacetonato), and $Cu(hfacac)_2 \cdot H_2O$ are added in equimolar ratios to a dipyrromethene, following the same synthesis as the addition of $Cu(acac)_2$, leading to the formation of new heteroleptic complexes [Cu(pyrdpm)(tfacac)] and [Cu(pyrdpm)(hfacac)]. However, unlike the unfluorinated copper(II) starting material, the amount of $Cu(tfacac)_2$ and $Cu(hfacac)_2 \cdot H_2O$ has to be controlled, because the presence of an excess metal salt leads to the formation of larger dinuclear and trinuclear species (vide infra). Purification by column chromatography yields red solids, which form orange or green crystals upon various crystallization methods.

Using the same 4- and 3-pyrdpm ligands, [Cu(4-pyrdpm)(tfacac)] [Cu(3-pyrdpm)(tfacac)], [Cu(4-pyrdpm)(hfacac)], and [Cu(3-pyrdpm)(hfacac)] were prepared. The complexes were characterized by mass spectrometry, infrared, and electronic absorbance spectroscopy. The complexes exhibit similar electronic absorbance maxima at 490-494 nm. The infrared spectra reveals new carbonyl stretches associated with the tfacac group at 1626-1627 cm^{-1} and 1648-1649 cm^{-1} for the hfacac group. Features associated with the trifluoromethyl groups are also observed at 1100-1300 cm^{-1}.

The crystal structure of [Cu(4-pyrdpm)(tfacac)] is isomorphic to [Cu(4-pyrdpm)(acac)], forming a zigzag polymer with chains along the crystallographic *a*-axis (Figure 4-7). A square pyramidal copper(II) center is formed with Cu–N_{dpm} bond distances of 1.96-1.98 Å. The Cu–O bond distances are unlike the unfluorinated counterparts, with one short and one long Cu–O bond distance of 1.95 Å and 1.98-1.99 Å respectively. The shorter Cu–O bond resides on the side of the tfacac closest to the CF_3 group. The Cu–N_{pyr} bond distance is comparable to that of the other heteroleptic complexes at 2.30-2.36 Å. There is also aggregation of the trifluoromethyl groups with two CF_3 moieties interacting at a F–F distance of 2.90 Å (Figure 4-8). As will be shown extensively, F–F interactions are shown to have a pronounced effect on the formation of structures in the solid state.

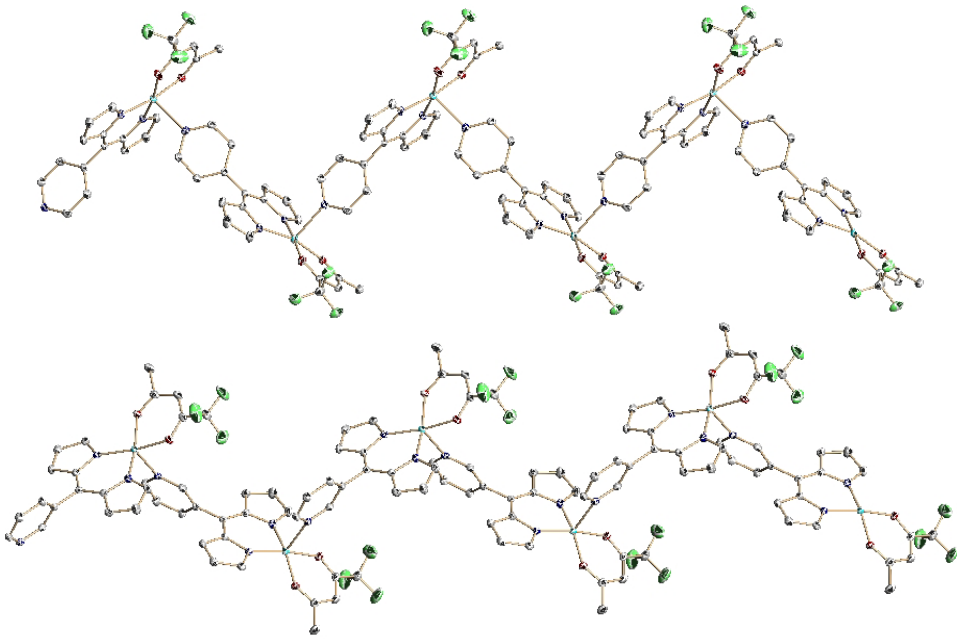

Figure 4-7. Structural diagram of the coordination polymers formed by [Cu(4-pyrdpm)(tfacac)] (top) and [Cu(3-pyrdpm)(tfacac)] (bottom) (ORTEP, 50% probability ellipsoids). Hydrogen atoms have been omitted for clarity.

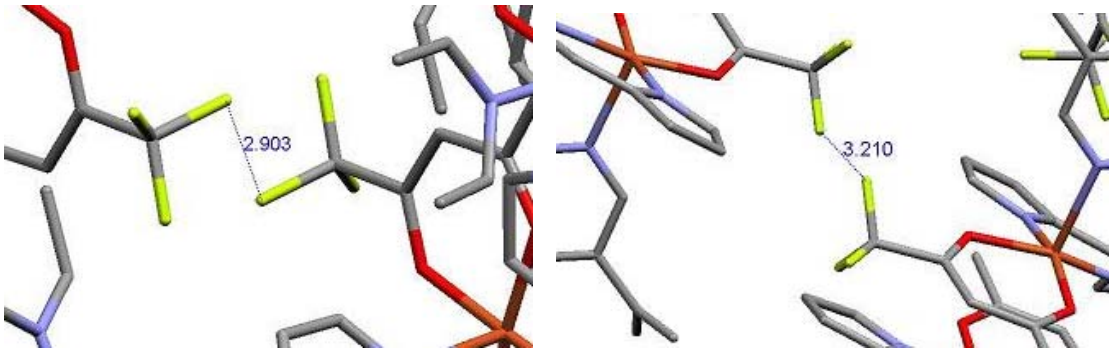

Figure 4-8. F–F interactions between neighboring trifluoromethyl groups of [Cu(4-pyrdpm)(tfacac)] (left) and [Cu(3-pyrdpm)(tfacac)] (right) between polymer chains. Hydrogen atoms and solvent molecules been omitted for clarity.

Like previous structures, [Cu(3-pyrdpm)(tfacac)] also forms a coordination polymer upon crystallization (Figure 4-7). The axial Cu–N_{pyr} bond distance is 2.28 Å, the Cu–N_{dpm} bond distance is 1.97 Å, and the Cu–O bond distances are 1.97 Å and 1.99 Å. A helical coordination polymer is observed, unlike its unfluorinated counterpart [Cu(3-pyrdpm)(acac)]. There is a twist to the chain, with the fluorinated groups directed outwards. Once again there is also aggregation of the trifluoromethyl groups with one trifluoromethyl group interacting with one group of a neighboring polymeric unit at a distance of 3.21 Å (Figure 4-8).

While the trifluoromethyl groups of tfacac have some effect on the overall packing structure and topology of the dipyrrin structures, as might be expected, the largest effect of the fluorination appears in the hfacac-containing dipyrrin structures. [Cu(4-pyrdpm)(hfacac)] was crystallized and analyzed by X-ray diffraction (Figure 4-30). A one-dimensional coordination polymer was anticipated because it was observed in all previous structures; however, a different topology emerges. The structure consists of two helical coordination polymers intertwined forming an

antiparallel, double helix, as well as a discrete hexameric ring consisting of six [Cu(4-pyrdpm)(hfacac)] groups (Figure 4-9). For the hexameric ring, the Cu–N_{dpm} bond distance is 1.95 Å, the Cu–O bond distance is 2.01 Å, and the axial Cu–N_{pyr} bond distance is 2.28 Å. The closest Cu–Cu distance is 9.72 Å, and the furthest Cu–Cu distance (two copper(II) centers on opposite sides of the ring, also corresponding to the approximate diameter of the ring) is 19.24 Å. For the double helical chains, the Cu–N_{dpm} bond distances are 1.94-1.95 Å, the Cu–O bond distances are 1.98-2.00 Å, and the Cu–N_{pyr} bond distance is 2.30 Å.

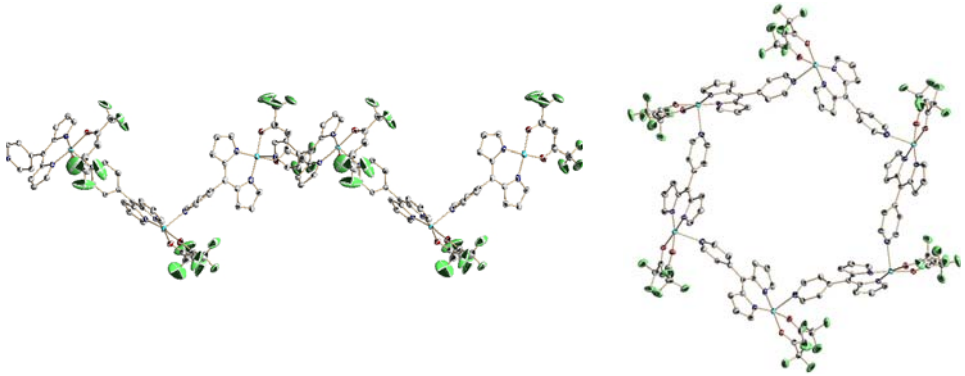

Figure 4-9. Individual components of [Cu(4-pyrdpm)(hfacac)] consisting of helical chains (left) that are intertwined (not shown) and a 6-membered ring (right) (ORTEP, 50% probability ellipsoids). Hydrogen atoms have been omitted for clarity.

The hexameric rings lie along the crystallographic *c*-axis and are spaced such that they form hexagonal channels throughout the structure (Figure 4-10). They do not lie directly on top of each other but are spaced at approximately 21 Å intervals (Cu–Cu distance of two eclipsed rings). As stated earlier, the two polymer components intertwine to form a double helix. The double helices lie parallel to the crystallographic *c*-axis and each hexameric ring is surrounded by six double helical chains.

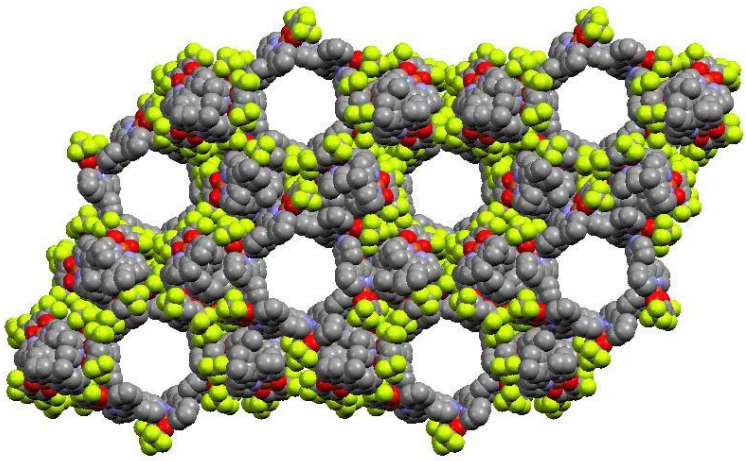

Figure 4-10. Space filling model of [Cu(4-pyrdpm)(hfacac)] viewed along the crystallographic *c*-axis. Hydrogen atoms have been omitted for clarity.

There are two types of hfacac groups of the [Cu(4-pyrdpm)(hfacac) structure: the hfacac groups of the hexameric ring and the hfacac groups of the helical chains. The complex aggregates such that each trifluoromethyl group of the hexameric ring interacts with between one and four trifluoromethyl groups of adjacent hexameric rings and polymeric chains with F–F distances of 3.1-3.5 Å (Figure 4-11). The trifluoromethyl groups of the helical chains strongly interact with between one and three trifluoromethyl groups of adjacent hexameric rings and polymeric chains with F–F distances of 2.9-3.4 Å (Figure 4-11).

The trifluoromethyl groups of the hexameric ring are directed outward, creating an unfluorinated core. The trifluoromethyl groups of the helical chains are also directed outward. Since the hexameric rings are at spaced intervals, the alternating space between the rings contain fluorinated groups from the helical chains. This leads to unfluorinated layers of the channels in the hexameric ring core, and alternate layers of fluorinated regions in the channels formed by the helical chains.

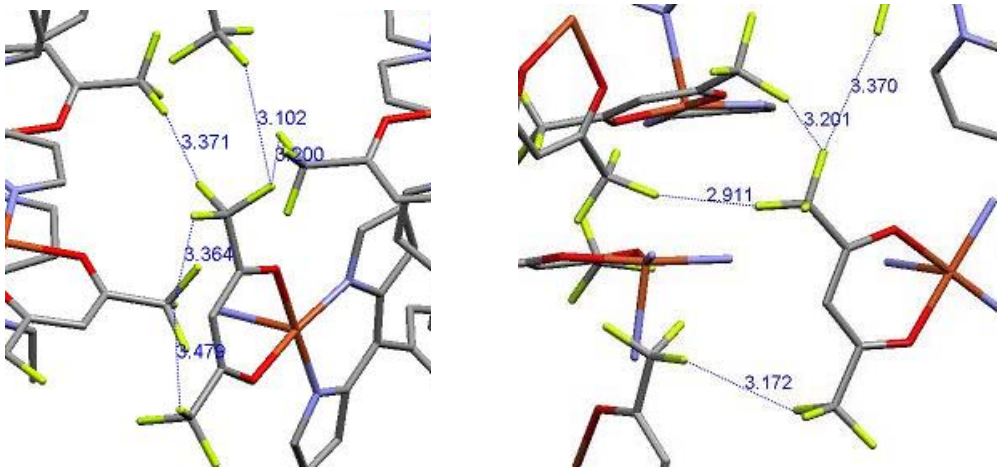

Figure 4-11. F–F interactions between neighboring trifluoromethyl groups of the [Cu(4-pyrdpm)(hfacac)] hexameric ring (left) and double helical polymer chains (right). Hydrogen atoms have been omitted for clarity.

While no ordered solvent molecules are observed in the X-ray structure, including in the large hexagonal channels, residual electron density peaks are detected, which suggests some disordered solvent molecules is present in the structure. However, TGA of air dried crystals shows no weight loss up to ~200 °C, indicating that no substantial amount of solvent is present. DSC was also performed and agrees with the TGA data, showing the first transition at 197 °C.

Finally, [Cu(3-pyrdpm)(hfacac)] was analyzed by X-ray diffraction (Figure 4-31). Like most of the previous structures described thus far, a one-dimensional coordination polymer is detected. The topology of the [Cu(3-pyrdpm)(hfacac)] coordination polymer is also helical, which is similar to [Cu(3-pyrdpm)(tfacac)] but different from the zigzag morphology of the unfluorinated counterpart [Cu(3-pyrdpm)(acac)]. The Cu–O and Cu–N_{dpm} bond distances are 1.98-2.00 Å and 1.94-

1.96 Å respectively. The chains are aligned along the crystallographic *b*-axis with an axial Cu–N_{pyr} bond distance of 2.28 Å. The trifluoromethyl groups are directed to the outside of the helical structure, oriented toward trifluoromethyl groups of neighboring polymer chains. The complex aggregates such that each trifluoromethyl group strongly interacts with three to four neighboring trifluoromethyl groups of adjacent chains with F–F distances of 2.9-3.4 Å (Figure 4-47). Examination of the overall packing shows layers of alternating fluorinated and unfluorinated regions (Figure 4-12).

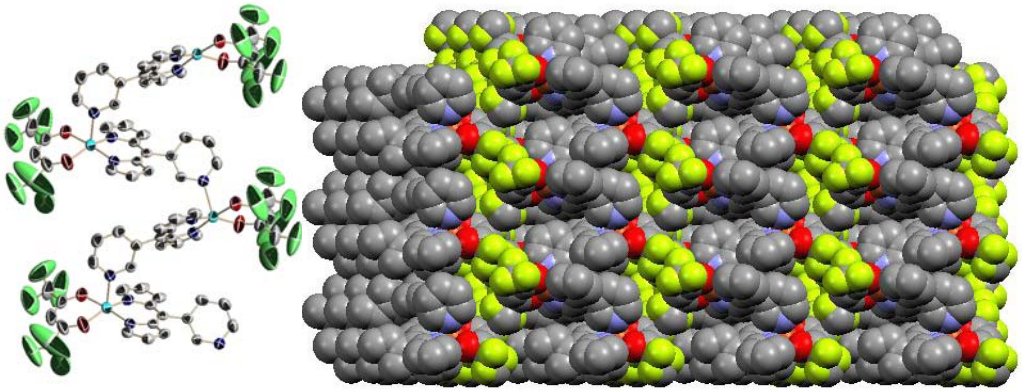

Figure 4-12. Structural diagram of the coordination polymer formed by [Cu(3-pyrdpm)(hfacac)] (ORTEP, 50% probability ellipsoids) (left), and packing diagram (space filling model, slightly off-set from crystallographic *a*-axis) (right). Hydrogen atoms and solvent molecules have been omitted for clarity.

4.2.3. *Meso*-Quinoline Dipyrrins

To probe the effects of modifying the donor group in the *meso*-position of the heteroleptic dipyrrin ligand, quinolyl derivatives were prepared. Quinoline-derived ligands have been previously shown to coordinate to $Cu(acac)_2$.[25] Condensation of 3-

quinolinecarboxaldehyde and 4-quinolinecarboxaldehyde with pyrrole, followed by oxidation with DDQ, gave the ligands 5-(3-quinolyl)dipyrromethene (3-quindpm) and 5-(4-quinolyl)dipyrromethene (4-quindpm), respectively. Addition of the copper(II) sources $Cu(acac)_2$, $Cu(tfacac)_2$, and $Cu(hfacac)_2 \cdot H_2O$ to the oxidized ligands in situ produces the various heteroleptic complexes. The complexes display electronic absorption and infrared spectroscopic features nearly identical to the pyridyl counterparts. Most of the complexes were also characterized by X-ray diffraction.

[Cu(3-quindpm)(acac)] crystallizes in a manner nearly identical to the structurally related complex [Cu(3-pyrdpm)(acac)] (Figure 4-32). The crystal structure reveals a one-dimensional polymer with the polymer chains packing in a herringbone fashion (Figure 4-13). The extra benzo ring on the quinoline ligand occupies the space where the co-crystallized methylene chloride solvent molecule resides in [Cu(3-pyrdpm)(acac)], and subsequently no co-crystallized solvent is found in [Cu(3-quindpm)(acac)]. The chains of [Cu(3-quindpm)(acac)] are aligned along the crystallographic *a*-axis with a $Cu–N_{quin}$ bond distance of ~2.46 Å, slightly longer than that found in the pyridyl system (~2.31 Å). The comparison of [Cu(3-pyrdpm)(acac)] and [Cu(3-quindpm)(acac)] suggests that moderate steric alterations at the *meso*-position has little effect on these supramolecular structures.

Figure 4-13. Structural diagram of the coordination polymer formed by [Cu(3-quindpm)(acac)] (ORTEP, 50% probability ellipsoids). Hydrogen atoms have been omitted for clarity.

[Cu(3-quindpm)(hfacac)] (Figure 4-33) also crystallizes as a one-dimensional coordination polymer with the chains aligned along the crystallographic *b*-axis (Figure 4-14) with a Cu–N_{quin} bond distance of 2.35 Å. Similar to [Cu(3-pyrdpm)(hfacac)], the polymer has a helical topology. The complex aggregates such that the trifluoromethyl groups strongly interact with two to three trifluoromethyl groups of adjacent polymer chains with F–F distances of 2.8-3.4 Å (Figure 4-49). As in [Cu(3-pyrdpm)(hfacac)], layers of alternating fluorinated and unfluorinated regions can be observed in the packing of the polymers (Figure 4-14). Examination of [Cu(3-pyrdpm)(hfacac)] and [Cu(3-quindpm)(hfacac)] clearly shows once again that the addition of fluorinated groups has a strong influence on supramolecular structure, while the additional aromatic surface of 3-quindpm versus 3-pyrdpm has comparatively little impact on the structure.

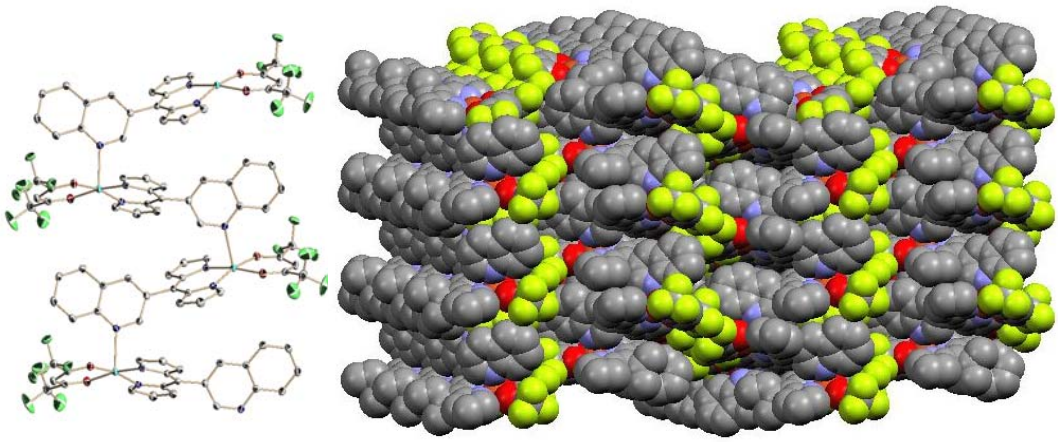

Figure 4-14. Structural diagram of the coordination polymer formed by [Cu(3-quindpm)(hfacac)] (ORTEP, 50% probability ellipsoids) (left) and packing diagram (space filling model, slightly off-set from crystallographic *a*-axis) of [Cu(3-quindpm)(hfacac)]. Hydrogen atoms and solvent molecules have been omitted for clarity.

Like the structure formed by [Cu(4-pyrdpm)(hfacac)], a dramatic effect of fluorination on supramolecular structure is found in the complex [Cu(4-quindpm)(hfacac)] (Figure 4-34). Instead of a one-dimensional coordination polymer, the compound crystallizes as a discrete hexameric ring (Figure 4-15). Again this parallels the chemistry found with the pyridyl analogue, where [Cu(4-pyrdpm)(hfacac)] is found to form a six-membered ring and a double helical coordination polymer in the same crystalline lattice. For [Cu(4-pyrdpm)(hfacac)], the copper(II) centers in hexameric ring are essentially coplanar; however, for [Cu(4-quindpm)(hfacac)] the ring is twisted in on itself and the copper(II) ions take on a cyclohexane 'chair' conformation (Figure 4-53). The Cu–N_{quin} bond lengths vary from 2.37-2.48 Å, which is significantly longer than the Cu–N_{pyr} bond distance of the hexamer formed with [Cu(4-pyrdpm)(hfacac)]. The benzo groups of the quinoline

ligand are directed toward the center of the ring, while the trifluoromethyl groups are pointed outward from the complex. This creates a supramolecular structure with a hydrophobic core and a fluorinated periphery. The hexamers pack such that the trifluoromethyl groups interact with one to three trifluoromethyl groups of nearby hexamers with F–F distances of 2.9-3.5 Å (Figure 4-48). No open channels or pores are present in the framework structure, in contrast to [Cu(4-pyrdpm)(hfacac)].

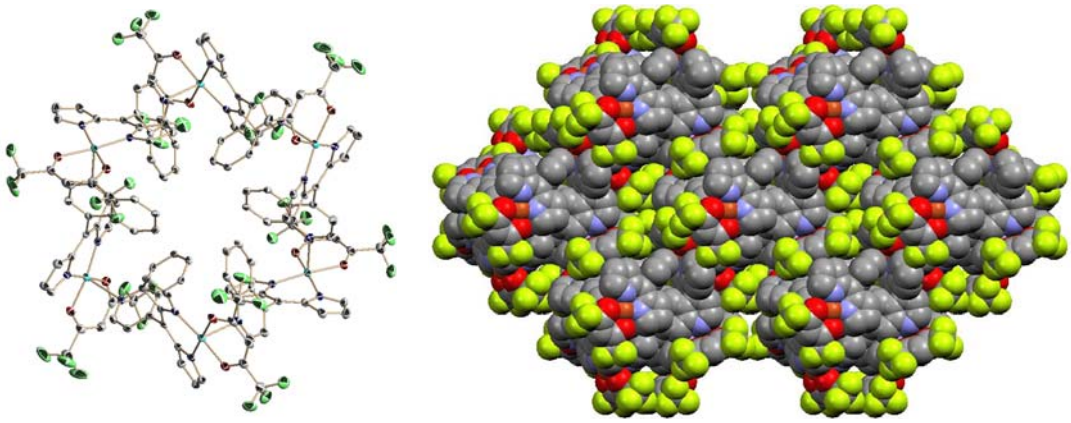

Figure 4-15. Structural diagram of the hexameric ring formed by [Cu(4-quindpm)(hfacac)] (ORTEP, 50% probability ellipsoids) (left) and packing diagram (space filling model, crystallographic *c*-axis) (right). Hydrogen atoms and solvent molecules have been omitted for clarity.

The relationships between the structures of [Cu(3-quindpm)(acac)], [Cu(3-quindpm)(hfacac)], and [Cu(4-quindpm)(hfacac)] and their pyridyl counterparts demonstrates the ability to modify the *meso*-ligand between pyridyl and quinolyl, while tuning the overall structure and packing by the introduction of acac versus hfacac spectator ligands. The results show the additional hydrophobic and steric properties of the quinoline-derived ligands have little effect on the overall morphology

of the solid-state structures. [Cu(3-quindpm)(tfacac)] and [Cu(4-quindpm)(tfacac)] did not produce single crystals suitable for X-ray diffraction, therefore similar comparisons could not be made between the related structures containing the pyridyl ligands.

4.2.4. Phenyl and Phenylacetylene Extended *Meso*-Pyridyl Dipyrrins

The chemistry of extended phenyl acetylene dipyrromethene ligands has been studied in detail (Chapter 2). In addition, phenylacetylpyridyl ligands have been appended to porphyrins for preparation of elaborate supramolecular structures, [26, 27] and boron-dipyrrin complexes for use as fluorophores.[28] In order to form coordination polymers and supramolecular structures with larger subunits, extended pyridyl dipyrrins are prepared and combined with copper(II) acac sources to form heteroleptic complexes. A series of phenyl pyridyl and phenylacetylene pyridyl dipyrromethene ligands 42b-pyrdpm 42-pyrdpm, 43-pyrdpm, and 44-pyrdpm (Figure 4-16) were synthesized from the corresponding aldehyde, which was either commercially available or prepared using Sonogashira reaction conditions, followed by condensation with pyrrole, oxidation with DDQ, and complexation with $Cu(acac)_2$, $Cu(tfacac)_2$, or $Cu(hfacac)_2 \cdot H_2O$ to form the heteroleptic metal complexes. All metal complexes were characterized by mass spectrometry, infrared, and electronic absorption spectroscopy. Most complexes were analyzed by X-ray diffraction. Upon crystallization of the metal complexes, various topologies emerge consisting of discrete complexes, one-dimensional zigzag polymers, and helical coordination

polymers. The remaining complexes produced crystals unsuitable for X-ray diffraction despite the variety of crystallization methods employed.

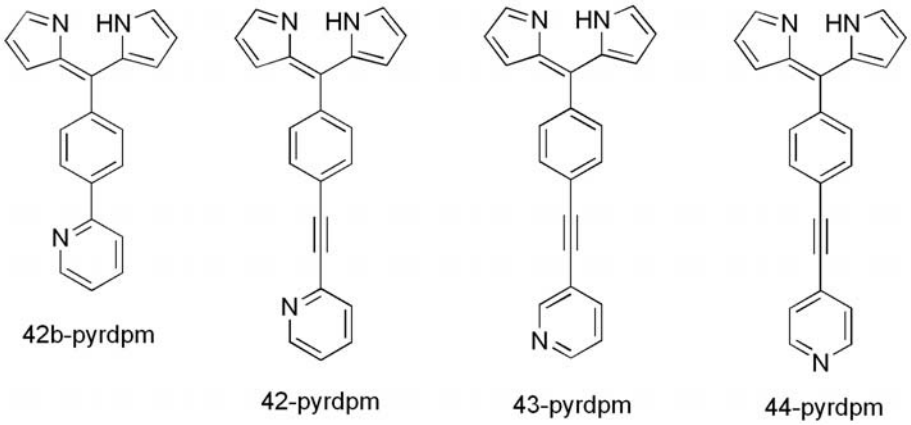

Figure 4-16. Large phenyl pyridine and phenylacetylene pyridine dipyrrin ligands used in the preparation of heteroleptic copper(II) complexes.

[Cu(2-pyrdpm)(acac)] did not form a coordination polymer because the nitrogen atom of the pyridyl ligand was not sterically accessible. Other nitrogen-containing dipyrrin ligands such as 42b-pyrdpm were prepared to explore the limits to which the pyridine can bind to a neighboring copper(II) center. The complex [Cu(42b-pyrdpm)(hfacac)] was synthesized and analyzed by X-ray diffraction (Figure 4-35). Upon crystallization, a discrete mononuclear metal complex is found. The Cu–N_{dpm} and Cu–O bond distances are comparable to all other heteroleptic structures at 1.94 Å and 1.96-1.98 Å respectively. The closest Cu–N_{pyr} distance is ~6.5 Å, showing no interaction between the pyridine nitrogen and any copper(II) center. However, despite the lack of a polymeric structure, there are F–F interactions of 2.9 Å between the trifluoromethyl groups (Figure 4-50). Metal complexes of the 42b-pyrdpm ligand

with acac and tfacac ancillary ligands were not synthesized because all prior data suggests they would also be discrete mononuclear complexes upon crystallization.

The dipyrrin ligand 42-pyrdpm was combined with $Cu(acac)_2$ to produce [Cu(42-pyrdpm)(acac)]. Like the previous two ligands, it was also a discrete mononuclear structure upon crystallization (Figure 4-36). The closest $Cu–N_{pyr}$ distance is ~6.0 Å, showing no interaction between the pyridyl nitrogen atom and any copper(II) center. The Cu–O bond distances are 1.92-1.93 Å, shorter then other dipyrrin structures, while the $Cu–N_{dpm}$ bond distance is similar at 1.96 Å.

The 42-pyrdpm ligand was also combined with $Cu(hfacac)_2 \cdot H_2O$ to form [Cu(42-pyrdpm)(hfacac)] and the metal complex was crystallized (Figure 4-37). Rather than a discrete structure like the unfluorinated counterpart, a one-dimensional coordination polymer is formed (Figure 4-17). Interestingly, the unfluorinated complex does not form a coordination polymer but the fluorinated complex does, suggesting that there are other subtle forces driving the formation of the frameworks other than sterics. The fluorinated ligand has an electronic withdrawing effect on the copper(II) center, making it more electron deficient then the unfluorinated counterpart. This electronic deficiency may be what is driving the polymer formation. Suitable single crystals for X-ray diffraction could not be obtained for [Cu(42-pyrdpm)(tfacac)] to determine if a coordination polymer is formed.

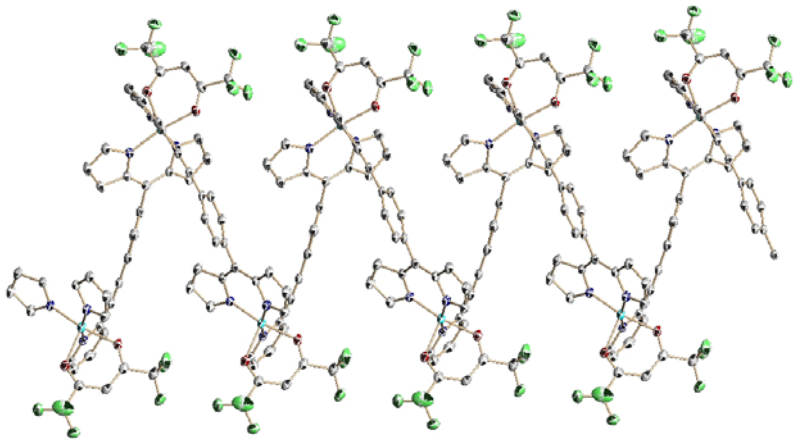

Figure 4-17. Structural diagram of the coordination polymer formed by [Cu(42-pyrdpm)(hfacac)] (ORTEP, 50% probability ellipsoids). Hydrogen atoms have been omitted for clarity.

Unlike all the square pyramidal copper(II) centers observed for this series of coordination polymers, the metal center of [Cu(42-pyrdpm)(hfacac)] does not contain the pyridine nitrogen atom in the axial position (Figure 4-18). One of the oxygen atoms from the acac ligand is elongated to form a Cu–O bond distance 2.20 Å and is located in the axial position. The other Cu–O bond distance is comparable to previous structures at 2.01 Å. The Cu–N_{dpm} bond distance is also comparable to previous structures at 1.95 Å. The Cu–N_{pyr} bond distance is very short at 2.04 Å and found in an equatorial position. The coordination polymer cannot be formed if the pyridine nitrogen atom resides in the axial position because the phenylacetylene component would overlap with the ancillary ligand or dipyrrin moiety of the copper(II) center. However, shifting of the ligands about the metal center would allow for accommodation of the fifth ligand. [Cu(42-pyrdpm)(hfacac)] also has numerous F–F interactions. The trifluoromethyl groups interact with three to five trifluoromethyl groups of neighboring complexes at 2.8-3.5 Å (Figure 4-51).

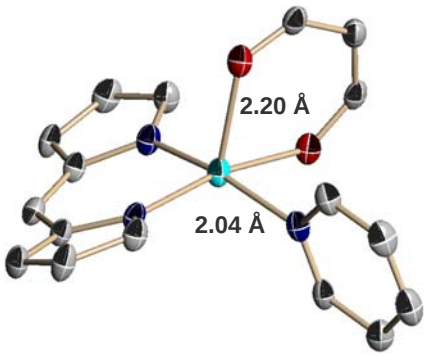

Figure 4-18. [Cu(42-pyrdpm)(hfacac)] metal center (ORTEP, 50% probability ellipsoids). Hydrogen atoms have been omitted for clarity.

To create an extended ligand similar to 3-pyrdpm, 43-pyrdpm was synthesized and combined with $Cu(acac)_2$, $Cu(tfacac)_2$, and $Cu(hfacac)_2{\cdot}H_2O$ to form [Cu(43-pyrdpm)(acac)], [Cu(43-pyrdpm)(tfacac)], and [Cu(43-pyrdpm)(hfacac)], respectively. All three complexes were characterized by X-ray diffraction (Figure 4-38) (Figure 4-39) (Figure 4-40).

[Cu(43-pyrdpm)(acac)] crystallizes as a helical one-dimensional coordination polymer with chains along the crystallographic *b*-axis (Figure 4-19). All coordination chemistry is similar to the previous 3- and 4-pyrdpm complexes with a square pyramidal copper(II) center, $Cu–N_{dpm}$ bond distance of 1.98 Å, Cu–O bond distances of 1.95-1.96 Å, and axial $Cu–N_{pyr}$ bond distances of 2.31-2.32 Å. The extended pyridyl ligand is very bent along the phenylacetylene bond similar to the extended phenylacetylene ligands appended to dipyrrin complexes (Chapter 2).

[Cu(43-pyrdpm)(tfacac)] crystallizes in a different crystal system and space group than [Cu(43-pyrdpm)(acac)]; however, the two structures look almost identical

in their packing. They both form helical coordination polymers (Figure 4-19) with chains aligned along the crystallographic *b*-axis. The copper(II) center is square pyramidal with Cu–N_{dpm} bond distances of 1.96-1.98 Å, Cu–O bond distances of 1.96-1.98 Å, and an axial Cu–N_{pyr} bond distance of 2.29 Å. There are F–F interactions between the trifluoromethyl group and two neighboring trifluoromethyl groups at 2.97 Å (Figure 4-52).

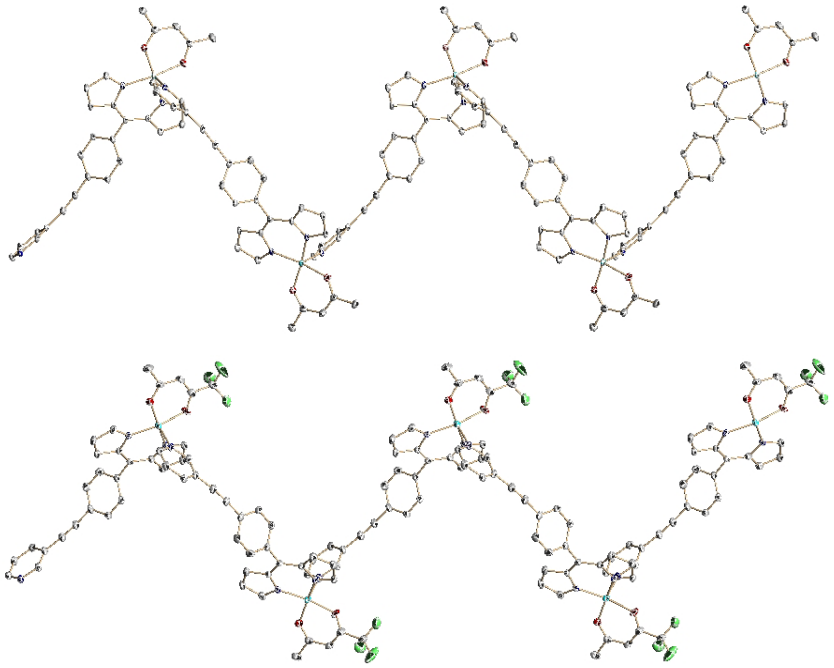

Figure 4-19. Structural diagram of the coordination polymer formed by [Cu(43-pyrdpm)(acac)] (top) and [Cu(43-pyrdpm)(tfacac)] (bottom) (ORTEP, 50% probability ellipsoids). Hydrogen atoms and solvent molecules have been omitted for clarity.

[Cu(43-pyrdpm)(hfacac)] was crystallized and analyzed by X-ray diffraction. A one-dimensional coordination polymer is formed but the overall topology is different then the previous two 43-pyrdpm complexes. The chains are not clearly

helical but are also not clearly zigzag. The chains are aligned along the crystallographic *b*-axis. The Cu–O bond distances are slightly elongated to 2.00-2.01 Å; however, the other bond distances are comparable to the previous structures with Cu–N_{dpm} bond distances of 1.95-1.96 Å, and an axial Cu–N_{pyr} bond distance of 2.30 Å. Each trifluoromethyl group interacts with three other trifluoromethyl groups at 2.8-3.4 Å (Figure 4-21), altering the formation of the frameworks.

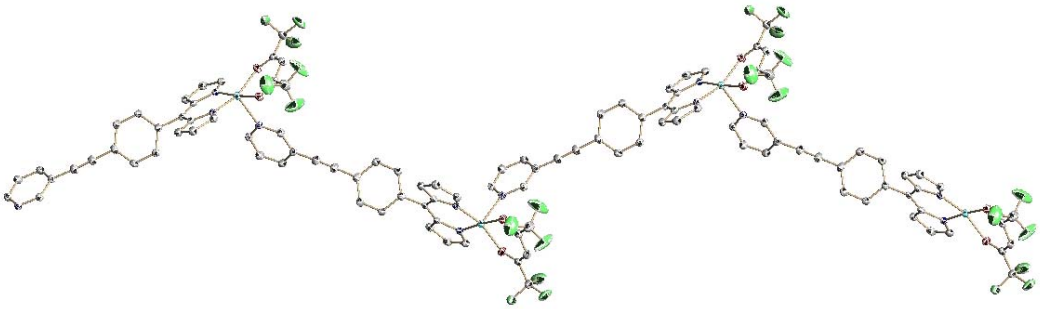

Figure 4-20. Structural diagram of the coordination polymer formed by [Cu(43-pyrdpm)(hfacac)] (ORTEP, 50% probability ellipsoids). Hydrogen atoms have been omitted for clarity.

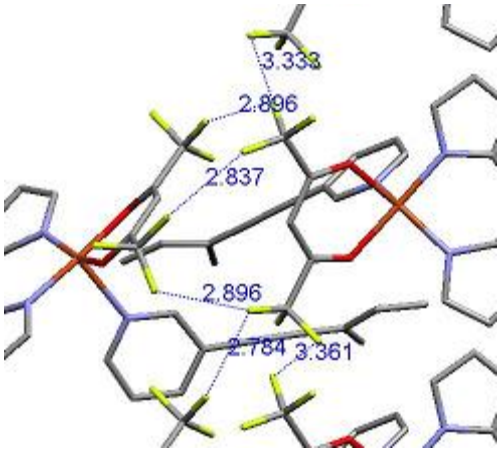

Figure 4-21. F–F interactions between neighboring trifluoromethyl groups of [Cu(43-pyrdpm)(hfacac)]. Hydrogen atoms have been omitted for clarity.

Finally, [Cu(44-pyrdpm)(acac)] was purified and crystallized (Figure 4-41). Surprisingly, the compound does not form a coordination polymer, but is a discrete mononuclear complex. The bond distances are comparable to other discrete heteroleptic dipyrrin complexes with Cu–N_{dpm} and Cu–O bond distances of 1.95-1.96 Å and 1.92-1.93 Å, respectively. The nearest Cu–N_{pyr} distance is ~5.0 Å. It is not clear why the complex did not form a coordination polymer.

4.2.5. Topology of the Coordination Polymers

Some coordination polymer topologies are easy to identify based on a visual inspection of the crystal structure. Some chains clearly display a helical or zigzag topology. Sometimes there can be subtle helical twists to a chain that may be hard to visually detect, thus complicating the identification of the topology of a polymeric chain. In order to more easily visualize and thereby ultimately determine the topology of the polymer chains, most atoms were removed (Figure 4-22), the central atoms were linked, and the polymer chains were expanded (Figure 4-23).

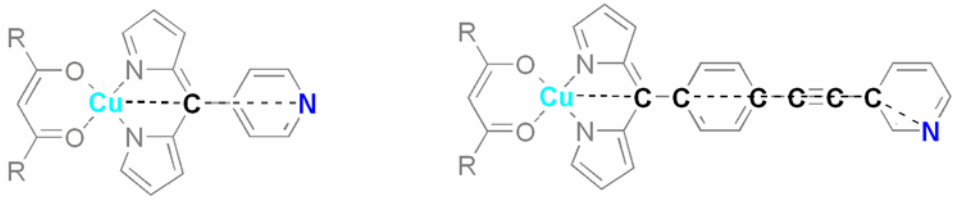

Figure 4-22. Structural diagram of the coordination polymer building blocks [Cu(4-pyrdpm)(acac)] (left) and [Cu(42-pyrdpm)(acac)] (right). Atoms highlighted in cyan black, and blue were used to form the polymeric chains in Figure 4-23.

From a visual examination of the networks that form one-dimensional coordination polymers, it was determined that [Cu(3-pyrdpm)(tfacac)], [Cu(3-pyrdpm)(hfacac)], [Cu(3-quindpm)(hfacac)], [Cu(42-pyrdpm)(hfacac)], [Cu(43-pyrdpm)(acac)], and [Cu(43-pyrdpm)(tfacac)] has helical topologies (Figure 4-23). In contrast, [Cu(4-pyrdpm)(acac)] has clearly a zigzag topology. For [Cu(43-pyrdpm)(hfacac)], the chain doe not appear to be helical but is also not clearly zigzag.

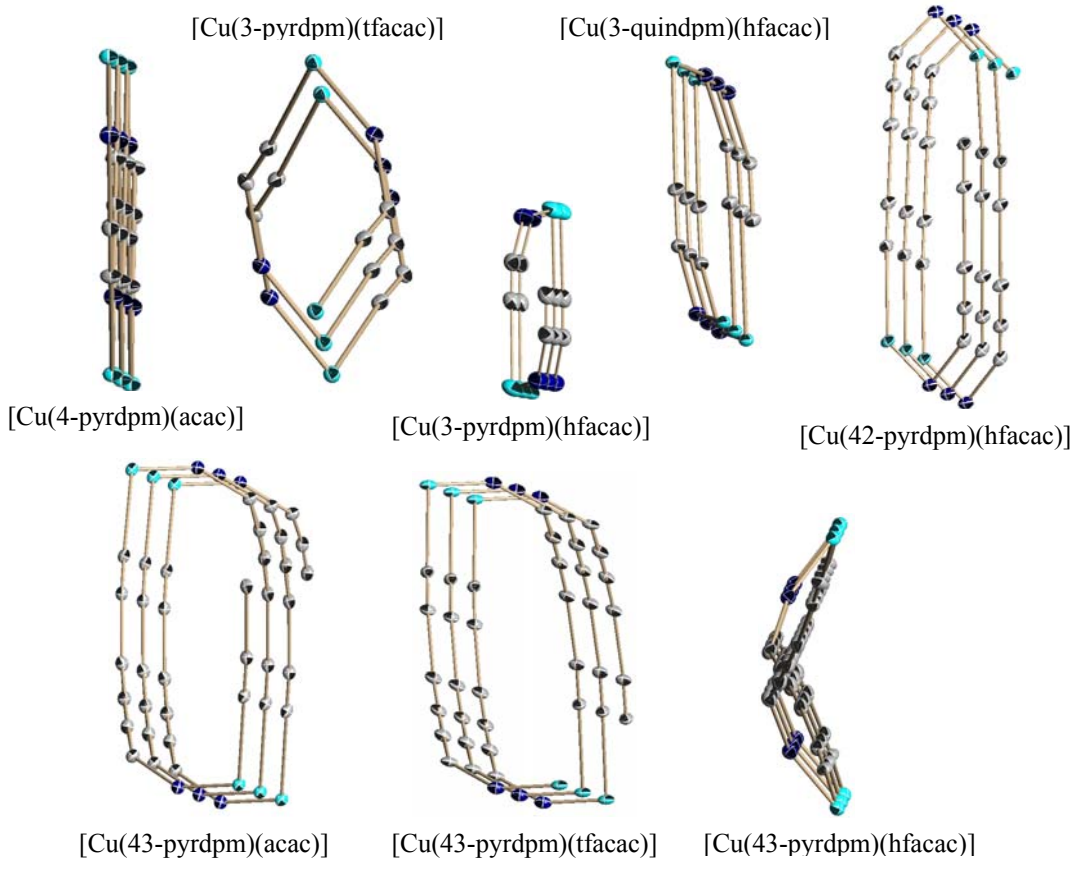

Figure 4-23. Simplified polymeric chains of the various coordination polymers viewed down the chains (cyan = copper(II), blue = nitrogen, grey = carbon). Atoms not highlighted in Figure 4-22 and solvent molecules have been removed for clarity.

It is worth noting that all of the helical coordination polymers have chains aligned along the crystallographic *b*-axis, while the zigzag structures have chains aligned along the crystallographic *a*-axis. Previously, most helical coordination polymers have been classified from a visual observation of the crystal structure. A more quantitative approach was desired to characterize the dipyrrin coordination polymers, because the topology of some polymers is not readily apparent.

Torsion angles are mathematically used to determine the twist of a chain. When consecutive torsion angles along a chain all are of the same sign, then they are twisting in the same direction, thus creating a helix. Torsion angles have been used in biochemistry to analyze peptides and amino acids[29, 30] and in polymer chemistry to analyze helical polymers.[31, 32] A few examples are found in supramolecular and coordination polymer chemistry that use torsion angles for analyzing a helical material.[33, 34] The torsion angles for all of the dipyrrin polymers were measured from consecutive copper (Cu1) and bridged *meso*-carbon atoms (C10) (Table 4-1). The structures of [Cu(3-pyrdpm)(hfacac)], [Cu(3-quindpm)(hfacac)], [Cu(42-pyrdpm)(hfacac)], [Cu(43-pyrdpm)(acac)], and [Cu(43-pyrdpm)(tfacac)], which appeared to be helical when viewed along the crystallographic *b*-axis, all have torsion angles of the same sign, thus confirming their helicity. However, [Cu(43-pyrdpm)(hfacac)] which was difficult to identify, has torsion angles of opposite signs, therefore is not helical.

Table 4-1. One-dimensional coordination polymers and physical properties

Compound	Torsion angles(º)	Geometry	Chain crystallographic axis	Pitch Cu–Cu diameter (Å)	Pitch Cu–Cu length (Å)
[Cu(3-pyrdpm)(acac)]	-180, 180	Zigzag	*a*	n/a	n/a
[Cu(4-pyrdpm)(acac)]	-180, 0	Zigzag	*a*	n/a	n/a
[Cu(4-pyrdpm)(tfacac)]	140.0, -2.8	Zigzag	*a*	n/a	n/a
[Cu(3-pyrdpm)(tfacac)]	45.9, 105.5	Helical	*b*	5.44	13.81
[Cu(3-pyrdpm)(hfacac)]	136.2, 11.6	Helical	*b*	6.84	9.69
[Cu(3-quindpm)(acac)]	-180, -180	Zigzag	*a*	n/a	n/a
[Cu(3-quindpm)(hfacac)]	-11.0,-149.8	Helical	*b*	6.94	9.66
[Cu(42-pyrdpm)(hfacac)]	38.6, 84.4	Helical	*b*	10.06	9.06
[Cu(43-pyrdpm)(acac)]	53.1, 86.7	Helical	*b*	11.11	18.13
[Cu(43-pyrdpm)(tfacac)]	92.3, 51.5	Helical	*b*	11.16	18.53
[Cu(43-pyrdpm)(hfacac)]	45.1, -153.2	Unknown	*c*	n/a	n/a

[Cu(4-pyrdpm)(acac)], [Cu(4-pyrdpm)(tfacac)], and [Cu(3-pyrdpm)(acac)] are zigzag, while [Cu(3-pyrdpm)(tfacac)] and [Cu(3-pyrdpm)(hfacac)] are helical. The quinoline structures are comparable to the pyridyl structures with [Cu(3-quindpm)(acac)] as zigzag and [Cu(3-quindpm)(hfacac)] as helical. When extending the ligand, [Cu(42-pyrdpm)(hfacac)], [Cu(43-pyrdpm)(acac)], and [Cu(43-pyrdpm)(tfacac)] are helical. [Cu(43-pyrdpm)(hfacac)] is determined to not be helical based on its torsion angles but it is also clearly not zigzag. A trend is observed in the structures because the helicity of the structures appears to be driven by the fluorination of the acac ligand along with the position of the nitrogen atom in the *meso*-substituted group.

With a series of helical polymers, other parameters such as pitch diameter and pitch length can be compared (Table 4-1). The pitch length was determined from the Cu–Cu distance of one helix rotation. The pitch diameter was calculated by forming a triangle with three copper(II) atoms in the helix twist and then calculating the distance of the line formed between the apex of the middle copper(II) atom and the center of the line between the two other copper(II) atoms. Interestingly, in addition to similar chemical properties and packing topologies, [Cu(3-pyrdpm)(hfacac)] and [Cu(3-quindpm)(hfacac)] have very similar pitch lengths and diameters.

4.2.6. Dinuclear and Trinuclear Species

As mentioned previously, the amount of $Cu(tfacac)_2$ and $Cu(hfacac)_2 \cdot H_2O$ had to be monitored because the presence of an excess metal salt can create larger dinuclear and trinuclear species. Initially, dipyrromethanes were oxidized and the amount of copper(II) salts were added in situ based on a complete conversion of the dipyrromethane to the dipyrromethene, which usually resulted in an excess of the copper(II) salt being added. Red solids, almost identical in color to the mononuclear complexes, were formed and the products were isolated and purified by column chromatography. The products were crystallized and analyzed by X-ray diffraction. In certain cases, rather then the desired heteroleptic dipyrrin structures, larger dinuclear and trinuclear species are formed by the binding of the *meso*-pyridine or quinoline to excess $Cu(tfacac)_2$ or $Cu(hfacac)_2$ (Scheme 4-1).

Scheme 4-1. Synthesis of the dinuclear and trinuclear species [Cu_2(4-pyrdpm)(Racac)$_3$] and [Cu_3(4-pyrdpm)$_2$(Racac)$_4$].

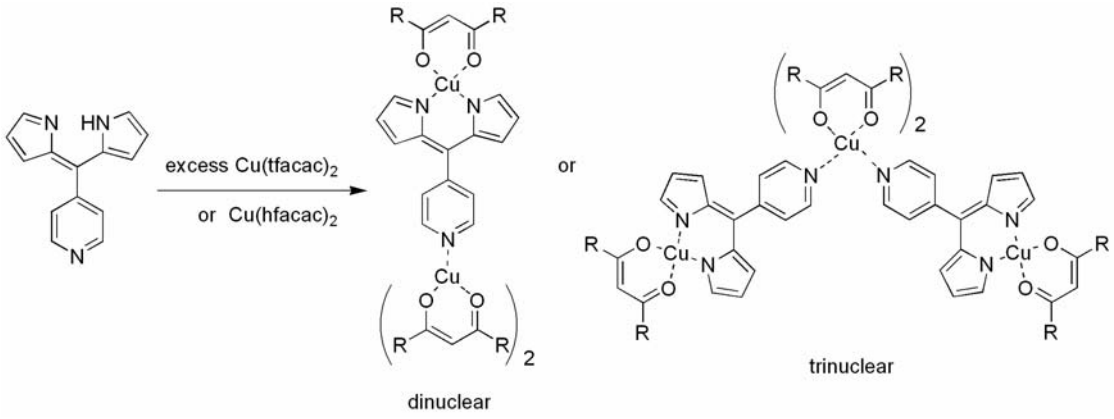

The first complex of this kind characterized by X-ray diffraction was a trinuclear complex consisting of 4-pyrdpm and an excess of Cu(hfacac)$_2$ ([Cu_3(4-pyrdpm)$_2$(hfacac)$_4$]) (Figure 4-42). Mass spectrometry does not show the parent ion peak, but only a peak for [Cu(4-pyrdpm)(hfacac)], which is a fragment of the complex. Electronic absorption spectroscopy shows very similar transitions at 232, 304, and 490 nm, compared to the mononuclear complex at 232, 312, and 492 nm. Infrared spectroscopy shows more intense carbonyl stretches, and elemental analysis is consistent with the new trinuclear complex as well. The X-ray crystal structure displays two units of [Cu(4-pyrdpm)(hfacac)] bridged by the pyridine nitrogen atoms to a single Cu(hfacac)$_2$ group. The two pyridine complexes bind in a *cis*-fashion to create a bent complex. The heteroleptic square planar dipyrrin copper(II) centers have slightly shortened Cu–N_{dpm} and Cu–O bond distances of 1.92-1.93 Å and 1.95-1.97 Å, respectively.

Additional dinuclear and trinuclear complexes were isolated and identified by

X-ray diffraction before the synthesis of the dipyrrin metal complexes was modified to control the amount of $Cu(tfacac)_2$ and $Cu(hfacac)_2$ added. Another complex was isolated from the addition of 4-pyrdpm and an excess of $Cu(tfacac)_2$ to produce the dinuclear complex $[Cu_2(4\text{-pyrdpm})(tfacac)_3]$ (Figure 4-43). Once again, more intense carbonyl stretches are detected by infrared spectroscopy. The crystal structure displays a slightly distorted square planar heteroleptic copper(II) center with one dipyrrin and one acac ligand, and a square pyramidal copper(II) center with two acac and one pyridine ligand.

While only a trinuclear complex is observed with the addition of $Cu(hfacac)_2$, and only a dinuclear complex is observed with the addition of $Cu(tfacac)_2$ to 4-pyrdpm, both trinuclear and dinuclear complexes are found in the same crystallization vial for 4-quindpm and $Cu(tfacac)_2$. The trinuclear complex (Figure 4-45) has two square planar copper(II) centers containing dipyrrin acac ligands and one octahedral copper(II) center with two tfacac and two pyridine ligands. It has a very elongated $Cu–N_{pyr}$ bond distance of 2.51 Å. In contrast to the other trinuclear complex with 4-pyrdpm, the two pyridine ligands are axial creating a linear complex. The dinuclear complex (Figure 4-44) displays a square planar copper(II) center and one square pyramidal copper(II) center with a $Cu–N_{pyr}$ bond distance of 2.33 Å.

Finally, a trinuclear complex is isolated from the addition of 42-pyrdpm and an excess of $Cu(tfacac)_2$ ($[Cu_3(42\text{-pyrdpm})_2(tfacac)_4]$) (Figure 4-46). The octahedral copper(II) center contains the pyridine ligands in the axial positions with a $Cu–N_{pyr}$ bond distance of 2.53 Å.

4.3. Conclusions

In summary, a variety of polymeric and supramolecular topologies are synthesized using self-complementary, self-assembling heteroleptic copper(II) complexes. Heteroleptic complexes of the formulation [Cu(dpm)(acac)] with the dipyrrin ligands 4-pyrdpm, 3-pyrdpm, 2-pyrdpm, 3-quindpm, 42-pyrdpm, 43-pyrdpm, and 44-pyrdpm, form a variety of topologies from discrete complexes to one-dimensional zigzag and helical polymers. The polymeric and supramolecular copper(II) complexes display square pyramidal coordination geometries with the acac and dipyrrin chelates occupying the square plane and the pyridyl or quinoline nitrogen atoms from a neighboring complex occupying the apical site.

The introduction of the perfluorinated spectator ligands tfacac and hfacac is found to have a large influence on the resulting supramolecular structure. Complexes of the formulation [Cu(dpm)(hfacac)] and [Cu(dpm)(tfacac)] with the dipyrrin ligands 4-pyrdpm, 3-pyrdpm, 4-quindpm, 3-quindpm, 42b-pyrdpm, 42-pyrdpm, and 43-pyrdpm also form a variety of topologies from discrete complexes, supramolecular hexagons, and one-dimensional zigzag and helical polymers.

The self-assembly of these molecular aggregates is driven by metal–ligand bonding, but is also modulated by F–F interactions. Perfluorination of the spectator ligand tends to generate more compact structures and is attributed to the self-aggregation of trifluoromethyl groups. The results presented here demonstrate that F–F contacts can be used to modulate supramolecular structure in the solid state. The use of F–F interactions as a way to influence solid-state self-assembly may prove

useful in fine-tuning the structure of crystalline materials. Finally, by modifying the dipyrrin and acac ligands in a stepwise fashion, guidelines have been established by which these supramolecular structures can be devised and manipulated.[35]

Pyridine and quinoline substituted dipyrrins were the only coordinating ligands studied in this analysis; however, other types of ligands may also coordinate to the copper(II) center of the dipyrrin metal complex, which would introduce even more types of dipyrrin coordination polymers and supramolecular structures. Other types of metals besides copper(II) may also be employed, which would also further expand the substitution capabilities of the polymers and supramolecular structures.

4.4. Experimental Section

General Procedures/Methods: Unless otherwise noted, starting materials were obtained from commercial suppliers and used without further purification. Pyrrole was freshly distilled. Elemental analyses were performed at NuMega Resonance Labs, San Diego, California. $^{1}H/^{13}C$NMR spectra were recorded on a Varian FT-NMR spectrometer running at 300 and 400 MHz at the Department of Chemistry and Biochemistry, University of California, San Diego. Infrared spectra were collected on a Mattson Research Series FT-IR instrument (using KBr pellets, laboratory of Prof. Clifford P. Kubiak) at the Department of Chemistry and Biochemistry, University of California, San Diego. UV-Visible spectra were recorded using a Perkin-Elmer Lambda 25 spectrophotometer with the UVWinLab 4.2.0.0230 software package. Mass spectra were acquired at the Small Molecule Mass Spectrometry Facility located

in the Department of Chemistry and Biochemistry, University of California, San Diego. A ThermoFinnigan LCQDECA mass spectrometer was used for the ESI or APCI analysis, and the data were analyzed using the Xcalibur software suite. A ThermoFinnigan MAT 900XL mass spectrometer was used to acquire the data for the high resolution mass spectra (HRMS).

Complex Synthesis and Characterization:

[Cu(4-pyrdpm)$_2$]. 5-(4-Pyridyl)dipyrromethane[22] (0.30 g, 1.34 mmol) was dissolved in 150 mL of $CHCl_3$, and the solution was stirred in an ice bath. DDQ (0.31 g, 1.34 mmol) was dissolved in 100 mL of benzene, and the solution was added slowly dropwise. After addition, the solvent was evaporated to half the volume and [$CuCl_2 \cdot 2H_2O$] (0.092 g, 0.54 mmol) dissolved in 50 mL of MeOH was added. The mixture was stirred for 10 min to form the copper(II) complex. The solution was evaporated to dryness, and the product was purified by column chromatography (SiO_2; $CHCl_3$/1% MeOH) to afford a dichroic red/green film. Yield: 25%. FAB-MS: *m*/*z* 504.5 $[M+H]^+$. Anal. Calcd for $C_{28}H_{20}N_6Cu$: C, 66.72; H, 4.00; N, 16.67. Found: C, 66.35; H, 3.70; N, 16.45. λ_{max} = 230, 302, 378, 470, 502 nm. IR (film from CH_2Cl_2): *ν* 995, 1022, 1037, 1244, 1335, 1376, 1404, 1536, 2924, 3094 cm^{-1}.

[Cu(3-pyrdpm)$_2$]. The same procedure was used as in the synthesis of [Cu(4-pyrdpm)$_2$] starting from 5-(3-pyridyl)dipyrromethane (0.50 g, 2.24 mmol).[22] Yield: 16%. FAB-MS: *m*/*z* 504.5 $[M+H]^+$. Anal. Calcd for $C_{28}H_{20}N_6Cu \cdot 0.5H_2O$: C, 64.42; H, 4.25; N, 16.10. Found: C, 64.50; H, 4.11; N, 15.90. λ_{max} = 232, 318, 372, 468, 502

nm. IR (film from CH_2Cl_2): *v* 995, 1023, 1037, 1244, 1335, 1376, 1405, 1547, 2925, 3094 cm^{-1}.

[Cu(4-pyrdpm)(acac)]. 5-(4-Pyridyl)dipyrromethane[22] (0.50 g, 2.24 mmol) was dissolved in 150 mL of $CHCl_3$ and the solution was stirred in an ice bath. DDQ (0.51 g, 2.24 mmol) was dissolved in 100 mL of benzene, and the solution was added slowly dropwise. $[Cu(acac)_2]$ (0.59 g, 2.24 mmol) was dissolved in 20 mL of $CHCl_3$ and the solution was added to the reaction mixture, which was stirred for 10 min to form the copper(II) complex. The solution was evaporated to dryness, and the product was purified by column chromatography (SiO_2; $CHCl_3$ with 0.5% MeOH) to afford brown/red crystals. Yield: 40%. FAB-MS: *m*/*z* 383.4 $[M+H]^+$, 283.2 $[M\text{-}acac]^+$. Anal. Calcd for $C_{19}H_{17}N_3O_2Cu$: C, 59.60; H, 4.48; N, 10.97. Found: C, 59.68; H, 4.68; N, 11.04. λ_{max} = 230, 300, 364, 496 nm. IR (film from CH_2Cl_2): *v* 993, 1025, 1245, 1338, 1387, 1520, 1557, 1592, 2920, 3045, 3093 cm^{-1}.

[Cu(3-pyrdpm)(acac)]. The same procedure was used as in the synthesis of [Cu(4-pyrdpm)(acac)] starting from 5-(3-pyridyl)dipyrromethane (0.30 g, 1.34 mmol).[22] Yield: 58%. FAB-MS: *m*/*z* 383.4 $[M+H]^+$. Anal. Calcd for $C_{19}H_{17}N_3O_2Cu{\cdot}0.5CH_2Cl_2$: C, 55.06; H, 4.27; N, 9.88. Found: C, 55.01; H, 4.67; N, 9.94. λ_{max} = 232, 302, 362, 496 nm. IR (film from CH_2Cl_2): *v* 993, 1026, 1244, 1337, 1378, 1520, 1549, 1591, 2919, 3094 cm^{-1}.

[Cu(2-pyrdpm)(acac)]. The same procedure was used as in the synthesis of [Cu(4-pyrdpm)(acac)] starting from 5-(2-pyridyl)dipyrromethane (0.90 g, 4.03 mmol).[22] Yield: 17%. ESI-MS: *m*/*z* 383.1 $[M+H]^+$. Anal. Calcd for

$C_{19}H_{17}N_3O_2Cu \cdot 0.5CH_2Cl_2$: C, 55.06; H, 4.27; N, 9.88. Found: C, 55.32; H, 4.34; N, 9.95. λ_{max} = 230, 300, 366, 498 nm. IR (film from CH_2Cl_2): *v* 996, 1028, 1246, 1337, 1384, 1520, 1555, 1586, 2854 cm^{-1}.

[Cu(4-pyrdpm)(tfacac)]. 5-(4-pyridyl)dipyrromethane[22] (0.30 g, 1.34 mmol) was dissolved in 150 mL of $CHCl_3$, and the solution was stirred in an ice bath. DDQ (0.31 g, 1.34 mmol) was dissolved in 125 mL of benzene, and the solution was added slowly dropwise. After addition, the solvent was evaporated to half the volume and filtered through celite. $Cu(tfacac)_2$ (0.60 g, 1.61 mmol) was dissolved in 50 mL $CHCl_3$ and added in small increments to the solution until all of the oxidized dipyrromethene had been converted to the metal complex as detected by TLC (yellow mobile band to a red mobile band) and UV/Vis. The solution was evaporated to dryness and the product was purified by column chromatography (SiO_2; CH_2Cl_2/1% MeOH) to afford a red/green solid. Yield: 13% (0.076 g). ESI-MS: *m/z* 436.9 $[M+H]^+$. Anal. Calcd for $C_{19}H_{14}F_3N_3O_2Cu \cdot 0.33CH_2Cl_2$: C, 49.92; H, 3.18; N, 9.03. Found C, 49.40; H, 3.57; N, 9.23. λ_{max} = 232, 304, 490 nm. IR (film from CH_2Cl_2): *v* 1627, 1558, 1568, 1408, 1379, 1340, 1296, 1246, 1140, 1028, 995 cm^{-1}.

[Cu(3-pyrdpm)(tfacac)]. The same procedure was used as in the synthesis of [Cu(4-pyrdpm)(tfacac)] with 5-(3-pyridyl)dipyrromethane[22] (0.30 g, 1.34 mmol) to afford a red/green solid. Yield: 21% (0.125 g). ESI-MS: *m/z* 436.9 $[M+H]^+$. Anal. Calcd for $C_{19}H_{14}F_3N_3O_2Cu$: C, 52.24; H, 3.23; N, 9.62. Found C, 51.85; H, 3.51; N, 9.61. λ_{max} = 232, 306, 492 nm. IR (film from CH_2Cl_2): *v* 1626, 1551, 1378, 1340, 1296, 1245, 1139, 109, 995 cm^{-1}.

[Cu(4-pyrdpm)(hfacac)]. The same procedure was used as in the synthesis of [Cu(4-pyrdpm)(tfacac)] with 5-(4-pyridyl)dipyrromethane[22] (0.30 g, 1.34 mmol) to afford a red solid. Yield: 22% (0.15 g). ESI-MS: *m/z* 490.9 $[M+H]^+$. Anal. Calcd for $C_{19}H_{11}F_6N_3O_2Cu$: C, 46.49; H, 2.26; N, 8.56. Found: C, 46.46; H, 2.23; N 8.75. λ_{max} = 232, 312, 492 nm. IR (film from CH_2Cl_2): *v* 1648, 1560, 1252, 1209, 1144, 1030, 997 cm^{-1}.

[Cu(3-pyrdpm)(hfacac)]. The same procedure was used as in the synthesis of [Cu(4-pyrdpm)(tfacac)] with 5-(3-pyridyl)dipyrromethane[22] (0.30 g, 1.34 mmol) to afford a red solid. Yield: 17% (0.11 g). FAB-MS: *m/z* 491.2 $[M+H]^+$. Anal. Calcd for $C_{19}H_{11}F_6N_3O_2Cu$: C, 46.49; H, 2.26; N, 8.56. Found: C, 46.65; H, 2.32; N, 8.88. λ_{max} = 232, 264, 320, 494 nm. IR (film from CH_2Cl_2): *v* 1649, 1553, 1379, 1341, 1252, 1209, 1144, 1030, 997 cm^{-1}.

5-(3-Quinolyl)dipyrromethane. 3-Quinolinecarboxaldehyde (0.50 g, 3.2 mmol) was dissolved in 15 mL of neat pyrrole and bubbled with nitrogen for 20 min. The solution was refluxed for 12 h under nitrogen. The pyrrole was evaporated and the product was purified by column chromatography (SiO_2; CH_2Cl_2/1% MeOH) to afford a yellow foam. Yield: 74% (0.64 g). ESI-MS: *m/z* 274.2 $[M+H]^+$, 207.3 [M-pyrrole]$^+$. ^{1}HNMR ($CDCl_3$ 400MHz, 25 °C): δ 5.60 (s,1H), 5.89 (s, 2H), 6.18 (q, 2H, *J* = 2.8 Hz), 6.75 (m, 2H), 7.50 (t, 1H, *J* = 7.2 Hz), 7.63-7.69 (m, 2H), 7.83 (s, 1H), 8.04 (d, 1H, *J* = 8.8 Hz), 8.48 (bs, 2H, NH), 8.65 ppm (s, 1H). ^{13}CNMR ($CDCl_3$ 100MHz, 25 °C): δ 41.7, 107.7, 108.4, 117.8, 126.7, 127.6, 127.8, 128.6, 129.2, 131.2, 134.4, 135.2, 146.7, 151.2 ppm. IR (film from CH_2Cl_2): *v* 3178, 3096, 2971, 1690, 1615,

1608, 1566, 1540, 1497, 1401, 1265, 1093, 1028, 7910, 773, 690 cm^{-1}.

[Cu(3-quindpm)(acac)]. The same procedure was used as in the synthesis of [Cu(4-pyrdpm)(acac)] from 5-(3-quinolyl)dipyrromethane (0.31 g, 1.12 mmol) to afford a red solid. Yield: 19% (0.095 g). FAB-MS: *m/z* 432.7 $[M+H]^+$. FAB-HRMS: *m/z* 433.0853 $[M+H]^+$ (Calcd. *m/z* 433.0846). λ_{max} = 235, 297, 497 nm. IR (film from CH_2Cl_2): *v* 1589, 1552, 1525, 1406, 1391, 1371, 1338, 1245, 1028, 996 cm^{-1}.

[Cu(3-quindpm)(tfacac)]. The same procedure was used as in the synthesis of [Cu(4-pyrdpm)(tfacac)] from 5-(3-quinolyl)dipyrromethane (0.14 g, 0.53 mmol) to afford a red solid. Yield: 63% (0.155 g). ESI-MS: *m/z* 486.95 $[M+H]^+$. EI-HRMS: *m/z* 486.0489 $[M+H]^+$ (Calcd. *m/z* 486.0485). λ_{max} = 234, 317, 492 nm. IR (film from CH_2Cl_2): *v* 1625, 1554, 1377, 1340, 1297, 1247, 1140, 1028, 997 cm^{-1}.

[Cu(3-quindpm)(hfacac)]. The same procedure was used as in the synthesis of [Cu(4-pyrdpm)(tfacac)] from 5-(3-quinolyl)dipyrromethane (0.30 g, 1.11 mmol) to afford a red solid. Yield: 38% (0.23 g). FAB-MS: *m/z* 541.4 $[M+H]^+$. FAB-HRMS: *m/z* 541.0287 $[M+H]^+$ (Calcd. *m/z* 541.0281). λ_{max} = 234, 262, 323, 492 nm. IR (film from CH_2Cl_2): *v* 2926, 1655, 1553, 1373, 1340, 1253, 1211, 1154, 1141, 1033, 999 cm^{-1}.

5-(4-Quinolyl)dipyrromethane. The same procedure was used as in the synthesis of 5-(3-quinolyl)dipyrromethane from 4-quinolinecarboxaldehyde (0.5 g, 3.18 mmol) to afford a yellow solid. Yield: 53% (0.46 g). ESI-MS: *m/z* 274.1 $[M+H]^+$. ^{1}HNMR ($CDCl_3$ 400MHz, 25 °C): δ 5.90 (m, 2H), 6.18 (q, 2H), 6.23 (s, 1H), 6.74 (m, 2H), 6.98 (d, 1H), 7.47 (td, 1H), 7.67 (td, 1H), 7.98 (d, 1H), 8.06 (d,

1H), 8.21 (bs, NH, 2H), 8.70 ppm (d, 1H). ^{13}CNMR ($CDCl_3$ 100MHz, 25 °C): δ 39.9, 107.9, 108.6, 117.6, 120.5, 1234, 126.6, 126.7, 129.1, 129.8, 130.3, 147.8, 148.0, 150.1 ppm. IR (film from CH_2Cl_2): *v* 3191, 3103, 2983, 2860, 1591, 1571, 1562, 1508, 1418, 1265, 1093, 1029, 799, 776, 723 cm^{-1}.

[Cu(4-quindpm)(acac)]. The same procedure was used as in the synthesis of [Cu(4-pyrdpm)(acac)] from 5-(4-quinolyl)dipyrromethane (0.38 g, 1.38 mmol) to afford a red solid.. Yield: 14% (0.084 g). FAB-MS: *m/z* 432.6 $[M+H]^+$. FAB-HRMS: *m/z* 433.0850 $[M+H]^+$ (Calcd. *m/z* 433.0846). λ_{max} = 230, 297, 499 nm. IR (film from CH_2Cl_2): *v* 1584, 1562, 1556, 1405, 1390, 1376, 1338, 1248, 1027, 995 cm^{-1}.

[Cu(4-quindpm)(tfacac)]. The same procedure was used as in the synthesis of [Cu(4-pyrdpm)(tfacac)] from 5-(4-quinolyl)dipyrromethane (0.33 g, 1.22 mmol) to afford a red solid. Yield: 43% (0.256 g). ESI-MS: *m/z* 487.0 $[M+H]^+$. Anal. Calcd for $C_{23}H_{16}F_3N_3O_2Cu$: C, 56.73; H, 3.31; N, 8.63. Found C, 57.01; H, 2.76; N, 8.79. λ_{max} = 230, 302, 494 nm. IR (film from CH_2Cl_2): *v* 1625, 1554, 1377, 1340, 1297, 1247, 1140, 1028, 997 cm^{-1}.

[Cu(4-quindpm)(hfacac)]. The same procedure was used as in the synthesis of [Cu(4-pyrdpm)(tfacac)] from 5-(4-quinolyl)dipyrromethane (0.27 g, 0.98 mmol) to afford red/green crystals. Yield: 34% (0.18 g). ESI-MS: *m/z* 540.9 $[M+H]^+$. Anal. Calcd for $C_{23}H_{16}F_3N_3O_2Cu$: C, 56.73; H, 3.31; N, 8.63. Found: C, 57.01; H, 2.76; N, 8.79. λ_{max} = 230, 263, 302, 317, 495 nm. IR (film from CH_2Cl_2): *v* 1648, 1555, 1378, 1341, 1251, 1212, 1145, 1029, 998 cm^{-1}.

[5-(4-pyridin-2-ylphenyl)dipyrromethane]. The same procedure was used as

in the synthesis of 5-(3-quinolyl)dipyrromethane with 4-(2-pyridyl)benzaldehyde (0.50 g, 2.7 mmol) to afford a yellow foam. Yield: 63% (0.51 g). ESI-MS: *m/z* 300.14 $[M+H]^+$, 258.3 [M-pyrrole]$^+$. ^{1}HNMR ($CDCl_3$ 400MHz, 25 °C): δ 5.48 (s, 1H), 5.94 (m, 2H), 6.19 (q, 2H, *J* = 2.8 Hz), 6.67 (m, 2H), 7.21 (m, 1H), 7.29 (d, 2H, *J* = 8.0 Hz), 7.68-7.75 (m, 2H), 7.91 (d, 2H, *J* = 8.0 Hz), 8.14 (bs, 2H, NH), 8.64 ppm (m, 1H). ^{13}CNMR ($CDCl_3$ 100MHz, 25 °C): δ 43.6, 107.1, 108.2, 117.2, 120.4, 121.9, 127.0, 128.6, 132.1, 136.6, 137.8, 142.8, 149.3, 156.8 ppm.

[Cu(42b-pyrdpm)(hfacac)]. The same procedure was used as in the synthesis of [Cu(4-pyrdpm)(tfacac)] with [5-(4-pyridin-2-ylphenyl)dipyrromethane] (0.26 g, 0.87 mmol) to afford a red/green solid. Yield: 18% (90 mg). ESI-MS: *m/z* 566.94 $[M+H]^+$. Anal. Calcd for $C_{25}H_{15}F_6N_3O_2Cu$: C, 52.96; H, 2.67; N, 7.41. Found C, 52.62; H, 2.92; N, 7.54. λ_{max} = 249, 331, 490 nm. IR (film from CH_2Cl_2): *v* 2911, 1642, 1562, 1547, 1250, 1207, 1156, 1139, 1033, 1002 cm^{-1}.

[4-(pyridin-2-ylethynyl)benzaldehyde]. A mixture of 4-bromobenzaldehyde (0.50 g, 2.70 mmol), 2-ethynylpyridine (0.56 g, 5.41 mmol), triethylamine (0.55 g, 5.41 mmol), $Pd(PPh_3)_2Cl_2$ (0.19 g, 0.27 mmol), triphenylphosphine (18 mg, 0.068 mmol), CuI (26 mg, 0.135 mmol), and 25 mL of dry THF was stirred under nitrogen for 24 h. It was diluted with 75 mL of CH_2Cl_2, washed with 75 mL 0.1 M EDTA and 75 mL brine then dried over $MgSO_4$. The solvent was evaporated and the product was purified by column chromatography (SiO_2; CH_2Cl_2/1% MeOH) to afford a yellow solid. Yield: 67% (0.38 g). GC-MS: *m/z* 207.1 $[M]^+$. ^{1}HNMR ($CDCl_3$ 400MHz, 25 °C): δ 7.07 (m, 1H), 7.35 (d, 1H, *J* = 7.6 Hz), 7.51 (m, 3H), 7.67 (d, 2H, *J* = 8.4 Hz)

8.45 (d, 1H, *J* = 4.8 Hz) 9.82 ppm (s, 1H, CHO). ^{13}CNMR ($CDCl_3$ 100MHz, 25 °C): δ 87.4, 91.6, 122.8, 126.9, 127.7, 128.9, 131.9, 135.2, 135.7, 141.9, 149.5, 190.6 ppm.

[5-(4-pyridin-2-ylethynylphenyl)dipyrromethane]. The same procedure was used as in the synthesis of 5-(3-quinolyl)dipyrromethane with [4-(pyridin-2-ylethynyl)benzaldehyde] (0.38 g, 1.82 mmol) to afford a yellow solid. Yield: 79% (0.46 g). ESI-MS: *m/z* 324.2 $[M+H]^+$. ^{1}HNMR ($CDCl_3$ 400MHz, 25 °C): δ 5.49 (s, 1H), 5.91 (m, 2H), 6.17 (m, 2H), 6.72 (m, 2H), 7.19-7.26 (m, 3H), 7.68 (td, 1H, *J* = 7.6 Hz, *J* = 2.0 Hz), 8.04 (2H, bs, NH), 8.58 ppm (d, 1H, *J* = 4.8 Hz). ^{13}CNMR ($CDCl_3$ 100MHz, 25 °C): δ 43.9, 88.5, 89.1, 107.3, 108.4, 117.4, 120.7, 122.6, 127.0, 128.3, 131.7, 132.1, 136.0, 143.0, 143.2, 149.8 ppm.

[Cu(42-pyrdpm)(acac)]. The same procedure was used as in the synthesis of [Cu(4-pyrdpm)(tfacac)] with [5-(4-pyridin-2-ylethynylphenyl)dipyrromethane] (0.31 g, 0.97 mmol) to afford a red solid. Yield: 6% (0.026 g). APCI-MS: *m/z* 482.97 $[M+H]^+$. FAB-HRMS: *m/z* 482.0930 $[M+H]^+$ (Calcd. *m/z* 482.0924). λ_{max} = 227, 298, 337, 495 nm. IR (film from CH_2Cl_2): *v* 2922, 1583, 1560, 1536, 1520, 1405, 1383, 1338, 1247, 1030, 997 cm^{-1}.

[Cu(42-pyrdpm)(tfacac)]. The same procedure was used as in the synthesis of [Cu(4-pyrdpm)(tfacac)] with [5-(4-pyridin-2-ylethynylphenyl)dipyrromethane] (0.20 g, 0.62 mmol) to afford a red solid. Yield: 48% (0.16 g). FAB-MS: *m/z* 537.4 $[M+H]^+$. FAB-HRMS: *m/z* 537.0730 $[M+H]^+$ (Calcd. *m/z* 537.0720). λ_{max} = 232, 298, 339, 490 nm. IR (film from CH_2Cl_2): *v* 2925, 1616, 1561, 1529, 1301, 1194, 1138, 1033, 1001 cm^{-1}.

[Cu(42-pyrdpm)(hfacac)]. The same procedure was used as in the synthesis of [Cu(4-pyrdpm)(tfacac)] with [5-(4-pyridin-2-ylethynylphenyl)dipyrromethane] (0.46 g, 1.43 mmol) to afford a red solid. Yield: 13% (0.11 g). APCI-MS: *m/z* 590.96 $[M+H]^+$. Anal. Calcd for $C_{27}H_{15}F_6N_3O_2Cu$: C, 54.87; H, 2.56; N, 7.11. Found C, 54.63; H, 2.43; N, 7.32. λ_{max} = 229, 270, 299, 332, 491 nm. IR (film from CH_2Cl_2): *v* 2919, 2851, 1649, 1556, 1532, 1247, 1142, 1032, 996 cm^{-1}.

[4-(pyridin-3-ylethynyl)benzaldehyde]. The same procedure was used as in the synthesis of [4-(pyridin-2-ylethynyl)benzaldehyde] with 4-bromobenzaldehyde (0.50 g, 2.70 mmol) and 3-ethynylpyridine (0.56 g, 5.41 mmol) to afford a yellow solid. Yield: 65% (0.36 g, 65%). GC-MS: *m/z* 207.1 $[M]^+$. ^{1}HNMR ($CDCl_3$ 400MHz, 25 °C): δ 7.19 (m, 1H), 7.58 (d, 2H, *J* = 8.0 Hz), 7.72 (dt, 1H, *J* = 8.0 Hz, *J* = 2.0 Hz), 7.76 (d, 2H, *J* = 8.4 Hz), 8.48, (d, 1H, *J* = 4.0 Hz), 8.69, (s, 1H), 9.91 ppm (s, 1H, CHO). ^{13}CNMR ($CDCl_3$ 100MHz, 25 °C): δ 89.4, 91.3, 119.2, 122.7, 128.1, 129.1, 131.7, 135.3, 138.1, 148.7, 151.8, 190.7 ppm.

[5-(4-pyridin-3-ylethynylphenyl)dipyrromethane]. The same procedure was used as in the synthesis of 5-(3-quinolyl)dipyrromethane from [4-(pyridin-3-ylethynyl)benzaldehyde] (0.36 g, 1.13 mmol) to afford a yellow solid. Yield: 41% (0.24 g). ESI-MS: *m/z* 324.2 $[M+H]^+$, 258.3 $[M–pyrrole]^+$. ^{1}HNMR ($CDCl_3$ 400MHz, 25 °C): δ 5.48 (s, 1H), 5.91 (m, 2H), 6.72 (m, 2H), 7.20 (d, 2H, *J* = 8.0 Hz), 7.28 (m, 1H), 7.48 (d, 2H, *J* = 8.4 Hz), 7.79 (dt, 1H, *J* = 8.0 Hz, *J* = 2.0 Hz), 8.16 (bs, 2H, NH), 8.50 (dd, 1H, *J* = 4.8 Hz, *J* = 2.0 Hz), 8.65 ppm (d, 1H, *J* = 1.6 Hz). ^{13}CNMR ($CDCl_3$ 100MHz, 25 °C): δ 43.9, 85.9, 92.4, 107.3, 108.3, 117.4, 120.9, 122.9, 128.4, 131.7,

132.1, 138.3, 142.9, 148.2, 151.9 ppm.

[Cu(43-pyrdpm)(acac)]. The same procedure was used as in the synthesis of [Cu(4-pyrdpm)(tfacac)] with [5-(4-pyridin-3-ylethynylphenyl)dipyrromethane] (0.36 g, 1.13 mmol) to afford a red/orange solid. Yield: 21% (0.11 g). EI-MS: *m/z* 482.2 $[M]^+$. FAB-HRMS: *m/z* 482.0928 $[M+H]^+$ (Calcd. *m/z* 482.0924). λ_{max} = 227, 297, 340, 494 nm. IR (film from CH_2Cl_2): *v* 2920, 1589, 1557, 1518, 1405, 1383, 1338, 1246, 1028, 996 cm^{-1}.

[Cu(43-pyrdpm)(tfacac)]. The same procedure was used as in the synthesis of [Cu(4-pyrdpm)(tfacac)] with [5-(4-pyridin-3-ylethynylphenyl)dipyrromethane] (0.24 g, 0.73 mmol) to afford a red/orange solid (0.063 g, 16% yield). ESI-MS: *m/z* 537.0 $[M+H]^+$. FAB-HRMS: *m/z* 537.0718 $[M+H]^+$ (Calcd. *m/z* 537.0720). λ_{max} = 228, 280, 343, 491 nm. IR (film from CH_2Cl_2): *v* 2924, 2853, 1625, 1555, 1380, 1339, 1296, 1140, 1029, 996 cm^{-1}.

[Cu(43-pyrdpm)(hfacac)]. The same procedure was used as in the synthesis of [Cu(4-pyrdpm)(tfacac)] with [5-(4-pyridin-3-ylethynylphenyl)dipyrromethane] (0.31 g, 0.95 mmol) to afford a red/orange solid. Yield: 9% (0.048 g). ESI-MS: *m/z* 590.93 $[M+H]^+$. Anal. Calcd for $C_{27}H_{15}F_6N_3O_2Cu$: C, 54.87; H, 2.56; N, 7.11. Found C, 55.04; H, 2.95; N, 7.31. λ_{max} = 228, 279, 336, 491 nm. IR (film from CH_2Cl_2): *v* 2922, 2852, 1649, 1557, 1251, 1207, 1147, 1031, 998 cm^{-1}.

[4-(pyridin-4-ylethynyl)benzaldehyde]. 4-(Ethynyl)benzaldehyde (0.33 g, 2.5 mmol), 4-bromopyridine hydrochloride (0.64 g, 3.3 mmol), $Pd(PPh_3)_2Cl_2$ (89 mg, 0.13 mmol), CuI (24 mg, 0.13 mmol), and 25 mL of dry diethylamine was stirred

under nitrogen for 24 h. It was evaporated and diluted with 75 mL of CH_2Cl_2, washed with 75 mL DI H_2O and 75 mL brine then dried over $MgSO_4$. The solvent was evaporated and the product was purified by column chromatography (SiO_2; CH_2Cl_2/1% MeOH) to afford a yellow solid. Yield: 58% (0.31 g). GC-MS: *m/z* 207.1 $[M]^+$. ^{1}HNMR ($CDCl_3$ 400MHz, 25 °C): δ 7.27 (d, 2H, *J* = 3.6 Hz), 7.55 (d, 2H, *J* = 8.4 Hz), 7.74 (d, 2H, *J* = 8.4 Hz), 8.51 (d, 2H, *J* = 4.0 Hz), 9.89 ppm (s, 1H, CHO). ^{13}CNMR ($CDCl_3$ 100MHz, 25 °C): δ 89.7, 92.2, 125.1, 127.6, 129.1, 130.1, 131.9, 135.6, 149.3, 190.6 ppm.

[5-(4-pyridin-4-ylethynylphenyl)dipyrromethane]. The same procedure was used as in the synthesis of 5-(3-quinolyl)dipyrromethane from [4-(pyridin-4-ylethynyl)benzaldehyde] (0.31 g, 1.5 mmol) to afford a yellow solid.. Yield: 40% (0.19 g). ESI-MS: *m/z* 324.12 $[M+H]^+$, 258.23 [M–pyrrole]$^+$. ^{1}HNMR ($CDCl_3$ 400MHz, 25 °C): δ 5.50 (s, 1H), 5.90 (m, 2H), 6.17 (m, 2H), 6.72 (m, 2H), 7.23 (d, 2H, *J* = 8.0 Hz), 7.37 (d, 2H, *J* = 6.0 Hz), 7.49 (d, 2H, *J* = 8.4 Hz), 8.07 (bs, 2H, NH), 8.57 (d, 2H, *J* = 6.4 Hz). ^{13}CNMR ($CDCl_3$ 100MHz, 25°C): δ 43.9, 86.6, 93.8, 107.3, 108.4, 117.4, 120.5, 125.4, 128.4, 131.3, 131.6, 132.0, 143.3, 149.5 ppm.

[Cu(44-pyrdpm)(acac)]. The same procedure was used as in the synthesis of [Cu(4-pyrdpm)(tfacac)] with [5-(4-pyridin-4-ylethynylphenyl)dipyrromethane] (0.163 g, 0.51 mmol) to afford a red/orange solid. Yield: 41% (0.101 g). FAB-MS: *m/z* 483.3 $[M+H]^+$. FAB-HRMS: *m/z* 483.0999 $[M+H]^+$ (Calcd. *m/z* 483.1003). λ_{max} = 228, 294, 340, 496 nm. IR (film from CH_2Cl_2): *v* 2921, 1592, 1551, 1515, 1404, 1384, 1338, 1246, 1027, 995 cm^{-1}.

[Cu(44-pyrdpm)(tfacac)]. The same procedure was used as in the synthesis of [Cu(4-pyrdpm)(tfacac)] with [5-(4-pyridin-4-ylethynylphenyl)dipyrromethane] (0.082 g, 0.25 mmol) to afford a red/orange solid. Yield: 44% (0.060 g). FAB-MS: *m/z* 537.3 $[M+H]^+$. FAB-HRMS: *m/z* 537.0714 $[M+H]^+$ (Calcd. *m/z* 537.0720). λ_{max} = 228, 294, 495 nm. IR (film from CH_2Cl_2): *v* 1626, 1556, 1380, 1340, 1296, 1246, 1140, 1029, 997 cm^{-1}.

[Cu(44-pyrdpm)(hfacac)]. The same procedure was used as in the synthesis of [Cu(4-pyrdpm)(tfacac)] with [5-(4-pyridin-4-ylethynylphenyl)dipyrromethane] (0.19 g, 0.59 mmol) to afford a red/orange solid. Yield: 8% (0.026 g). ESI-MS: *m/z* 590.98 $[M+H]^+$. FAB-HRMS: *m/z* 591.0433 $[M+H]^+$ (Calcd. *m/z* 591.0437). λ_{max} = 228, 293, 320, 491 nm. IR (film from CH_2Cl_2): *v* 2926, 2854, 1650, 1603, 1556, 1407, 1381, 1341, 1252, 1207, 1153, 1031, 998 cm^{-1}.

$[Cu_3(4\text{-pyrdpm})_2(hfacac)_4]$. 5-(4-Pyridyl)dipyrromethane[22] (0.30 g, 1.34 mmol) was dissolved in $CHCl_3$ (150 mL) and stirred in an ice bath. DDQ (0.31 g, 1.34 mmol) was dissolved in benzene (100 mL) and added dropwise. $Cu(hfacac)_2 \cdot H_2O$ (0.64 g, 1.34 mmol) dissolved in $CHCl_3$ (50 mL) was added and stirred for 10 min to form the copper(II) complex. The reaction mixture was evaporated to dryness, and the product was purified by column chromatography (SiO_2; $CHCl_3$/1% MeOH) to afford a red solid. Yield: 27% (0.27 g). Anal. Calcd for $C_{48}H_{24}F_{24}N_6O_8Cu_3 \cdot 0.5CHCl_3$: C, 38.35; H, 1.63; N, 5.53. Found: C, 38.02; H, 1.27; N, 5.56. λ_{max} = 232, 304, 490 nm. IR (film from CH_2Cl_2): *v* 1644, 1562, 1255, 1214, 1145, 1029, 1000 cm^{-1}.

Differential Scanning Calorimetry and Thermogravimetric Analysis. Differential scanning calorimetry (DSC) experiments were performed on a Shimadzu DSC-50 instrument in a helium atmosphere with a flow rate of 30 cm^3/min. Crystalline samples were heated from ~25 to 500 °C at a rate of 10 °C/min. Thermogravimetric analysis (TGA) experiments were performed on a Shimadzu TGA-50 with a flow rate of 40 cm^3/min of nitrogen. Crystalline samples were heated from ~25 to 800 °C at a rate of 4 °C/min.

4.5. Acknowledgment

Text, schemes, and figures of this chapter, in part, are reprints of the materials published in the following papers: Sara R. Halper, Mitchell R. Malachowski, Heather M. Delaney, and Seth M. Cohen, "Heteroleptic Copper Dipyrromethene Complexes: Synthesis, Structure, and Coordination Polymers" *Inorg. Chem.* **2004**, 43, 1242-1249; Sara R. Halper and Seth M. Cohen, "Self-Assembly of Two Distinct Supramolecular Motifs in a Single Crystalline Framework" *Angew. Chem. Intl. Ed*. **2004**, 43, 2385-2388; Sara R. Halper and Seth M. Cohen, "Self-Assembly of Heteroleptic [Cu(dipyrrinato)(hfacac)] Complexes Driven by Fluorine–Fluorine Interactions" *Inorg. Chem.* **2005**, 44, 4139-4141. The co-authors listed in these publications also participated in the research. The permissions to reproduce these papers were granted by John Wiley & Sons Inc., and the American Chemistry Society.

4.6. Appendix

X-ray Crystal Structure Determination

Details: Single crystals of each compound suitable for X-ray diffraction structural determination were mounted on quartz capillaries with Paratone oil and were cooled in a nitrogen stream on the diffractometer. Data were collected on either a Bruker AXS or a Bruker P4 diffractometer each equipped with area detectors. Peak integrations were performed with the Siemens SAINT software package. Absorption corrections were applied using the program SADABS. Space group determinations were performed by the program XPREP. The structures were solved by either Patterson or direct methods and refined with the SHELXTL software package (Sheldrick, G. M. *SHELXTL vers. 5.1 Software Reference Manual*; Bruker AXS: Madison, WI, 1997). All hydrogen atoms were fixed at calculated positions with isotropic thermal parameters, and all non-hydrogen atoms were refined anisotropically unless otherwise noted.

Structure of [Cu(4-pyrdpm)$_2$]. Dark green blocks were grown by diffusion of pentane into a toluene solution containing the complex. No solvent molecules were found co-crystallized with the complex.

Structure of [Cu(4-pyrdpm)(acac)]. Brown/red blocks were grown by diffusion of pentane into a solution of the complex in benzene. Suitable crystals could also be obtained by slow evaporation of a CH_2Cl_2 solution containing the complex. The compound was found to have a continuous one-dimensional polymeric structure. No solvent molecules were found co-crystallized.

Structure of [Cu(3-pyrdpm)(acac)]. Dark green blocks were grown by slow evaporation of a CH_2Cl_2 solution containing the complex. The compound was found to have a continuous one-dimensional polymeric structure. The complex co-crystallized with one molecule of CH_2Cl_2 in the asymmetric unit. A relatively large residual peak (3.44 e $Å^{-3}$) was found near one of the chlorine atoms of the CH_2Cl_2 molecule. This may represent some disorder in the otherwise well ordered solvent molecule; however, this residual density was not further modeled or refined.

Structure of [Cu(2-pyrdpm)(acac)]. Dark green blocks suitable for X-ray diffraction were grown by slow evaporation of a CH_2Cl_2/hexanes mixture containing the complex. No solvent molecules were found co-crystallized.

Structure of [Cu(4-pyrdpm)(tfacac)]. Green rods suitable for X-ray diffraction structural determination were grown by evaporation from a solution of the complex dissolved in CH_2Cl_2. The complex co-crystallized with two molecules of methylene chloride in the asymmetric unit.

Structure of [Cu(3-pyrdpm)(tfacac)]. Green blocks suitable for X-ray diffraction structural determination were grown by evaporation from a solution of the complex dissolved in CH_2Cl_2. No solvent molecules were found co-crystallized.

Structure of [Cu(4-pyrdpm)(hfacac)]. Red-green blocks suitable for X-ray diffraction were grown from a solution of the complex in $CHCl_3$ diffused with hexanes. No solvent molecules were found co-crystallized.

Structure of [Cu(3-pyrdpm)(hfacac)]. Green blocks suitable for X-ray diffraction structural determination were grown by evaporation from a solution of the

complex dissolved in $CHCl_3$. Samples cooled to 100 K were unstable (crystals fractured); therefore, the data was collected at 223 K. The complex co-crystallized with one disordered molecule of $CHCl_3$, which was treated as a diffuse contribution using the program SQUEEZE (A. Spek, Platon Library). Electron count/unit cell: 221 (found), 256 (expected).

Structure of [Cu(3-quindpm)(acac)]. Orange rods suitable for X-ray diffraction structural determination were grown by evaporation from a solution of the complex dissolved in CH_2Cl_2. No solvent molecules were found co-crystallized.

Structure of [Cu(3-quindpm)(hfacac)]. Red rods suitable for X-ray diffraction structural determination were grown from a solution of the complex dissolved in $CHCl_3$ diffused with pentane. The complex co-crystallized with one molecule of chloroform in the asymmetric unit.

Structure of [Cu(4-quindpm)(hfacac)]. Green blocks suitable for X-ray diffraction structural determination were grown from a solution of the complex dissolved in $CHCl_3$ diffused with hexane. The complex co-crystallized with one molecule of hexane in the asymmetric unit.

Structure of [Cu(42b-pyrdpm)(hfacac)]. Red rods suitable for X-ray diffraction structural determination were grown by slow evaporation of the complex dissolved in CH_2Cl_2. No solvent molecules were found co-crystallized.

Structure of [Cu(42-pyrdpm)(acac)]. Orange plates suitable for X-ray diffraction structural determination were grown by slow evaporation of the complex dissolved in CH_2Cl_2. No solvent molecules were found co-crystallized.

Structure of [Cu(42-pyrdpm)(hfacac)]. Green plates suitable for X-ray diffraction structural determination were grown by slow evaporation of the complex dissolved in CH_2Cl_2. No solvent molecules were found co-crystallized.

Structure of [Cu(43-pyrdpm)(acac)]. Green/orange blocks suitable for X-ray diffraction structural determination were grown by slow evaporation of the complex dissolved in CH_2Cl_2. The complex co-crystallized with one molecule of methylene chloride in the asymmetric unit.

Structure of [Cu(43-pyrdpm)(tfacac)]. Orange plates suitable for X-ray diffraction structural determination were grown from a solution of the complex dissolved in $CHCl_3$ diffused with pentane. No solvent molecules were found co-crystallized.

Structure of [Cu(43-pyrdpm)(hfacac)]. Green blocks suitable for X-ray diffraction structural determination were grown from a solution of the complex dissolved in $CHCl_3$ diffused with pentane. No solvent molecules were found co-crystallized with the complex. One CF_3 group found in two independent orientations, and was modeled as such.

Structure of [Cu(44-pyrdpm)(acac)]. Orange blocks suitable for X-ray diffraction structural determination were grown by slow evaporation of the complex dissolved in CH_2Cl_2. No solvent molecules were found co-crystallized.

Structure of [Cu_3(4-pyrdpm)$_2$(hfacac)$_4$]. Red plates suitable for X-ray diffraction structural determination were grown from a solution of the complex in $CHCl_3$ diffused with pentane. The complex co-crystallized with one molecule of

$CHCl_3$ in the asymmetric unit.

Structure of [Cu_2(4-pyrdpm)(tfacac)$_3$]. Green blocks suitable for X-ray diffraction structural determination were grown by slow evaporation of the complex dissolved in CH_2Cl_2. No solvent molecules were found co-crystallized.

Structure of [Cu_2(4-quindpm)(tfacac)$_3$]. Orange rods suitable for X-ray diffraction structural determination were grown from a solution of the complex in $CHCl_3$ diffused with hexane. No solvent molecules were found co-crystallized.

Structure of [Cu_3(4-quindpm)$_2$(tfacac)$_4$]. Red needles suitable for X-ray diffraction structural determination were grown from the same solution as [Cu_2(4-quindpm)(tfacac)$_3$] ($CHCl_3$ diffused with hexane). No solvent molecules were found co-crystallized.

Structure of [Cu_3(42-pyrdpm)$_2$(tfacac)$_4$]. Green blocks suitable for X-ray diffraction structural determination were grown by slow evaporation of the complex dissolved in CH_2Cl_2. No solvent molecules were found co-crystallized.

X-ray Crystal Structure Details for [Cu(4-pyrdpm)$_2$]

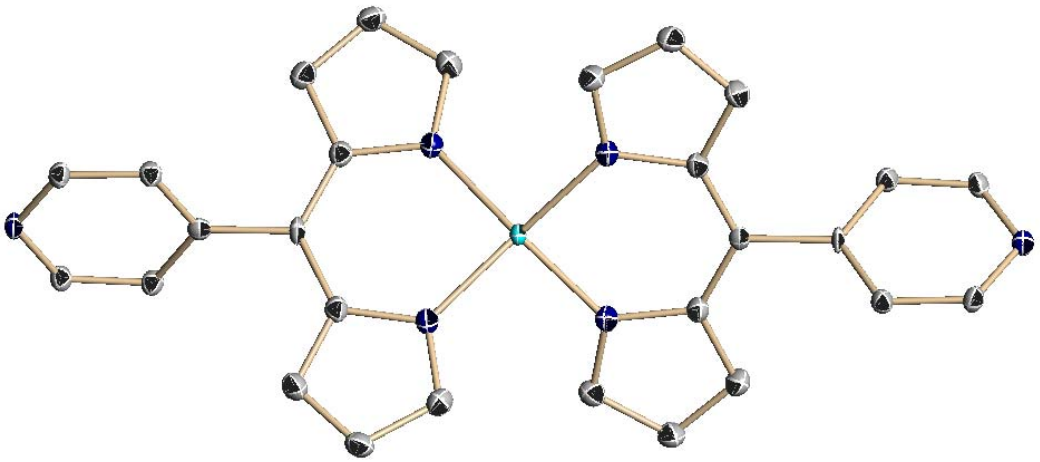

Figure 4-24. Structural Diagram of [Cu(4-pyrdpm)$_2$] (ORTEP, 50% probability ellipsoids). Hydrogen atoms have been omitted for clarity.

Table 4-2. Crystal Data for [Cu(4-pyrdpm)$_2$].

Empirical formula	Cu C_{28} H_{20} N_6	
Temperature	100(2) K	
Crystal system	Orthorhombic	
Space group	*Aba*2	
Unit cell dimensions	a = 8.9282(7) Å	α = 90°
	b = 8.9150(7) Å	β = 90°
	c = 28.113(2) Å	γ = 90°
Volume	2237.7(3) Å^3	
Z	4	
Crystal size	0.45 × 0.30 × 0.20 mm^3	
Reflections collected	6241	
Independent reflections	2046 [R(int) = 0.0164]	
Data / restraints / parameters	2046 / 1 / 162	
Goodness-of-fit on F^2	1.141	
Final R indices [I>2σ(I)]	R1 = 0.0266, wR2 = 0.0728	
R indices (all data)	R1 = 0.0268, wR2 = 0.0730	

X-ray Crystal Structure Details for [Cu(4-pyrdpm)acac]

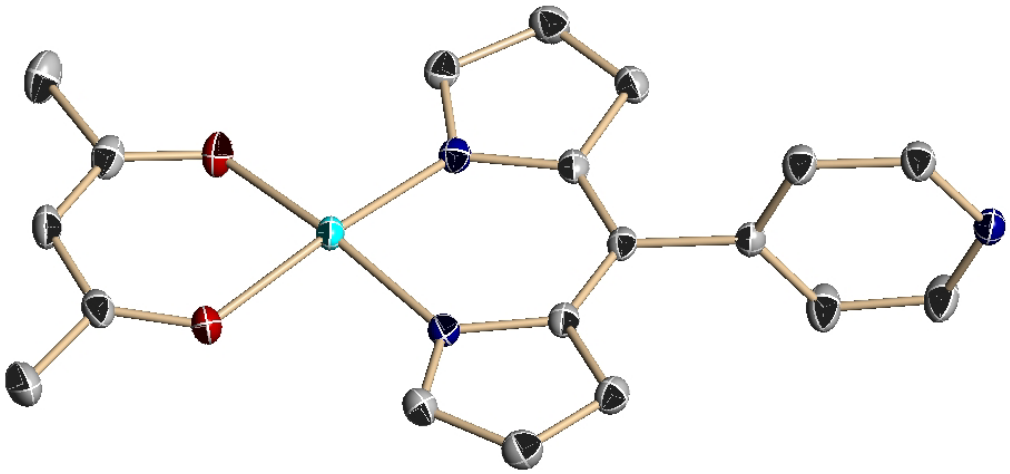

Figure 4-25. Structural Diagram of [Cu(4-pyrdpm)acac] (ORTEP, 50% probability ellipsoids). Hydrogen atoms have been omitted for clarity.

Table 4-3. Crystal Data for [Cu(4-pyrdpm)acac].

Empirical formula	$Cu_{1.33}\ C_{25.33}\ H_{22.67}\ N_4\ O_{2.67}$	
Temperature	100(2) K	
Crystal system	Orthorhombic	
Space group	*Pnma*	
Unit cell dimensions	a = 14.0337(10) Å	α = 90°
	b = 11.9862(9) Å	β = 90°
	c = 10.4162(7) Å	γ = 90°
Volume	1752.1(2) Å^3	
Z	4	
Crystal size	0.50 × 0.35 × 0.30 mm^3	
Reflections collected	10150	
Independent reflections	2107 [R(int) = 0.0229]	
Data / restraints / parameters	2107 / 0 / 128	
Goodness-of-fit on F^2	1.112	
Final R indices [I>2σ(I)]	$R1$ = 0.0268, $wR2$ = 0.0778	
R indices (all data)	$R1$ = 0.0293, $wR2$ = 0.0787	

X-ray Crystal Structure Details for [Cu(3-pyrdpm)acac]

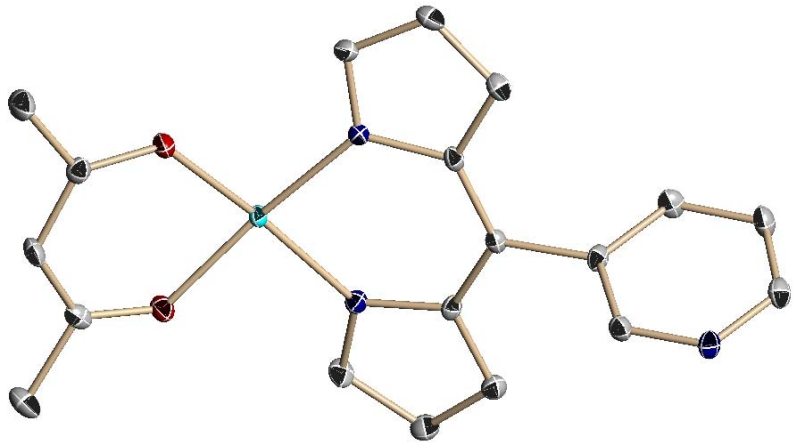

Figure 4-26. Structural Diagram of [Cu(3-pyrdpm)acac] (ORTEP, 50% probability ellipsoids). Hydrogen atoms and solvent molecules have been omitted for clarity.

Table 4-4. Crystal Data for [Cu(3-pyrdpm)acac].

Empirical formula	Cu $C_{19.5}$ H_{18} N_3 O_2 Cl	
Temperature	100(2) K	
Crystal system	Triclinic	
Space group	*P*-1	
Unit cell dimensions	a = 8.3811(5) Å	α = 117.520(1)°
	b = 15.5837(10) Å	β = 91.737(1)°
	c = 116.5921(11) Å	γ = 98.950(1)°
Volume	1714.7(2) $Å^3$	
Z	4	
Crystal size	0.30 × 0.15 × 0.15 mm^3	
Reflections collected	16478	
Independent reflections	8431 [R(int) = 0.0229]	
Data / restraints / parameters	8431 / 0 / 482	
Goodness-of-fit on F^2	1.052	
Final R indices [I>2σ(I)]	$R1$ = 0.0545, $wR2$ = 0.1472	
R indices (all data)	$R1$ = 0.0647, $wR2$ = 0.1543	

X-ray Crystal Structure Details for [Cu(2-pyrdpm)acac]

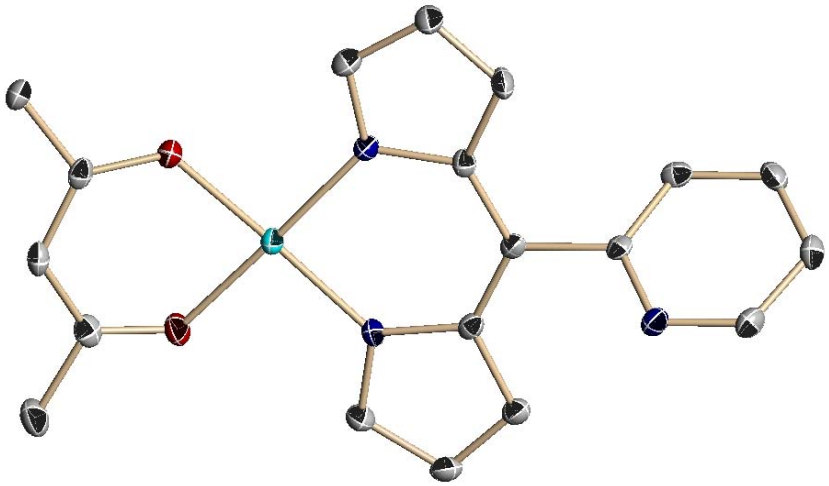

Figure 4-27. Structural Diagram of [Cu(2-pyrdpm)acac] (ORTEP, 50% probability ellipsoids). Hydrogen atoms have been omitted for clarity.

Table 4-5. Crystal Data for [Cu(2-pyrdpm)acac].

Empirical formula	Cu C_{19} H_{17} N_3 O_2	
Temperature	100(2) K	
Crystal system	Orthorhombic	
Space group	*P*2(1)2(1)2(1)	
Unit cell dimensions	a = 9.4788(6) Å	α = 90°
	b = 9.9354(6) Å	β = 90°
	c = 35.677(2) Å	γ = 90°
Volume	3359.9(4) $Å^3$	
Z	8	
Crystal size	0.35 × 0.30 × 0.10 mm^3	
Reflections collected	21289	
Independent reflections	7640 [R(int) = 0.0296]	
Data / restraints / parameters	7640 / 0 / 455	
Goodness-of-fit on F^2	1.044	
Final R indices [I>2σ(I)]	$R1$ = 0.0330, $wR2$ = 0.0727	
R indices (all data)	$R1$ = 0.0359, $wR2$ = 0.0738	

X-ray Crystal Structure Details for [Cu(4-pyrdpm)(tfacac)]

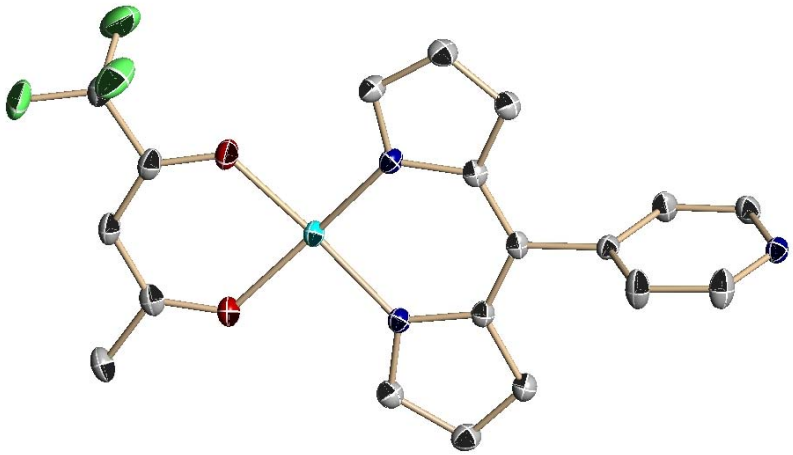

Figure 4-28. Structural Diagram of [Cu(4-pyrdpm)(tfacac)] (ORTEP, 50% probability ellipsoids). Hydrogen atoms and solvent molecules have been omitted for clarity.

Table 4-6. Crystal Data for [Cu(4-pyrdpm)(tfacac)].

Empirical formula	$Cu\ C_{20}\ H_{16}\ F_3\ N_3\ O_2\ Cl_2$	
Temperature	100(2) K	
Crystal system	Monoclinic	
Space group	*P*2(1)/c	
Unit cell dimensions	a = 14.3951(10) Å	α = 90°
	b = 21.1481(15) Å	β = 106.849(10)°
	c = 14.6063(11) Å	γ = 90°
Volume	4255.7(5) $Å^3$	
Z	8	
Crystal size	0.23 × 0.19 × 0.13 mm^3	
Reflections collected	36307	
Independent reflections	9747 [R(int) = 0.0285]	
Data / restraints / parameters	9747 / 0 / 561	
Goodness-of-fit on F^2	1.064	
Final R indices [I>2σ(I)]	$R1$ = 0.0390, $wR2$ = 0.0945	
R indices (all data)	$R1$ = 0.0485, $wR2$ = 0.0994	

X-ray Crystal Structure Details for [Cu(3-pyrdpm)(tfacac)]

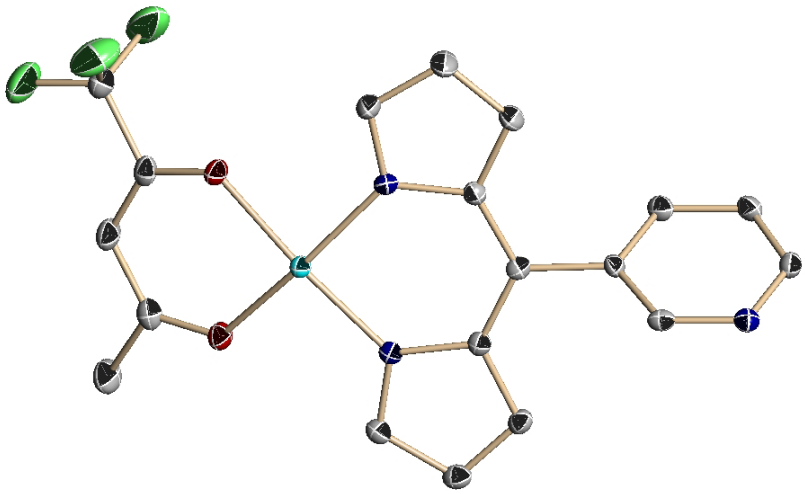

Figure 4-29. Structural Diagram of [Cu3-pyrdpm)(tfacac)] (ORTEP, 50% probability ellipsoids). Hydrogen atoms have been omitted for clarity.

Table 4-7. Crystal Data for [Cu(3-pyrdpm)(tfacac)].

Empirical formula	$Cu\ C_{19}\ H_{14}\ F_3\ N_3\ O_2$	
Temperature	100(2) K	
Crystal system	Monoclinic	
Space group	*P*2(1)/n	
Unit cell dimensions	$a = 9.0165(5)$ Å	$\alpha = 90°$
	$b = 13.8073(8)$ Å	$\beta = 91.324(10)°$
	$c = 13.8996(8)$ Å	$\gamma = 90°$
Volume	1729.95(17) $Å^3$	
Z	4	
Crystal size	$0.13 \times 0.10 \times 0.09\ mm^3$	
Reflections collected	14759	
Independent reflections	3944 [*R*(int) = 0.0233]	
Data / restraints / parameters	3944 / 0 / 254	
Goodness-of-fit on F^2	1.107	
Final *R* indices [I>2σ(I)]	*R*1 = 0.0447, *wR*2 = 0.1161	
R indices (all data)	*R*1 = 0.0480, *wR*2 = 0.1180	

X-ray Crystal Structure Details for [Cu(4-pyrdpm)(hfacac)]

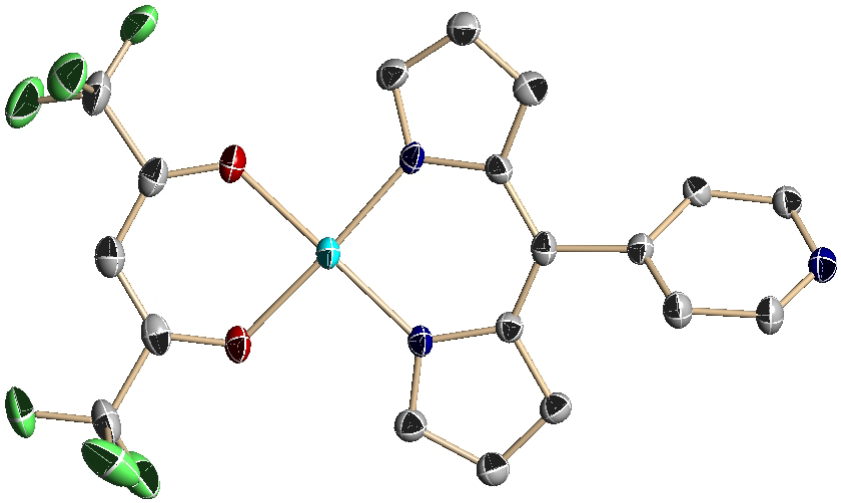

Figure 4-30. Structural Diagram of [Cu(4-pyrdpm)(hfacac)] (ORTEP, 50% probability ellipsoids). Hydrogen atoms have been omitted for clarity.

Table 4-8. Crystal Data for [Cu(4-pyrdpm)(hfacac)].

Empirical formula	Cu C_{19} H_{11} F_6 N_3 O_2	
Temperature	100(2) K	
Crystal system	Rhombohedral	
Space group	*R*-3	
Unit cell dimensions	a = 44.2373(18) Å	α = 90°
	b = 44.2373(18) Å	β = 90°
	c = 21.3285(18) Å	γ = 120°
Volume	36147(4) Å^3	
Z	54	
Crystal size	0.42 × 0.32 × 0.29 mm^3	
Reflections collected	70495	
Independent reflections	17300 [R(int) = 0.0612]	
Data / restraints / parameters	17300 / 0 / 838	
Goodness-of-fit on F^2	1.078	
Final R indices [I>2σ(I)]	$R1$ = 0.0780, $wR2$ = 0.2416	
R indices (all data)	$R1$ = 0.1105, $wR2$ = 0.2598	

X-ray Crystal Structure Details for [Cu(3-pyrdpm)(hfacac)]

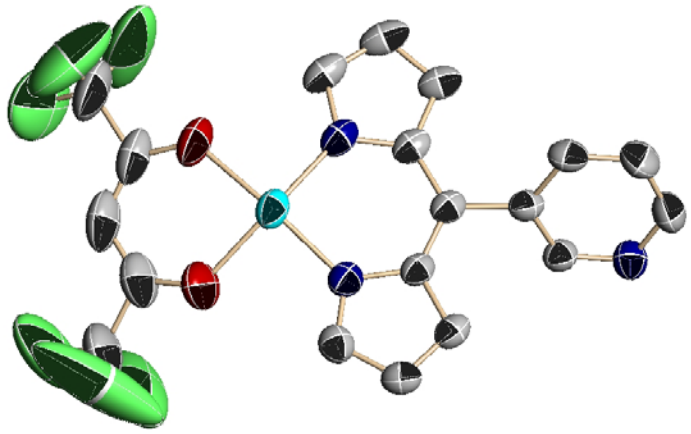

Figure 4-31. Structural Diagram of [Cu(3-pyrdpm)(hfacac)] (ORTEP, 50% probability ellipsoids). Hydrogen atoms and solvent molecules have been omitted for clarity.

Table 4-9. Crystal Data for [Cu(3-pyrdpm)(hfacac)].

Empirical formula	$Cu\ C_{20}\ H_{12}\ F_6\ N_3\ O_2\ Cl_3$	
Temperature	223(2) K	
Crystal system	Monoclinic	
Space group	*P*2(1)/c	
Unit cell dimensions	a = 15.5323(10) Å	α = 90°
	b = 9.6926(6) Å	β = 97.406(10)°
	c = 16.0408(11) Å	γ = 90°
Volume	2394.8(3) $Å^3$	
Z	4	
Crystal size	0.20 × 0.18 × 0.12 mm^3	
Reflections collected	20217	
Independent reflections	5473 [R(int) = 0.0256]	
Data / restraints / parameters	5473 / 0 / 280	
Goodness-of-fit on F^2	1.079	
Final R indices [I>2σ(I)]	$R1$ = 0.0553, $wR2$ = 0.1714	
R indices (all data)	$R1$ = 0.0680, $wR2$ = 0.1790	

X-ray Crystal Structure Details for [Cu(3-quindpm)(acac)]

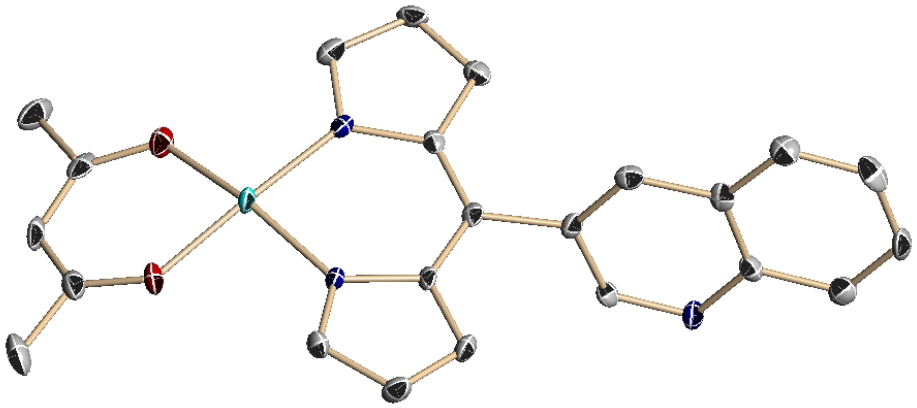

Figure 4-32. Structural Diagram of [Cu(3-quindpm)(acac)] (ORTEP, 50% probability ellipsoids). Hydrogen atoms have been omitted for clarity.

Table 4-10. Crystal Data for [Cu(3-quindpm)(acac)].

Empirical formula	Cu C_{23} H_{19} N_3 O_2	
Temperature	100(2) K	
Crystal system	Monoclinic	
Space group	*P*2(1)/c	
Unit cell dimensions	*a* = 8.4016(5) Å	$\alpha = 90°$
	b = 28.5805(18) Å	$\beta = 95.745(10)°$
	c = 16.3187(10) Å	$\gamma = 90°$
Volume	3898.8(4) $Å^3$	
Z	8	
Crystal size	0.18 × 0.08 × 0.03 mm^3	
Reflections collected	32963	
Independent reflections	8749 [*R*(int) = 0.0779]	
Data / restraints / parameters	8749 / 0 / 527	
Goodness-of-fit on F^2	1.0974	
Final *R* indices [I>2σ(I)]	*R*1 = 0.0667, *wR*2 = 0.1183	
R indices (all data)	*R*1 = 0.0986, *wR*2 = 0.1288	

X-ray Crystal Structure Details for [Cu(3-quindpm)(hfacac)]

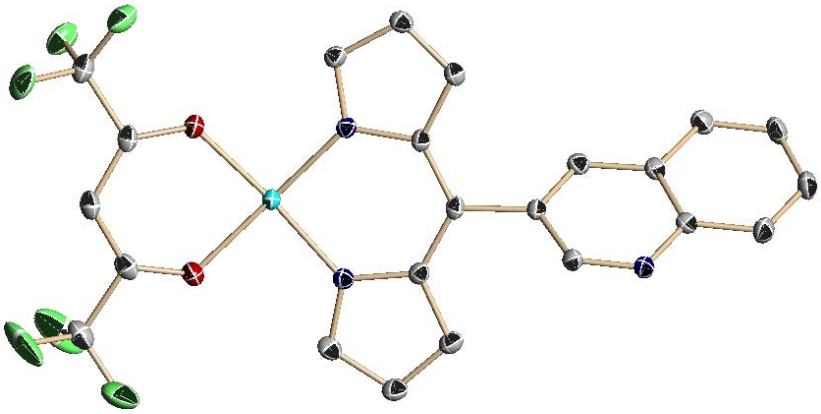

Figure 4-33. Structural Diagram of [Cu(3-quindpm)(hfacac)] (ORTEP, 50% probability ellipsoids). Hydrogen atoms and solvent molecules have been omitted for clarity.

Table 4-11. Crystal Data for [Cu(3-quindpm)(hfacac)].

Empirical formula	$Cu\ C_{23.5}\ H_{13.5}\ F_6\ N_3\ O_2\ Cl_{1.5}$	
Temperature	100(2) K	
Crystal system	Monoclinic	
Space group	*P*2(1)/n	
Unit cell dimensions	*a* = 15.7479(14) Å	$\alpha = 90°$
	b = 9.6616(8) Å	$\beta = 94.283(10)°$
	c = 32.162(3) Å	$\gamma = 90°$
Volume	4879.8(7) $Å^3$	
Z	8	
Crystal size	0.51 × 0.06 × 0.05 mm^3	
Reflections collected	41306	
Independent reflections	1694 [*R*(int) = 0.0314]	
Data / restraints / parameters	1694 / 0 / 667	
Goodness-of-fit on F^2	1.051	
Final *R* indices [I>2σ(I)]	*R*1 = 0.0659, *wR*2 = 0.1815	
R indices (all data)	*R*1 = 0.0756, *wR*2 = 0.1898	

X-ray Crystal Structure Details for [Cu(4-quindpm)(hfacac)]

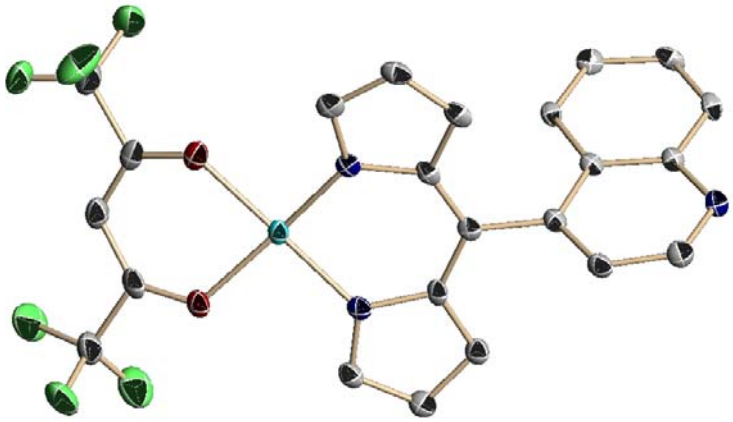

Figure 4-34. Structural Diagram of [Cu(4-quindpm)(hfacac)] (ORTEP, 50% probability ellipsoids). Hydrogen atoms and solvent molecules have been omitted for clarity.

Table 4-12. Crystal Data for [Cu(4-quindpm)(hfacac)].

Empirical formula	$Cu_6\ C_{150}\ H_{106}\ F_{36}\ N_{18}\ O_{12}$	
Temperature	100(2) K	
Crystal system	Monoclinic	
Space group	*C*2/c	
Unit cell dimensions	a = 22.6062(13) Å	α = 90°
	b = 21.8773(12) Å	β = 93.968(10)°
	c = 31.0283(17) Å	γ = 90°
Volume	15308.7(15) Å^3	
Z	4	
Crystal size	0.19 × 0.18 × 0.10 mm^3	
Reflections collected	64258	
Independent reflections	17420 [*R*(int) = 0.0618]	
Data / restraints / parameters	17420 / 0 / 1002	
Goodness-of-fit on F^2	1.084	
Final *R* indices [I>2σ(I)]	*R*1 = 0.0647, *wR*2 = 0.1517	
R indices (all data)	*R*1 = 0.0922, *wR*2 = 0.1639	

X-ray Crystal Structure Details for [Cu(42b-pyrdpm)(hfacac)]

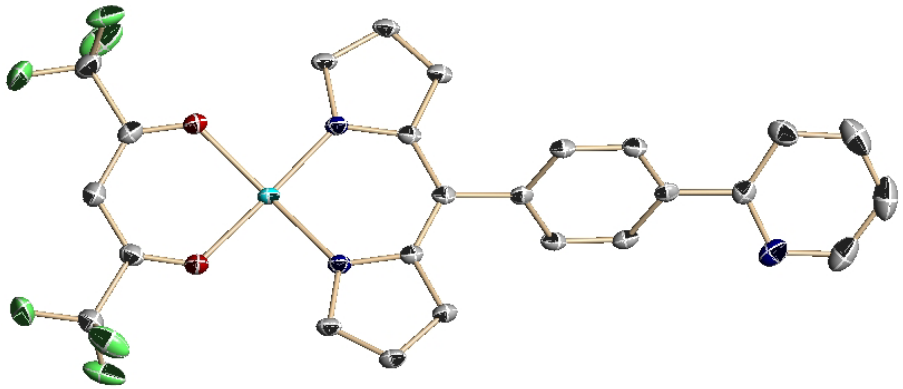

Figure 4-35. Structural Diagram of [Cu(42b-pyrdpm)(hfacac)] (ORTEP, 50% probability ellipsoids). Hydrogen atoms have been omitted for clarity.

Table 4-13. Crystal Data for [Cu(42b-pyrdpm)(hfacac)].

Empirical formula	$Cu\ C_{25}\ H_{15}\ F_6\ N_3\ O_2$	
Temperature	100(2) K	
Crystal system	Monoclinic	
Space group	*P*2(1)/c	
Unit cell dimensions	*a* = 16.0549(11) Å	$\alpha = 90°$
	b = 14.9864(10) Å	$\beta = 96.620(10)°$
	c = 9.3776(6) Å	$\gamma = 90°$
Volume	2241.3(3) $Å^3$	
Z	4	
Crystal size	0.20 × 0.08 × 0.01 mm^3	
Reflections collected	19026	
Independent reflections	5100 [*R*(int) = 0.0243]	
Data / restraints / parameters	5100 / 0 / 334	
Goodness-of-fit on F^2	1.063	
Final *R* indices [I>2σ(I)]	*R*1 = 0.0395, *wR*2 = 0.1084	
R indices (all data)	*R*1 = 0.0425, *wR*2 = 0.1120	

X-ray Crystal Structure Details for [Cu(42-pyrdpm)(acac)]

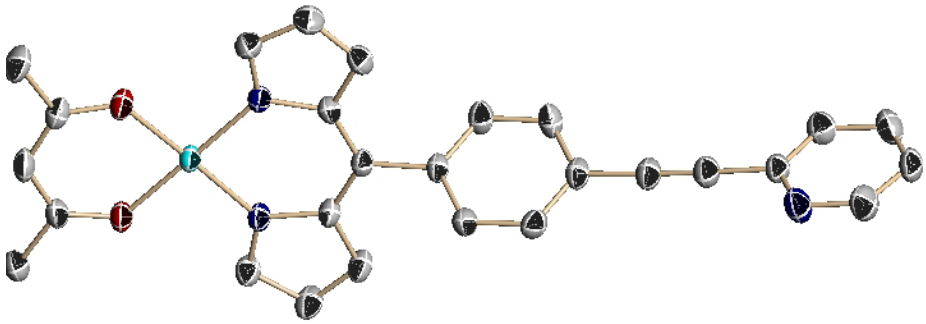

Figure 4-36. Structural Diagram of [Cu(42-pyrdpm)(acac)] (ORTEP, 50% probability ellipsoids). Hydrogen atoms have been omitted for clarity.

Table 4-14. Crystal Data for [Cu(42-pyrdpm)(acac)].

Empirical formula	Cu C_{27} H_{21} N_3 O_2	
Temperature	200(2) K	
Crystal system	Triclinic	
Space group	*P*-1	
Unit cell dimensions	a = 7.0891(6) Å	α = 80.0780(10)°
	b = 11.8956(10) Å	β = 83.8090(10)°
	c = 14.2247(12) Å	γ = 74.2010(10)°
Volume	1134.63(17) $Å^3$	
Z	2	
Crystal size	0.27 × 0.24 × 0.02 mm^3	
Reflections collected	9658	
Independent reflections	4943 [R(int) = 0.0169]	
Data / restraints / parameters	4943 / 0 / 300	
Goodness-of-fit on F^2	1.055	
Final R indices [I>2σ(I)]	$R1$ = 0.0337, $wR2$ = 0.0930	
R indices (all data)	$R1$ = 0.0388, $wR2$ = 0.0964	

X-ray Crystal Structure Details for [Cu(42-pyrdpm)(hfacac)]

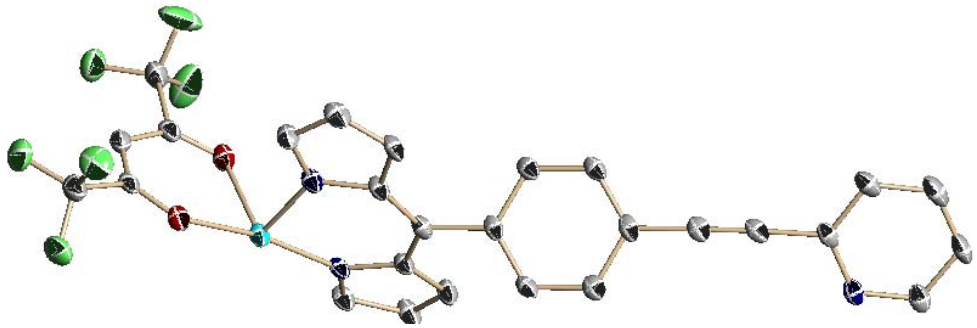

Figure 4-37. Structural Diagram of [Cu(42-pyrdpm)(hfacac)] (ORTEP, 50% probability ellipsoids). Hydrogen atoms have been omitted for clarity.

Table 4-15. Crystal Data for [Cu(42-pyrdpm)(hfacac)].

Empirical formula	Cu C_{27} H_{15} F_6 N_3 O_2	
Temperature	100(2) K	
Crystal system	Monoclinic	
Space group	*P*2(1)/c	
Unit cell dimensions	*a* = 17.689(4) Å	α = 90°
	b = 9.055(2) Å	β = 92.043(4)°
	c = 15.052(3) Å	γ = 90°
Volume	2409.5(9) $Å^3$	
Z	4	
Crystal size	0.24 × 0.16 × 0.04 mm^3	
Reflections collected	20079	
Independent reflections	5522 [*R*(int) = 0.0682]	
Data / restraints / parameters	5522 / 0 / 352	
Goodness-of-fit on F^2	1.081	
Final *R* indices [I>2σ(I)]	*R*1 = 0.0571, *wR*2 = 0.1260	
R indices (all data)	*R*1 = 0.0861, *wR*2 = 0.1426	

X-ray Crystal Structure Details for [Cu(43-pyrdpm)(acac)]

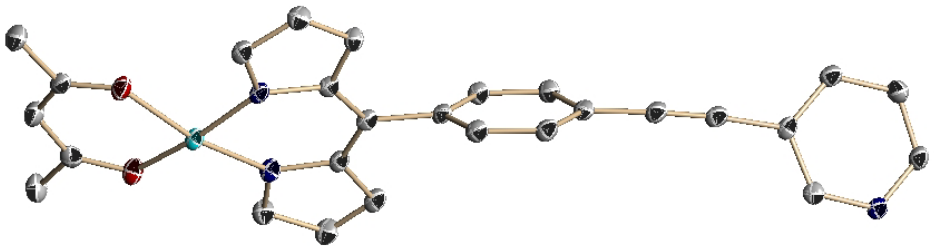

Figure 4-38. Structural Diagram of [Cu(43-pyrdpm)(acac)] (ORTEP, 50% probability ellipsoids). Hydrogen atoms and solvent molecules have been omitted for clarity.

Table 4-16. Crystal Data for [Cu(43-pyrdpm)(acac)].

Empirical formula	Cu $C_{27.5}$ H_{22} N_3 O_2 Cl	
Temperature	100(2) K	
Crystal system	Monoclinic	
Space group	*P*2(1)/n	
Unit cell dimensions	a = 15.9263(18) Å	α = 90°
	b = 18.127(2) Å	β = 106.687(2)°
	c = 17.2934(19) Å	γ = 90°
Volume	4782.3(9) Å^3	
Z	8	
Crystal size	0.10 × 0.07 × 0.05 mm^3	
Reflections collected	29613	
Independent reflections	10830 [R(int) = 0.0302]	
Data / restraints / parameters	10830 / 0 / 626	
Goodness-of-fit on F^2	1.068	
Final R indices [I>2σ(I)]	$R1$ = 0.0534, $wR2$ = 0.1454	
R indices (all data)	$R1$ = 0.0662, $wR2$ = 0.1542	

X-ray Crystal Structure Details for [Cu(43-pyrdpm)(tfacac)]

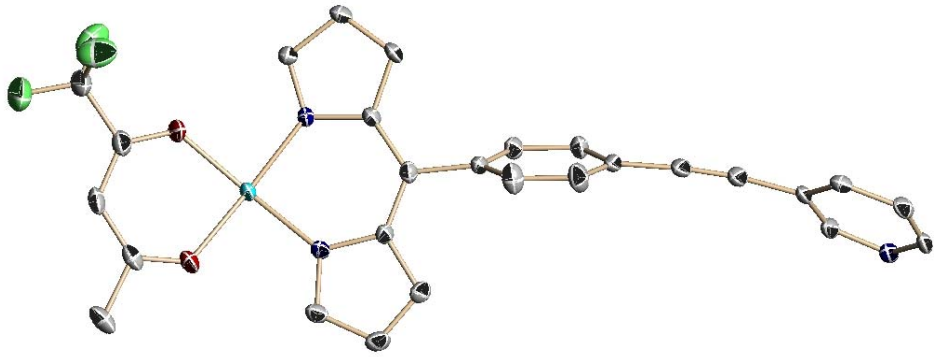

Figure 4-39. Structural Diagram of [Cu(43-pyrdpm)(tfacac)] (ORTEP, 50% probability ellipsoids). Hydrogen atoms have been omitted for clarity.

Table 4-17. Crystal Data for [Cu(43-pyrdpm)(tfacac)].

Empirical formula	Cu C_{27} H_{18} F_3 N_3 O_2	
Temperature	100(2) K	
Crystal system	Orthorhombic	
Space group	*P*bca	
Unit cell dimensions	a = 9.129(2) Å	α = 90°
	b = 18.529(4) Å	β = 90°
	c = 27.143(7) Å	γ = 90°
Volume	4591.2(19) $Å^3$	
Z	8	
Crystal size	0.54 × 0.43 × 0.01 mm^3	
Reflections collected	27016	
Independent reflections	5259 [R(int) = 0.0583]	
Data / restraints / parameters	5259 / 0 / 326	
Goodness-of-fit on F^2	1.133	
Final R indices [I>2σ(I)]	$R1$ = 0.0569, $wR2$ = 0.1465	
R indices (all data)	$R1$ = 0.0757, $wR2$ = 0.1562	

X-ray Crystal Structure Details for [Cu(43-pyrdpm)(hfacac)]

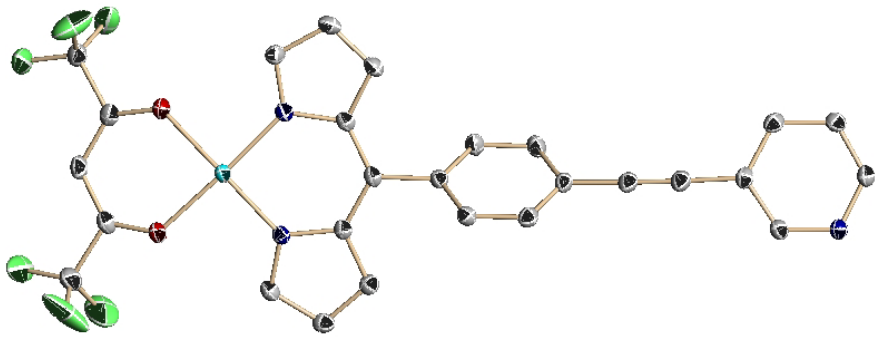

Figure 4-40. Structural Diagram of [Cu(43-pyrdpm)(hfacac)] (ORTEP, 50% probability ellipsoids). Hydrogen atoms have been omitted for clarity.

Table 4-18. Crystal Data for [Cu(43-pyrdpm)(hfacac)].

Empirical formula	Cu C_{27} H_{15} F_6 N_3 O_2	
Temperature	100(2) K	
Crystal system	Orthorhombic	
Space group	*P*bcn	
Unit cell dimensions	a = 8.1808(6) Å	α = 90°
	b = 21.9900(16) Å	β = 90°
	c = 27.108(2) Å	γ = 90°
Volume	4876.6(6) $Å^3$	
Z	8	
Crystal size	0.27 × 0.14 × 0.10 mm^3	
Reflections collected	29320	
Independent reflections	5610 [R(int) = 0.0308]	
Data / restraints / parameters	5610 / 0 / 380	
Goodness-of-fit on F^2	1.054	
Final R indices [I>2σ(I)]	$R1$ = 0.0386, $wR2$ = 0.0931	
R indices (all data)	$R1$ = 0.0457, $wR2$ = 0.0972	

X-ray Crystal Structure Details for [Cu(44-pyrdpm)(acac)]

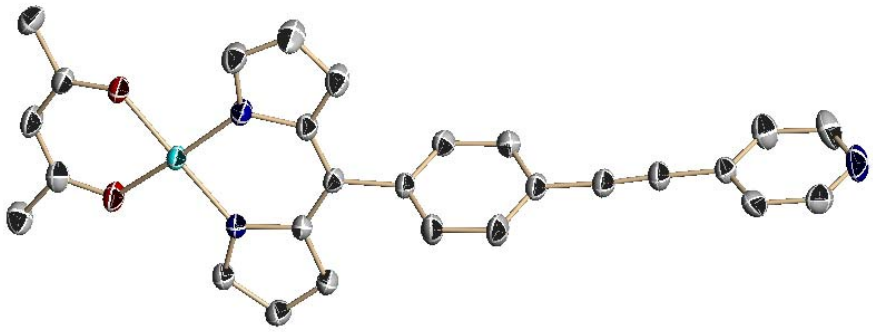

Figure 4-41. Structural Diagram of [Cu(44-pyrdpm)(acac)] (ORTEP, 50% probability ellipsoids). Hydrogen atoms have been omitted for clarity.

Table 4-19. Crystal Data for [Cu(44-pyrdpm)(acac)].

Empirical formula	Cu C_{27} H_{21} N_3 O_2	
Temperature	100(2) K	
Crystal system	Triclinic	
Space group	*P*-1	
Unit cell dimensions	a = 7.4629(11) Å	α = 84.439(2)°
	b = 11.0023(16) Å	β = 89.193(2)°
	c = 14.430(2) Å	γ = 72.687(2)°
Volume	1125.7(3) Å^3	
Z	2	
Crystal size	0.34 × 0.32 × 0.25 mm^3	
Reflections collected	5445	
Independent reflections	2916 [R(int) = 0.0270]	
Data / restraints / parameters	2916 / 0 / 300	
Goodness-of-fit on F^2	1.055	
Final R indices [I>2σ(I)]	R1 = 0.0394, wR2 = 0.1036	
R indices (all data)	R1 = 0.0452, wR2 = 0.1152	

X-ray Crystal Structure Details for $[Cu_3(4\text{-pyrdpm})_2(hfacac)_4]$

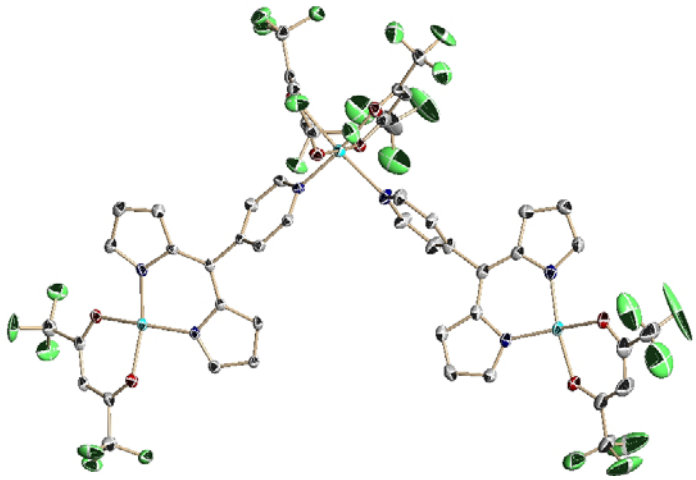

Figure 4-42. Structural Diagram of $[Cu_3(4\text{-pyrdpm})_2(hfacac)_4]$ (ORTEP, 50% probability ellipsoids). Hydrogen atoms and solvent molecules have omitted for clarity.

Table 4-20. Crystal Data for $[Cu_3(4\text{-pyrdpm})_2(hfacac)_4]$.

Empirical formula	$Cu_3\ C_{49}\ H_{25}\ F_{24}\ N_6\ O_8\ Cl_3$	
Temperature	100(2) K	
Crystal system	Monoclinic	
Space group	*P*2(1)/c	
Unit cell dimensions	a = 15.5903(14) Å	α = 90°
	b = 12.1048(11) Å	β = 94.612(2)°
	c = 30.364(3) Å	γ = 90°
Volume	5711.6(9) $Å^3$	
Z	4	
Crystal size	0.25 × 0.15 × 0.03 mm^3	
Reflections collected	47720	
Independent reflections	13055 [R(int) = 0.0559]	
Data / restraints / parameters	13055 / 0 / 838	
Goodness-of-fit on F^2	1.061	
Final R indices [I>2σ(I)]	$R1$ = 0.0687, $wR2$ = 0.1513	
R indices (all data)	$R1$ = 0.0984, $wR2$ = 0.1642	

X-ray Crystal Structure Details for $[Cu_2(4\text{-pyrdpm})(tfacac)_3]$

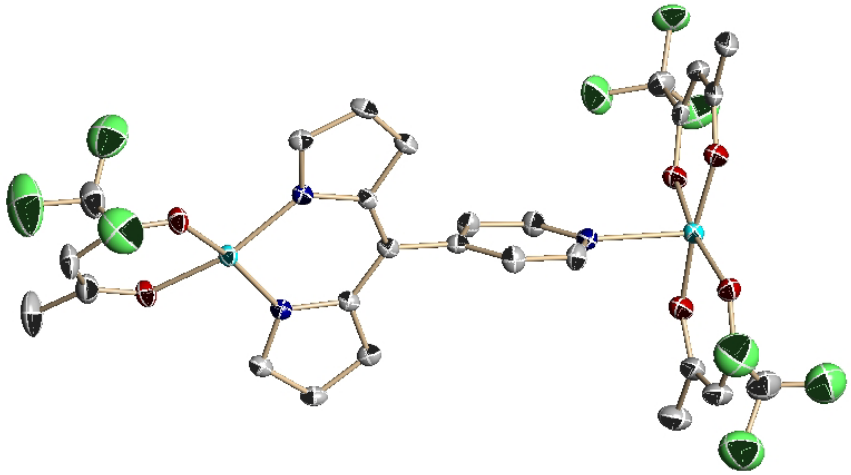

Figure 4-43. Structural Diagram of $[Cu_2(4\text{-pyrdpm})(tfacac)_3]$ (ORTEP, 50% probability ellipsoids). Hydrogen atoms have been omitted for clarity.

Table 4-21. Crystal Data for $[Cu_2(4\text{-pyrdpm})(tfacac)_3]$.

Empirical formula	$Cu_2\ C_{29}\ H_{22}\ F_9\ N_3\ O_6$	
Temperature	100(2) K	
Crystal system	Monoclinic	
Space group	*P*2(1)/c	
Unit cell dimensions	*a* = 8..5688(4) Å	$\alpha = 90°$
	b = 143003(7) Å	$\beta = 90.5430(10)°$
	c = 25.9059(13) Å	$\gamma = 90°$
Volume	3174.3(3) $Å^3$	
Z	4	
Crystal size	$0.36 \times 0.30 \times 0.25\ mm^3$	
Reflections collected	19488	
Independent reflections	7240 [*R*(int) = 0.0264]	
Data / restraints / parameters	7240 / 0 / 445	
Goodness-of-fit on F^2	1.063	
Final *R* indices [I>2σ(I)]	*R*1 = 0.0849, *wR*2 = 0.2619	
R indices (all data)	*R*1 = 0.0901, *wR*2 = 0.2670	

X-ray Crystal Structure Details for $[Cu_2(4\text{-quindpm})(tfacac)_3]$

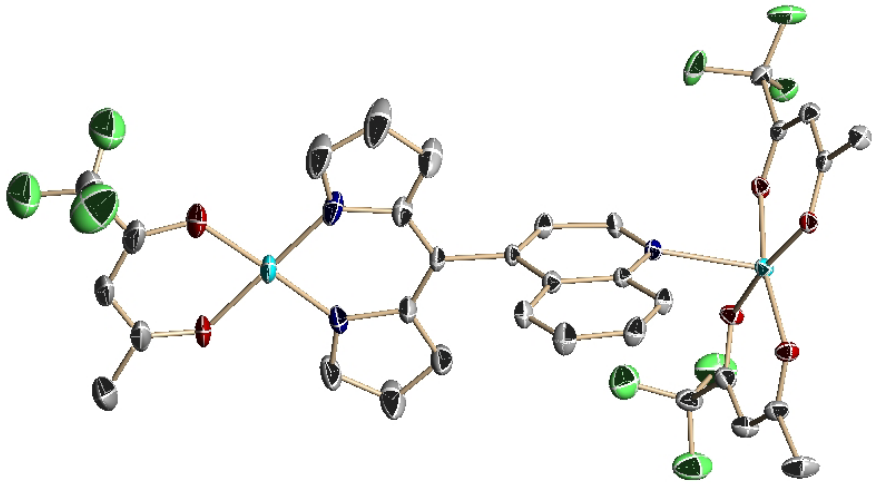

Figure 4-44. Structural Diagram of $[Cu_2(4\text{-quindpm})(tfacac)_3]$ (ORTEP, 50% probability ellipsoids). Hydrogen atoms have been omitted for clarity.

Table 4-22. Crystal Data for $[Cu_2(4\text{-quindpm})(tfacac)_3]$.

Empirical formula	$Cu_2\ C_{33}\ H_{24}\ F_9\ N_3\ O_6$	
Temperature	100(2) K	
Crystal system	Triclinic	
Space group	*P*-1	
Unit cell dimensions	a = 8.2369(14) Å	α = 84.117(3)°
	b = 8.3530(15) Å	β = 86.502(3)°
	c = 24.707(4) Å	γ = 88.938(3)°
Volume	1687.7(5) $Å^3$	
Z	2	
Crystal size	0.16 × 0.08 × 0.03 mm^3	
Reflections collected	14291	
Independent reflections	7316 [R(int) = 0.0252]	
Data / restraints / parameters	7316 / 0 / 482	
Goodness-of-fit on F^2	1.076	
Final R indices [I>2σ(I)]	$R1$ = 0.0779, $wR2$ = 0.2228	
R indices (all data)	R1 = 0.0897, $wR2$ = 0.2326	

X-ray Crystal Structure Details for $[Cu_3(4\text{-quindpm})_2(tfacac)_4]$

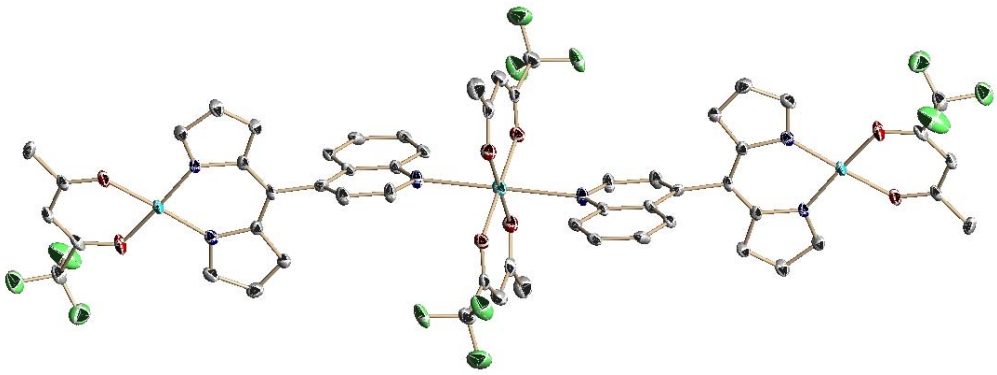

Figure 4-45. Structural Diagram of $[Cu_3(4\text{-quindpm})_2(tfacac)_4]$ (ORTEP, 50% probability ellipsoids). Hydrogen atoms have been omitted for clarity.

Table 4-23. Crystal Data for $[Cu_3(4\text{-quindpm})_2(tfacac)_4]$.

Empirical formula	$Cu_3\ C_{56}\ H_{40}\ F_{12}\ N_6\ O_8$	
Temperature	100(2) K	
Crystal system	Monoclinic	
Space group	*P*2(1)/n	
Unit cell dimensions	*a* = 16.756(4) Å	$\alpha = 90°$
	b = 8.379(2) Å	$\beta = 106.142(5)°$
	c = 19.966(5) Å	$\gamma = 90°$
Volume	2692.8(12) $Å^3$	
Z	2	
Crystal size	0.20 × 0.05 × 0.03 mm^3	
Reflections collected	21944	
Independent reflections	6058 [*R*(int) = 0.1077]	
Data / restraints / parameters	6058 / 0 / 387	
Goodness-of-fit on F^2	1.096	
Final *R* indices [I>2σ(I)]	*R*1 = 0.0825, *wR*2 = 0.1495	
R indices (all data)	*R*1 = 0.1373, *wR*2 = 0.1666	

X-ray Crystal Structure Details for $[Cu_3(42\text{-pyrdpm})_2(tfacac)_4]$

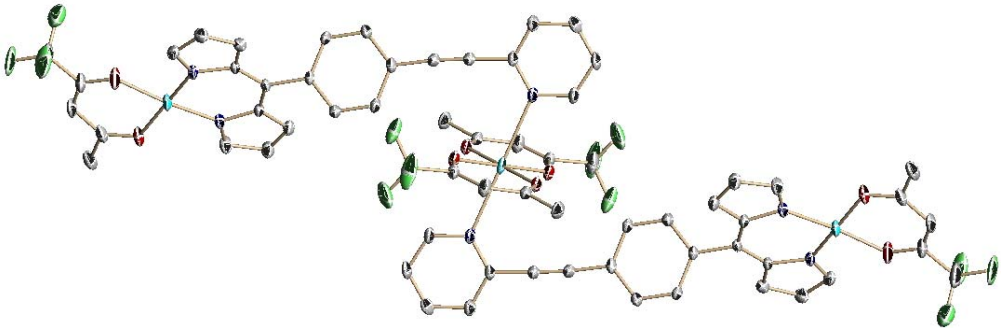

Figure 4-46. Structural Diagram of $[Cu_3(42\text{-pyrdpm})_2(tfacac)_4]$ (ORTEP, 50% probability ellipsoids). Hydrogen atoms have been omitted for clarity.

Table 4-24. Crystal Data for $[Cu_3(42\text{-pyrdpm})_2(tfacac)_4]$.

Empirical formula	$Cu_{1.5}\ C_{32}\ H_{22}\ F_6\ N_3\ O_4$	
Temperature	100(2) K	
Crystal system	Monoclinic	
Space group	*P*2(1)/c	
Unit cell dimensions	$a = 21.546(3)$ Å	$\alpha = 90°$
	$b = 18.012(2)$ Å	$\beta = 91.067(2)°$
	$c = 7.7451(10)$ Å	$\gamma = 90°$
Volume	3005.3(7) Å^3	
Z	4	
Crystal size	$0.32 \times 0.14 \times 0.12$ mm^3	
Reflections collected	25571	
Independent reflections	6738 [*R*(int) = 0.0490]	
Data / restraints / parameters	6738 / 0 / 423	
Goodness-of-fit on F^2	1.029	
Final *R* indices [I>2σ(I)]	*R*1 = 0.0469, *wR*2 = 0.1206	
R indices (all data)	*R*1 = 0.0630, *wR*2 = 0.1336	

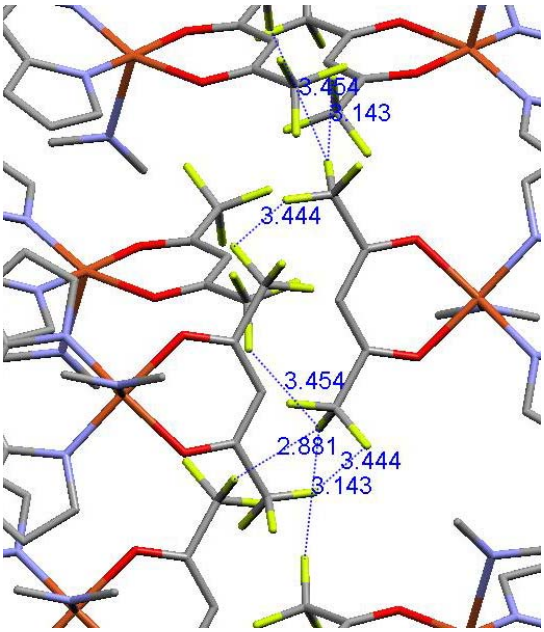

Figure 4-47. F–F interactions of [Cu(3-pyrdpm)(hfacac)]. Hydrogen atoms have been omitted for clarity.

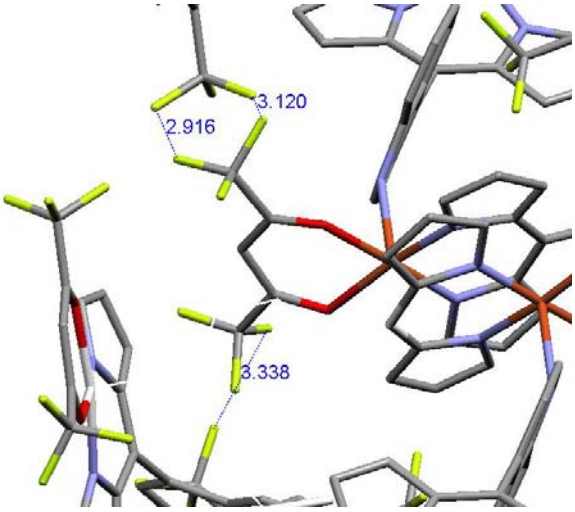

Figure 4-48. F–F interactions of [Cu(4-quindpm)(hfacac)]. Hydrogen atoms have been omitted for clarity.

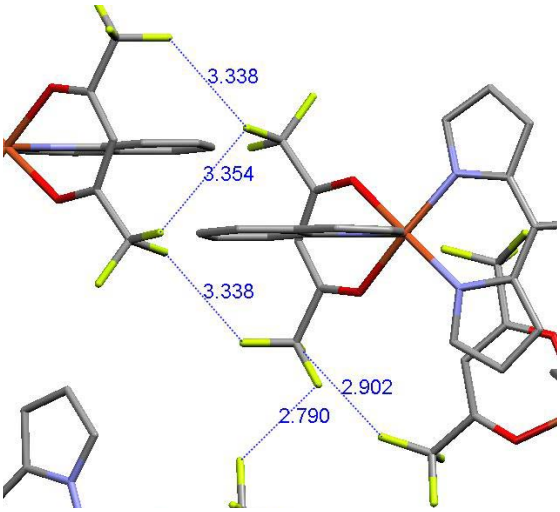

Figure 4-49. F–F interactions of [Cu(3-quindpm)(hfacac)]. Hydrogen atoms have been omitted for clarity.

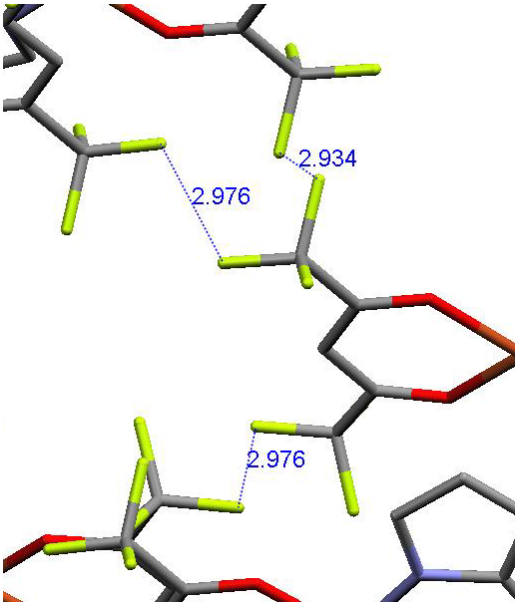

Figure 4-50. F–F interactions of [Cu(42b-pyrdpm)(hfacac)]. Hydrogen atoms have been omitted for clarity.

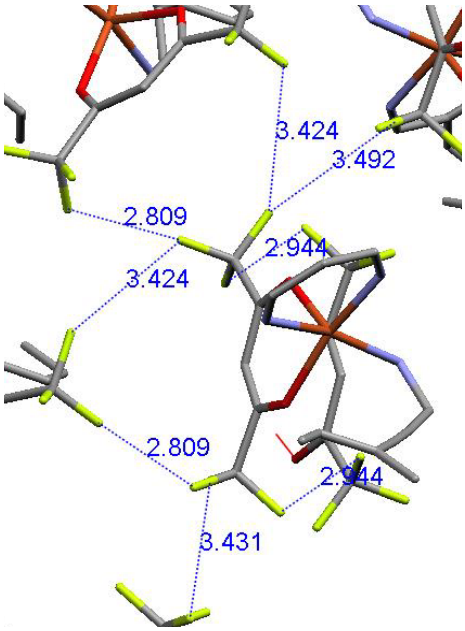

Figure 4-51. F–F interactions of [Cu(42-pyrdpm)(hfacac)]. Hydrogen atoms have been omitted for clarity.

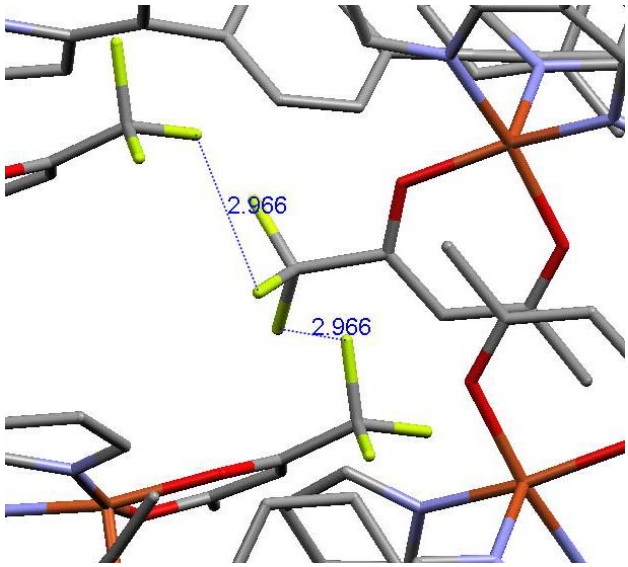

Figure 4-52. F–F interactions of [Cu(43-pyrdpm)(tfacac)]. Hydrogen atoms have been omitted for clarity.

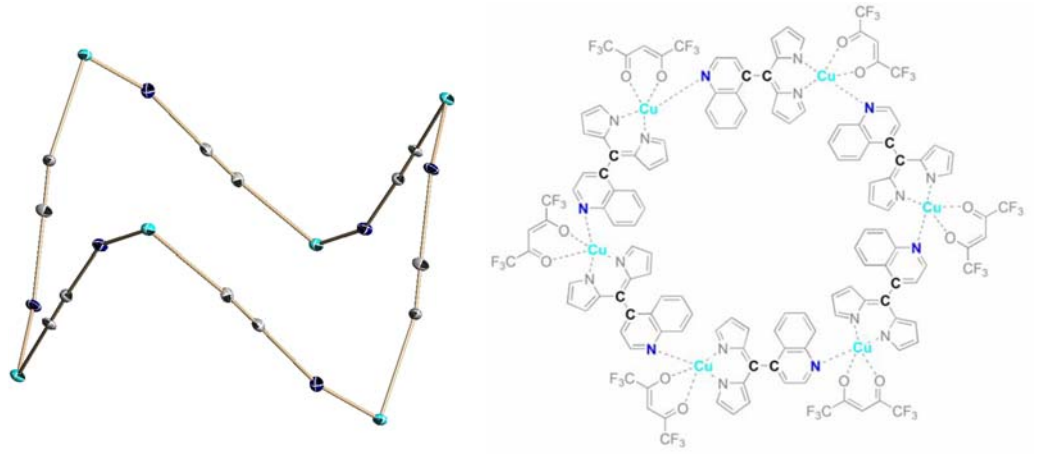

Figure 4-53. Cyclohexane 'chair' conformation (left, copper(II) ions in cyan) of the hexameric structure formed by [Cu(4-quindpm)(hfacac)]. All atoms have been removed except those indicated in the chemical drawing (right) to highlight the 'chair' structure.

4.7. References

[1] B. Moulton, M. J. Zaworotko, *Chem. Rev.* **2001**, *101*, 1629.

[2] Y. Kubota, M. Takata, R. Matsuda, R. Kitaura, S. Kitagawa, K. Kato, M. Sakata, T. C. Kobayashi, *Angew. Chem. Int. Ed.* **2005**, *44*, 920.

[3] J. X. Xie, X. Bu, N. Zheng, P. Feng, *Chem. Commun.* **2005**, 4916.

[4] J. Y. Ryu, J. H. Han, J. Y. Lee, S. J. Hong, S. H. Choi, C. Kim, S.-J. Kim, Y. Kim, *Inorg. Chim. Acta* **2005**, *358*, 3659.

[5] X.-C. Huang, J.-P. Zhang, Y.-Y. Lin, X.-M. Chen, *Chem. Commun.* **2005**, 2232.

[6] C. Kaes, M. W. Hosseini, C. E. F. Rickard, B. W. Skelton, A. H. White, *Angew. Chem. Int. Ed.* **1998**, *37*, 920.

[7] K. Biradha, C. Seward, M. J. Zaworotko, *Angew. Chem. Int. Ed.* **1999**, *38*, 492.

[8] A. Erxleben, *Inorg. Chem.* **2001**, *40*, 412.

[9] S. Sailaja, K. R. Reddy, M. V. Rajasekharan, C. Hureau, E. Riviere, J. Cano, J.-J. Girerd, *Inorg. Chem.* **2003**, *42*, 180.

[10] W. Blitz, J. A. Clinch, *Z. Anorg. Chem.* **1904**, *40*, 218.

[11] J. Pradilla-Sorzano, J. P. J. Fackler, *Inorg. Chem.* **1973**, *12*, 1174.

[12] B.-W. Lee, B. Twamley, J. M. Shreeve, *J. Fluorine Chem.* **2001**, *108*, 111.

[13] A. Mayr, J. Guo, *Inorg. Chem.* **1999**, *38*, 921.

[14] G. S. Papaefstathiou, T. D. Hamilton, T. Friscic, L. R. MacGillivray, *Chem. Commun.* **2004**, 270.

[15] Y. Sano, M. Tanaka, N. Koga, K. Matsuda, H. Iwamura, P. Rabu, M. Drillon, *J. Am. Chem. Soc.* **1997**, *119*, 8246.

[16] Y.-B. Dong, M. D. Smith, R. C. Layland, H.-C. zur Loye, *Inorg. Chem.* **1999**, *38*, 5027.

[17] R. Horikoshi, T. Mochida, H. Moriyama, *Inorg. Chem.* **2001**, *40*, 2430.

[18] F. M. Tabellion, S. R. Seidel, A. M. Arif, P. J. Stang, *J. Am. Chem. Soc.* **2001**, *123*, 7740.

[19] G. W. Coates, A. R. Dunn, L. M. Henling, D. A. Dougherty, R. H. Grubbs, *Angew. Chem. Int. Ed.* **1997**, *36*, 248.

[20] M. Gdaniec, W. Jankowski, M. J. Milewska, T. Polonski, *Angew. Chem. Int. Ed.* **2003**, *42*, 3903.

[21] F. Ponzini, R. Zagha, K. Hardcastle, J. S. Siegel, *Angew. Chem. Int. Ed.* **2000**, *39*, 2323.

[22] D. Gryko, J. S. Lindsey, *J. Org. Chem.* **2000**, *65*, 2249.

[23] C. Brückner, V. Karunaratne, S. J. Rettig, D. Dolphin, *Can. J. Chem.* **1996**, *74*, 2182.

[24] D. B. Rorabacher, *Chem. Rev.* **2004**, *104*, 651.

[25] P. Jose, S. Ooi, Q. Fernando, *J. Inorg. Nucl. Chem.* **1969**, *31*, 1971.

[26] A. Ambroise, J. Li, L. Yu, J. S. Lindsey, *Org. Lett.* **2000**, *2*, 2563.

[27] L. Yu, J. S. Lindsey, *J. Org. Chem.* **2001**, *66*, 7402.

[28] G. Ulrich, R. Ziessel, *J. Org. Chem.* **2004**, *69*, 2070.

[29] C. Baldauf, R. Gunther, H.-J. Hoffmann, *J. Org. Chem.* **2004**, *69*, 6214.

[30] C. J. Margulis, H. A. Stern, B. J. Berne, *J. Phys. Chem. B* **2002**, *106*, 10748.

[31] S. Y. Hong, D. Y. Kim, C. Y. Kim, R. Hoffmann, *Macromolecules* **2001**, *34*, 6474.

[32] S. Toyoda, M. Fujiki, *Macromolecules* **2001**, *34*.

[33] E.-Q. Gao, S.-Q. Bai, Z.-M. Wang, C.-H. Yan, *J. Am. Chem. Soc.* **2003**, *125*, 4984.

[34] M. Tominaga, H. Masu, K. Katagiri, T. Kato, I. Azumaya, *Org. Lett.* **2005**, *7*, 3785.

[35] *Comprehensive Supramolecular Chemistry, Vol. 6*, Elsevier, Oxford, **1996**.

V. Heterometallic Dipyrrin Metal-Organic Frameworks

5.1. Introduction

As described in Chapter 1, metal-organic frameworks (MOFs) are materials consisting of an organic ligand (building block) linked via metal ions or metal clusters to form a framework structure. When an organic building block is replaced with an inorganic complex, termed a 'metalloligand', new properties can be introduced into the framework.[1-6] Dipyrrin metal complexes can be incorporated into MOFs in a similar fashion to organic ligands because they are neutral complexes and can have parallel organic functional groups and symmetry. However, dipyrrin metal complexes also possess physical, chemical, and optical properties that are not possible in an organic building block. For example, dipyrrins are strong chromophores, due to strong metal-ligand charge transfer bands. In addition, octahedral metal dipyrrin complexes are chiral, and thus could be used to make a chiral framework.

5.1.1. Silver-Containing MOFs

Metal dipyrrin complexes have the potential to be used as metalloligands and substituted for common organic linkers in the preparation of silver-containing MOFs. MOFs constructed from silver(I) salts and multitopic coordinating ligands such as pyridines and nitriles have been studied in detail.[7-9] Dipyrrin complexes can be decorated on their periphery with these donor groups, thereby mimicking the symmetry and structure of the organic building blocks. The studies described here focus on silver-containing MOFs bound through pyridine ligands of three-fold symmetric metalloligand building blocks.

5.1.2. MOF Topologies

A variety of one-, two-, and three-dimensional topologies have been achieved with different building blocks and metal ions. Silver(I) ions can coordinate from one to three ligands; however, they usually coordinate to three ligands forming a three-fold symmetric node.[9] Depending on the coordination strength of the counterion, the silver(I) ion is sometimes weakly coordinated to an anion. One advantage of using dipyrrin building blocks is the variety of two- and three-dimensional topologies that can be obtained from two- and three-fold symmetric dipyrrin complexes when combined with silver(I) ions (Figure 5-1). Octahedral metal complexes such as cobalt(III) and iron(III) dipyrrins contain three ligands, whereas tetrahedral and square planar metal complexes such as copper(II) and zinc(II) dipyrrins contain two coordinating linear ligands.

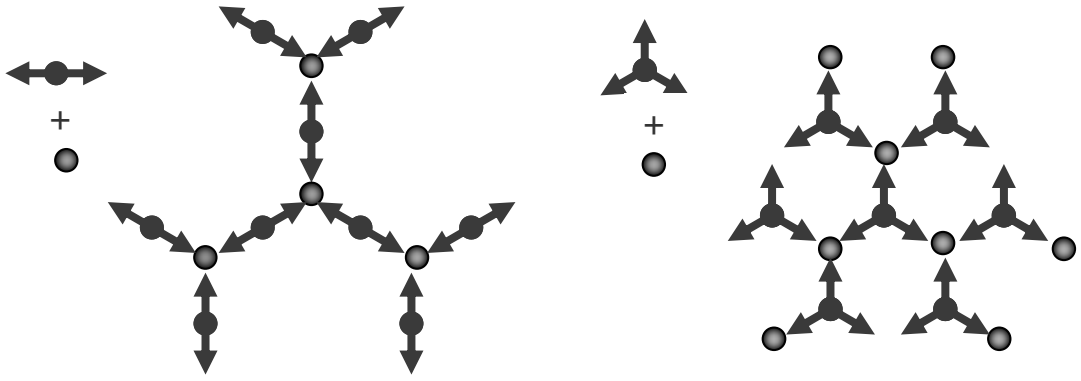

Figure 5-1. Possible framework topologies from two-fold ligands (left) and three-fold ligands (right) with three-fold nodes (metal ions).

The (n,p) nomenclature was established to help identify different nets, with 'n' being the number of sides that make up the smallest closed ring in the system, and 'p' being the number of links that coordinate to each node.[11] As long as the silver(I) ion is bound to three ligands and the dipyrrin metal centers remain octahedral with three dipyrrin ligands, then p = 3. The (6,3) net, a closed ring of 6 sides, is more commonly known as a two-dimensional hexagonal or honeycomb structure.[11] There is only one type of (6,3) net; however, the hexagonal sheets can layer with other sheets in different patterns.[12] Theoretically, there are eleven different three-dimensional topologies consisting of ten sides and three-fold nodes, i.e. (10,3) nets.[10] While each (10,3) net is chemically equivalent when using the same building block, each net contains different torsion and bond angles. For example the (10,3)-d net requires deviation from the ideal 120° bond angles at each three fold node to be formed. The (6,3), (10,3)-a, (10,3)-b, and (10,3)-d nets are the most common nets created with tris-chelate metal complex building blocks (Figure 5-2).[10] (10,3) Nets are very interesting because they can contain large open pores or channels, and can also be topologically chiral. There are also a number of (8,3), (9,3), and (12,3) type nets that can also be formed;[13] however, these types of nets are less common.

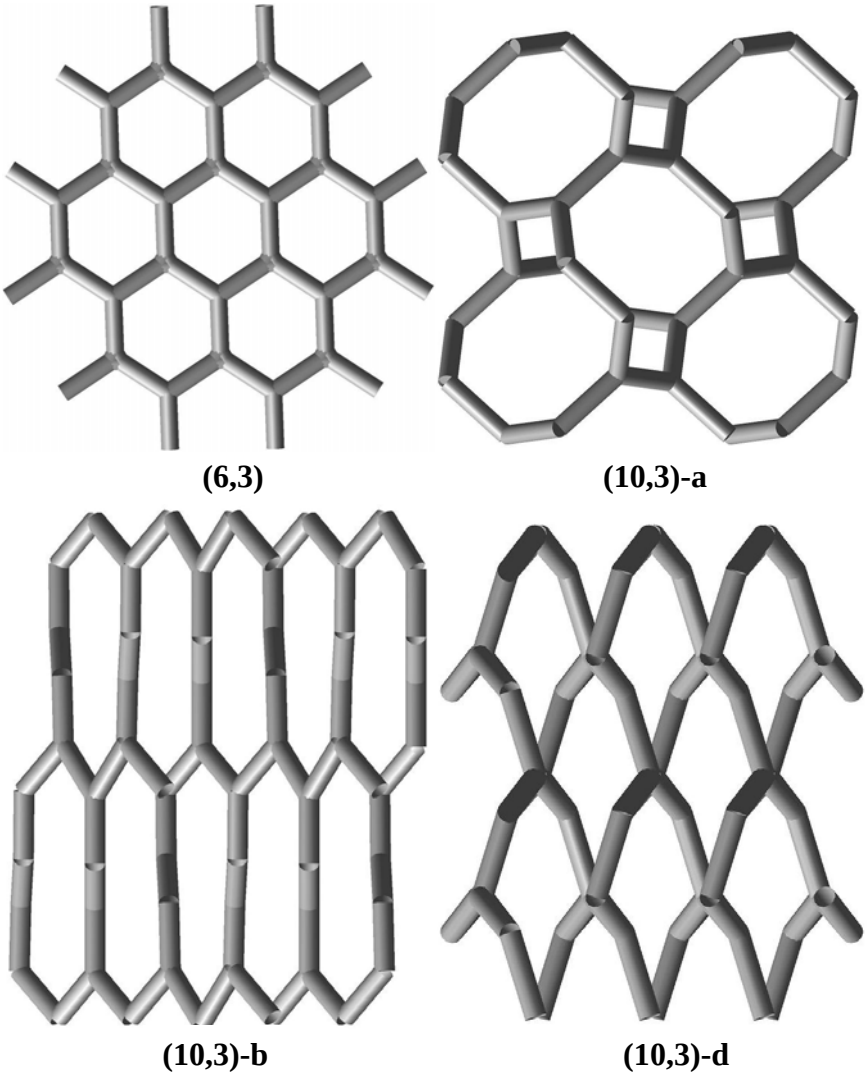

Figure 5-2. Topological diagrams of a two-dimensional (6,3) net (top left) and common three-dimensional (10,3) nets (top right and bottom) that can be formed with three-fold nodes. Note: nets can appear different when viewed along different symmetric axes.

There are several challenges when choosing to prepare a class of MOFs. First, it is difficult to predict the exact (10,3), (6,3), or other topology that will emerge from a specific set of building blocks. Second, various degrees of interpenetration are very common and also unpredictable.[14] Most MOF syntheses are empirical, i.e. mixing the various components and then identifying the topology of the MOF once it has

formed by using X-ray diffraction methods. Because the topology often cannot be controlled, one feature that can be controlled is the chemical functionality. The building block can be selected for its chemical properties, and when incorporated into a framework, should retain those properties.

5.1.3. Anion Templating and Anion Exchange

There are various forces driving the formation of the different framework topologies. One factor is the templating effect by the counterions in silver(I) frameworks. Anions have been known to template the formation of solid-state materials,[15] and the templating effect of counterions in several silver(I) frameworks has been studied.[16-23] When the building block remains unchanged but the counterion is altered for a series of silver(I) frameworks, the effects of the silver(I) counterions on the topology and overall functionality of the frameworks can be determined. For example, thiobis(pyridine) organic ligands used by Jung and coworkers were combined with silver(I) salts to produce one-dimensional helices and chains, and two-dimensional networks.[24, 25] The organic linker 2,4′-thiobis(pyridine) (2,4′-Py_2S) and the silver(I) salts $AgNO_3$, $AgBF_4$, $AgClO_4$, $AgPF_6$, $AgCF_3CO_2$, and $AgCF_3SO_3$ produced four different topologies (Figure 5-3) because the counterion had an effect on the formation of the structure. Anion exchange experiments were performed to exchange counterions between networks of the same topology. For example, the two-dimensional network $[Ag_3(2,4'\text{-}Py_2S)_4](BF_4)_3$ was suspended in a solution of $NaPF_6$. After 24 hours, the original BF_4^- counterion had completely exchanged for PF_6^-, as

determined by elemental analysis and infrared spectroscopy. X-ray powder diffraction (XRD) data showed the network retained its overall topology. The reverse anion exchange experiment of BF_4^- for PF_6^- was performed under identical conditions, but was unsuccessful, which was attributed to the relative coordinating strength of the counterions. The same anion exchange experiment was carried out for a variety of other silver(I) networks with sodium salts of several counterions to help confirm the overall binding strengths of the anions in the networks. This trend was further confirmed by the distance between the counterion and the silver(I) ion in the X-ray structures. Strongly coordinating anions bound directly to the silver(I) ion at <2.5 Å, while weakly coordination anions were not found in any close proximity to the metal ion in the crystal structure. The coordination trend was determined to be NO_3^- > $CF_3CO_2^-$ > $CF_3SO_3^-$ > PF_6^- > ClO_4^- > BF_4^-.

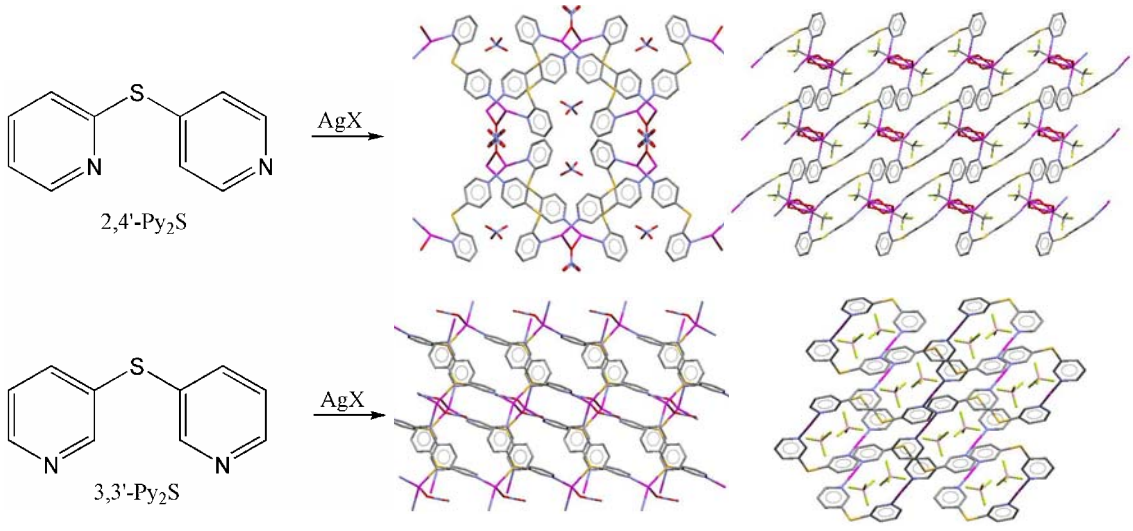

Figure 5-3. Thiobispyridine ligands (left) and the silver(I) networks $[Ag_3(2,4'\text{-}Py_2S)_4](NO_3)_3$ (top middle), $[Ag_3(2,4'\text{-}Py_2S)_4](CF_3CO_2)_3$ (top right), $[Ag_3(3,3'\text{-}Py_2S)_4](NO_3)_3$ (bottom middle), and $[Ag_3(3,3'\text{-}Py_2S)_4](BF_4)_3$ (bottom right) formed with different counterions.

Because anions can template different topologies, under certain conditions, anion exchange has induced supramolecular transformation in the solid-state.[8, 26] A second series of one-dimensional helices and two-dimensional networks were prepared with a slightly different pyridine ligand, 3,3′-thiobis(pyridine) (3,3′-Py_2S) (Figure 5-3), and the silver(I) salts $AgNO_3$, $AgBF_4$, $AgClO_4$, and $AgPF_6$.[25] Once again, an effect of the counterion on the formation of the supramolecular topology was observed. Several anion exchange experiments were performed on these networks; however, this time amongst networks of different topologies. For example, the two-dimensional network [Ag(3,3′-Py_2S)(NO_3)] was suspended in an aqueous solution of the sodium salts $AgBF_4$, $AgClO_4$, and $AgPF_6$, where the corresponding silver(I) complexes of the salts formed one-dimensional helicates. Not only did the counterions exchange but the two-dimensional networks converted into the one-dimensional helicates, as determined by XRD. The reverse experiment of the helicates to the networks only proceeded slightly. This observation showed the counterion dictated the network topology. Topological conversion upon anion exchange has also been observed for other types of silver(I) frameworks.[8]

5.1.4. Silver-Containing Pyridine-Substituted Dipyrrin MOFs

Pyridine-substituted dipyrrin ligands and metal complexes have been prepared and combined with silver(I) salts to make a series of two- and three-dimensional frameworks, mimicking the nitrile systems prepared by Lee and coworkers (Chapter 1).[9, 27-29] Tris-chelate metal dipyrrin complexes were prepared from cobalt(III) and

iron(III) metal salts. Mixed-metal MOFs were also prepared, which contained both cobalt(III) and iron(III) metalloligands in the same crystalline framework. Finally, a lengthened phenylacetylene pyridine dipyrrin building block was prepared and used for the preparation of MOFs.

In depth studies of the anion templating effect of the pyridine-substituted dipyrrin MOFs was performed to help elucidate the driving forces for the formation of MOFs. Anion exchange experiments were then performed to help determine the effect of the counterion on the topology.

5.2. Results and Discussion

5.2.1. Three-Dimensional (10,3) Frameworks

Pyridine-substituted dipyrrin ligands were prepared as described in Chapter 4. $[Fe(4\text{-pyrdpm})_3]$ was prepared in a manner similar to previous iron(III) dipyrrin complexes, and exhibits identical metal-ligand charge transfer bands (Chapter 2). $[Co(4\text{-pyrdpm})_3]$ was prepared by the addition of triethylamine and $Na_3[Co(NO_2)_6]$ to the oxidized dipyrrin, followed by heat and stirring. The cobalt(III) complex displays metal-ligand charge transfer bands at 469 and 506 nm. Both metal complexes were analyzed by X-ray diffraction (Figure 5-4). The complexes each display a pseudo-octahedral geometry as expected. The iron(III) complex has Fe–N bond distances of 1.95-1.98 Å. The cobalt(III) complex has slightly shorter Co–N bond distances of 1.93-1.94 Å. The pyridine ligands are directed outward in a three-fold fashion.

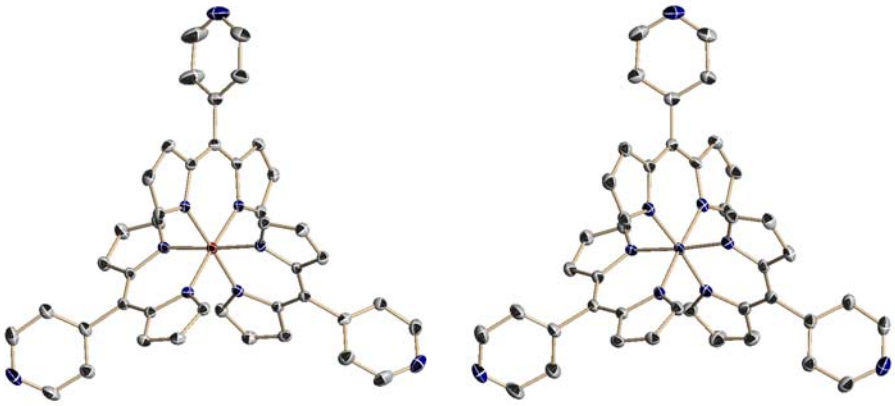

Figure 5-4. Structural diagram of [Fe(4-pyrdpm)$_3$] (left) and [Co(4-pyrdpm)$_3$] (right) (ORTEP, 50% probability ellipsoids). Hydrogen atoms and solvent molecules have been omitted for clarity.

To prepare the silver(I) MOFs, a general synthetic procedure was designed. The dipyrrin metal complex is dissolved in benzene and is added to a silver(I) salt also dissolved in benzene in an equimolar ratio. A red precipitate forms immediately, which is redissolved with acetonitrile. The solution is then allowed to slowly evaporate, causing the framework to crystallize. Single crystals are taken from the solution and analyzed by X-ray diffraction. The bulk crystals can also be collected and washed with benzene for use in other characterization methods and further studies.

Silver(I) triflate (AgOTf, $OTf^- = CF_3SO_3^-$, triflate, trifluoromethanesulfonate) is the most widely used silver(I) salt for the preparation of MOFs.[27-29] The first network involved the combination of [Co(4-pyrdpm)$_3$] and AgOTf to form the framework MOF-Co/AgOTf-1. Red crystals were obtained and analyzed by X-ray diffraction (Figure 5-5). As expected, each cobalt(III) center retains its three-fold symmetry, and each silver(I) ion coordinates to pyridine ligands of three distinct dipyrrin complexes to form an extended framework. The Ag–N bond distances are

2.23-2.24 Å. The silver(I) ion is also weakly coordinated to the OTf^- counterion with an Ag–O bond distance of 2.56 Å. The framework was compared to known three-dimensional topologies and was identified to be a (10,3)-d net. This was confirmed by generating the vertex symbols[30] of the framework using the OLEX software program[31] and comparing them to the known vertex symbols of the frameworks.[10] The framework is also found to be double-interpenetrated. Alternating Δ and Λ isomers of the dipyrrin metal complex are located regularly throughout the structure and the framework is achiral.

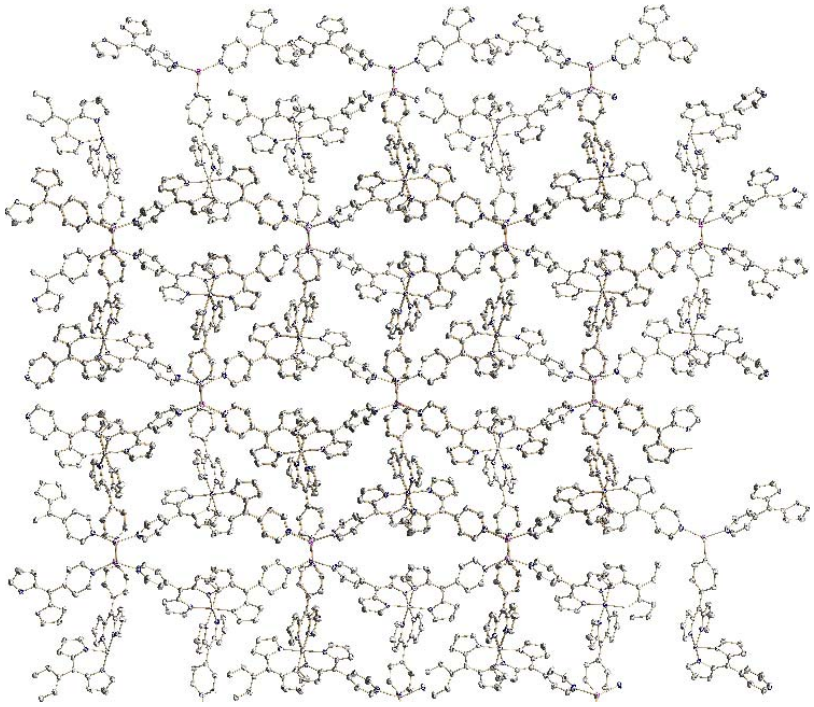

Figure 5-5. Packing diagram of the two interpenetrated nets of MOF-Co/AgOTf-1 viewed along the crystallographic *b*-axis (ORTEP, 50% probability ellipsoids). Hydrogen atoms, counterions, and solvent molecules have been omitted for clarity.

Additional silver(I) salts were employed to prepare more MOFs. A second MOF was synthesized from the combination of [Co(4-pyrdpm)$_3$] and $AgBF_4$ to create MOF-Co/$AgBF_4$-1. Red crystals were formed and analyzed by X-ray diffraction (Figure 5-19). The cobalt(III) center was also octahedral with Co–N bond distances of 1.90-1.95 Å. Each silver(I) ion is bound to three pyridines with Ag–N bond distances of 2.19-2.24 Å. The BF_4^- counterion is weakly bound with an Ag–F bond distance of 2.68 Å. The structural parameters are nearly identical to MOF-Co/AgOTf-1, and analysis of the overall topology reveals an isostructural three-dimensional (10,3)-d net, which is also double-interpenetrated.

In addition to altering the silver(I) salt, the dipyrrin metal center could also be changed. A third MOF involved the combination of [Fe(4-pyrdpm)$_3$] and $AgBF_4$ to form MOF-Fe/$AgBF_4$-1. Single crystals were obtained by the same conditions as the previous two networks. The X-ray structural parameters are once again isostructural to the previous two structures revealing a three-dimensional (10,3)-d net that is double interpenetrated (Figure 5-20). The bond distances are comparable with Fe–N bond distances of 1.92-1.97 Å, Ag–N bond distances of 2.22-2.24 Å, and a weakly coordinated BF_4^- counterion bound at 2.67 Å.

Using the program SOLV included in the PLATON software package[32] calculations were performed to determine the free volume of the (10,3)-d MOFs. Omitting all solvent molecules but including counterions, MOF-Co/AgOTf-1, MOF-Co/$AgBF_4$-1, and MOF-Fe/$AgBF_4$-1 generates a free volume of 39-42%.

Thus far, minor changes such as the metal center and counterion did not have an effect on the overall topology. Surprisingly, when [Fe(4-pyrdpm)$_3$] and AgOTf were used to prepare MOF-Fe/AgOTf-1, and the framework was analyzed by X-ray diffraction, a different topology emerges (Figure 5-21). A three-dimensional (10,3)-b net rather then a (10,3)-d net is formed (Figure 5-6). This topology is confirmed not to be an anomaly by repeated crystallization of the same components yielding the same X-ray cell parameters. Similar to the previous three MOFs, MOF-Fe/AgOTf-1 contains an octahedral iron(III) center and silver(I) ions bound to three pyridines. The network is also double interpenetrated. The Fe–N bond distances range from 1.94-1.99 Å, which are slightly elongated from the (10,3)-d nets. The Ag–N bond distances range from 2.19-2.32 Å. In contrast to the previous structure containing AgOTf, the OTf^- counterions are bridging in between two silver(I) ions, creating a trigonal bipyramidal environment at each silver(I) center (Figure 5-7). The Ag–O bond distances range from 2.61-3.03 Å. The OTf^- counterions are actually bridging silver(I) ions between the two interpenetrated nets. The (10,3)-b net generates a free volume of 30%.

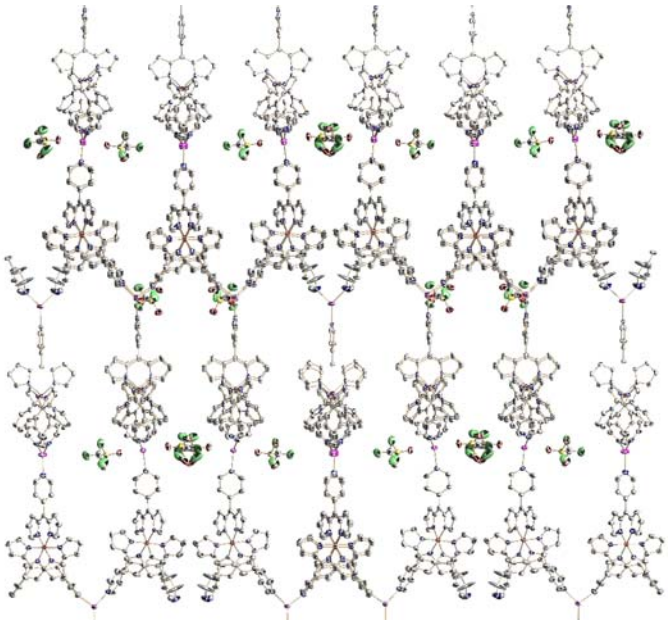

Figure 5-6. Packing diagram of MOF-Fe/AgOTf-1 viewed along the crystallographic *c*-axis (ORTEP, 50% probability ellipsoids). Hydrogen atoms and solvent molecules have been omitted for clarity.

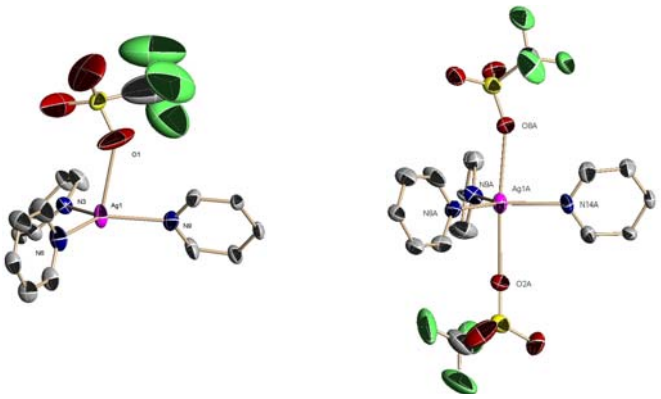

Figure 5-7. Silver(I) center of MOF-Co/AgOTf-1 (left) and MOF-Fe/AgOTf-1 (right) displaying the pyridine ligands and OTf^- counterions, with partial atom numbering schemes (ORTEP, 50% probability ellipsoids). Partial structure, hydrogen, and solvent atoms have been omitted for clarity.

It is not readily apparent why a (10,3)-b net is formed versus a (10,3)-d net for MOF-Fe/AgOTf-1. Crystals of all networks were grown under identical conditions. Despite the differences in topologies, these (10,3) frameworks have many similarities

and required only minor alterations to interchange from one topology to another.[10] Interestingly, the (10,3)-b and (10,3)-d nets formed with the dipyrrin MOFs are similar too because they contain pseudo-hexagonal channels (Figure 5-8). Both frameworks are also double interpenetrated.

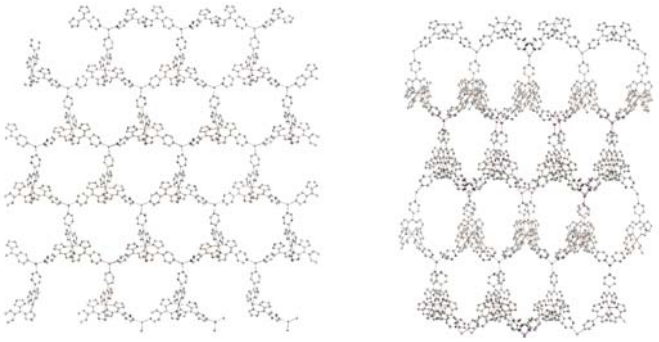

Figure 5-8. Structural diagram of MOF-Co/AgOTf-1 ((10,3)-d, *c*-axis, left), and MOF-Fe/AgOTf-1 ((10,3)-b, off-axis, right). Hydrogen atoms, counterions, and solvent molecules have been omitted for clarity.

5.2.2. Two-Dimensional (6,3) Frameworks

The same building blocks [Co(4-pyrdpm)$_3$] and [Fe(4-pyrdpm)$_3$] were used to prepare MOFs with the silver(I) salts $AgPF_6$ and $AgSbF_6$. Synthesis of the MOFs and crystallization conditions were identical to the previous (10,3) MOFs. Single crystals were obtained for MOF-Co/$AgPF_6$-1, MOF-Fe/$AgPF_6$-1, MOF-Co/$AgSbF_6$-1, and MOF-Fe/$AgSbF_6$-1 and their structures were determined by X-ray diffraction (Figure 5-22) (Figure 5-23) (Figure 5-24) (Figure 5-25). All of the cobalt(III) and iron(III) metal centers retain their pseudo-octahedral geometry and the silver(I) ions coordinate to three pyridine ligands. In contrast to the networks formed with AgOTf and $AgBF_4$,

the networks formed with $AgPF_6$ and $AgSbF_6$ yield two-dimensional (6,3) hexagonal nets.

The two frameworks formed by the combination of [Co(4-pyrdpm)$_3$], [Fe(4-pyrdpm)$_3$] and $AgPF_6$ (MOF-Co/$AgPF_6$-1 and MOF-Fe/$AgPF_6$-1) have nearly identical structural parameters and are isostructural, forming (6,3) nets (Figure 5-9). In contrast to the three-dimensional nets, each silver(I) ion contains two short Ag–N bond distances of 2.20-2.23 Å and one long bond distance of 2.34-2.35 Å. The counterion has an Ag–F distance of >4.0 Å, and is not coordinated to the silver(I) ion. However, in both structures, the nitrogen atom of an acetonitrile solvent molecule is weakly coordinated to the silver(I) ion with bond distances of 2.58-2.69 Å.

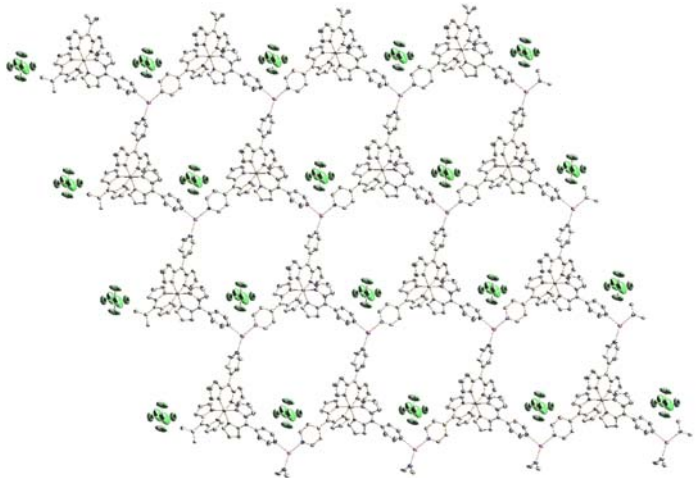

Figure 5-9. Structural diagram of MOF-Co/$AgPF_6$-1 (ORTEP, 50% probability ellipsoids). Hydrogen atoms and solvent molecules have been omitted for clarity.

The two frameworks formed by the combination of [Co(4-pyrdpm)$_3$], [Fe(4-pyrdpm)$_3$] and $AgSbF_6$ (MOF-Co/$AgSbF_6$-1 and MOF-Fe/$AgSbF_6$-1) are also isostructural to each other forming a (6,3) net. Each silver(I) ion also contains two

short Ag–N bond distances of 2.21-2.24 Å and one long bond distance of 2.35-2.36 Å. The counterion also has an Ag–F distance of >4.0 Å, therefore is non-coordinating, and again the nitrogen atom of an acetonitrile solvent molecule is weakly coordinated to the silver(I) ion with bond distances of 2.52-2.58 Å.

While the two different counterions PF_6^- and SbF_6^-, in combination with the cobalt(III) and iron(III) dipyrrins, all form (6,3) nets, the two sets of frameworks containing the different counterions produce two different types of overall topologies due to the different packing natures of the hexagonal sheets (Figure 5-10). For the PF_6^- nets, two neighboring sheets strongly interact. The distance between the center of two sheets is shorter, and the spacing between each set of two sheets is slightly longer (Figure 5-37). The number of sheets required before the pattern of layering is repeated, or the peridocity, is two for MOF-M/$AgPF_6$-1 (M = Co, Fe). The two hexagonal sheets are not eclipsed, but also not perfectly staggered. Fully eclipsed sheets would have perfect hexagonal channels throughout the structure, while perfectly staggered sheets would prevent the formation of large hexagonal channels. The sheets of MOF-M/$AgPF_6$-1 are slightly offset from one sheet to the next (Figure 5-10). The closest metal–metal distances are Ag–Ag and Co–Co at 6.93 Å and 8.45 Å, respectively. For the SbF_6^- nets, all the sheets are approximately equally spaced (Figure 5-37). The periodicity of MOF-M/$AgSbF_6$-1 is four and each sheet is also slightly offset from the previous sheet (Figure 5-10). The two closest metal–metal distances are Co–Co and Co–Ag at 7.28 Å, and 8.16 Å, respectively. The (6,3) nets with $AgPF_6$ generate a free volume of 36%, and the (6,3) nets with $AgSbF_6$ generate a free volume of 36-37%.

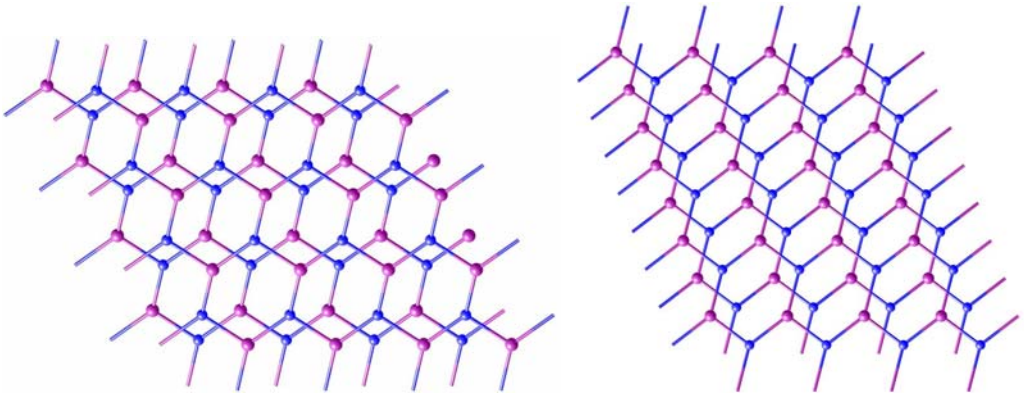

Figure 5-10. Topological diagram of two sheets of MOF-Co/$AgPF_6$-1 (*a*-axis, left) and two sheets of MOF-Co/$AgSbF_6$-1 (*b*-axis, right). Silver(I) ions are shown in purple and cobalt(III) ions are shown in blue. All other atoms, counterions, and solvent molecules have been omitted for clarity.

As emphasized, in contrast to frameworks of the weakly coordinating counterions OTf^- and BF_4^-, a new (6,3) topology is formed with $AgPF_6$ and $AgSbF_6$. The PF_6^- and SbF_6^- counterions are clearly influencing the topology of the frameworks. The dipyrrin complexes have no effect on the topology because the frameworks were identical with different metal centers and identical counterions.

Once again the (6,3) nets formed with the dipyrrin MOFs are similar to the (10,3)-b and (10,3)-d nets because they contain pseudo-hexagonal channels. The remarkable similarity between the (10,3)-d nets and the (6,3) nets has been previously described.[29] Interpenetration does alter the hexagonal channels of each framework. All (10,3) and (6,3) structures reported, except for MOF-Co/$AgNO_3$-1b contain alternating Δ and Λ isomers of the octahedral metal centers, therefore are achiral. While crystals of every preceding MOF could all be extracted from solution and analyzed by X-ray diffraction, air dried crystals lost their crystallinity.

5.2.3. Alternate Two-Dimensional Frameworks

Previously, NO_3^- counterions have shown to bind in a monodentate and bidentate fashion to a single silver(I) ion, as well as monodentate bridging between to two silver(I) ions.[33] A new framework involving the combination of [Co(4-pyrdpm)$_3$] and $AgNO_3$ was prepared. The new MOF was clearly different from the previous MOFs because copious amounts of acetonitrile was needed to redissolve the initial precipitate that formed. The crystals also took substantially longer to grow and large single crystals were difficult to obtain. The first structure solved from crystals obtained in solution was labeled MOF-Co/$AgNO_3$-1a, for reasons that will be apparent later. The structure did not refine well, due to the poor quality of the crystal. Many atoms could not refine anisotropically, and therefore the structure is solved isotropically. Despite the low quality of the crystallographic data, the positioning of the atoms and topology is readily apparent. The cobalt(III) center remains pseudo-octahedral with Co–N bond distances of 1.92-1.96 Å. The silver(I) ion, is only bound to *two* pyridine ligands with Ag–N bond distances of 2.19-2.21 Å. Rather then a single counterion bound to one silver(I) ion, each counterion is bound to two silver(I) ions with an Ag–O bond distance of 2.55 Å. Each NO_3^- counterion is bridging between two silver(I) ions. The silver(I) ion is bound to two pyridines, and bound to two NO_3^- counterions, generating a four-fold node with two different bound ligands. The cobalt(III) centers act as two-fold bent linkers giving a (4,4) net. The overall structure consists of sheets of [Co(4-pyrdpm)$_3$] and $AgNO_3$ (Figure 5-11). The (4,4) sheets are in the plane of the crystallographic *b*- and *c*-axis. The unbound pyridine

ligands are pointing outward from the sheets. A large residual electron density peak (5.37 e $Å^{-3}$) is detected at 1.97 Å from the unbound pyridine nitrogen. It is attributed to a partially disordered solvent molecule. A well ordered benzene molecule is also observed in the crystal structure.

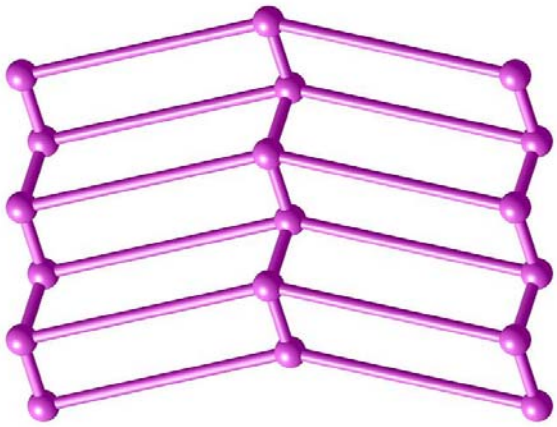

Figure 5-11. Topological diagram of a single sheet of MOF-Co/$AgNO_3$-1a viewed down the crystallographic *a*-axis. Silver(I) ions are shown in purple. All other atoms, counterions, and solvent molecules have been omitted for clarity.

As the initial benzene/acetonitrile solution of MOF-Co/$AgNO_3$-1a was allowed to further evaporate, the initial crystals appeared to dissolve and reform. The mother liquor was allowed to fully evaporate, and the crystals were allowed to air dry. The dried crystals appeared to retain their crystallinity. X-ray structural analysis of the dried crystals was performed (Figure 5-27). The presence of a new framework, labeled MOF-Co/$AgNO_3$-1b, is revealed by the new structural parameters that are obtained. Structural analysis reveals the metal binding mode is identical to the previous (10,3) and (6,3) networks with pseudo-octahedral dipyrrin metal centers and Co–N bond distances of 1.93-1.95 Å. The silver(I) ions are bound to *three*

corresponding pyridine ligands with Ag–N bond distances of 2.29-2.43 Å. The NO_3^- counterion, however, is bound *bidentate* to the silver(I) ion with Ag–O bond distances of 2.34 Å and 2.81 Å. The bidentate coordination of the counterion drastically alters the bond angles between the pyridine ligands on the silver(I) ion. This in turn alters the overall topology.

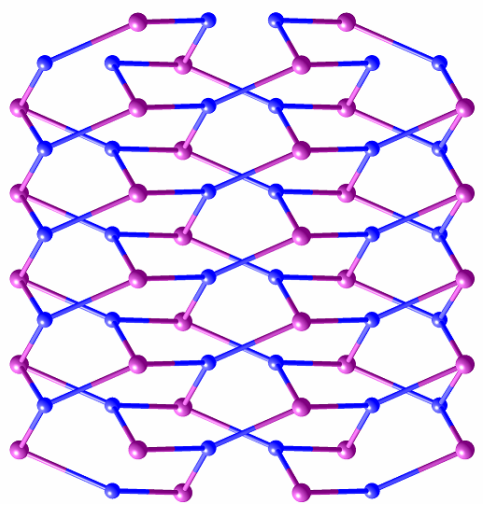

Figure 5-12. Topological diagram of MOF-Co/$AgNO_3$-1b viewed along the crystallographic *b*-axis. Silver(I) ions are shown in purple and cobalt(III) ions are shown in blue. All other atoms, counterions, and solvent molecules have been omitted for clarity.

The MOF-Co/$AgNO_3$-1b framework appears to be an (8,3) type net. However, it appears to only be two-dimensional, and is not a regular type two-dimensional net. Visual inspection shows eight sides make up the smallest closed circuit of the framework. The vertex symbols of the framework were calculated using the OLEX software program. The exact net is unclear, as there are no reports of nets containing the same vertex symbols and there are very few reports of (8,3) nets[13]. Surprisingly,

a single octahedral metal center is found in the asymmetric unit of a chiral space group, therefore the new framework is chiral. The framework, as solved, consists of all Δ isomers of the cobalt(III) dipyrrin complex. While an (8,3)-a net is also chiral, comparison of the structure to other known (8,3)-a nets displays a different topology.[13]

5.2.4. Anion Templating

Despite the fact that it is difficult to predict the exact topology that will form, a clear trend was starting to emerge between the coordinating ability of the counterions and the topology. OTf^- and BF_4^- are weakly coordinating counterions that form three-dimensional networks, SbF_6^- and PF_6^- are non-coordinating counterions that form two-dimensional sheets, and finally NO_3^- is a strongly coordinating counterion that form a combination of unusual topologies. The inclusion of the NO_3^- counterion is shown to have the largest effect on the topology of the frameworks. MOF-Co/$AgNO_3$-1a involves the binding of two separate NO_3^- counterions and form a (4,4) net, while MOF-Co/$AgNO_3$-1b involves the bidentate binding of a single NO_3^- counterion and form an (8,3) net.

The coordinating ability of the counterion effects the overall topology because when a counterion coordinates to the silver(I) ion, the bond angles between the dipyrrin ligands and the silver(I) center are altered. It may be the subtle differences between the bond angles that drive the formation of the overall topology. This information will help to predict the formation of other MOFs in the future. The N–

Ag–N bond angles of the nets are comparable amongst the same (n,p) type nets (Table 5-1). The ideal bond angles of a trigonal planar metal center is 120º; however, they can all deviate from the ideal geometry of their adapted structure. The (10,3)-d nets MOF-Co/AgOTf-1, MOF-Co/$AgBF_4$-1, and MOF-Fe/$AgBF_4$-1 are all comparable with three medium bond angles (110º-130º). The (10,3)-b net MOF-Fe/AgOTf-1 has four silver(I) centers in the asymmetric unit, therefore has four sets of N–Ag–N bond angles. There does not appear to be any sort of uniformity to the bond angles, which range from 92-138º, thus agreeing with the theory that the (10,3)-d net cannot form with bond angles of 120º.[10] The (6,3) nets MOF-Co/$AgPF_6$-1 and MOF-Fe/$AgPF_6$-1 have one small/medium bond angle, one medium bond angle, and one large bond angle. The (6,3) nets MOF-Co/$AgSbF_6$-1 and MOF-Fe/$AgSbF_6$-1 have one small bond angle, one small/medium bond angle, and one large bond angle. And finally, the (8,3) net MOF-Co/$AgNO_3$-1b has two small bond angles and one medium bond angle.

Table 5-1. Bond angles for the MOFs.

Compound	**Net**	**N–Ag–N**	**N–Ag–N**	**N–Ag–N**
MOF-Co/AgOTf-1	(10,3)-d	111º	124º	124º
MOF-Co/$AgBF_4$-1	(10,3)-d	113º	123º	123º
MOF-Fe/$AgBF_4$-1	(10,3)-d	115º	118º	125º
MOF-Fe/AgOTf-1	(10,3)-b	92º	134º	134º
		104º	117º	138º
		113º	116º	131º
		118º	121º	121º
MOF-Co/$AgPF_6$-1	(6,3)	110º	112º	145º
MOF-Fe/$AgPF_6$-1	(6,3)	102º	110º	145º
MOF-Co/$AgSbF_6$-1	(6,3)	99º	107º	151º
MOF-Fe/$AgSbF_6$-1	(6,3)	98º	110º	148º
MOF-Co/$AgNO_3$-1b	(8,3)	88º	99º	122º

5.2.5. Anion Exchange

Previous anion exchange studies on MOFs have been performed under a variety of solvent conditions with an assortment of anion sources.[24, 25, 34] Anion exchange of the dipyrrin MOFs was performed for multiple of reasons. First was to determine if the frameworks are robust to withstand anion exchange. Second was to confirm the size of the counterion is not driving the formation of the nets. If counterion size and not coordinating ability is dictating the topology, then the larger PF_6^- and SbF_6^- counterions should not be exchanged into the (10,3)-nets. Third was to show these frameworks could be useful for various applications such as anion purification. Finally, because anion exchange has been shown to induce solid-state transformation, the effect of the topology upon anion exchange of these specific MOFs would be determined. Initial anion exchange studies on the dipyrrin MOFs were performed in aqueous solvents with sodium salts. The crystals were not stable under these conditions. More gentle conditions were desired for anion exchange, which would allow for crystals to still be analyzed by single crystal X-ray diffraction. Single crystal X-ray diffraction was desired so that the inclusion of the new counterion, and the new topology could be definitively determined.

Organic tetrabutylammonium salts have been used in anion exchange studies[35] and are useful because they can be dissolved in common organic solvents, including benzene/acetonitrile, which is the solvent conditions of all the MOF crystallizations. With this in mind, large single crystals of MOF-Co/AgOTf-1 were grown under the standard conditions. The mother liquor was removed and a solution

containing excess amount of a tetrabutylammonium salt dissolved in benzene/acetonitrile was added. The solution was gently shaken for one day and the crystals were then removed and analyzed by single crystal X-ray diffraction. Some amount of the MOF redissolved during the exchange process, as could be seen by the slight red color of the solution. This is due to the small amount of acetonitrile that was used. Anion exchange experiments in solutions containing only benzene did not dissolve any of the crystals; however, the crystals became cloudy, probably due to the solvent changes.

The first successful anion exchange experiment involved replacing an OTf^- counterion of MOF-Co/AgOTf-1with a BF_4^- counterion to form MOF-Co/AgOTf/BF_4-1. Both anions have shown to template a (10,3)-d net. A crystal from the anion exchange solution was extracted and analyzed by single-crystal X-ray diffraction (Figure 5-28). The structural parameters reveal the same (10,3)-d net after anion exchange. In addition, the BF_4^- counterion is detected in the asymmetric unit and is well ordered. The Ag–F bond distance is comparable at 2.68 Å versus 2.69 Å in the crystal structure of MOF-Co/$AgBF_4$-1. The full exchange of the counterion is confirmed by rinsing the crystals with benzene, dissolving the network in d^6-DMSO, and analyzing the resulting solution by ^{19}FNMR for the disappearance of the OTf^- peak and the appearance of the BF_4^- peak (Figure 5-38).

A second anion exchange study involved replacing an OTf^- counterion of MOF-Co/AgOTf-1 with a PF_6^- counterion to form MOF-Co/AgOTf/PF_6-1. The OTf^- counterion templates a (10,3)-d net while the PF_6^- counterion templates a (6,3) net.

After anion exchange, single crystals of MOF-Co/AgOTf/PF_6-1 were once again analyzed by X-ray diffraction (Figure 5-29). The structural parameters reveal the framework did not undergo a structural transformation and remained a (10,3)-d net. In addition, the PF_6^- counterion is detected and well ordered in the asymmetric unit, and resides in the same location as the original OTf^- counterion (Figure 5-13). The Ag–F bond distance is significantly shortened to 2.85 Å (versus 4.83 Å in the crystal structure MOF-Co/AgPF_6-1). A network containing a two-dimensional templating anion in a three-dimensional framework is formed. The full exchange of the counterion is also confirmed by ^{19}FNMR with the disappearance of the OTf^- peak and the appearance of the two PF_6^- peaks (Figure 5-39).

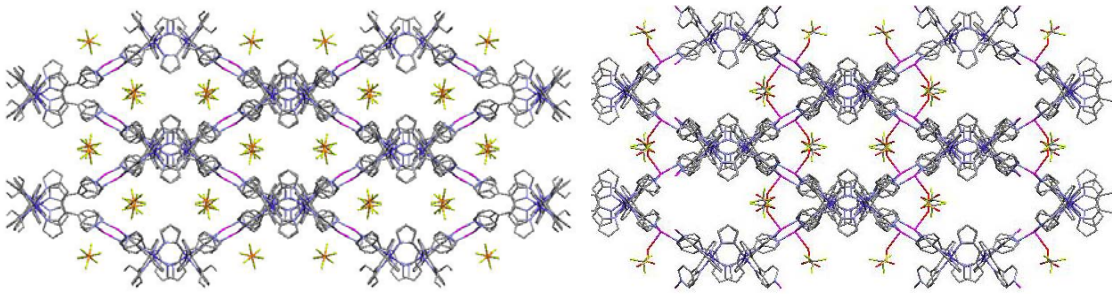

Figure 5-13. Structural diagram of MOF-Co/AgOTf/PF_6-1 (left) and MOF-Co/AgOTf-1 (right) viewed along the crystallographic *c*-axis. Hydrogen and solvent atoms have been omitted for clarity.

Anion exchange studies clearly reveal a (6,3) templating counterion can be exchanged in to a (10,3) net. The exchange of the OTf^- counterion with the PF_6^- counterion goes against the anion exchange trend established by Jung and

coworkers.[24, 25] The framework also does not undergo a solid-state transformation when introducing a counterion that dictates a different topology.

Identification and characterization of anion exchange usually involves X-ray powder diffraction or other spectroscopic techniques such as NMR and IR.[8, 24, 25, 36, 37] This is probably due to the difficulty to obtain good single crystals after anion exchange. An example was found utilizing single crystal X-ray diffraction for analyzing an anion exchanged material.[38] However, the initial framework was grown in a solution containing an excess of the second anion, rather then growing crystals first, then exchanging the anion. Other examples found in the literature involved anion exchange of materials but recrystallization was needed to obtain single crystals for X-ray diffraction.[15, 35] We believe this is the first anion exchange study of this type analyzed by single crystal X-ray diffraction. The dipyrrin MOFs are able to undergo specific gentle anion exchange conditions and still retain crystallinity. We have also yet to find an example where one anion templates a topology and is exchanged with another anion that would template another topology, without altering the framework.

5.2.6. Mixed Metals

Crystallizing mixed metal MOFs was sought for two reasons. First, mixed metal systems have been utilized for donor/acceptor pairs in energy transfer processes.[39-41] Second, because the cobalt(III) and iron(III) dipyrrin form two different (10,3) type nets with AgOTf when grown under identical conditions, we

were curious as to the topology that would form when the two metals are mixed in equal ratios.

Mixed metal MOFs were first prepared with [Co(4-pyrdpm)$_3$], [Fe(4-pyrdpm)$_3$], and $AgBF_4$ (MOF-CoFe/$AgBF_4$-1). Dark green single crystals were obtained and X-ray diffraction reveal the same (10,3)-d observed for MOF-Co/$AgBF_4$-1 and MOF-Fe/$AgBF_4$-1 (Figure 5-31). The counterion is weakly bound to the silver(I) ion with a bond distance of 2.71 Å. The presence of both iron(III) and cobalt(III) dipyrrin complexes in the same single crystal is confirmed by electronic absorption analysis of the single crystals dissolved in acetonitrile and diluted with methylene chloride (Figure 5-40). Single crystals were also obtained for [Co(4-pyrdpm)$_3$], [Fe(4-pyrdpm)$_3$], and $AgSbF_6$ (MOF-CoFe/$AgSbF_6$-1). Matrix parameters reveal the same (6,3) net observed for MOF-Co/$AgSbF_6$-1 and MOF-Fe/$AgSbF_6$-1; however, a full data set was not collected.

Finally, mixed metal MOFs were prepared with [Co(4-pyrdpm)$_3$], [Fe(4-pyrdpm)$_3$], and AgOTf (MOF-CoFe/AgOTf-1). Single crystals were obtained and X-ray diffraction reveals the (10,3)-d net, which was originally observed for MOF-Co/AgOTf-1 (Figure 5-30). The presence of both iron(III) and cobalt(III) dipyrrin complexes is also confirmed by electronic absorption analysis of dissolved single crystals. The (10,3)-d net appears to be the predominant framework over the (10,3)-b net in the dipyrrin MOFs.

5.2.7. Additional Dipyrrin Ligands for MOFs

All structures reported thus far utilized the 4-pyrdpm ligand. Many other dipyrrin ligands could potentially be employed. The 3-pyrdpm ligand has also been used extensively in the formation of coordination polymers and has yielded interesting results (Chapter 4); therefore, the cobalt(III) dipyrrin complex [Co(3-pyrdpm)$_3$] with the 3-pyrdpm ligand was prepared. Single crystals of the metal dipyrrin building block were obtained and the structure was determined by X-ray analysis (Figure 5-32). The complex displays a pseudo-octahedral cobalt(III) geometry. The pyridine ligands are all directing outward with accessible space around the nitrogen to allow for silver(I) coordination. The metal complex was mixed with various silver(I) salts under various solvent conditions; however, only microcrystalline fibers were obtained. The material could not be analyzed by X-ray diffraction to determine the structure. Focus was diverted to other dipyrrin building blocks.

Varying the size of the building block can alter particular features of MOFs such as framework size and porosity. The dipyrrin building block can be lengthened with chemical groups such as phenylacetylene spacers (Chapter 2). Phenylacetylene spacers have been used to make extended organic ligands for nitrile silver(I) networks.[29, 42] A phenylacetylene-substituted cobalt(III) dipyrrin pyridine building block [Co[44-pyrdpm)$_3$] was prepared from the dipyrrin ligand 44-pyrdpm (Chapter 4). The cobalt(III) complex was characterized by a variety of methods including X-ray diffraction (Figure 5-14). The crystal structure reveals a distorted octahedral cobalt(III) center with Co–N bond distances of 1.93-1.95 Å. Despite the rigidity of

phenylacetylenes, the ligands appear to be bent, similar to the previous extended dipyrrin metal complexes (Chapter 2).

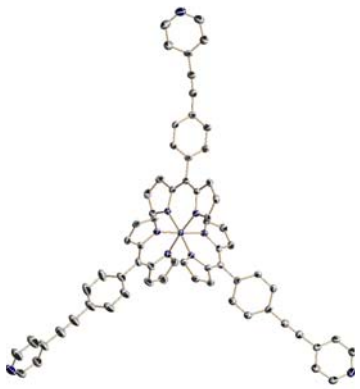

Figure 5-14. Structural diagram of [Co(44-pyrdpm)$_3$] (ORTEP, 50% probability ellipsoids). Hydrogen atoms and solvent molecules have been omitted for clarity.

The new cobalt(III) dipyrrin building block was used for the preparation of silver(I) MOFs. [Co(44-pyrdpm)$_3$] was combined with AgOTf, $AgBF_4$, and $AgPF_6$ to form MOF-Co/AgOTf-3, MOF-Co/$AgBF_4$-3, and MOF-Co/$AgPF_6$-3, respectively. Single crystals of each MOF were analyzed by X-ray diffraction. Surprisingly, rather than a combination of three-dimensional frameworks and two-dimensional nets, only two-dimensional (6,3) nets are formed for all three structures.

As stated, MOF-Co/AgOTf-3 crystallizes as a (6,3) net (Figure 5-15). The cobalt(III) center retains its pseudo-octahedral geometry. The silver(I) ion contains two shorter Ag–N bond distances of 2.21-2.23 Å and one long bond distance of 2.35-2.38 Å, with an average bond distance of 2.27 Å, slightly longer then the other two and three-dimensional nets formed with [Co(4-pyrdpm)$_3$] and [Fe(4-pyrdpm)$_3$]. The counterion is bound with an Ag–O bond distance of 2.60 Å. MOF-Co/$AgBF_4$-3

crystallizes in an identical space group to MOF-Co/AgOTf-3 (Figure 5-35). The Ag–N bond distances are similar with two short and one long bond length at 2.21-2.37 Å. The counterion is weakly coordinated with an Ag–F bond distance of 2.87 Å. Finally, MOF-Co/$AgPF_6$-3 also crystallizes in an identical space group to the preceding two MOFs. It has Ag–N bond distances of 2.21-2.35 Å. Surprisingly, the counterion is weakly bound with an Ag–F bond distance of 2.81 Å. This distance is comparable to the Ag–F bond distance of the PF_6^- counterion that was exchanged in to the MOF-Co/AgOTf-1 framework (vide infra). The (6,3) nets formed with [Co(44-pyrdpm)$_3$] generate a free volume of 41-42%. As expected, the larger building blocks generate structures with larger void volumes.

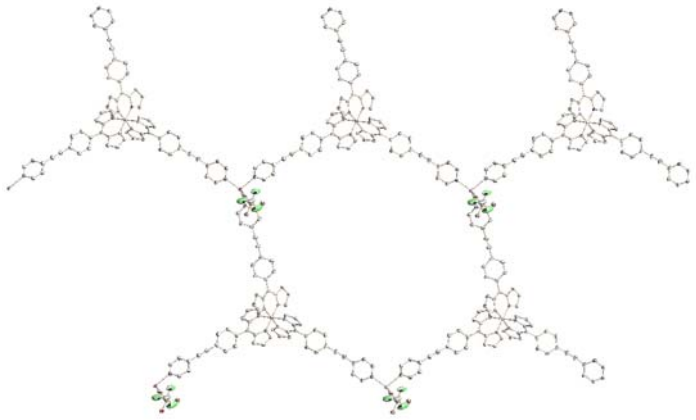

Figure 5-15. Structural diagram of MOF-Co/AgOTf-3 viewed off-axis (ORTEP, 50% probability ellipsoids). Hydrogen atoms and solvent molecules have been omitted for clarity.

The formation of only (6,3) nets with very large building blocks has been observed before.[29] For all MOFs built with 4-pyrdpm, the Fe–Ag and Co–Ag distances (from one metal node to another) are ~9.8 Å. For all MOFs built with 44-

pyrdpm, the Fe–Ag and Co–Ag distances are ~16.7 Å. In comparison to the previously reported framework TEB·AgOTf, which formed a (10,3) net, it had a three-fold benzene center to silver(I) distance (from the center of the organic node to the metal node) of ~12.9 Å.[9] The previously reported extended framework 1,3,5-Tris(4-(4-ethynylbenzonitrile)phenyl)benzene·AgOTf, which formed a (6,3) net, had a three-fold benzene center to silver(I) distance of ~17.1 Å.[29] The smaller dipyrrin building block and parallel organic nitrile ligand both form (10,3) nets, while the larger dipyrrin building block and parallel larger organic nitrile ligand both form (6,3) nets.

5.3. Conclusions

In summary, heterometallic metal-organic frameworks (MOFs) based on neutral [Co(4-pyrdpm)$_3$] and [Fe(4-pyrdpm)$_3$] complexes bound to silver(I) ions are presented. The topology of the MOFs is dictated by the silver(I) counterion. Both two- and three-dimensional topologies are prepared. Anion exchange studies are carried out consisting of replacing the counterion a three-dimensional framework with a two-dimensional templating counterion without disrupting the topology. In addition, mixed-metal MOFs containing both iron(III) and cobalt(III) dipyrrin complexes bound to silver(I) ions in the same crystalline framework are prepared. Finally, a larger pyridine-containing dipyrrin ligand extended with a phenylacetylene spacer (44-pyrdpm) is prepared and incorporated in to a variety of silver(I) MOFs to determine the effect of the size of the building block on the topology of the framework.

It is shown that weakly coordinating counterions template (10,3)-type nets with dipyrrin building blocks while non-coordinating counterions and really large dipyrrin building blocks template (6,3) nets. The strongly coordinating NO_3^- counterion template a variety of unusual topologies. Now that a trend has been established and the factors which drive the formation of the frameworks have been identified, the ability to predict the topology of other structures form will be easier.

With a series of frameworks already prepared with different topologies and different types of porosity, each type of framework will behave differently when it comes to applications such as gas an solvent storage. Each type framework will exhibit higher or lower storage capabilities of certain components compared to the other frameworks, and thus be selective. Further studies measuring the storage capabilities will need to be performed to confirm the analysis.

5.4. Experimental Section

General Procedures/Methods: Unless otherwise noted, starting materials were obtained from commercial suppliers and used without further purification. Pyrrole was freshly distilled. Mass spectrometry was performed either at the University of California, San Diego Mass Spectrometry Facility in the Department of Chemistry and Biochemistry, or at University of Arizona Mass Spectrometry Facility in the Department of Chemistry. A ThermoFinnigan LCQ-DECA mass spectrometer was used for the ESI or APCI analysis, and the data were analyzed using the Xcalibur software suite. A ThermoFinnigan MAT 900XL mass spectrometer was used to

acquire the data for the high resolution mass spectra (HRMS). Elemental analysis was performed at the University of California, Berkeley Analytical Facility or NuMega Resonance Labs, Inc. San Diego, CA. Infrared spectra were collected on a Mattson Research Series FT-IR instrument (using KBr pellets or NaCl plates, laboratory of Prof. Clifford P. Kubiak) at the Department of Chemistry and Biochemistry, University of California, San Diego. $^{1}H/^{13}C$NMR spectra were recorded on a Varian FT-NMR spectrometer running at 300 MHz, 400 MHz and 500 MHz at the Department of Chemistry and Biochemistry, University of California, San Diego. UV-visible spectra were recorded in CH_2Cl_2 using a Hewlett-Packard 4582A spectrophotometer under PC control using the ChemStation software suite or a Perkin-Elmer Lambda 25 spectrophotometer with the UVWinLab 4.2.0.0230 software package.

Complex Synthesis and Characterization:

[Co(4-pyrdpm)$_3$]. 5-(4-Pyridyl)dipyrromethane[43] (0.40 g, 1.79 mmol) was dissolved in 150 mL $CHCl_3$ and stirred in an ice bath. 2,3-Dichloro-5,6-dicyano-1,4-benzoquinone (DDQ, 0.41 g, 1.79 mmol) was dissolved in 100 mL benzene and added slowly dropwise. After addition, the reaction mixture was evaporated to dryness and the resulting dark residue was dissolved in 100 mL of acetonitrile. Triethylamine (1 mL) was added and $Na_3[Co(NO_2)_6]$ (0.24 g, 0.59 mmol) dissolved in a mixture of 2 mL of H_2O and 1 mL of acetonitrile was added to the solution. The resulting solution was heated to reflux overnight (~14 h) under a nitrogen atmosphere. The mixture was

evaporated to dryness and the product was purified by column chromatography (SiO_2; CH_2Cl_2/2% MeOH) to afford an orange solid. Yield: 38% (0.165 g). ^{1}HNMR ($CDCl_3$ 400 MHz, 25 °C): δ 6.36 (d, 6H, *J* = 4.0 Hz), 6.42 (s, 6H), 6.65 (d, 6H, *J* = 4.0 Hz), 7.38 (d, 6H, *J* = 6.0 Hz), 8.70 ppm (d, 6H, *J* = 5.6 Hz). ^{13}CNMR ($CDCl_3$ 100 MHz, 25 °C): δ 119.4, 124.9, 132.7, 134.4, 142.6, 145.6, 148.9, 152.4 ppm. ESI-MS: *m/z* 720.00 $[M+H]^+$. HR-FABMS: *m/z* 720.2021 $[M+H]^+$ (Calcd. *m/z* 720.2029). λ_{max} (CH_2Cl_2 solution) = 228 (38,800), 297 (17,500), 469 (48,300), 506 (41,700) nm. λ_{max} (solid) = 533, >570 nm. IR (KBr pellet): *v* 3100, 3028, 1595, 1561, 1538, 1410, 1380, 1346, 1247, 1207, 1032, 995, 889, 776, 770, 739, 719, 656 cm^{-1}.

[Fe(4-pyrdpm)$_3$]. 5-(4-Pyridyl)dipyrromethane[43] (0.30 g, 1.34 mmol) was dissolved in 150 mL $CHCl_3$ and stirred in an ice bath. 2,3-Dichloro-5,6-dicyano-1,4-benzoquinone (DDQ, 0.31 g, 1.34 mmol) was dissolved in 100 mL benzene and added slowly dropwise. After addition, the reaction mixture was evaporated to dryness and the resulting dark residue was dissolved in 100 mL of a 1:1 mixture of $CHCl_3$/MeOH. Triethylamine (1 mL) was added and $FeCl_3 \cdot 6H_2O$ (0.11 g, 0.40 mmol) dissolved in 2 mL of MeOH was added to the $CHCl_3$/MeOH solution. The resulting mixture was heated to reflux overnight (~14 h) under a nitrogen atmosphere. The solution was evaporated to dryness and the product was purified by column chromatography (SiO_2; CH_2Cl_2/2% MeOH) to afford a dichroic red/green solid. Yield: 60% (0.192 g). ESIMS: *m/z* 717.01 $[M+H]^+$. HR-FABMS: *m/z* 717.2061 $[M+H]^+$ (Calcd. *m/z* 717.2046). λ_{max} (CH_2Cl_2 solution) = 227 (42,900), 294 (18,900), 444 nm (50,700).

λ_{max} (solid) = 535, >600 nm. IR (KBr pellet): *v* 3100, 3034, 1596, 1563, 1529, 1401, 1379, 1336, 1242, 1205, 1189, 1039, 997, 890, 798, 764, 739, 721, 656 cm^{-1}.

[Co(4-pyrdpm)$_3$AgOTf] (MOF-Co/AgOTf-1). In the following order, 1 equiv of a benzene solution containing 3.5 mM [Co(4-pyrdpm)$_3$], neat benzene, and 1 equiv of a benzene solution containing 3.5 mM AgOTf were placed into a glass test tube. A precipitate formed immediately upon addition of AgOTf, which was dissolved with the addition of ~1.0 mL of acetonitrile. Different volumes of solution were used in order to obtain mixtures containing from ~0.22-1.3 mM of each reactant. The solutions were stored in the dark and left to slowly evaporate. Orange crystals grew from all solutions after ~7-15 days. For a solution containing 0.66 mM [Co(4-pyrdpm)$_3$], 0.66 mM AgOTf, 1.0 mL acetonitrile (total volume 4.0 mL) the isolated yield of crystalline material was 1.0 mg (39%). λ_{max} (solid) = 535, >600 nm. IR (KBr pellet): *v* 3094, 2921, 2852, 1607, 1563, 1537, 1411, 1380, 1346, 1282, 1247, 1221, 1160, 1021, 995, 890, 801, 769, 738, 718, 636 cm^{-1}. Anal. Calcd for $CoC_{43}H_{30}N_9O_3SF_3Ag \cdot 2/3$Benzene: C, 54.88; H, 3.33; N, 12.25. Found: C, 54.93; H, 3.63; N, 11.90.

[Co(4-pyrdpm)$_3$AgBF$_4$] (MOF-Co/AgBF$_4$-1). The same procedure as MOF-Co/AgOTf-1 was used. For a solution containing 1.3 mM [Co(4-pyrdpm)$_3$], 1.3 mM $AgBF_4$, and 1.0 mL acetonitrile (total volume 4.0 mL) the isolated yield of crystalline material was 1.7 mg (36%). IR (KBr pellet): *v* 3111, 1606, 1559, 1536, 1402, 1391, 1336, 1242, 1203, 1190, 1039, 995, 890, 796, 719, 673 cm^{-1}.

[Fe(4-pyrdpm)$_3$BF$_4$] (MOF-Fe/AgBF$_4$-1). The same procedure as MOF-Co/AgOTf-1 was used. For a solution containing 0.65 mM [Fe(4-pyrdpm)$_3$], 0.65 mM $AgBF_4$, and 1.0 mL acetonitrile (total volume 4.0 mL) the isolated yield of crystalline material was 0.5 mg (21%). λ_{max} (solid) = 542, >650 nm. IR (KBr pellet): *v* 3111, 1606, 1559, 1536, 1402, 1391, 1336, 1242, 1203, 1190, 1039, 995, 890, 796, 719, 673 cm^{-1}. Anal. Calcd for $FeC_{42}H_{30}N_9BF_4Ag$: C, 55.36; H, 3.32; N, 13.83. Found: C, 55.49; H, 3.70; N, 13.84.

[Fe(4-pyrdpm)$_3$AgOTf] (MOF-Fe/AgOTf-1). The same procedure as MOF-Co/AgOTf-1 was used. For a solution containing 2.6 mM [Fe(4-pyrdpm)$_3$], 2.6 mM AgOTf, and 1.0 mL acetonitrile (total volume 4.0 mL) the isolated yield of crystalline material was 4.6 mg (32%). IR (KBr pellet): *v* 3089, 1606, 1560, 1539, 1403, 1379, 1337, 1281, 1243, 1189, 1162, 1040, 1014, 997, 891, 802, 771, 738, 720, 672, 636 cm^{-1}.

[Co(4-pyrdpm)$_3$AgPF$_6$] (MOF-Co/AgPF$_6$-1). The same procedure as MOF-Co/AgOTf-1 was used. For a solution containing 1.7 mM [Co(4-pyrdpm)$_3$], 1.7 mM $AgPF_6$, and 1.0 mL acetonitrile (total volume 4.0 mL) the isolated yield of crystalline material was 4.8 mg (80%). IR (KBr pellet): *v* 3118, 1608, 1562, 1538, 1411, 1382, 1346, 1247, 1221, 1207, 1083, 1070, 1034, 995, 889, 802, 781, 738, 717, 670 cm^{-1}.

[Fe(4-pyrdpm)$_3$AgPF$_6$] (MOF-Fe/AgPF$_6$-1). The same procedure as (MOF-Co/AgOTf-1 was used. For a solution containing 1.7 mM [Fe(4-pyrdpm)$_3$], 1.7 mM $AgPF_6$, and 1.0 mL acetonitrile (total volume 4.0 mL) the isolated yield of crystalline

material was 3.9 mg (65%). IR (KBr pellet): *v* 3105, 1607, 1555, 1537, 1402, 1379, 1336, 1242, 1203, 1189, 1039, 995, 890, 840, 808, 770, 719, 669, 659, 557 cm^{-1}.

[Co(4-pyrdpm)$_3$AgSbF$_6$] (MOF-Co/AgSbF$_6$-1). The same procedure as MOF-Co/AgOTf-1 was used. For a solution containing 0.43 mM [Co(4-pyrdpm)$_3$], 0.43 mM $AgSbF_6$, and 1.0 mL acetonitrile (total volume 4.0 mL) the isolated yield of crystalline material was 0.9 mg (49%). IR (KBr pellet): *v* 3105, 3025, 1607, 1561, 1537, 1410, 1379, 1345, 1251, 1220, 1209, 1192, 1032, 995, 890, 801, 769, 738, 718, 657, 639, 624 cm^{-1}.

[Fe(4-pyrdpm)$_3$AgSbF$_6$] (MOF-Fe/AgSbF$_6$-1). The same procedure as MOF-Co/AgOTf-1 was used. For a solution containing 1.4 mM [Fe(4-pyrdpm)$_3$], 1.4 mM $AgSbF_6$, and 1.0 mL acetonitrile (total volume 5.6 mL) the isolated yield of crystalline material was 3.4 mg (32%). IR (KBr pellet): *v* 3092, 3025, 1607, 1561, 1539, 1402, 1379, 1336, 1243, 1219, 1204, 1189, 1040, 996, 891, 802, 769, 721, 657 cm^{-1}.

[Co(4-pyrdpm)$_3$Fe(4-pyrdpm)$_3$(AgOTf)$_2$] (MOF-CoFe/AgOTf-1). In the following order, 1 equiv of a benzene solution containing 3.5 mM [Fe(4-pyrdpm)$_3$] 3.5 mM [Co(4-pyrdpm)$_3$], neat benzene, and 1 equiv of a benzene solution containing 7.0 mM AgOTf were placed into a glass test tube. A precipitate formed immediately upon addition of AgOTf, which was dissolved with the addition of ~1.0 mL of acetonitrile. Different volumes of solution were used in order to obtain mixtures containing from ~0.22 - 1.3 mM of each reactant. The solutions were stored in the dark and left to slowly evaporate. For a solution containing 0.88 mM [Fe(4-pyrdpm)$_3$], 0.88 mM

[Co(4-pyrdpm)$_3$], 1.75 mM AgOTf, 1.0 mL acetonitrile (total volume 4.0 mL) the isolated yield of crystalline material was 2.8 mg (42%). IR (KBr pellet): *v* 3110, 1606, 1563, 1537, 1408, 1381, 1346, 1282, 1221, 1190, 1164, 1031, 995, 890, 802, 770, 738, 719, 664, 636 cm^{-1}.

[Co(4-pyrdpm)$_3$Fe(4-pyrdpm)$_3$(AgBF$_4$)$_2$] (MOF-CoFe/AgBF$_4$-1). The same procedure as MOF-CoFe/AgOTf-1 was used. For a solution containing 0.88 mM [Fe(4-pyrdpm)$_3$], 0.88 mM [Co(4-pyrdpm)$_3$], 1.75 mM AgBF$_4$, and 1.0 mL acetonitrile (total volume 4.0 mL) the isolated yield of crystalline material was 5.5 mg (87%). IR (KBr pellet): *v* 3111, 1606, 1559, 1536, 1402, 1391, 1336, 1242, 1203, 1190, 1039, 995, 890, 796, 719, 673 cm^{-1}.

[Co(3-pyrdpm)$_3$]. Was prepared in a manner similar to [Co(4-pyrdpm)$_3$] from 5-(3-Pyridyl)dipyrromethane[43] (0.30 g, 1.34 mmol). Yield: 47% (0.104 g). ^{1}HNMR ($CDCl_3$ 400 MHz, 25 °C): δ 6.35 (m, 6H), 6.43 (m, 6H), 6.67 (m, 6H), 7.40 (m, 6H), 7.78 (d, 3H, *J* = 7.2 Hz), 8.70 ppm (d, 3H, *J* = 11.2 Hz). FAB-MS: *m/z* 720.6 [M+H]$^+$. HR-FABMS: *m/z* 720.2034 [M+H]$^+$ (Calcd. *m/z* 720.2029). λ_{max} (CH_2Cl_2 solution) = 229, 305, 401, 469, 506 nm. IR (KBr pellet): *v* 3118, 3039, 1566, 1547, 1411, 1378, 1346, 1252, 1210, 1191, 1038, 1030, 997, 901, 885, 843, 797, 772, 721, 687 cm^{-1}.

[Co(44-pyrdpm)$_3$]. Was prepared in a manner similar to [Co(4-pyrdpm)$_3$] from 5-(4-pyridin-4-ylethynylphenyl)dipyrromethane (Chapter 4) (0.50 g, 1.55 mmol). Yield: 38% (0.20 g). ESI-MS: *m/z* 1020.08 [M+H]$^+$. HR-FABMS: *m/z* 1020.2957 [M+H]$^+$ (Calcd. *m/z* 1020.2968). ^{1}HNMR ($CDCl_3$ 400MHz, 25 °C): δ 6.36 (m, 6H), 6.43 (s, 6H), 6.72 (m, 6H), 9.41 (d, 6H, *J* = 5.6 Hz), 7.48 (d, 6H, *J* = 8.0 Hz), 7.62 (d,

6H, J = 8.4 Hz), 8.62 ppm (d, 6H, J = 5.2 Hz). ^{13}CNMR ($CDCl_3$ 100MHz, 25 °C): δ 87.6, 93.3, 118.9, 122.2, 125.4, 130.3, 130.6, 131.0, 132.7, 135.0, 138.6, 144.8, 149.5, 151.7 ppm. λ_{max} (CH_2Cl_2 solution) = 228, 279, 293, 335, 398, 469, 506 nm. IR (KBr pellet): ν 3111, 1606, 1559, 1536, 1402, 1391, 1336, 1242, 1203, 1190, 1039, 995, 890, 796, 719, 673 cm^{-1}.

[Co(44-pyrdpm)$_3$AgOTf] (MOF-Co/AgOTf-3). The same procedure as MOF-Co/AgOTf-1 was used. For a solution containing 1.7 mM [Co(44-pyrdpm)$_3$], 1.7 mM AgOTf, and 1.0 mL acetonitrile (total volume 4.0 mL) the isolated yield of crystalline material was 6.11 mg (69%). IR (KBr pellet): ν 3094, 2921, 2852, 1607, 1563, 1537, 1411, 1380, 1346, 1282, 1247, 1221, 1160, 1021, 995, 890, 801, 769, 738, 718, 636 cm^{-1}.

[Co(44-pyrdpm)$_3$AgBF$_4$] (MOF-Co/AgBF$_4$-3). The same procedure as MOF-Co/AgOTf-1 was used. For a solution containing 1.7 mM [Co(44-pyrdpm)$_3$], 1.7 mM $AgBF_4$, and 1.0 mL acetonitrile (total volume 4.0 mL) the isolated yield of crystalline material was 7.5 mg (89%). IR (KBr pellet): ν 3111, 1606, 1559, 1536, 1402, 1391, 1336, 1242, 1203, 1190, 1039, 995, 890, 796, 719, 673 cm^{-1}.

[Co(44-pyrdpm)$_3$PF$_6$] (MOF-Co/AgPF$_6$-3). The same procedure as MOF-Co/AgOTf-1 was used. For a solution containing 1.7 mM [Co(44-pyrdpm)$_3$], 1.7 mM $AgPF_6$, and 1.0 mL acetonitrile (total volume 4.0 mL) the isolated yield of crystalline material was 6.9 mg (77%). IR (KBr pellet): ν 3095, 1608, 1561, 1540, 1411, 1382, 1345, 1247, 1207, 1034, 996, 890, 849, 802, 769, 738, 717, 669, 557 cm^{-1}.

Anion Exchange Studies

[Co(4-pyrdpm)$_3$AgOTf] exchanged with BF_4 (MOF-Co/AgOTf/BF_4-1). Crystals of MOF-Co/AgOTf-1 were grown according to the procedure above. Before the solution fully evaporated, the mother liquor was removed and was quickly replaced with a solution of tetrabutylammonium tetrafluoroborate (30 mM) in benzene:acetonitrile 4:1. The solution was shaken for 24 h. Single crystals for X-ray diffraction were extracted from the anion exchange solution. The remaining crystals were washed with a benzene/acetonitrile solution. ^{19}FNMR ($CDCl_3$ 300MHz, 25 °C): δ - 152.1 ppm.

[Co(4-pyrdpm)$_3$AgOTf] exchanged with PF_6 (MOF-Co/AgOTf/PF_6-1). The same procedure as above was used with tetrabutylammonium hexafluorophosphate (26 mM). ^{19}FNMR ($CDCl_3$ 300MHz, 25 °C): δ -69.3, -71.8 ppm.

Solid State Electronic Spectroscopy

Spectra were collected on a Perkin Elmer Lambda 25 spectrophotometer by using a Labsphere RSA-PE-20F Fiber Optic Reflectance Spectroscopy Accessory. Crystalline samples (10-30 mg) were mounted between glass slides and the percent reflectance spectra were collected at a scan rate of 960 nm/min with a 1.0 nm resolution. All spectra were modified using the smooth command provided with the UV WinLab spectrophotometer software.

5.5. Acknowledgment

Text, schemes, and figures of this chapter, in part, are reprints of the materials published in the following paper: Sara R. Halper and Seth M. Cohen, "Heterometallic Metal-Organic Frameworks Based on Tris(dipyrrinato) Coordination Complexes" *Inorg. Chem.* **2005**, 44, 486-488. The dissertation author was the primary researcher.

The permissions to reproduce this paper was granted by the American Chemical Society, Copyright 2005.

5.6. Appendix

X-ray Crystal Structure Determination

Details: Single crystals of each compound suitable for X-ray diffraction structural determination were mounted on quartz capillaries with Paratone oil and were cooled in a nitrogen stream on the diffractometer. Data were collected on either a Bruker AXS or a Bruker P4 diffractometer each equipped with area detectors. Peak integrations were performed with the Siemens SAINT software package. Absorption corrections were applied using the program SADABS. Space group determinations were performed by the program XPREP. The structures were solved by either Patterson or direct methods and refined with the SHELXTL software package (Sheldrick, G. M. *SHELXTL vers. 5.1 Software Reference Manual*; Bruker AXS: Madison, WI, 1997). All hydrogen atoms were fixed at calculated positions with isotropic thermal parameters, and all non-hydrogen atoms were refined anisotropically unless otherwise noted.

Structure of [Co(4-pyrdpm)$_3$]. Orange blocks of [Co(4-pyrdpm)$_3$] suitable for X-ray diffraction structural determination were grown from a solution with the complex dissolved in chloroform diffused with pentane. The complex co-crystallized with two molecules of chloroform and two molecules of pentane. One of the molecules of pentane was disordered and treated as a diffuse contribution using the program SQUEEZE (A. Spek, Platon Library). Electron count/unit cell: 191 (found), 210 (expected).

Structure of [Fe(4-pyrdpm)$_3$]. Green blocks of [Fe(4-pyrdpm)$_3$] suitable for X-ray diffraction structural determination were grown from a solution with the complex dissolved in chloroform diffused with pentane. The complex co-crystallized with one molecule of unidentified solvent, which was disordered and treated as a diffuse contribution using the program SQUEEZE (A. Spek, Platon Library). Electron count/unit cell: 104 (found), 168 (expected, for a pentane molecule). The poor correlation between the found and calculated electron density may indicate that the solvent was both disordered and only partially occupied.

Structure of [Co(4-pyrdpm)$_3$AgOTf] (MOF-Co/AgOTf-1). Orange blocks of MOF-Co/AgOTf-1 suitable for X-ray diffraction structural determination were grown from evaporation of a solution of [Co(4-pyrdpm)$_3$] and AgOTf dissolved in benzene and acetonitrile as described above. The complex co-crystallized with two ordered molecules of acetonitrile, which were refined isotropically and hydrogen atoms were not calculated. Several additional disordered and partially occupied solvent molecules were treated as a diffuse contribution using the program SQUEEZE (A. Spek, Platon Library). Electron count/unit cell: 747 (found). The presence of four additional molecules of acetonitrile in the asymmetric unit gives an expected electron count/unit cell of 704, in good agreement with the SQUEEZE refinement.

Structure of [Fe(4-pyrdpm)$_3$AgBF$_4$] (MOF-Fe/AgBF$_4$-1). Red blocks of MOF-Fe/AgBF$_4$-1 suitable for X-ray diffraction structural determination were grown from evaporation of a solution of [Fe(4-pyrdpm)$_3$] and AgBF$_4$ dissolved in benzene and acetonitrile as described above. The complex co-crystallized with one ordered

molecule of acetonitrile, which was refined isotropically and hydrogen atoms were not calculated. Several additional disordered and partially occupied solvent molecules were treated as a diffuse contribution using the program SQUEEZE (A. Spek, Platon Library). Electron count/unit cell: 954 (found). The presence of four additional molecules of acetonitrile in the asymmetric unit gives an expected electron count/unit cell of 1056, in good agreement with the SQUEEZE refinement.

Structure of [Fe(4-pyrdpm)$_3$AgOTf] (MOF-Fe/AgOTf-1). Red plates of MOF-Fe/AgOTf-1 suitable for X-ray diffraction were grown from evaporation of a solution of [Fe(4-pyrdpm)$_3$] and AgOTf dissolved in benzene and acetonitrile as described above. Three molecules of [Fe(4-pyrdpm)$_3$AgOTf] were in the asymmetric unit. The complex co-crystallized with 4 ½ molecules of benzene and two molecules of acetonitrile, which were refined anisotropically. An additional ½ molecule of benzene was found however it was disordered, therefore were treated as a diffuse contribution using the program SQUEEZE (A. Spek, Platon Library). Electron count/unit cell: 177 (found), 168 (expected).

Structure of [Co(4-pyrdpm)$_3$AgBF$_4$] (MOF-Co/AgBF$_4$-1). Red rods of MOF-Co/AgBF$_4$-1 suitable for X-ray diffraction were grown from evaporation of a solution of [Co(4-pyrdpm)$_3$] and AgBF$_4$ dissolved in benzene and acetonitrile as described above. The complex co-crystallized with at least 2 molecules of acetonitrile and two molecules of benzene in the asymmetric unit which were disordered and partially occupied, therefore were treated as a diffuse contribution using the program SQUEEZE (A. Spek, Platon Library). Electron count/unit cell: 974 (found). The

presence of 2 molecules of acetonitrile and two molecules of benzene has an electron count/unit cell: 1024, in good agreement with the SQUEEZE refinement.

Structure of [Co(4-pyrdpm)$_3$AgPF$_6$] (MOF-Co/AgPF$_6$-1). Red blocks of MOF-Co/AgPF$_6$-1 suitable for X-ray diffraction were grown from evaporation of a solution of [Co(4-pyrdpm)$_3$] and AgPF$_6$ dissolved in benzene and acetonitrile as described above. The counterion is located in three in three independent positions with two on mirror planes from each other. They were determined and then set to be 50%, 25%, and 25% respectively. The complex co-crystallized with 1 molecule of benzene and 1 molecule of acetonitrile that were refined isotropically. An additional molecule of benzene and two additional molecules of acetonitrile were present but disordered and partially occupied, therefore were treated as a diffuse contribution using the program SQUEEZE (A. Spek, Platon Library). Electron count/unit cell: 151 (found). The presence of 2 molecules of acetonitrile and 1 molecule of benzene has an electron count/unit cell: 172, in good agreement with the SQUEEZE refinement.

Structure of [Fe(4-pyrdpm)$_3$AgPF$_6$] (MOF-Fe/AgPF$_6$-1). Green blocks of MOF-Fe/AgPF$_6$-1 suitable for X-ray diffraction were grown from evaporation of a solution of [Fe(4-pyrdpm)$_3$] and AgPF$_6$ dissolved in benzene and acetonitrile as described above. The counterion is located in three in three independent positions with two on mirror planes from each other. They were determined and then set to be 50%, 25%, and 25% respectively. The complex co-crystallized with 1 molecules of benzene and 3 molecules of acetonitrile that were refined isotropically. An additional molecule of benzene was present but disordered and partially occupied, therefore were

treated as a diffuse contribution using the program SQUEEZE (A. Spek, Platon Library). Electron count/unit cell: 73 (found). The presence of 1 molecule of benzene has an electron count/unit cell: 84, in good agreement with the SQUEEZE refinement.

Structure of [Co(4-pyrdpm)$_3$AgSbF$_6$] (MOF-Co/AgSbF$_6$-1). Red hexagons of MOF-Co/AgSbF$_6$-1 suitable for X-ray diffraction were grown from evaporation of a solution of [Co(4-pyrdpm)$_3$] and AgSbF$_6$ dissolved in benzene and acetonitrile as described above. The counterion is located in three independent positions with two on inversion centers. They were determined based on the Sb occupancy and then set to be 35%, 31%, and 34% respectively. The third counterion is disordered and a benzene molecule also partially occupies the position and could not be refined anisotropically, therefore the counterion was only partially identified and refined isotropically. The complex co-crystallized with one molecule of benzene and one molecule of acetonitrile which were refined isotropically. Several other molecules of benzene and acetonitrile were present but disordered and partially occupied, therefore were treated as a diffuse contribution using the program SQUEEZE (A. Spek, Platon Library). Electron count/unit cell: 288 (found). The presence of two molecules of acetonitrile and one molecule of benzene has an electron count/unit cell: 344, in good agreement with the SQUEEZE refinement.

Structure of [Fe(4-pyrdpm)$_3$AgSbF$_6$] (MOF-Fe/AgSbF$_6$-1). Red plates of MOF-Fe/AgSbF$_6$-1 suitable for X-ray diffraction were grown from evaporation of a solution of [Fe(4-pyrdpm)$_3$] and AgSbF$_6$ dissolved in benzene and acetonitrile as described above. The counterion is also located in three independent positions with

two on inversion centers. They were determined and then set to be 36%, 27%, and 37% occupancy respectively. The third counterion is disordered and a benzene molecule also partially occupies the position and could not be refined anisotropically, therefore the counterion was only partially identified and refined isotropically. The complex co-crystallized with one ordered molecule of benzene and one ordered molecule of acetonitrile which were refined isotropically. Other molecules of benzene and acetonitrile were present but disordered and partially occupied, therefore were treated as a diffuse contribution using the program SQUEEZE (A. Spek, Platon Library). Electron count/unit cell: 220 (found). The presence of one molecule of acetonitrile and one molecule of benzene has an electron count/unit cell: 256, in good agreement with the SQUEEZE refinement.

Structure of $[Co(4\text{-pyrdpm})_3Fe(4\text{-pyrdpm})_3(AgOTf)_2]$ (MOF-CoFe/AgOTf-1). Green blocks of MOF-CoFe/AgOTf-1 suitable for X-ray diffraction were grown from evaporation of a solution of $[Co(4\text{-pyrdpm})_3]$, $[Fe(4\text{-pyrdpm})_3]$ and AgOTf dissolved in benzene and acetonitrile as described above. The complex co-crystallized with two molecules of benzene and three molecules of acetonitrile, which were disordered and partially occupied, therefore were treated as a diffuse contribution using the program SQUEEZE (A. Spek, Platon Library). Electron count/unit cell: 1106 (found), 1200 (expected).

Structure of $[Co(4\text{-pyrdpm})_3Fe(4\text{-pyrdpm})_3(AgBF_4)_2]$ (MOF-CoFe/$AgBF_4$-1). Green blocks of MOF-CoFe/$AgBF_4$-1 suitable for X-ray diffraction were grown from evaporation of a solution of $[Co(4\text{-pyrdpm})_3]$, $[Fe(4\text{-pyrdpm})_3]$ and $AgBF_4$

dissolved in benzene and acetonitrile as described above. The complex co-crystallized with two molecules of benzene and one molecule of acetonitrile, which were disordered and partially occupied. Additional solvent molecules were found however they were disordered. All solvent was treated as a diffuse contribution using the program SQUEEZE (A. Spek, Platon Library). Electron count/unit cell: 1057 (found). The presence of two molecules of benzene and three molecules of acetonitrile in the asymmetric unit gives an expected electron count/unit cell of 1200 in good agreement with the SQUEEZE refinement.

Structure of [Co(4-pyrdpm)$_3$AgOTf] exchanged with BF_4 (MOF-Co/AgOTf/BF_4-1). Red blocks of MOF-Co/AgOTf/BF_4-1 suitable for X-ray diffraction were grown from evaporation of a solution of [Co(4-pyrdpm)$_3$] and AgOTf exchanged with tetrabutylammonium tetrafluoroborate dissolved in benzene and acetonitrile as described above. The complex co-crystallized with one molecule of benzene and one molecule of acetonitrile, which were disordered and partially occupied. Additional solvent molecules were found however they were disordered. All solvent was treated as a diffuse contribution using the program SQUEEZE (A. Spek, Platon Library). Electron count/unit cell: 1226 (found). The presence of two molecules of benzene and three molecules of acetonitrile in the asymmetric unit gives an expected electron count/unit cell of 1200 in good agreement with the SQUEEZE refinement.

Structure of [Co(4-pyrdpm)$_3$AgOTf] exchanged with PF_6 (MOF-Co/AgOTf/PF_6-1). Red blocks of MOF-Co/AgOTf/PF_6-1 suitable for X-ray

diffraction were grown from evaporation of a solution of [Co(4-pyrdpm)$_3$] and AgOTf exchanged with tetrabutylammonium hexafluorophosphate dissolved in benzene and acetonitrile as described above. Electron count/unit cell: 963 (found), (expected). The complex co-crystallized with one molecule of benzene and one molecule of acetonitrile, which were disordered and partially occupied. Additional solvent molecules were found however they were disordered. All solvent was treated as a diffuse contribution using the program SQUEEZE (A. Spek, Platon Library). Electron count/unit cell: 963 (found). The presence of two molecules of benzene and two molecules of acetonitrile in the asymmetric unit gives an expected electron count/unit cell of 1024 in good agreement with the SQUEEZE refinement.

Structure of [Co(44-pyrdpm)$_3$]. Red plates of [Co(44-pyrdpm)$_3$] suitable for X-ray diffraction structural determination were grown from a solution with the complex dissolved in chloroform diffused with hexane. The complex co-crystallized with 2 molecules of hexane and one molecule of chloroform. One hexane molecule was partially occupied and disordered therefore was treated as a diffuse contribution using the program SQUEEZE (A. Spek, Platon Library). Electron count/unit cell: 171 (found), 200 (expected).

Structure of [Co(44-pyrdpm)$_3$AgOTf] (MOF-Co/AgOTf-3). Red rods of MOF-Co/Ag-OTf-3 suitable for X-ray diffraction were grown from evaporation of a solution of [Co(44-pyrdpm)$_3$] and AgOTf dissolved in benzene and acetonitrile as described above. The complex co-crystallized with four ordered molecules of benzene and one ordered molecule of acetonitrile, which were refined anisotropically. Two

molecules of benzene and were detected but disordered and partially occupied therefore were treated as a diffuse contribution using the program SQUEEZE (A. Spek, Platon Library). Electron count/unit cell: 63 (found), 84 (expected).

Structure of [Co(44-pyrdpm)$_3$AgBF$_4$] (MOF-Co/AgBF$_4$-3). Red rods of MOF-Co/AgBF$_4$-3 suitable for X-ray diffraction were grown from evaporation of a solution of [Co(44-pyrdpm)$_3$] and AgBF$_4$ dissolved in benzene and acetonitrile as described above. The complex co-crystallized with one ordered molecule of benzene and one ordered molecule of acetonitrile, which were refined anisotropically. Four molecules of benzene and two molecules of acetonitrile were detected but disordered therefore were treated as a diffuse contribution using the program SQUEEZE (A. Spek, Platon Library). Electron count/unit cell: 447 (found), 424 (expected).

Structure of [Co(44-pyrdpm)$_3$AgPF$_6$] (MOF-Co/AgPF$_6$-3). Red plates of MOF-Co/AgPF$_6$-3 suitable for X-ray diffraction were grown from evaporation of a solution of [Co(44-pyrdpm)$_3$] and AgPF$_6$ dissolved in benzene and acetonitrile as described above. The complex co-crystallized with four ordered molecules of benzene, which were refined anisotropically. One molecule of benzene and two molecules of acetonitrile were detected but disordered therefore were treated as a diffuse contribution using the program SQUEEZE (A. Spek, Platon Library). Electron count/unit cell: 177 (found), 172 (expected).

X-ray Crystal Structure Details for [Co(4-pyrdpm)$_3$]

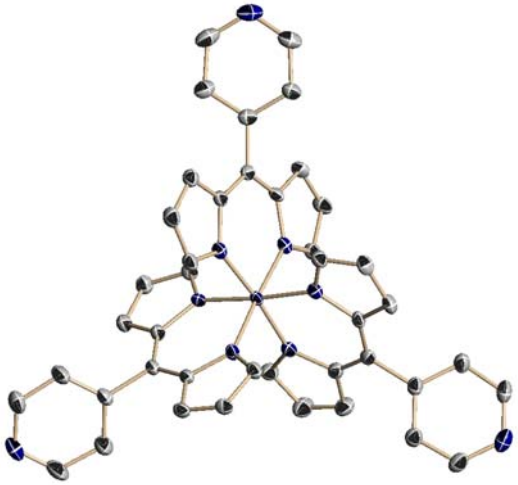

Figure 5-16. Structural Diagram of [Co(4-pyrdpm)$_3$] with partial atom numbering schemes (ORTEP, 50% probability ellipsoids). Hydrogen atoms and solvent molecules have been omitted for clarity.

Table 5-2. Crystal Data for [Co(4-pyrdpm)$_3$].

Empirical formula	$CoC_{54}H_{56}N_9Cl_6$	
Temperature	100(2) K	
Crystal system	Monoclinic	
Space group	*P*2(1)/c	
Unit cell dimensions	a = 20.9151(14) Å	α = 90°
	b = 18.4021(13) Å	β = 102.5010(10)°
	c = 23.3326(16) Å	γ = 90°
Volume	8767.4 (11) Å^3	
Z	8	
Crystal size	0.38 × 0.17 × 0.02 mm^3	
Reflections collected	72950	
Independent reflections	19754 [R(int) = 0.0387]	
Data / restraints / parameters	19754 / 0 / 1056	
Goodness-of-fit on F^2	1.105	
Final R indices [I>2sigma(I)]	R1 = 0.0521, wR2 = 0.1434	
R indices (all data)	R1 = 0.0685, wR2 = 0.1516	

X-ray Crystal Structure Details for [Fe(4-pyrdpm)$_3$]

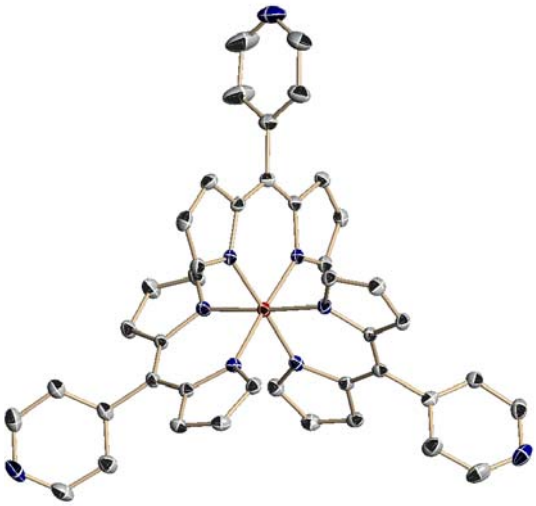

Figure 5-17. Structural Diagram of [Fe(4-pyrdpm)$_3$] with partial atom numbering schemes (ORTEP, 50% probability ellipsoids). Hydrogen atoms and disordered solvent molecules have been omitted for clarity.

Table 5-3. Crystal Data for [Fe(4-pyrdpm)$_3$].

Empirical formula	$FeC_{48}H_{44}N_9$	
Temperature	100(2) K	
Crystal system	Monoclinic	
Space group	*P*2(1)/c	
Unit cell dimensions	a = 9.2370(9) Å	α = 90°
	b = 30719(3) Å	β = 102.8780(10)°
	c = 13.0514(12) Å	γ = 90°
Volume	3610.3 (6) Å^3	
Z	4	
Crystal size	0.23 × 0.18 × 0.17 mm^3	
Reflections collected	30925	
Independent reflections	8104 [R(int) = 0.0388]	
Data / restraints / parameters	8104 / 0 / 469	
Goodness-of-fit on F^2	1.071	
Final R indices [I>2sigma(I)]	$R1$ = 0.0415, w$R2$ = 0.0962	
R indices (all data)	$R1$ = 0.0553, w$R2$ = 0.1007	

X-ray Crystal Structure Details for MOF-Co/AgOTf-1

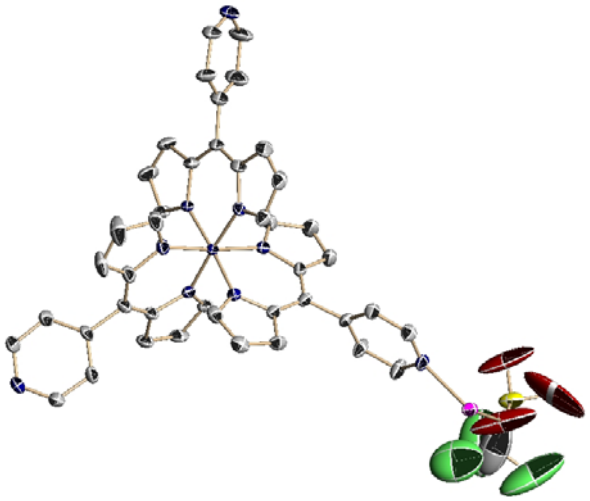

Figure 5-18. Structural Diagram of MOF-Co/AgOTf-1 (ORTEP, 50% probability ellipsoids). Hydrogen atoms and solvent molecules have been omitted for clarity.

Table 5-4. Crystal Data for MOF-Co/AgOTf-1.

Empirical formula	$CoC_{55}H_{48}N_{15}AgO_3F_3S$	
Temperature	100(2) K	
Crystal system	Orthorhombic	
Space group	*Pbcn*	
Unit cell dimensions	a = 26.713(3) Å	α = 90°
	b = 12.5800(13) Å	β = 90°
	c = 33.455(3) Å	γ = 90°
Volume	11243 (2) $Å^3$	
Z	8	
Crystal size	0.40 × 0.33 × 0.15 mm^3	
Reflections collected	93010	
Independent reflections	12681 [R(int) = 0.0828]	
Data / restraints / parameters	12681 / 0 / 574	
Goodness-of-fit on F^2	1.041	
Final R indices [I>2sigma(I)]	$R1$ = 0.0704, $wR2$ = 0.1842	
R indices (all data)	$R1$ = 0.0921, $wR2$ = 0.1946	

X-ray Crystal Structure Details for MOF-Co/$AgBF_4$-1

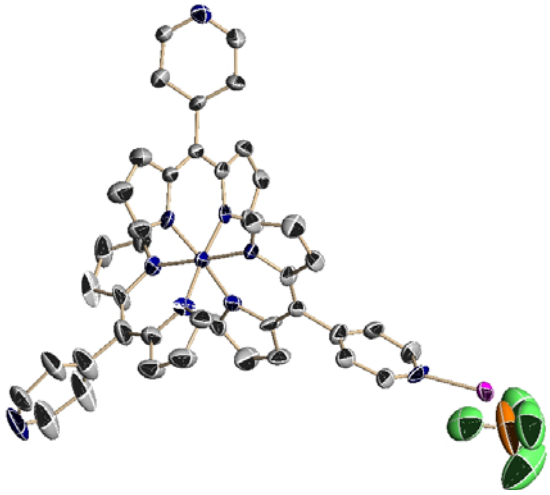

Figure 5-19. Structural Diagram of MOF-Co/$AgBF_4$-1 (ORTEP, 50% probability ellipsoids). Hydrogen atoms and solvent molecules have been omitted for clarity.

Table 5-5. Crystal Data for MOF-Co/$AgBF_4$-1.

Empirical formula	$CoC_{58}H_{48}N_{11}AgBF_4$	
Temperature	100(2) K	
Crystal system	Orthorhombic	
Space group	*Pbcn*	
Unit cell dimensions	a = 26.902(7) Å	α = 90°
	b = 12.349(3) Å	β = 90°
	c = 33.378(8) Å	γ = 90°
Volume	11089 (5) $Å^3$	
Z	8	
Crystal size	0.30 × 0.22 × 0.16 mm^3	
Reflections collected	89619	
Independent reflections	12782 [R(int) = 0.2904]	
Data / restraints / parameters	12782 / 0 / 523	
Goodness-of-fit on F^2	1.117	
Final R indices [I>2sigma(I)]	$R1$ = 0.1437, $wR2$ = 0.3225	
R indices (all data)	$R1$ = 0.1733, $wR2$ = 0.3389	

X-ray Crystal Structure Details for MOF-Fe/$AgBF_4$-1

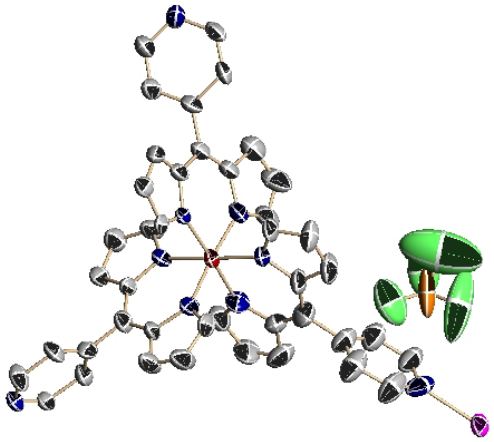

Figure 5-20. Structural Diagram of MOF-Fe/$AgBF_4$-1 (ORTEP, 50% probability ellipsoids). Hydrogen atoms and solvent molecules have been omitted for clarity.

Table 5-6. Crystal Data for MOF-Fe/$AgBF_4$-1.

Empirical formula	$FeC_{53}H_{49}N_{14}AgBF_4$	
Temperature	100(2) K	
Crystal system	Orthorhombic	
Space group	*Pbcn*	
Unit cell dimensions	a = 26.959(3) Å	α = 90°
	b = 12.3089(2) Å	β = 90°
	c = 33.493(4) Å	γ = 90°
Volume	11114 (4) $Å^3$	
Z	8	
Crystal size	0.32 × 0.22 × 0.15 mm^3	
Reflections collected	92491	
Independent reflections	12659 [R(int) = 0.0826]	
Data / restraints / parameters	12659 / 0 / 535	
Goodness-of-fit on F^2	1.041	
Final R indices [I>2sigma(I)]	$R1$ = 0.0984, $wR2$ = 0.2691	
R indices (all data)	$R1$ = 0.1461, $wR2$ = 0.2910	

X-ray Crystal Structure Details for MOF-Fe/AgOTf-1

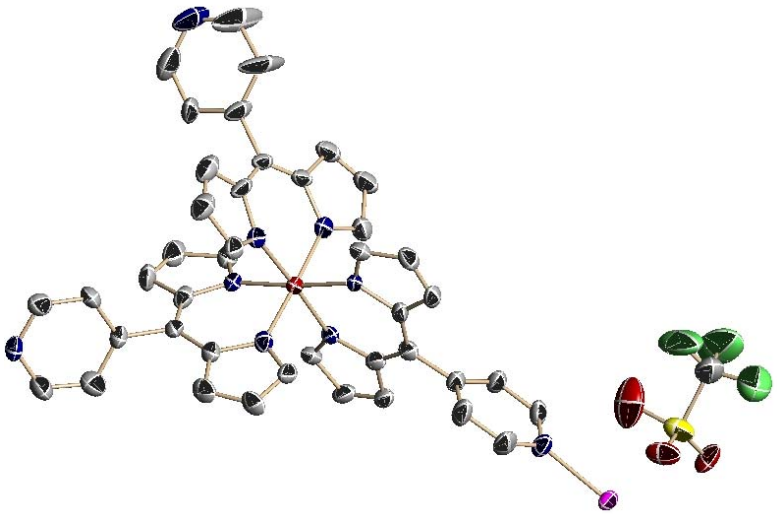

Figure 5-21. Structural Diagram of MOF-Fe/AgOTf-1 (ORTEP, 50% probability ellipsoids). Hydrogen atoms and solvent molecules have been omitted for clarity.

Table 5-7. Crystal Data for MOF-Fe/AgOTf-1.

Empirical formula	$Fe_3C_{163}H_{126}N_{29}Ag_3S_3F_9O_9$	
Temperature	100(2) K	
Crystal system	Monoclinic	
Space group	*C2/c*	
Unit cell dimensions	a = 33.186(5) Å	α = 90°
	b = 66.054(10) Å	β = 110.699(2)°
	c = 14.882(2) Å	γ = 90°
Volume	30516 (8) Å^3	
Z	8	
Crystal size	0.32 × 0.15 × 0.02 mm^3	
Reflections collected	132639	
Independent reflections	34378 [R(int) = 0.1385]	
Data / restraints / parameters	34378 / 0 / 1953	
Goodness-of-fit on F^2	0.976	
Final R indices [I>2sigma(I)]	$R1$ = 0.0906, $wR2$ = 0.2000	
R indices (all data)	$R1$ = 0.1844, $wR2$ = 0.2322	

X-ray Crystal Structure Details for MOF-Co/$AgPF_6$-1

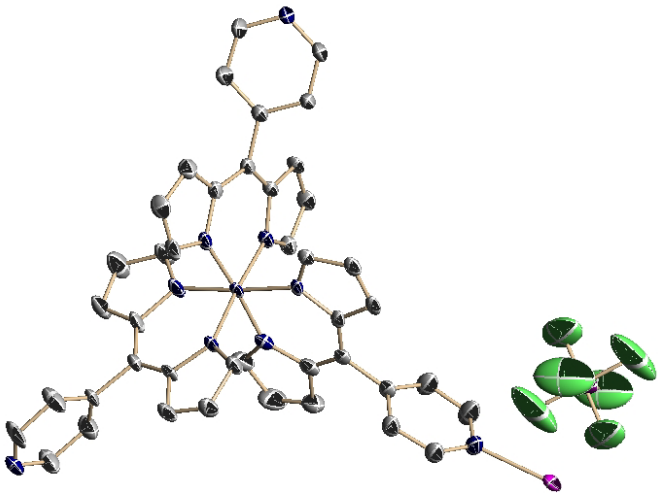

Figure 5-22. Structural Diagram of MOF-Co/$AgPF_6$-1 (ORTEP, 50% probability ellipsoids). Hydrogen atoms and solvent molecules have been omitted for clarity.

Table 5-8. Crystal Data for MOF-Co/$AgPF_6$-1.

Empirical formula	$CoC_{60}H_{51}N_{11}AgPF_6$	
Temperature	100(2) K	
Crystal system	Triclinic	
Space group	*P*-1	
Unit cell dimensions	a = 13.120(3) Å	α = 110.178(3)°
	b = 16.111(3) Å	β = 112.416(3)°
	c = 16.134(3) Å	γ = 97.335(3)°
Volume	2824.0(10) $Å^3$	
Z	2	
Crystal size	0.50 × 0.30 × 0.23 mm^3	
Reflections collected	23611	
Independent reflections	12243 [R(int) = 0.0354]	
Data / restraints / parameters	12243 / 0 / 610	
Goodness-of-fit on F^2	1.033	
Final R indices [I>2sigma(I)]	$R1$ = 0.0866, $wR2$ = 0.2452	
R indices (all data)	$R1$ = 0.0993, $wR2$ = 0.2545	

X-ray Crystal Structure Details for MOF-Fe/$AgPF_6$-1

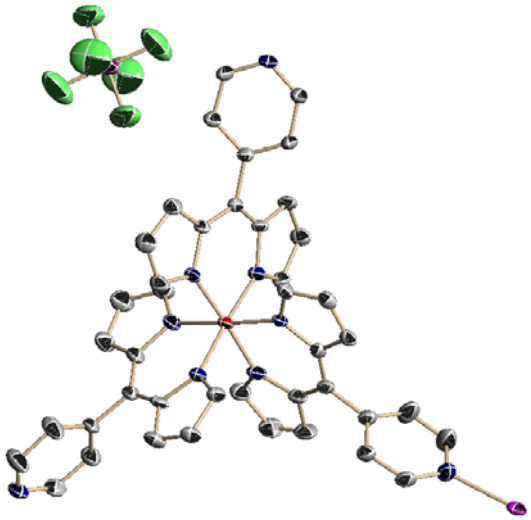

Figure 5-23. Structural Diagram of MOF-Fe/$AgPF_6$-1 (ORTEP, 50% probability ellipsoids). Hydrogen atoms and solvent molecules have been omitted for clarity.

Table 5-9. Crystal Data for MOF-Fe/$AgPF_6$-1.

Empirical formula	$FeC_{60}H_{51}N_{12}AgPF_6$	
Temperature	100(2) K	
Crystal system	Triclinic	
Space group	*P*-1	
Unit cell dimensions	a = 13.115(2) Å	α = 110.161(2)°
	b = 16.116(3) Å	β = 98.523(2)°
	c = 16.297(3) Å	γ = 112.103(3)°
Volume	2838.8 (8) $Å^3$	
Z	2	
Crystal size	0.47 × 0.41 × 0.18 mm^3	
Reflections collected	23676	
Independent reflections	12281 [R(int) = 0.0299]	
Data / restraints / parameters	11281 / 0 / 625	
Goodness-of-fit on F^2	1.092	
Final R indices [I>2sigma(I)]	$R1$ = 0.0812, $wR2$ = 0.2554	
R indices (all data)	$R1$ = 0.1029, $wR2$ = 0.2726	

X-ray Crystal Structure Details for MOF-Co/$AgSbF_6$-1

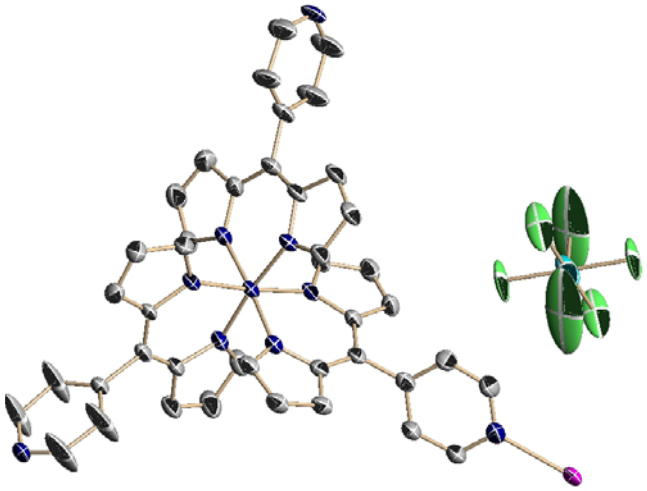

Figure 5-24. Structural Diagram of MOF-Co/$AgSbF_6$-1 (ORTEP, 50% probability ellipsoids). Hydrogen atoms and solvent molecules have been omitted for clarity.

Table 5-10. Crystal Data for MOF-Co/$AgSbF_6$-1.

Empirical formula	$CoC_{60}H_{51}N_{12}AgSbF_6$	
Temperature	100(2) K	
Crystal system	Monoclinic	
Space group	*P*2(1)/c	
Unit cell dimensions	a = 15.7911(14) Å	α = 90°
	b = 25.454(2) Å	β = 109.8240(10)°
	c = 16.3779(14) Å	γ = 90°
Volume	6193.0 (9) $Å^3$	
Z	4	
Crystal size	0.53 × 0.50 × 0.45 mm^3	
Reflections collected	51670	
Independent reflections	13879 [R(int) = 0.0415]	
Data / restraints / parameters	13879 / 0 / 611	
Goodness-of-fit on F^2	1.051	
Final R indices [I>2sigma(I)]	$R1$ = 0.0842, $wR2$ = 0.2480	
R indices (all data)	$R1$ = 0.0973, $wR2$ = 0.2581	

X-ray Crystal Structure Details for MOF-Fe/$AgSbF_6$-1

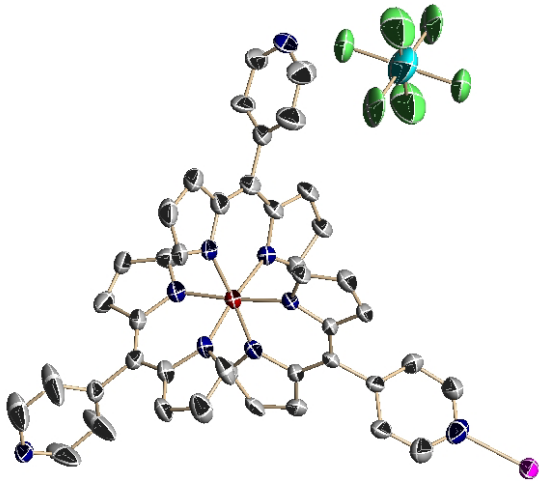

Figure 5-25. Structural Diagram of MOF-Fe/$AgSbF_6$-1 (ORTEP, 50% probability ellipsoids). Hydrogen atoms and solvent molecules have been omitted for clarity.

Table 5-11. Crystal Data for MOF-Fe/$AgSbF_6$-1.

Empirical formula	$FeC_{58}H_{48}N_{11}AgSbF_6$	
Temperature	100(2) K	
Crystal system	Monoclinic	
Space group	*P*2(1)/*c*	
Unit cell dimensions	*a* = 15.874(2) Å	$\alpha = 90°$
	b = 24.606(3) Å	$\beta = 110.009(2)°$
	c = 16.377(2) Å	$\gamma = 90°$
Volume	6010.7 (13) $Å^3$	
Z	4	
Crystal size	0.22 × 0.20 × 0.04 mm^3	
Reflections collected	50692	
Independent reflections	13559 [*R*(int) = 0.0648]	
Data / restraints / parameters	13559 / 0 / 610	
Goodness-of-fit on F^2	1.031	
Final *R* indices [I>2sigma(I)]	*R*1 = 0.1274, *wR*2 = 0.3374	
R indices (all data)	*R*1 = 0.1640, *wR*2 = 0.3562	

X-ray Crystal Structure Details for MOF-Co/$AgNO_3$-1a

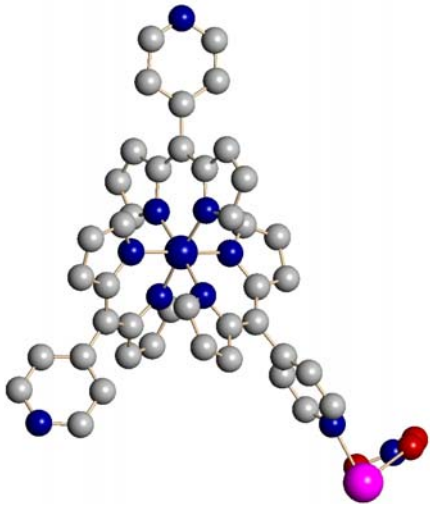

Figure 5-26. Structural Diagram of MOF-Co/$AgNO_3$-1a (ORTEP, 50% probability ellipsoids). Hydrogen atoms and solvent molecules have been omitted for clarity.

Table 5-12. Crystal Data for MOF-Co/$AgNO_3$-1a.

Empirical formula	$CoC_{48}H_{36}N_{10}AgO_3$	
Temperature	100(2) K	
Crystal system	Monoclinic	
Space group	*P*2(1)/c	
Unit cell dimensions	a = 14.128(3) Å	α = 90°
	b = 8.827(2) Å	β = 112.889(4)°
	c = 35.763(9) Å	γ = 90°
Volume	4108.7 (17) $Å^3$	
Z	4	
Crystal size	0.22 × 0.20 × 0.13 mm^3	
Reflections collected	32976	
Independent reflections	9249 [R(int) = 0.0486]	
Data / restraints / parameters	9249 / 0 / 568	
Goodness-of-fit on F^2	1.145	
Final R indices [I>2sigma(I)]	$R1$ = 0.2312, $wR2$ = 0.5505	
R indices (all data)	$R1$ = 0.2346, $wR2$ = 0.5514	

X-ray Crystal Structure Details for MOF-Co/$AgNO_3$-1b

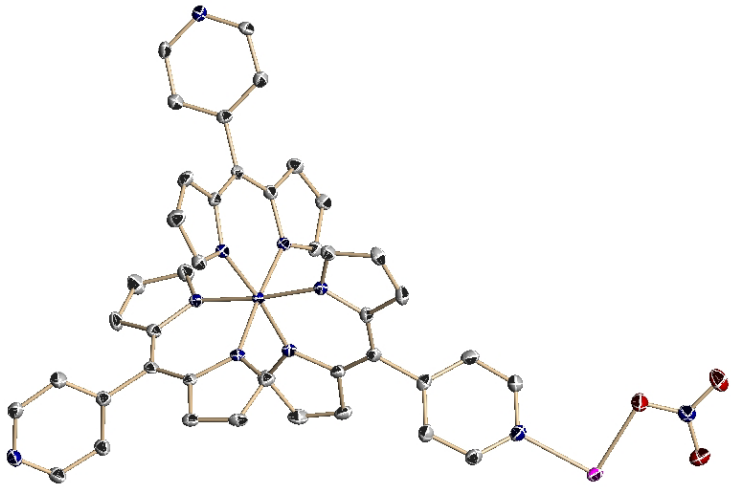

Figure 5-27. Structural Diagram of MOF-Co/$AgNO_3$-1b (ORTEP, 50% probability ellipsoids). Hydrogen atoms and solvent molecules have been omitted for clarity.

Table 5-13. Crystal Data for MOF-Co/$AgNO_3$-1b.

Empirical formula	$CoC_{43}H_{33.50}N_{10.50}AgO_3$	
Temperature	100(2) K	
Crystal system	Monoclinic	
Space group	*C*2	
Unit cell dimensions	a = 34.721(4) Å	α = 90°
	b = 8.3253(9) Å	β = 112.7000(10)°
	c = 14.2738(16) Å	γ = 90°
Volume	3778.0 (7) $Å^3$	
Z	4	
Crystal size	0.60 × 0.24 × 0.22 mm^3	
Reflections collected	16019	
Independent reflections	7969 [R(int) = 0.0248]	
Data / restraints / parameters	7969 / 1 / 532	
Goodness-of-fit on F^2	1.109	
Final R indices [I>2sigma(I)]	$R1$ = 0.0264, $wR2$ = 0.0704	
R indices (all data)	$R1$ = 0.0268, $wR2$ = 0.0706	

X-ray Crystal Structure Details for MOF-Co/AgOTf/BF_4-1

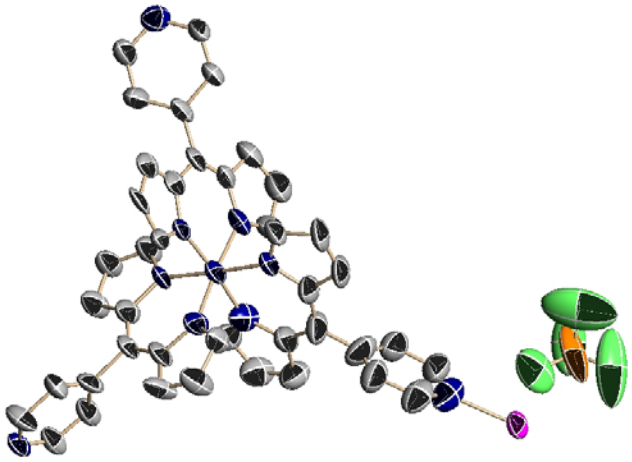

Figure 5-28. Structural Diagram of MOF-Co/AgOTf/BF_4-1 (ORTEP, 50% probability ellipsoids). Hydrogen atoms and solvent molecules have been omitted for clarity.

Table 5-14. Crystal Data for MOF-Co/AgOTf/BF_4-1.

Empirical formula	$CoC_{60}H_{51}N_{12}AgBF_4$	
Temperature	100(2) K	
Crystal system	Orthorhombic	
Space group	*Pbcn*	
Unit cell dimensions	a = 26.973(4) Å	α = 90°
	b = 12.3571(17) Å	β = 90°
	c = 33.438(5) Å	γ = 90°
Volume	11145 (3) $Å^3$	
Z	8	
Crystal size	0.30 × 0.20 × 0.10 mm^3	
Reflections collected	91138	
Independent reflections	12795 [R(int) = 0.1231]	
Data / restraints / parameters	12795 / 0 / 523	
Goodness-of-fit on F^2	0.994	
Final R indices [I>2sigma(I)]	$R1$ = 0.1024, $wR2$ = 0.2819	
R indices (all data)	$R1$ = 0.1896, $wR2$ = 0.3117	

X-ray Crystal Structure Details for MOF-Co/AgOTf/PF_6-1

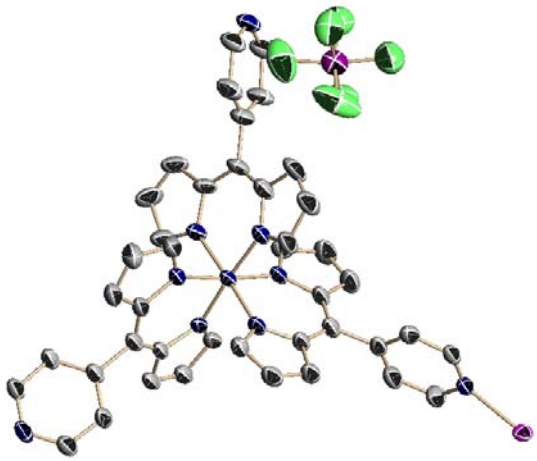

Figure 5-29. Structural Diagram of MOF-Co/AgOTf/PF_6-1 (ORTEP, 50% probability ellipsoids). Hydrogen atoms and solvent molecules have been omitted for clarity.

Table 5-15. Crystal Data for MOF-Co/AgOTf/PF_6-1.

Empirical formula	$CoC_{58}H_{48}N_{11}AgPF_6$	
Temperature	100(2) K	
Crystal system	Orthorhombic	
Space group	*Pbcn*	
Unit cell dimensions	a = 26.847(2) Å	α = 90°
	b = 12.6272(10) Å	β = 90°
	c = 33.438(3) Å	γ = 90°
Volume	11335.5 (15) $Å^3$	
Z	8	
Crystal size	0.55 × 0.34 × 0.22 mm^3	
Reflections collected	91578	
Independent reflections	12952 [R(int) = 0.0557]	
Data / restraints / parameters	12952 / 0 / 541	
Goodness-of-fit on F^2	1.093	
Final R indices [I>2sigma(I)]	$R1$ = 0.0584, $wR2$ = 0.1628	
R indices (all data)	$R1$ = 0.0824, $wR2$ = 0.1730	

X-ray Crystal Structure Details for MOF-CoFe/AgOTf-1

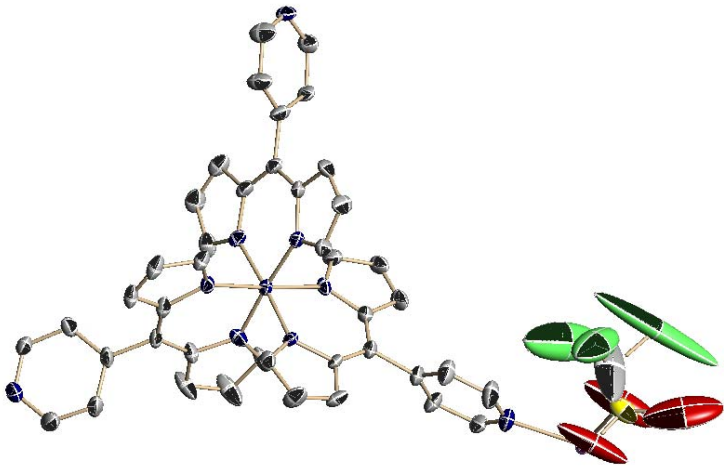

Figure 5-30. Structural Diagram of MOF-CoFe/AgOTf-1 (ORTEP, 50% probability ellipsoids). Hydrogen atoms and solvent molecules have been omitted for clarity.

Table 5-16. Crystal Data for MOF-CoFe/AgOTf-1.

Empirical formula	Co/Fe $C_{61}H_{51}N_{12}AgSF_3O_3$	
Temperature	100(2) K	
Crystal system	Orthorhombic	
Space group	*Pbcn*	
Unit cell dimensions	a = 26.846(3) Å	α = 90°
	b = 12.6198(12) Å	β = 90°
	c = 33.523(3) Å	γ = 90°
Volume	11357.1 (19) $Å^3$	
Z	8	
Crystal size	0.35 × 0.26 × 0.18 mm^3	
Reflections collected	93132	
Independent reflections	13366 [R(int) = 0.0465]	
Data / restraints / parameters	13366 / 0 / 550	
Goodness-of-fit on F^2	1.074	
Final R indices [I>2sigma(I)]	$R1$ = 0.0846, $wR2$ = 0.2013	
R indices (all data)	$R1$ = 0.0984, $wR2$ = 0.2077	

X-ray Crystal Structure Details for MOF-CoFe/$AgBF_4$-1

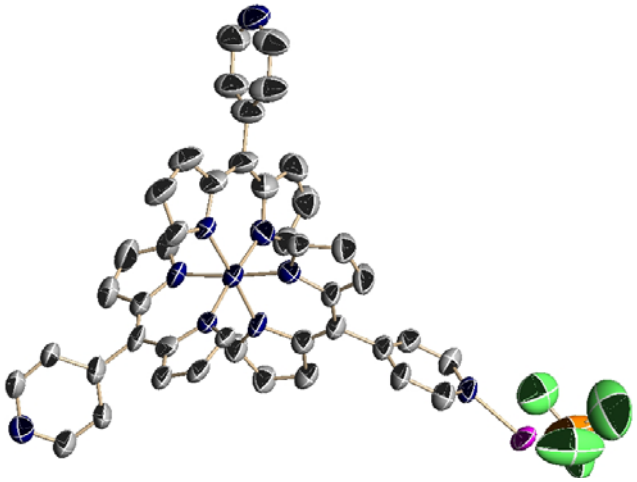

Figure 5-31. Structural Diagram of MOF-CoFe/$AgBF_4$-1 (ORTEP, 50% probability ellipsoids). Hydrogen atoms and solvent molecules have been omitted for clarity.

Table 5-17. Crystal Data for MOF-CoFe/$AgBF_4$-1.

Empirical formula	Co/Fe $C_{60}H_{51}N_{12}AgBF_4$	
Temperature	100(2) K	
Crystal system	Orthorhombic	
Space group	*Pbcn*	
Unit cell dimensions	a = 27.111(3) Å	α = 90°
	b = 12.4180(12) Å	β = 90°
	c = 33.668(3) Å	γ = 90°
Volume	11334.9 (18) $Å^3$	
Z	8	
Crystal size	0.38 × 0.34 × 0.30 mm^3	
Reflections collected	95024	
Independent reflections	13373 [R(int) = 0.1029]	
Data / restraints / parameters	13373 / 0 / 523	
Goodness-of-fit on F^2	0.974	
Final R indices [I>2sigma(I)]	$R1$ = 0.0861, $wR2$ = 0.2196	
R indices (all data)	$R1$ = 0.1744, $wR2$ = 0.2596	

X-ray Crystal Structure Details for [Co(3-pyrdpm)$_3$]

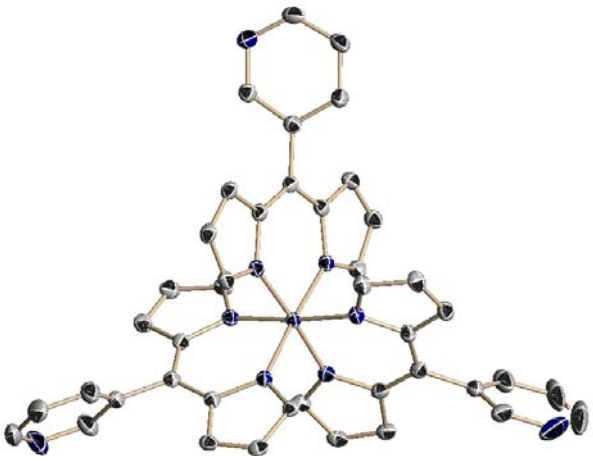

Figure 5-32. Structural Diagram of [Co(3-pyrdpm)$_3$] (ORTEP, 50% probability ellipsoids) with partial atom numbering schemes. Hydrogen atoms have been omitted for clarity.

Table 5-18. Crystal Data for [Co(3-pyrdpm)$_3$].

Empirical formula	$CoC_{42}H_{30}N_9$	
Temperature	100(2) K	
Crystal system	Monoclinic	
Space group	*P*2(1)/c	
Unit cell dimensions	a = 9.4021(5) Å	α = 90°
	b = 25.4016(13) Å	β = 102.0150(10)°
	c = 14.1149(7) Å	γ = 90°
Volume	3297.2 (3) Å^3	
Z	4	
Crystal size	0.27 × 0.26 × 0.05 mm^3	
Reflections collected	27732	
Independent reflections	7421 [R(int) = 0.0272]	
Data / restraints / parameters	7421 / 0 / 469	
Goodness-of-fit on F^2	1.036	
Final R indices [I>2sigma(I)]	R1 = 0.0386, wR2 = 0.0966	
R indices (all data)	R1 = 0.0457, wR2 = 0.1008	

X-ray Crystal Structure Details for [Co(44-pyrdpm)$_3$]

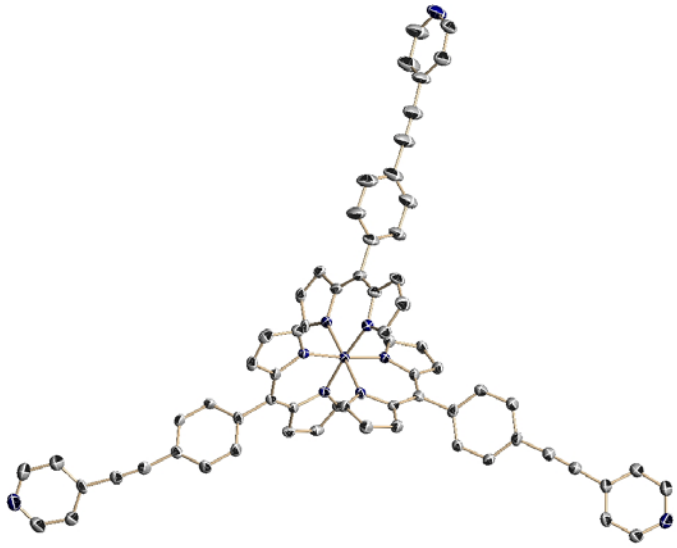

Figure 5-33. Structural Diagram of [Co(44-pyrdpm)$_3$] (ORTEP, 50% probability ellipsoids). Hydrogen atoms and solvent molecules have been omitted for clarity.

Table 5-19. Crystal Data for [Co(44-pyrdpm)$_3$].

Empirical formula	$CoC_{79}H_{71}N_9Cl_3$	
Temperature	100(2) K	
Crystal system	Triclinic	
Space group	*P*-1	
Unit cell dimensions	a = 15.2681(12) Å	α = 69.4900(10)°
	b = 20.2619(16) Å	β = 84.2850(10)°
	c = 21.5668(17) Å	γ = 87.069(2)°
Volume	6217.0 (8) Å^3	
Z	4	
Crystal size	0.27 × 0.26 × 0.10 mm^3	
Reflections collected	53738	
Independent reflections	27331 [R(int) = 0.0465]	
Data / restraints / parameters	27331 / 0 / 1461	
Goodness-of-fit on F^2	0.972	
Final R indices [I>2sigma(I)]	$R1$ = 0.0662, $wR2$ = 0.1581	
R indices (all data)	$R1$ = 0.1080, $wR2$ = 0.1743	

X-ray Crystal Structure Details for MOF-Co/AgOTf-3

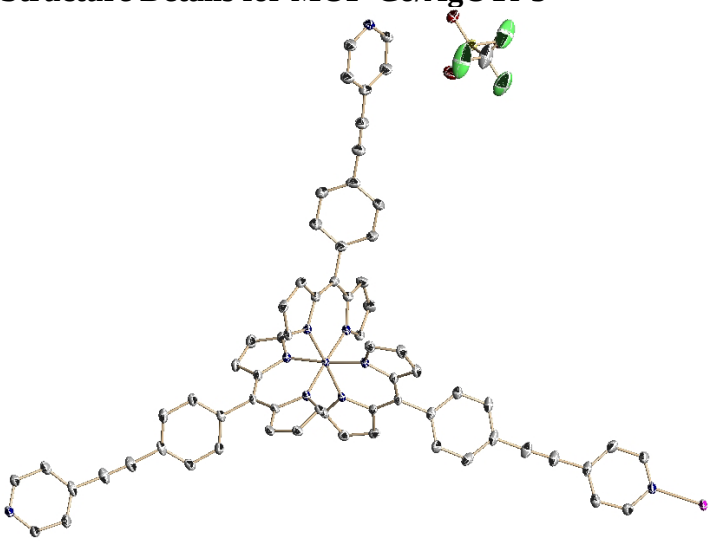

Figure 5-34. Structural Diagram of MOF-Co/AgOTf-3 (ORTEP, 50% probability ellipsoids). Hydrogen atoms and solvent molecules have been omitted for clarity.

Table 5-20. Crystal Data for MOF-Co/AgOTf-3.

Empirical formula	$CoC_{105}H_{81}N_{10}AgF_3O_3S$	
Temperature	100(2) K	
Crystal system	Triclinic	
Space group	*P*-1	
Unit cell dimensions	a = 9.3693(9) Å	α = 94.659(2)°
	b = 19.3886(19) Å	β = 94.855(2)°
	c = 22.869(2) Å	γ = 91.655(2)°
Volume	4123.0 (7) $Å^3$	
Z	2	
Crystal size	0.90 × 0.24 × 0.22 mm^3	
Reflections collected	35002	
Independent reflections	17956 [R(int) = 0.0273]	
Data / restraints / parameters	17956 / 0 / 1010	
Goodness-of-fit on F^2	1.041	
Final R indices [I>2sigma(I)]	$R1$ = 0.0501, $wR2$ = 0.1276	
R indices (all data)	$R1$ = 0.0643, $wR2$ = 0.1332	

X-ray Crystal Structure Details for MOF-Co/$AgBF_4$-3

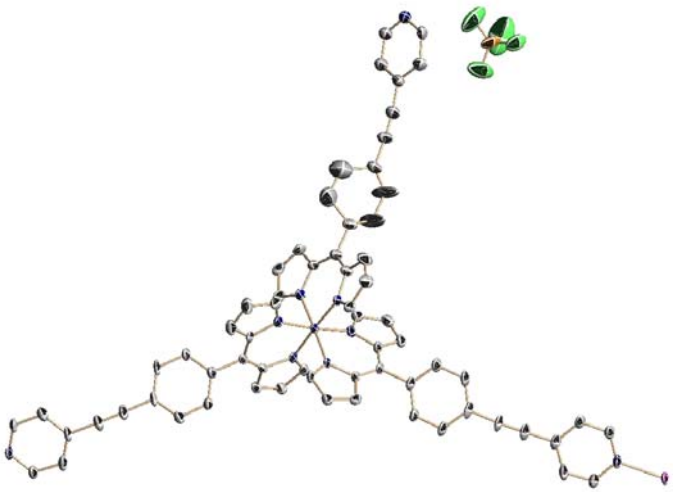

Figure 5-35. Structural Diagram of MOF-Co/$AgBF_4$-3 (ORTEP, 50% probability ellipsoids). Hydrogen atoms and solvent molecules have been omitted for clarity.

Table 5-21. Crystal Data for MOF-Co/$AgBF_4$-3.

Empirical formula	$CoC_{102}H_{81}N_{12}AgBF_4$	
Temperature	100(2) K	
Crystal system	Triclinic	
Space group	*P*-1	
Unit cell dimensions	a = 9.4031(17) Å	α = 91.311(3)°
	b = 18.794(4) Å	β = 94.990(3)°
	c = 22.803(4) Å	γ = 94.994(3)°
Volume	3997.5 (13) $Å^3$	
Z	2	
Crystal size	0.50 × 0.15 × 0.09 mm^3	
Reflections collected	33394	
Independent reflections	17297 [R(int) = 0.0433]	
Data / restraints / parameters	17297 / 0 / 821	
Goodness-of-fit on F^2	0.940	
Final R indices [I>2sigma(I)]	$R1$ = 0.0765, $wR2$ = 0.2017	
R indices (all data)	$R1$ = 0.1015, $wR2$ = 0.2127	

X-ray Crystal Structure Details for MOF-Co/$AgPF_6$-3

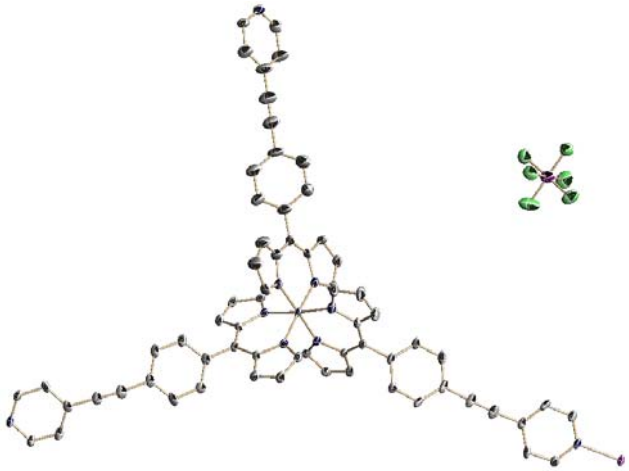

Figure 5-36. Structural Diagram of MOF-Co/$AgPF_6$-3 with partial atom numbering schemes (ORTEP, 50% probability ellipsoids). Hydrogen atoms and solvent molecules have been omitted for clarity.

Table 5-22. Crystal Data for MOF-Co/$AgPF_6$-3.

Empirical formula	$CoC_{100}H_{78}N_{11}AgPF_6$	
Temperature	100(2) K	
Crystal system	Triclinic	
Space group	*P*-1	
Unit cell dimensions	a = 9.4026(13) Å	α = 93.820(2)°
	b = 19.385(3) Å	β = 95.353(2)°
	c = 22.645(3) Å	γ = 92.800(2)°
Volume	4094.0 (10) $Å^3$	
Z	2	
Crystal size	0.44 × 0.17 × 0.07 mm^3	
Reflections collected	33968	
Independent reflections	17705 [R(int) = 0.0585]	
Data / restraints / parameters	17705 / 0 / 973	
Goodness-of-fit on F^2	1.020	
Final R indices [I>2sigma(I)]	$R1$ = 0.0891, $wR2$ = 0.2319	
R indices (all data)	$R1$ = 0.1383, $wR2$ = 0.2499	

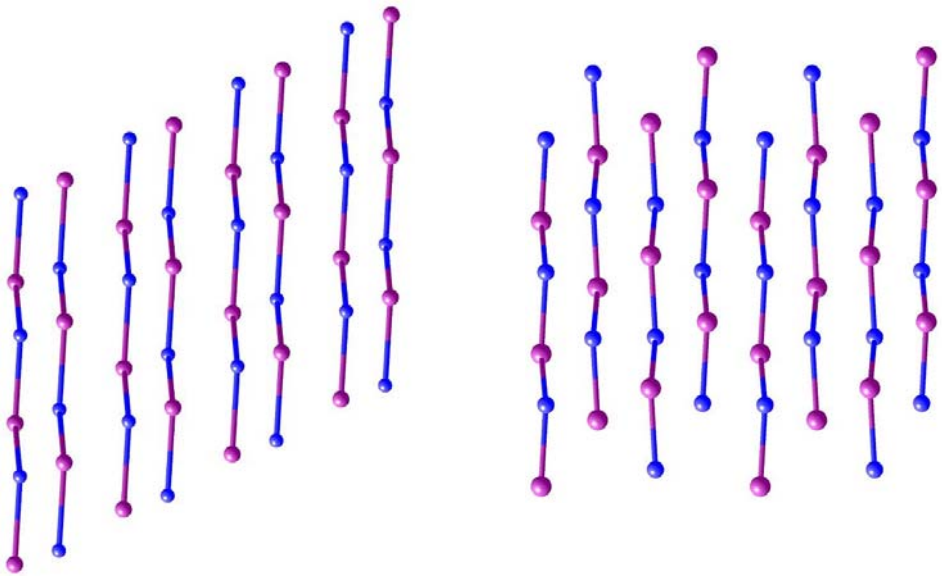

Figure 5-37. Topological diagram of sheets of MOF-Co/$AgPF_6$-1 (*b*-axis, left) and two sheets of MOF-Co/$AgSbF_6$-1 (*a*-axis, right). Silver(I) ions are shown in purple and cobalt(III) ions are shown in blue. All other atoms, counterions, and solvent molecules have been omitted for clarity.

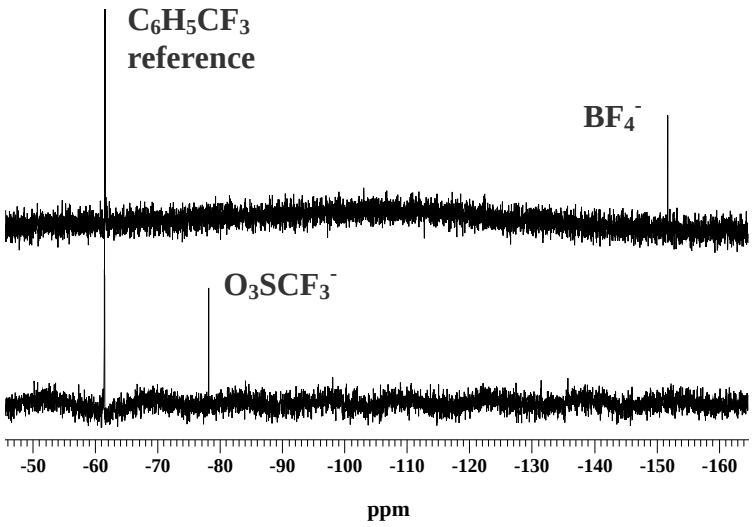

Figure 5-38. ^{19}FNMR of MOF-Co/AgOTf/BF_4-1 (top) and MOF-Co/AgOTf-1 (bottom).

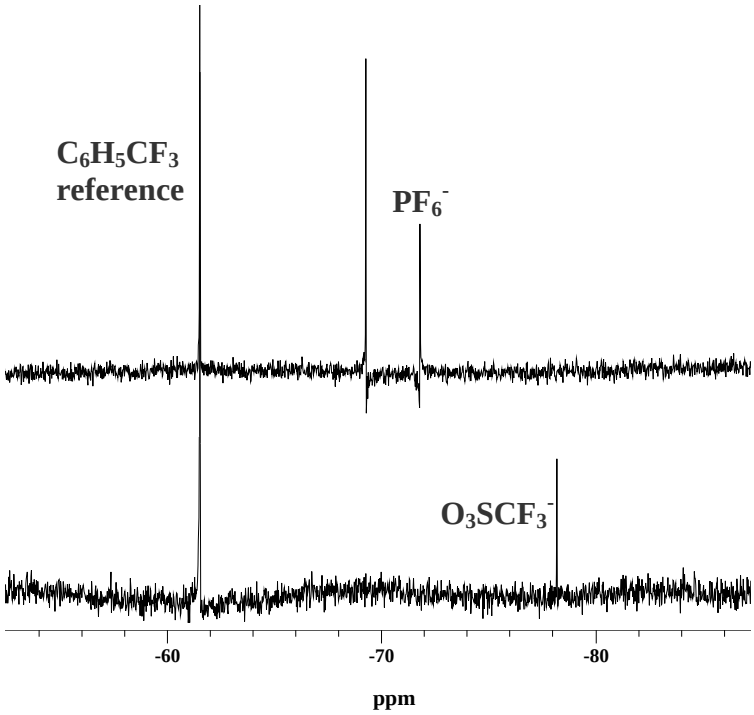

Figure 5-39. ^{19}FNMR of MOF-Co/AgOTf/PF_6-1 (top) and MOF-Co/AgOTf-1 (bottom).

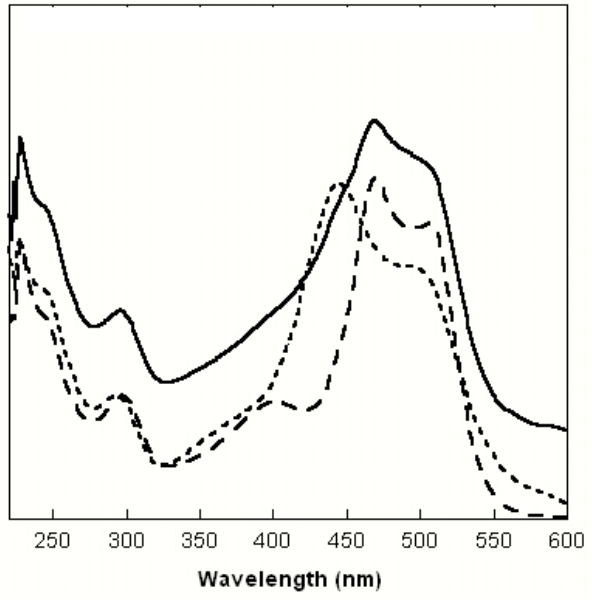

Figure 5-40. Electronic absorption spectra of MOF-CoFe/$AgBF_4$-1 (——), [Co(4-pyrdpm)$_3$] (---), and [Fe(4-pyrdpm)$_3$] (····).

5.7. References

[1] C. V. K. Sharma, G. A. Broker, J. G. Huddleston, J. W. Baldwin, R. M. Metzger, R. D. Rogers, *J. Am. Chem. Soc.* **1999**, *121*, 1137.

[2] T. N. Milic, N. Chi, D. G. Yablon, G. W. Flynn, J. D. Batteas, C. M. Drain, *Angew. Chem. Int. Ed.* **2002**, *41*, 2117.

[3] B. F. Abrahams, B. F. Hoskins, D. M. Michail, R. Robson, *Nature* **1994**, *369*, 727.

[4] D. Hagrman, P. J. Hagrman, J. Zubieta, *Angew. Chem. Int. Ed.* **1999**, *38*, 3165.

[5] R. Kitaura, G. Onoyama, H. Sakamoto, R. Matsuda, S. Noro, S. Kitagawa, *Angew. Chem. Int. Ed.* **2004**, *43*, 2684.

[6] S. Decurtins, H. W. Schmalle, P. Schneuwly, J. Ensling, P. A. Gtlich, *J. Am. Chem. Soc.* **1994**, *116*, 9521.

[7] O. M. Yaghi, H. Li, *J. Am. Chem. Soc.* **1996**, *118*, 295.

[8] K. S. Min, M. P. Suh, *J. Am. Chem. Soc.* **2000**, *122*, 6834.

[9] G. B. Gardner, D. Venkataraman, J. S. Moore, S. Lee, *Nature* **1995**, *374*, 792.

[10] L. Öhrström, K. Larsson, *Dalton Trans.* **2004**, 347.

[11] A. F. Wells, *Three-dimensional nets, polyhedra*, John Wiley & Sons, New York, **1977**.

[12] B. Chen, S. Lee, D. Venkataraman, F. J. DiSalvo, E. B. Lobkovsky, M. Nakayama, *Cryst. Growth Des.* **2002**, *2*, 101.

[13] L. Ohrstrom, K. Larsson, *Molecule-based materials*, Elsevier, **2005**.

[14] S. R. Batten, R. Robson, *Angew. Chem. Int. Ed.* **1998**, *37*, 1460.

[15] M. Du, Y.-M. Guo, S.-T. Chen, X.-H. Bu, S. R. Batten, J. Ribas, S. Kitagawa, *Inorg. Chem.* **2004**, *43*, 1287.

[16] O. M. Yaghi, H. L. Li, *J. Am. Chem. Soc.* **1996**, *118*, 295.

[17] Z. Ni, J. J. Vittal, *Crystal Growth & Design* **2001**, *1*, 195.

[18] Y. Kang, S. S. Lee, K.-M. Park, S. H. Lee, S. O. Kang, J. Ko, *Inorg. Chem.* **2001**, *40*, 7027.

[19] L. Raehm, L. Mimassi, C. Guyard-Duhayon, H. Amouri, *Inorg. Chem.* **2003**, *42*, 5654.

[20] X.-H. Bu, Y.-B. Xie, J.-R. Li, R.-H. Zhang, *Inorg. Chem.* **2003**, *42*, 7422.

[21] F. C. Pigge, M. D. Burgard, N. P. Rath, *Crystal Growth & Design* **2003**, *3*, 331.

[22] D. L. Reger, R. P. Watson, J. R. Gardinier, M. D. Smith, *Inorg. Chem.* **2004**, *43*, 6609.

[23] C. Seward, J. Chan, D. Song, S. Wang, *Inorg. Chem.* **2003**, *42*, 1112.

[24] O.-S. Jung, Y. J. Kim, Y.-A. Lee, K.-M. Park, S. S. Lee, *Inorg. Chem.* **2003**, *42*, 844.

[25] O.-S. Jung, Y. J. Kim, Y.-A. Lee, H. K. Chae, H. G. Jang, J. Hong, *Inorg. Chem.* **2001**, *40*, 2105.

[26] H. J. Choi, M. P. Suh, *Inorg. Chem.* **2003**, *42*, 1151.

[27] D. Venkataraman, G. B. Gardner, S. Lee, J. S. Moore, *J. Am. Chem. Soc.* **1995**, *117*, 11600.

[28] G. B. Gardner, Y.-H. Kiang, S. Lee, A. Asgaonkar, D. Venkataraman, *J. Am. Chem. Soc.* **1996**, *118*, 6946.

[29] Y.-H. Kiang, G. B. Gardner, S. Lee, Z. Xu, E. B. Lobkovsky, *J. Am. Chem. Soc.* **1999**, *121*, 8204.

[30] M. O'Keeffe, S. T. Hyde, *Zeolites* **1997**, *19*, 370.

[31] http://www.ccp14.ac.uk/ccp/web-mirrors/lcells/olex_index.htm.

[32] A. L. Spek, *Acta Crystallogr.* **1990**, *A46*, C34.

[33] L. Carlucci, G. Ciani, D. M. Prosperio, F. Porta, *Angew. Chem. Int. Ed.* **2003**, *42*, 317.

[34] J. Fan, W.-Y. Sun, T. Okamura, Y.-Q. Zheng, B. Sui, W.-X. Tang, N. Ueyama, *Crystal Growth & Design* **2004**, *4*, 579.

[35] C. S. Campos-Fernandez, B. L. Schottel, H. T. Chifotides, J. K. Bera, J. Bacsa, J. M. Koomen, D. H. Russell, K. R. Dunbar, *J. Am. Chem. Soc.* **2005**, *127*, 12909.

[36] B. H. Hamilton, K. A. Kelly, T. A. Wagler, M. P. Espe, C. J. Ziegler, *Inorg. Chem.* **2002**, *41*, 4984.

[37] B. H. Hamilton, K. A. Kelly, T. A. Wagler, M. P. Espe, C. J. Ziegler, *Inorg. Chem.* **2004**, *43*, 50.

[38] B. H. Hamilton, T. A. Wagler, M. P. Espe, C. J. Ziegler, *Inorg. Chem.* **2005**, *44*, 4891.

[39] Q. Li, T. Li, J. Wu, *J. Phys. Chem. B* **2001**, *105*, 12293.

[40] C. Chiorboli, M. A. Rodgers, F. Scandola, *J. Am. Chem. Soc.* **2003**, *125*, 483.

[41] J. C. F. Colis, R. Staples, C. Tripp, D. Labrecque, H. Patterson, *J. Phys. Chem. B* **2005**, *109*, 102.

[42] W. Choe, Y.-H. Kiang, Z. Xu, S. Lee, *Chem. Mater.* **1999**, *11*, 1776.

[43] D. Gryko, J. S. Lindsey, *J. Org. Chem.* **2000**, *65*, 2249.